PhD Thesis

Towards Crystalline Carbon dots for Improved Application Potential

By

Ayan Pal

Department of Chemistry
Indian Institute of Technology Guwahati

Towards Crystalline Carbon dots for Improved Application Potential

A thesis submitted By

Ayan Pal

Roll No. 146122026

to

Indian Institute of Technology Guwahati

for the award of the degree of

Doctor of Philosophy

Department of Chemistry
Indian Institute of Technology Guwahati
Guwahati – 781039
India

July 2019

Statement

This thesis entitled **"*Towards Crystalline Carbon dots for Improved Application Potential*"** is a work of research and investigation carried out by me under the supervision of Dr. Arun Chattopadhyay, Professor, Department of Chemistry, Indian Institute of Technology Guwahati. This thesis has been submitted by me to the Department of Chemistry, Indian Institute of Technology Guwahati for the award of the degree of Doctor of Philosophy. I further declare that this work has not been submitted anywhere else for the award of any degree in any Institute or University to the best of my knowledge.

_____

Ayan Pal
Department of Chemistry
IIT Guwahati,
Guwahati-781039, Assam
India
Date:
Place: Guwahati, Assam

Certificate

It is certified that the thesis entitled **"*Towards Crystalline Carbon dots for Improved Application Potential*"** being submitted to the Indian Institute of Technology Guwahati by *Ayan Pal (Roll. No. 146122026)* for the award of the degree of Doctor of Philosophy in Chemistry, is a bona fide record of research work carried out by him. The information and data reported by him are solely the results of his original findings. He has meticulously carried out the investigations and followed the guidelines of the laboratory. This work has not been submitted elsewhere for awarding any degree or diploma to the best of my knowledge.

_____

Arun Chattopadhyay
Thesis Supervisor
Professor,
Department of Chemistry,
IIT Guwahati,
Guwahati-781039, Assam,
India.
Date:
Place: Guwahati, Assam

Dedicated to my beloved Parents

Mr. Ramesh Pal

and

Mrs. Sarbani Pal

Acknowledgements

I would like to express my sincere gratitude to my thesis supervisor Prof. Arun Chattopadhyay, for his guidance, constant support, encouragement and valuable advice during the entire course of my doctoral studies. His discipline, sincerity, dedication towards research work and persuasive innovation ideas have inspired me a lot during my research career. I feel fortunate to have opportunity working under the supervision of such a dynamic personality. Thank you very much Sir for your support.

I am thankful to my doctoral committee chairman Dr. Lal Mohan Kundu, and the other committee members, Dr. Chandan K. Jana and Dr. A.S. Achalkumar for their constructive criticism as well as important suggestions regarding research works.

I offer my heartfelt thanks to my collaborators, Dr. Niramala Devi, Dr. Palashuddin Sk, Dr. Gayatri Natu, Dr. Deepanjalee Dutta, Kafeel Ahmad and Arin Bhakat for their tremendous input in my research works.

I would like to acknowledge all the faculty and staff members from Department of Chemistry and Centre for Nanotechnology for their continuous support and for providing advanced research facilities. Also, I thank Centre for Environment, Central Instruments Facility, Department of Physics IIT Guwahati.

I am extremely thankful to all my past and present lab members for their help and providing me a friendly atmosphere in the lab.

I am highly grateful to all of my friends who made my hostel life enjoyable. Also, I acknowledge their help and encouragement in various aspects.

Last but not least, I would like to give my heartfelt acknowledgment to my parents for their endless support, sacrifice and unconditional love.

Thank you
Blessed to have you all

Ayan

Contents

Abstract

Present thesis addresses that apart from being a good optical material, carbon dots (Cdots) can be highly crystalline in nature, turning them into a quality nano material for energy storage and conversion. The aim of this thesis is to pursue detailed investigations on the structural characteristics of Cdots. In this thesis we try to pinpoint on probing the hetero atom doping, which influenced the photophysical property of Cdots through surface modifications and heteroatom induced structural arrangement. In spite of being an emerging class of "nano light" the origin of optical properties of Cdots is still not well explained. That is the motivation of this thesis to investigate detailed photophysical properties of Cdots and implementation of the same for sensing application. Besides, exact geometry inside Cdot nano structure is not known. Structural randomness restricts utilization of this state-of-the-art environment friendly and easy-to-synthesize nano material in the field of organic electronics, photovoltaics, energy storage and conversion. Present thesis also imparts light on preparing highly crystalline Cdots. Origin of the observed structural characteristics were investigated in details and were finally utilized for efficient energy conversion and energy storage applications.

The present thesis is comprised of six chapters as described below.

Chapter 1 consists of the introduction part and literature review of carbon dots, properties and applications.

Chapter 2 describes dopant induced improved photoluminescence phenomenon of amorphous Cdots. Taking advantage of the enhanced photoluminescence efficiency of Cdots due to doping, a duel light emitting nano composite system was fabricated for ratiometric intracellular pH sensing.

Chapter 3 consists discovery of conducting nature in Cdots. The conducting property was investigated based on *I-V* characteristic studies of Cdot films. A Cdot based semi-crystalline polymeric nano composite system with polypyrrole (PPy) was synthesized

where Cdots were found to enhance the conducting nature of the composite system. Finally, the improved conducting nature of the composite system was successfully utilized for sensing nitro explosive compounds based on *I-V* characteristic studies.

Chapter 4 demonstrates synthesis of dopant induced non-graphitic crystalline nature in Cdots. Generation of excellent crystallinity was found to be advantageous for efficient photothermal conversion and phonon transportation. Finally, this phenomenon in Cdot system was successfully implied for solar light assisted sea water desalination.

Chapter 5 describes facile synthesis of highly crystalline Cdot assembly. Assisted by excellent crystallinity, the as-prepared assembled Cdot system was found to boost the electrochemical performance and charge storage ability in electrodes, which was finally implied to fabricated Cdot based supercapacitors.

Chapter 6 includes conclusion and future prospects.

Chapter 1

Introduction

The distinctive quality of carbon forming robust covalent bonds with neighboring carbon atoms in different hybridization states such as the sp^3, sp^2 and sp enables to be present in diverse structures with unique characteristics, also known as the allotropes of carbon. Among allotropes, existence of carbon was first identified in diamond in the year 1772 followed by graphite in 1890s. Besides, in past few decades, findings of a range of new carbon structures are noteworthy such as the C_{60} molecule also known as fullerene (along with C_{20} and C_{70}), carbon nanotubes (CNTs), onion-like carbon (OLC) spheres, graphene quantum dots (GQDs). However, lately another class of carbon nano structure that has been studied extensively is carbon dots (or Cdots). Unique optical properties along with structural flexibility and their wide range of applications have made this state-of-the-art carbon allotrope a promising candidate in the field of nano science and technology, thus opening up a newer avenue for the current research work based on carbon materials.

1.1 Carbon dots

Carbon dots (Cdots) are the luminescent zero-dimensional nanostructured carbon materials with size ranging between 1-10 nm. As an emerging class of nanomaterials, Cdots exhibit several outstanding qualities such as low toxicity, excellent water solubility, ease of synthesis and functionalization, and high photo-stability substantiating them apt for multifaceted applications.

1.1.1 Discovery of Carbon dots (Cdots)

The journey of Cdots started in the year 2004 with the separation of "impure" fluorescent carbon by Xu *et al.* during purification of single-walled carbon nanotubes. [1] Later in 2006, Sun *et al.* reported formation of quantum-sized nanoscale carbon particles termed as "carbon dots" during laser ablation of carbon target. [2] Next year, in 2007, Liu *et al.* reported synthesis of fluorescent "carbon nanoparticles" (size < 2 nm) by using combustion oxidation method. [3] After 2007, the field of Cdots has been

significantly expanded and till date they are being extensively studied by the researchers for various applications.

1.1.2 Synthetic Methods

The synthesis procedure of Cdots could be classified in to two categories, "top-down" and "bottom-up". In "top-down" approach, Cdots are synthesized from macroscopic carbon structures such as the carbon nanotubes, graphite and activated carbon by using arc discharge, chemical oxidation, laser ablation and electrochemical oxidation methods. On the other hand, "bottom-up" approach corresponds to synthesis of Cdots starting with small molecular precursors such as citric acid, glucose, amino acids, polyethylene glycol (PEG) and sucrose through microwave treatment, hydrothermal treatment, combustion/thermal decomposition, and plasma treatment. [4-10] Also, in order to introduce environmentally and cost-effective techniques, several "green" resources have been used for synthesizing Cdots such as organogel, natural silk, hair fiber, bovine serum albumin, chitosan, egg shell membrane, gelatin and so on. [11-17].

1.1.3 Composition and Structure

Typically, Cdots are composed of three fundamental elements- carbon (C), nitrogen (N) and oxygen (O). Since the main constituent element is carbon, these nano materials are termed as "carbon dots" or Cdots. Depending upon synthetic strategies and the starting materials, the compositions of these three fundamental constituents differ resulting interesting optical phenomena. [18] The carbogenic core is formed with sp^2 and/or sp^3 hybridized carbon attached to various surface functional groups (such as the -COOH, -CONH, $-NH_2$, -OH). Though the emission characteristics of Cdots are predominantly controlled by surface functional groups (known as extrinsic emission resulting tunable emission), carbogenic core directed emission could also be found, which is known as intrinsic emission. Emission properties of Cdots could also be tuned by doping several other hetero atoms such as boron (B) and phosphorus (P). Besides, Cdots are mostly amorphous in nature. However, depending upon reaction conditions and precursors graphitic crystallization can take place. [19-21]

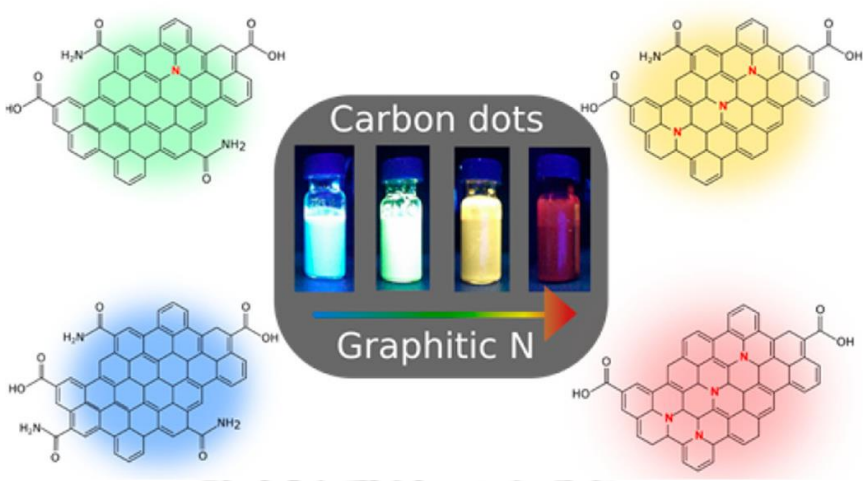

Figure 1.1. Schematic for the graphitic structure proposed to be formed during high temperature carbonization and corresponding emission.[22] (Reprinted with permission from reference 22. Copyright 2017 American Chemical Society).

1.1.4 Properties of Cdots

1.1.4.1 Absorption and Photoluminescence Properties

Typically, Cdots are observed to have strong absorbance in the UV region along with tail extended up to visible region. The peak appearing between 250-290 nm corresponds to π–π* transitions whereas strong absorbance appearing ~ 350 nm is attributed to n-π* transitions inside carbon nanostructure. However, some Cdot systems exhibit absorbance above 400 nm wavelength, due to surface functional group induced smaller electronic bandgap transitions (Figure 1.2a).

The photoluminescence (PL) property, on the other hand, commonly known as "excitation dependent tunability" is one of the most exciting phenomena discovered for Cdot systems.[23] So far, numerous reports have been published based on full-color-tunable emission of Cdots, which turns these state-of-the-art nanomaterials in to powerful tool for bio- and chemical sensing. Even though Cdots exhibit excellent PL property with high quantum efficiency, comprehensive explanations for such unique PL origin has not been proposed yet. Indeed, presently three different viewpoints exist for the explanation of Cdot PL characteristics such as (i) defect state emission caused by surface functional groups, (ii) core state emission, and (iii) molecular luminescence, caused due to formation of fluorescent impurities as the side product during Cdot synthesis.

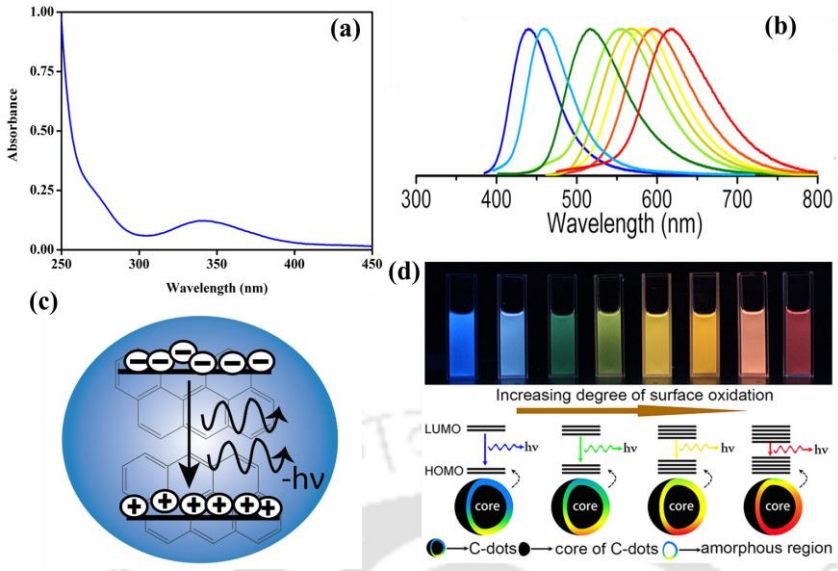

Figure 1.2. (a) Typical absorption spectrum shown by Cdots. (b) Excitation dependent tenability in emission of Cdots.[24] (Reprinted with permission from reference 24. Copyright 2016 American Chemical Society). (c) Schematic for core state emission also known as intrinsic emission. (d) Surface functional group induced tunable emission in Cdots.[24] (Reprinted with permission from reference 24. Copyright 2016 American Chemical Society).

1.1.4.2 Electroluminescence and Chemiluminescence Properties

Electroluminescence (ECL) is an optoelectrical phenomenon of a material for generating light by passing strong electric field. In this regard, as an emerging class of "nano light" Cdots have been found to be viable alternate to semiconducting quantum dots in the field of electroluminescent light-emitting diodes (LEDs). Wang *et al.* demonstrated the electroluminescent phenomenon of Cdots by developing white light-emitting devices showing an efficiency of 0.083% at 5 mA cm^{-2} current density (CRI 82). [25] Afterwards, Zhang *et. al.* have shown color-switchable electroluminescence property of Cdots, based on variations in device structure and applied current density. [26] Also, Cdots have been used as emitting layer in LEDs by Veca *et al.*[27] Similarly, Yuan *et. al.* reported monochrome electroluminescent LEDs using Cdot bandgap emission. [28]

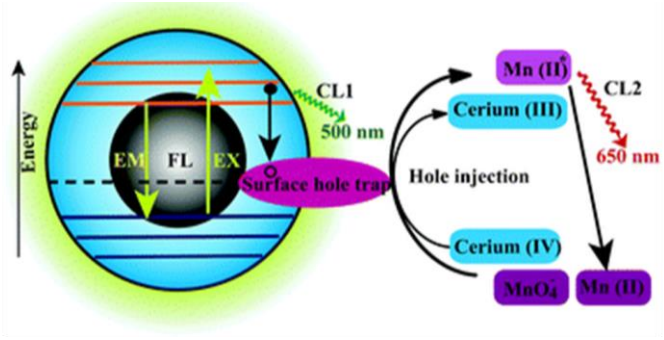

Figure 1.3. (a) Schematic for the photoluminescence and chemiluminescence mechanisms of Cdots in presence of oxidizing species such as $KMnO_4$ and cerium (IV).[29] (Reprinted with permission from reference 29. Copyright 2012 Royal Society of Chemistry).

On the other hand, the term chemiluminescence (CL) corresponds to the generation of light using chemical reaction. Cdot chemiluminescence (CL) phenomenon was first invented by Lin *et al.* in presence of oxidizing species such as cerium (IV) and potassium permanganate ($KMnO_4$). Detailed investigations revealed that the presence of oxidizing species helped injecting holes inside the carbon nano structure, which assists in electron-hole annihilation. The resulting energy is emitted in the form of CL. [29] Interestingly, CL phenomenon of Cdots is found to be very much dependent upon nature of surface functional groups. [30] Thus, the observed CL phenomenon in Cdots and its ability towards both the electron donation/acceptance make them potential candidate for catalysis and optronics.

1.1.4.3 Photoinduced Electron Transfer Properties

Recent reposts corresponding to photoinduced electron transfer properties of Cdots have introduced a newer avenue for their potential applications in light energy conversion, photocatalysis along with detailed mechanistic studies. For example, Xu *et al.* reported that Cdots can efficiently trap photo excited electrons corresponding to semiconductors, resulting in efficient separation between photoinduced electrons and holes. [31] Wang *et al.* showed that the PL intensity of Cdots could be affected efficiently in the presence of electron donor (N, N-diethylaniline) or electron acceptor (2,4-dinitrotoluene or 4-nitrotoluene) molecules, proving photoexcited Cdots as effective electron donor and/or accepter. [32] Besides, electron transfer mechanisms in Cdot based nanocomposite systems such as Cdots/MWCNTs, Cdots/GO, Cdots/TiO_2 have been studied extensively as well.[33]

1.1.4.4 Up-conversion Properties

Fluorescence up-conversion is a phenomenon in which emission wavelength is shorter than the excitation wavelength, and is mostly useful for bio imaging purposes because of reduced background auto fluorescence and better photon tissue penetration. Apart from conventional down-conversion PL, Cdots are found to exhibit up-conversion PL as well. This interesting property in Cdot system was first found by Cao *et. al.*, showing emission in visible region by Cdots upon excitation with an 800 nm pulsed laser source. [34] Later, detailed investigations on the same phenomenon in Cdot systems have been done by several other research groups by taking different precursors and following separate synthetic strategies. [35-37]

1.1.5 Applications of Cdots

1.1.5.1 Bio-imaging and Bio-sensing

Being a good optical material, Cdots have widely been used for bio-imaging and biomolecule sensing purpose. Unlike metal based semiconducting quantum dots, Cdots are found to be biocompatible, making them apt for biological applications. In the year 2007, Cao *et al.* reported imaging of cancer cells using two photon photoluminescence microscopy. [34] Later, Yang *et al.* (in 2009) reported excellent biocompatibility and non-toxicity of Cdots by which they showed in vivo optical imaging in mice model. [38] Since then several reports have been published claiming Cdots as excellent bio-imaging probes for cancer cell lines, mitochondria, tissues and tumor cells.[39-44]

Along with bio-imaging, Cdots are found to be efficient probes for detecting bio molecule because of structural flexibility, nontoxicity, good biocompatibility, cell permeability and photo stability. Cdots have been reported as the biosensor for proteins, [45] nucleic acid, [46] phosphates, [47] glucose,[48] pH, [49] metal ions like potassium,[50] iron,[51] cellular copper,[52] bio-thiols,[53] dopamine,[54] ascorbic acid, [55] and reactive oxygen species (ROS).[56]

1.1.5.2 Drug Delivery

Due to smaller size, good biocompatibility and sustained drug release, Cdots have been used as good nano carrier and drug release tool. For example, Zheng *et al.* reported

oxaliplatin conjugated Cdots, which showed efficient therapeutic performance especially targeted drug release by Cdots. [57] Lai *et al.* showed efficient doxorubicin (DOX; anticancer drug) release performance by Cdots in HeLa cells.[58] Mewada *et al.* prepared bovine serum albumin (BSA) passivated Cdots, which showed better DOX release efficiency to cancer cells.[59] Thus various reports corresponding to surface functional group modified Cdots suggest them as a potential candidate for targeted drug delivery. [60-62]

1.1.5.3 Chemical Sensing

So far, exceptional optical properties of Cdots have been extensively used to design noble sensing probes. Cdots have been used to detect several small molecules such as melamine, [63] picric acid, [64] 2,4-dinitrophenol, [65] tetracyclines,[66] quercetin, [67] amoxicillin. [68] For example, Yang *et al.* synthesized Cdots from l-cysteine in presence of diphosphorus pentoxide, which was used to detect different tetracyclines with calculated LOD of 4.2-7.5 nM. [66] Sk *et al.* reported selective and sensitive detection of picric acid by using photoluminescence quenching phenomenon of Cdots, synthesized from citric acid and ethylene diamine. Calculated detection limit was reported to be 75.6 ppb. [64]

1.1.5.4 Light Emitting Devices (LED) and Photodetectors

As a state-of-the-art luminescent material, low cost, photo stable, high quantum yield and less toxic Cdots are expected to replace heavy metals such as lead, cadmium and rare earth metals in devising light emitting diodes. Yuan *et al.* synthesized multicolor emitting Cdots, which were used as the active emissive layer for fabricating LEDs. Maximum luminescence was reported to be 136 cd m^{-2}.[69] Similarly, warm white light-emitting diodes were fabricated by Jia *et al.* with maximum measured luminance of 5248–5909 cd m^{-2} and a current efficiency of 3.65-3.85 cd A^{-1} where Cdots acted as the emissive layer.[70] Thus several groups have used the efficient electroluminescence property of Cdots to device light-emitting devices. [71-75] Besides, efforts have been given by many research groups on devising Cdot based photo detectors. Xie *et al.* made "Core-shell heterojunction" between silicon nanowire arrays and Cdots to prepare self-

driven photodetectors. [76] Similarly, MoS_2-Cdot hybrid system has been used by Sahatiya *et al.* to prepare paper based UV-vis-NIR photodetector. [77]

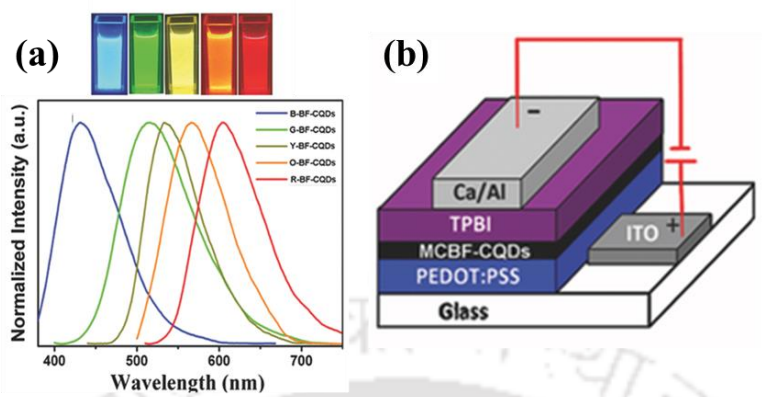

Figure 1.4. (a), (b) Multicolor emitting Cdot based LED.[69] Reprinted with permission.[69] Copyright 2017, John Wiley and Sons.

1.1.5.5 Photocatalysis

The ability of absorbing longer wavelength light and energy exchange by Cdots into solution species has made them excellent photocatalysts for organic reactions. Indeed, Sk *et al.* demonstrated synthesis of carbon nanoparticle supported gold (Au) nanoparticles, which could be used as efficient photocatalyst during the homocoupling reaction of phenylboronic acid. [78] In another study, Cdots of 1-4 nm were synthesized, which were found to exhibit catalytic activity in presence of NIR light, resulting in the selective oxidation of alcohols to benzaldehyde. The conversion efficiency was found to be 92 % with 100 % selectivity. [79] Similarly, Cdots of size between 5-10 nm was synthesized by Li *et al.* by using chemical ablation of graphite, which was finally used to catalyze several organic reactions. [80] Also, the photocatalytic activities of Cdots have been utilized for removal of organic pollutants, [81] oxidizing cyclohexane in to cyclohexanone,[82] hydrocarbon oxidation,[83] and H_2 generation by irradiating visible light. [84]

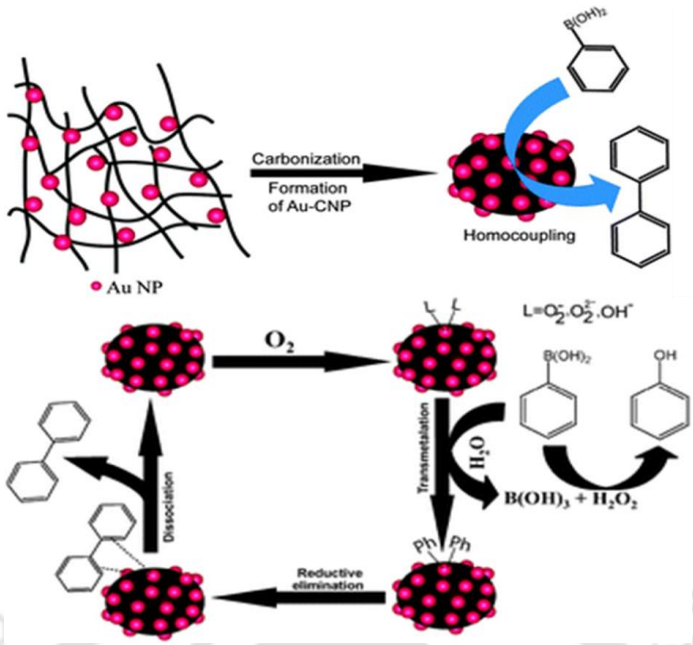

Figure 1.5. Schematic representation for the photocatalytic activity by Cdots.[78] (Reproduced with permission from ref. 78.).

1.1.5.6 Electrocatalysis

Current surge for the development of clean energy resources, devoid of traditional fossil fuels necessitates further research over oxygen reduction and oxygen evolution reaction. Till date, various metal based catalysts and their composite systems have been used in order to improve reaction kinetics. However, due to complicated synthesis procedures along with high cost of these metal based electro catalysts, carbon based materials have been introduced. Use of Cdots is noteworthy for the same. Zhu *et al.* synthesized bifunctional Cdots using hydrothermal method, which showed efficient electrocatalytic activity for oxygen reduction reaction. [85] Tang *et al.* used Cdots deposited over Ni-Fe layered double-hydroxide nanoplates for better electrocatalytic activity. Good stability along with small over potential can be observed (~305 mV in 0.1 M KOH and ~235 mV in 1 M KOH at 10 mA cm^{-2} current density), which are effective for efficient oxygen evolution reactions.[86]

1.1.5.7 Solar Cells

As explained in the preceding sections, due to wide absorbance range in the UV region along with tail extended in the visible range, Cdots are being utilized successfully in

photovoltaics such as devising solar cells. Recently, several Cdot based composites have been reported as the photosensitizer for dye sensitized solar cells,[87] hole transporter in perovskite solar cells, [88] counter electrode for quantum dot sensitized solar cells.[89] Zhang *et al.* reported nitrogen doped Cdots, which were used as sensitizers for fabricating TiO_2-based dye sensitized solar cells. Here Cdots were found to exhibit better photo induced electron transfer to the conduction band of TiO_2. [87] Briscoe *et al.* synthesized biomass derived Cdot based ZnO nanohybrid in order to device solid-state solar cells. [90] Nitrogen and sulfur co-doped Cdots have been used as the surface modifier of ZnO by Wang *et al.* It has been observed that embedding Cdots reduce surface energy of the ZnO layer, facilitating efficient transportation and collection of photo generated carriers. Maximum power conversion efficiency (PCE) was reported to be 9.31% in this work. [91] Zhang *et al.* developed ZnO/Cdots bilayer "electron extraction layer" where Cdots assisted in ZnO surface passivation along with exciton dissociation.[92] The results revealed that using such bilayer system enabled suppressing of quenching of excitons and further reducing Shockley-Read-Hall (SRH) recombination. Improved PCE was measured to be 9.64% in this work. [92]

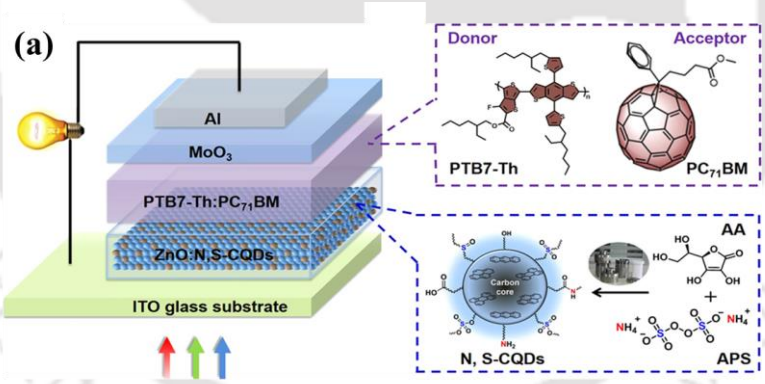

Figure 1.6. Schematic representation for the device fabrication of inverted organic solar cells along with structural formula of the active layer constituents and Cdots synthesis procedure.[91] (Reprinted with permission from ref. 91). Copyright 2019 American Chemical Society.

1.2 Motivation

The introduction section of this thesis includes various aspects of Cdots proving themselves a viable alternate to metal based semiconductors especially quantum dots. So far Cdots have been primarily portrayed as amorphous nanomaterials having no structural alignment. Though researches have been able to generate limited graphitic

arrangement in Cdots structure, the question still remains - 'Should Cdots be considered as crystalline nanomaterial?' It is important mentioning here that understanding crystalline nature in carbon nanostructures is important as crystallinity induces completely different mechanical characteristics, providing structural rigidity as compared to amorphous carbon nanomaterials. Long range order can provide better structural stability, phonon and electronic transport ability as compared to randomly oriented substances.

As discussed in the preceding sections, only graphitic characteristics and corresponding phenomena of Cdots have been studied widely so far. Presently, Cdots are considered as an emerging class of nano light owing to their exceptional optical properties, substantially high photoluminescence quantum yield, ease of synthesis and functionalization, and environmental friendliness. Most of the implementations are based on their so called top-notch optical properties. Although a few results have been reported on their catalytic behavior and their use in photovoltaics, lack of structural arrangement further restricts their successful implementations, ending up with lower efficiency values. Thus, there is clear need of introducing simple methodology for gaining high quality crystalline nature in this green and easy-to-synthesize carbon allotrope so that it could be successfully implemented in fabricating miniaturized devices related to energy conversion and organic photovoltaics.

1.3 Overview of the Thesis

The thesis is focused on facile synthesis of luminescent Cdots and generating noble characteristics such as conductivity and structural symmetry or crystallinity by heteroatom doping and finally utilize the same for sensing, efficient photothermal heat generation and in improving charge storage performance. The thesis contains four chapters and the kernel of each chapter is highlighted below.

Chapter 2 represents synthesis of boron and phosphorus doped Cdots (termed as B-Cdots and P-Cdots, respectively) and detailed studies of their exceptional photophysical properties. Results revealed that boron doping can improve luminescence quantum yield significantly whereas the opposite trend could be monitored in case of phosphorus doping in the similar system. Heteroatom induced surface modifications such as oxidation or reduction to the surface functional groups along with consequential surface

passivation were surmised to be the determining factors for such exceptional photophysical behavior. Finally, optically stable and high quantum yield B-Cdots were used to synthesize a white light emitting nanocomposite material, the emission of which was found to be highly sensitive towards pH of the local environment. Such pH dependent emission characteristics were successfully utilized towards monitoring intracellular pH in cancerous cells (HeLa cells here).

Chapter 3 delineates the finding of conducting property in Cdots. Cdots were synthesized from citric acid monohydrate and ethylene diamine. Chemically synthesized conducting nanocomposite was prepared, which consisted of Cdots and polypyrrole (PPy). The composite showed higher electrical conductivity as compared to the components i.e., Cdots or PPy. The conductive film of the composite material was prepared whused for highly sensitive and selective detection of picric acid in water as well as in soil.

Chapter 4 demonstrates a simple but efficient method of generating excellent crystalline property in carbon nano structures. Microwave treatment of citric acid monohydrate and thiourea in the presence of *ortho* phosphoric acid resulted in the formation of well-ordered structure in Cdot where the extent of crystallinity was solely dependent of phosphorus doping percentage. Generation of well-ordered crystalline structure in Cdot system was found to be appropriate for efficient photothermal conversion and phonon transportations. These phenomena were successfully implemented for solar-light assisted sea-water desalination in the presence of crystalline Cdots.

Chapter 5 portrays zinc ion induced assembly of Cdots with enhanced crystalline nature. Crystallinity in Cdots helped improve electrochemical performance and charge storage ability of electrodes significantly. Finally, this phenomenon was successfully applied towards fabrication of Cdot based supercapacitor electrodes with outstanding specific capacitance and excellent energy density.

Chapter 6 contains conclusion of the thesis and future prospects.

References

1. Xu, X.; Ray, R.; Gu, Y.; Ploehn, H. J.; Gearheart, L.; Raker, K.; Scrivens, W. A. Electrophoretic Analysis and Purification of Fluorescent Single-Walled Carbon Nanotube Fragments. *J. Am. Chem. Soc.* **2004,** *126* (40), 12736-12737.

2. Sun, Y.-P.; Zhou, B.; Lin, Y.; Wang, W.; Fernando, K. A. S.; Pathak, P.; Meziani, M. J.; Harruff, B. A.; Wang, X.; Wang, H.; Luo, P. G.; Yang, H.; Kose, M. E.; Chen, B.; Veca, L. M.; Xie, S.-Y. Quantum-Sized Carbon Dots for Bright and Colorful Photoluminescence. *J. Am. Chem. Soc.* **2006,** *128* (24), 7756-7757.

3. Liu, H.; Ye, T.; Mao, C. Fluorescent Carbon Nanoparticles Derived from Candle Soot. *Angew. Chem. Int. Ed.* **2007**, *46*, 6473 -6475.

4. Iqbal, A.; Iqbal, K.; Xu, L.; Li, B.; Gong, D.; Liu, X.; Guo, Y.; Liu, W.; Qin, W.; Guo, H. Heterogeneous Synthesis of Nitrogen-doped Carbon Dots Prepared via Anhydrous Citric Acid and Melamine for Selective and Sensitive Turn on-off-on Detection of Hg (II), Glutathione and its Cellular Imaging. *Sens. Actuators, B* **2018**, *255*, 1130-1138.

5. Ma, Z.; Ming, H.; Huang, H.; Liu, Y.; Kang, Z., One-step Ultrasonic Synthesis of Fluorescent N-doped Carbon Dots from Glucose and their Visible-light Sensitive Photocatalytic Ability. *New J. Chem.* **2012**, *36*, 861-864.

6. Jiang, J.; He, Y.; Li, S.; Cui, H. Amino Acids as the Source for Producing Carbon Nanodots: Microwave Assisted One-step Synthesis, Intrinsic Photoluminescence Property and Intense Chemiluminescence Enhancement. *Chem. Commun.* **2012**, *48*, 9634-9636.

7. Zhang, B.-X.; Zhang, G.-Y.; Gao, H.; Wu, S.-H.; Chen, J.-H.; Li, X.-L. One-step Hydrothermal Synthesis and Optical Properties of PEG-passivated Nitrogen-doped Carbon Dots. *RSC Adv.* **2015**,*5*, 7395-7400.

8. Liu, X.; Liu, J.; Zheng, B.; Yan, L.; Dai, J.; Zhuang, Z.; Du, J.; Guo, Y.; Xiao, D. N-Doped Carbon Dots: Green and Efficient Synthesis on a Large-scale and their Application in Fluorescent pH Sensing. *New J. Chem.* **2017,** *41* (19), 10607-10612.

9. Jaiswal, A.; Ghosh, S. S.; Chattopadhyay, A. One Step Synthesis of C-dots by Microwave Mediated Caramelization of Poly(ethylene glycol). *Chem. Commun.* **2012,** *48* (3), 407-409.

10. Park, S. Y.; Lee, C. Y.; An, H. R.; Kim, H.; Lee, Y. C.; Park, E. C.; Chun, H. S.; Yang, H. Y.; Choi, S. H.; Kim, H. S.; Kang, K. S.; Park, H. G.; Kim, J. P.; Choi, Y.; Lee, J.; Lee, H. U. Advanced Carbon Dots via Plasma-induced Surface Functionalization for Fluorescent and Bio-medical Applications. *Nanoscale* **2017,** *9 (26)*, 9210-9217.

11. Neabo, J. R.; Vigier-Carriere, C.; Rondeau-Gagne, S.; Morin, J. F. Room-Temperature Synthesis of Soluble, Fluorescent Carbon Nanoparticles from Organogel Precursors. *Chem. Commun*. **2012,** *48 (81)*, 10144-10146.

12. Wu, Z. L.; Zhang, P.; Gao, M. X.; Liu, C. F.; Wang, W.; Leng, F.; Huang, C. Z. One-pot Hydrothermal Synthesis of Highly Luminescent Nitrogen-doped Amphoteric Carbon Dots for Bioimaging from Bombyx Mori Silk – Natural Proteins. *J. Mater. Chem. B* **2013**, *1*, 2868-2873.

13. Sun, D.; Ban, R.; Zhang, P.-H.; Wu, G.-H.; Zhang, J.-R.; Zhu, J.-J. Hair Fiber as a Precursor for Synthesizing of Sulfur- and Nitrogen-co-doped Carbon Dots with Tunable Luminescence Properties. *Carbon* **2013,** *64*, 424-434.

14. Liu, J.-M.; Lin, L.-p.; Wang, X.-X.; Lin, S.-Q.; Cai, W.-L.; Zhang, L.-H.; Zheng, Z.-Y. Highly Selective and Sensitive Detection of Cu^{2+} with Lysine Enhancing Bovine Serum Albumin Modified-Carbon Dots Fluorescent Probe. *Analyst* **2012**, *137*, 2637-2642.

15. Liu, X.; Pang, J.; Xu, F.; Zhang, X. Simple Approach to Synthesize Amino-Functionalized Carbon Dots by Carbonization of Chitosan. *Sci. Rep*. **2016,** *6*, 31100.

16. Wang, Q.; Liu, X.; Zhang, L.; Lv, Y. Microwave-assisted Synthesis of Carbon Nanodots through an Eggshell Membrane and their Fluorescent Application. *Analyst* **2012**, *137 (22)*, 5392–5397.

17. Liang, Q.; Ma, W.; Shi, Y.; Li, Z.; Yang, X. Easy Synthesis of Highly Fluorescent Carbon Quantum Dots from Gelatin and their Luminescent Properties and Applications. *Carbon* **2013,** *60*, 421-428.

18. Lim, S. Y.; Shen, W.; Gao, Z., Carbon Quantum Dots and their Applications. *Chem. Soc. Rev*. **2015,** *44 (1)*, 362-381.

19. Baker, S. N.; Baker, G. A. Luminescent Carbon Nanodots: Emergent Nanolights. *Angew. Chem. Int. Ed.* **2010,** *49* (38), 6726-6744.

20. Li, H.; Kang, Z.; Liu, Y.; Lee, S.-T. Carbon nanodots: Synthesis, Properties and Applications. *J. Mater. Chem*. **2012**, *22*, 24230-24253.

21. Wu, H.; Chen, Y.; Dai, X.; Li, P.; Stoddart, J. F.; Liu, Y. In Situ Photoconversion of Multicolor Luminescence and Pure White Light Emission Based on Carbon Dot-Supported Supramolecular Assembly. *J. Am. Chem. Soc.* **2019,** *141 (16)*, 6583-6591.

22. Hola, K.; Sudolska, M.; Kalytchuk, S.; Nachtigallova, D.; Rogach, A. L.; Otyepka, M.; Zboril, R. Graphitic Nitrogen Triggers Red Fluorescence in Carbon Dots. *ACS Nano* **2017**, *11*, 12402-12410.

23. Hu, S.; Trinchi, A.; Atkin, P.; Cole, I. Tunable photoluminescence across the entire visible spectrum from carbon dots excited by white light. *Angew. Chem. Int. Ed.* **2015**, *54*, 2970-2974.

24. Ding, H.; Yu, S. B.; Wei, J. S.; Xiong, H. M. Full-Color Light-Emitting Carbon Dots with a Surface-State-Controlled Luminescence Mechanism. *ACS Nano* **2016**, *10*, 484-491.

25. Wang, F.; Chen, Y. H.; Liu, C. Y.; Ma, D. G. White Light-emitting Devices Based on Carbon Dots' Electroluminescence. *Chem. Commun.* **2011**, *47*, 3502-3504.

26. Zhang, X.; Zhang, Y.; Wang, Y.; Kalytchuk, S.; Kershaw, S. V.; Wang, Y.; Wang, P.; Zhang, T.; Zhao, Y.; Zhang, H.; Cui, T.; Wang, Y.; Zhao, J.; Yu, W. W.; Rogach, A. L. Color-Switchable Electroluminescence of Carbon Dot Light-Emitting Diodes. *ACS Nano* **2013**, *7* , 11234-11241.

27. Veca, L. M.; Diac, A.; Mihalache, I.; Wang, P.; LeCroy, G. E.; Pavelescu, E. M.; Gavrila, R.; Vasile, E.; Terec, A.; Sun, Y.-P. Electroluminescence of Carbon 'Quantum' Dots – From Materials to Devices. *Chem. Phys. Lett.* **2014,** *613*, 40-44.

28. Yuan, F.; Wang, Z.; Li, X.; Li, Y.; Tan, Z.; Fan, L.; Yang, S. Bright Multicolor Bandgap Fluorescent Carbon Quantum Dots for Electroluminescent Light-Emitting Diodes. *Adv. Mater.* **2017**, *29*, 1604436.

29. Lin, Z.; Xue, W.; Chen, H.; Lin, J. M. Classical Oxidant Induced Chemiluminescence of Fluorescent Carbon Dots. *Chem. Commun.* **2012**, *48*, 1051-1053.

30. Teng, P.; Xie, J.; Long, Y.; Huang, X.; Zhu, R.; Wang, X.; Liang, L.; Huang, Y.; Zheng, H., Chemiluminescence Behavior of the Carbon Dots and the Reduced State Carbon dots. *J. Lumin.* **2014,** *146*, 464-469.

31. Xu, J.; Sahu, S.; Cao, L.; Bunker, C. E.; Peng, G.; Liu, Y.; Fernando, K. A.; Wang, P.; Guliants, E. A.; Meziani, M. J.; Qian, H.; Sun, Y. P. Efficient Fluorescence Quenching in Carbon Dots by Surface-Doped Metals-Disruption of Excited State Redox Processes and Mechanistic Implications. *Langmuir* **2012**, *28*, 16141-16147.

32. Wang, X.; Cao, L.; Lu, F.; Meziani, M. J.; Li, H.; Qi, G.; Zhou, B.; Harruff, B. A.; Kermarrec, F.; Sun, Y. P. Photoinduced Electron Transfers With Carbon Dots. *Chem. Commun.* **2009**, 3774-3776. DOI: 10.1039/b906252a.

33. Yu, P.; Wen, X.; Toh, Y.-R.; Lee, Y.-C.; Huang, K.-Y.; Huang, S.; Shrestha, S.; Conibeer, G.; Tang, J. Efficient Electron Transfer in Carbon Nanodot–Graphene Oxide Nanocomposites. *J. Mater. Chem. C* **2014**, *2*, 2894-2901.

34. Cao, L.; Wang, X.; Meziani, M. J.; Lu, F.; Wang, H.; Luo, P. G.; Lin, Y.; Harruff, B. A.; Veca, L. M.; Murray, D.; Xie, S.-Y.; Sun, Y.-P. Carbon Dots for Multiphoton Bioimaging. *J. Am. Chem. Soc.* **2007**, *129*, 11318-11319.

35. Shen, J.; Zhu, Y.; Chen, C.; Yang, X.; Li, C. Facile Preparation and Upconversion Luminescence of Graphene Quantum Dots. *Chem. Commun.* **2011,** *47*, 2580-2582.

36. Li, H.; He, X.; Kang, Z.; Huang, H.; Liu, Y.; Liu, J.; Lian, S.; Tsang, C. H.; Yang, X.; Lee, S. T. Water-soluble Fluorescent Carbon Quantum Dots and Photocatalyst Design. *Angew. Chem. Int. Ed.* **2010**, *49*, 4430-4434.

37. Zong, J.; Zhu, Y.; Yang, X.; Shen, J.; Li, C. Synthesis of Photoluminescent Carbogenic Dots Using Mesoporous Silica Spheres as Nanoreactors. *Chem. Commun.* **2011**, *47*, 764-766.

38. Yang, S.-T.; Cao, L.; Luo, P. G.; Lu, F.; Wang, X.; Wang, H.; Meziani, M. J.; Liu, Y.; Qi, G.; Sun, Y.-P. Carbon Dots for Optical Imaging in Vivo. *J. Am. Chem. Soc.* **2009**, *131*, 11308-11309.

39. Zhang, J.; Yu, S.-H., Carbon dots: Large-Scale Synthesis, Sensing and Bioimaging. *Mater. Today* **2016**, *19*, 382-393.

40. Gao, G.; Jiang, Y. W.; Yang, J.; Wu, F. G. Mitochondria-Targetable Carbon Quantum Dots for Differentiating Cancerous Cells from Normal Cells. *Nanoscale* **2017**, *9*, 18368-18378.

41. Kong, B.; Zhu, A.; Ding, C.; Zhao, X.; Li, B.; Tian, Y. Carbon Dot-based Inorganic-Organic Nanosystem for Two-Photon Imaging and Biosensing of pH Variation in Living Cells and Tissues. *Adv. Mater.* **2012**, *24*, 5844-5848.

42. Ko, H. Y.; Chang, Y. W.; Paramasivam, G.; Jeong, M. S.; Cho, S.; Kim, S. In vivo Imaging of Tumour Bearing Near-infrared Fluorescence-Emitting Carbon Nanodots Derived from Tire Soot. *Chem. Commun.* **2013**, *49*, 10290-10292.

43. Jiang, K.; Sun, S.; Zhang, L.; Lu, Y.; Wu, A.; Cai, C.; Lin, H. Red, Green, and Blue Luminescence by Carbon dots: Full-color Emission Tuning and Multicolor Cellular Imaging. *Angew. Chem. Int. Ed.* **2015**, *54*, 5360-5363.

44. Tao, H.; Yang, K.; Ma, Z.; Wan, J.; Zhang, Y.; Kang, Z.; Liu, Z. In Vivo NIR Fluorescence Imaging, Biodistribution, and Toxicology of Photoluminescent Carbon Dots Produced from Carbon Nanotubes and Graphite. *Small* **2012,** *8*, 281-290.

45. Freire, R. M.; Le, N. D. B.; Jiang, Z.; Kim, C. S.; Rotello, V. M.; Fechine, P. B. A. NH_2-rich Carbon Quantum Dots: A Protein-Responsive Probe for Detection and Identification. *Sens. Actuators, B* **2018,** *255*, 2725-2732.

46. Li, H.; Zhang, Y.; Wang, L.; Tian, J.; Sun, X. Nucleic Acid Detection Using Carbon Nanoparticles as a Fluorescent Sensing Platform. *Chem. Commun.* **2011**, *47*, 961-963.

47. Zhao, H. X.; Liu, L. Q.; Liu, Z. D.; Wang, Y.; Zhao, X. J.; Huang, C. Z. Highly Selective Detection of Phosphate in Very Complicated Matrixes with an Off-On Fluorescent Probe of Europium-Adjusted Carbon Dots. *Chem. Commun.* **2011**,*47*, 2604-2606.

48. Wang, H.; Yi, J.; Velado, D.; Yu, Y.; Zhou, S. Immobilization of Carbon Dots in Molecularly Imprinted Microgels for Optical Sensing of Glucose at Physiological pH. *ACS Appl. Mater. Interfaces* **2015**, *7*, 15735-157445.

49. Shi, W.; Li, X.; Ma, H. A Tunable Ratiometric pH Sensor Based on Carbon Nanodots for the Quantitative Measurement of the Intracellular pH of Whole Cells. *Angew. Chem. Int. Ed.* **2012**, *51*, 6432 -6435.

50. Wei, W.; Xu, C.; Ren, J.; Xu, B.; Qu, X. Sensing Metal Ions with Ion Selectivity of a Crown Ether and Fluorescence Resonance Energy Transfer between Carbon Dots and Graphene. *Chem. Commun.* **2012**, *48*, 1284-1286.

51. Wang, R.; Wang, X.; Sun, Y. One-step Synthesis of Self-doped Carbon Dots with Highly Photoluminescence as Multifunctional Biosensors for Detection of Iron Ions and pH. *Sens. Actuators, B* **2017**, *241*, 73-79.

52. Zhu, A.; Qu, Q.; Shao, X.; Kong, B.; Tian, Y. Carbon-Dot-Based Dual-Emission Nanohybrid Produces a Ratiometric Fluorescent Sensor for In Vivo Imaging of Cellular Copper Ions. *Angew. Chem. Int. Ed.* **2012**, *51*, 7185-7189.

53. Tang, Z.; Lin, Z.; Li, G.; Hu, Y. Amino Nitrogen Quantum Dots-Based Nanoprobe for Fluorescence Detection and Imaging of Cysteine in Biological Samples. *Anal. Chem.* **2017**, *89*, 4238-4245.

54. Naik, V.; Zantye, P.; Gunjal, D.; Gore, A.; Anbhule, P.; Kowshik, M.; Bhosale, S. V.; Kolekar, G. Nitrogen-Doped Carbon Dots via Hydrothermal Synthesis: Naked Eye Fluorescent Sensor for Dopamine and Used for Multicolor Cell Imaging. *ACS Appl. Bio Mater.***2019**, *2*, 2069-2077.

55. Zheng, M.; Xie, Z.; Qu, D.; Li, D.; Du, P.; Jing, X.; Sun, Z. On−Off−On Fluorescent Carbon Dot Nanosensor for Recognition of Chromium(VI) and Ascorbic Acid Based on the Inner Filter Effect. *ACS Appl. Mater. Interfaces* **2013**, *5*, 13242-13247.

56. Wang, Y.; Wang, Z.; Rui, Y.; Li, M. Horseradish Peroxidase Immobilization on Carbon Nanodots/CoFe Layered Double Hydroxides: Direct Electrochemistry and Hydrogen Peroxide Sensing. *Biosens. Bioelectron.* **2015**, *64*, 57-62.

57. Zheng, M.; Liu, S.; Li, J.; Qu, D.; Zhao, H.; Guan, X.; Hu, X.; Xie, Z.; Jing, X.; Sun, Z. Integrating Oxaliplatin with Highly Luminescent Carbon Dots: an Unprecedented Theranostic Agent for Personalized Medicine. *Adv. Mater.* **2014**, *26*, 3554-3560.

58. Lai, C.-W.; Hsiao, Y.-H.; Peng, Y.-K.; Chou, P.-T. Facile Synthesis of Highly Emissive Carbon Dots from Pyrolysis of Glycerol; Gram Scale Production of Carbon Dots/mSiO2 for Cell Imaging and Drug Release. *J. Mater. Chem.* **2012**, *22*, 14403-14409.

59. Mewada, A.; Pandey, S.; Thakur, M.; Jadhav, D.; Sharon, M. Swarming Carbon Dots For Folic Acid Mediated Delivery of Doxorubicin and Biological Imaging. *J. Mater. Chem. B* **2014**, *2*, 698-705.

60. Tang, J.; Kong, B.; Wu, H.; Xu, M.; Wang, Y.; Wang, Y.; Zhao, D.; Zheng, G. Carbon Nanodots Featuring Efficient FRET for Real-Time Monitoring of Drug Delivery and Two-Photon Imaging. *Adv. Mater.* **2013**, *25*, 6569-6574.

61. Zhang, M.; Zhao, X.; Fang, Z.; Niu, Y.; Lou, J.; Wu, Y.; Zou, S.; Xia, S.; Sun, M.; Du, F. Fabrication Of HA/PEI-Functionalized Carbon Dots for Tumor Targeting, Intracellular Imaging and Gene Delivery. *RSC Adv.* **2017**, *7*, 3369-3375.

62. Zheng, M.; Ruan, S.; Liu, S.; Sun, T.; Qu, D.; Zhao, H.; Xie, Z.; Gao, H.; Jing, X.; Sun, Z. Self-Targeting Fluorescent Carbon Dots for Diagnosis of Brain Cancer Cells. *ACS Nano* **2015**, *9*, 11455-11461.

63. Qian, Z.; Shan, X.; Chai, L.; Ma, J.; Chen, J.; Feng, H. Si-Doped Carbon Quantum Dots: A Facile and General Preparation Strategy, Bioimaging Application, and Multifunctional Sensor. *ACS Appl. Mater. Interfaces* **2014**, *6*, 6797-6805.

64. Sk, M. P.; Chattopadhyay, A. Induction Coil Heater Prepared Highly Fluorescent Carbon Dots as Invisible Ink and Explosive Sensor. *RSC Adv.* **2014**, *4*, 31994-31999.

65. Cayuela, A.; Soriano, M. L.; Valcarcel, M. Strong Luminescence of Carbon Dots Induced by Acetone Passivation: Efficient Sensor for a Rapid Analysis of Two Different Pollutants. *Anal. Chim. Acta* **2013**, *804*, 246-251.

66. Yang, X.; Luo, Y.; Zhu, S.; Feng, Y.; Zhuo, Y.; Dou, Y. One-Pot Synthesis of High Fluorescent Carbon Nanoparticles and their Applications as Probes for Detection of Tetracyclines. *Biosens. Bioelectron.* **2014,** *56*, 6-11.

67. Xiao, D.; Yuan, D.; He, H.; Gao, M. Microwave Assisted One-Step Green Synthesis of Fluorescent Carbon Nanoparticles from Ionic Liquids and their Application as Novel Fluorescence Probe for Quercetin Determination. *J. Lumin.* **2013**, *140*, 120-125.

68. Niu, J.; Gao, H. Synthesis and Drug Detection Performance of Nitrogen-Doped Carbon Dots. *J. Lumin.* **2014**, *149*, 159-162.

69. Yuan, F.; Wang, Z.; Li, X.; Li, Y.; Tan, Z.; Fan, L.; Yang, S. Bright Multicolor Bandgap Fluorescent Carbon Quantum Dots for Electroluminescent Light-Emitting Diodes. *Adv. Mater* **2017**, *29*, 1604436.

70. Jia, H.; Wang, Z.; Yuan, T.; Yuan, F.; Li, X.; Li, Y.; Tan, Z. a.; Fan, L.; Yang, S. Electroluminescent Warm White Light-Emitting Diodes Based on Passivation Enabled Bright Red Bandgap Emission Carbon Quantum Dots. *Adv. Sci.* **2019**, 1900397. DOI: 10.1002/advs.201900397.

71. Yuan, B.; Xie, Z.; Chen, P.; Zhou, S. Highly Efficient Carbon Dots and their Nanohybrids for Trichromatic White LEDs. *J. Mater. Chem. C* **2018,** *6* (22), 5957-5963.

72. Yuan, F.; Yuan, T.; Sui, L.; Wang, Z.; Xi, Z.; Li, Y.; Li, X.; Fan, L.; Tan, Z.; Chen, A.; Jin, M.; Yang, S. Engineering Triangular Carbon Quantum Dots with Unprecedented Narrow Bandwidth Emission for Multicolored LEDs. *Nat. Commun.* **2018,** *9* , 2249. DOI: 10.1038/s41467-018-04635-5.

73. Miao, X.; Qu, D.; Yang, D.; Nie, B.; Zhao, Y.; Fan, H.; Sun, Z. Synthesis of Carbon Dots with Multiple Color Emission by Controlled Graphitization and Surface Functionalization. *Adv. Mater.* **2018**, *30*, 1704740.

74. Xu, J.; Miao, Y.; Zheng, J.; Yang, Y.; Liu, X. Ultrahigh Brightness Carbon Dot-Based Blue Electroluminescent LEDs by Host-Guest Energy Transfer Emission Mechanism. *Adv. Optical Mater.* **2018**, *6*, 1800181.

75. Wang, H.; Sun, C.; Chen, X.; Zhang, Y.; Colvin, V. L.; Rice, Q.; Seo, J.; Feng, S.; Wang, S.; Yu, W. W. Excitation Wavelength Independent Visible Color Emission of Carbon Dots. *Nanoscale* **2017**, *9*, 1909-1915.

76. Xie, C.; Nie, B.; Zeng, L.; Liang, F.-X.; Wang, M.-Z.; Luo, L.; Feng, M.; Yu, Y.; Wu, C.-Y.; Wu, Y.; Yu, S.-H. Core–Shell Heterojunction of Silicon Nanowire Arrays and Carbon Quantum Dots for Photovoltaic Devices and Self-Driven Photodetectors. *ACS Nano* **2014**, *8*, 4015-4022.

77. Sahatiya, P.; Jones, S. S.; Badhulika, S. 2D MoS_2-Carbon Quantum Dot Hybrid Based Large Area, Flexible UV–Vis–NIR Photodetector on Paper Substrate. *Appl. Mater. Today* **2018**, *10*, 106-114.

78. Sk, M.P.; Jana, C. K.; Chattopadhyay, A. A Gold-Carbon Nanoparticle Composite as an Efficient Catalyst for Homocoupling Reaction. *Chem. Commun.* **2013**, *49*, 8235-8237.

79. Li, H.; Liu, R.; Lian, S.; Liu, Y.; Huang, H.; Kang, Z. Near-Infrared Light Controlled Photocatalytic Activity of Carbon Quantum Dots for Highly Selective Oxidation Reaction. *Nanoscale* **2013**, *5*, 3289-3297.

80. Li, H.; Liu, R.; Kong, W.; Liu, J.; Liu, Y.; Zhou, L.; Zhang, X.; Lee, S. T.; Kang, Z. Carbon Quantum Dots with Photo-Generated Proton Property as Efficient Visible Light Controlled Acid Catalyst. *Nanoscale* **2014**, *6*, 867-873.

81. Jiang, X.-H.; Wang, L.-C.; Yu, F.; Nie, Y.-C.; Xing, Q.-J.; Liu, X.; Pei, Y.; Zou, J.-P.; Dai, W.-L. Photodegradation of Organic Pollutants Coupled with Simultaneous Photocatalytic Evolution of Hydrogen Using Quantum-Dot-Modified g-C3N4 Catalysts under Visible-Light Irradiation. *ACS Sustainable Chem. Eng.* **2018**, *6*, 12695-12705.

82. Liu, R.; Huang, H.; Li, H.; Liu, Y.; Zhong, J.; Li, Y.; Zhang, S.; Kang, Z. Metal Nanoparticle/Carbon Quantum Dot Composite as a Photocatalyst for High-Efficiency Cyclohexane Oxidation. *ACS Catal.* **2013**, *4*, 328-336.

83. Han, X.; Han, Y.; Huang, H.; Zhang, H.; Zhang, X.; Liu, R.; Liu, Y.; Kang, Z. Synthesis of Carbon Quantum Dots/SiO_2 Porous Nanocomposites and their Catalytic ability for Photo-Enhanced Hydrocarbon Selective Oxidation. *Dalton Trans.* **2013**, *42*, 10380-10383.

84. Martindale, B. C.; Hutton, G. A.; Caputo, C. A.; Reisner, E. Solar Hydrogen Production Using Carbon Quantum Dots and a Molecular Nickel Catalyst. *J. Am. Chem. Soc.* **2015**, *137*, 6018-6025.

85. Zhu, C.; Zhai, J.; Dong, S. Bifunctional Fluorescent Carbon Nanodots: Green Synthesis via Soy Milk and Application as Metal-Free Electrocatalysts for Oxygen Reduction. *Chem. Commun.* **2012**, *48*, 9367-9369.

86. Tang, D.; Liu, J.; Wu, X.; Liu, R.; Han, X.; Han, Y.; Huang, H.; Liu, Y.; Kang, Z. Carbon Quantum Dot/NiFe Layered Double-Hydroxide Composite as a Highly Efficient Electrocatalyst for Water Oxidation. *ACS Appl. Mater. Interfaces* **2014**, *6*, 7918-7925.

87. Zhang, Y.-Q.; Ma, D.-K.; Zhang, Y.-G.; Chen, W.; Huang, S.-M. N-Doped Carbon Quantum Dots for TiO_2-Based Photocatalysts and Dye-Sensitized Solar Cells. *Nano Energy* **2013**, *2*, 545-552.

88. Ma, Y.; Zhang, H.; Zhang, Y.; Hu, R.; Jiang, M.; Zhang, R.; Lv, H.; Tian, J.; Chu, L.; Zhang, J.; Xue, Q.; Yip, H. L.; Xia, R.; Li, X.; Huang, W. Enhancing the Performance of Inverted Perovskite Solar Cells via Grain Boundary Passivation with Carbon Quantum Dots. *ACS Appl. Mater. Interfaces* **2019**, *11*, 3044-3052.

89. Dao, V.-D.; Kim, P.; Baek, S.; Larina, L. L.; Yong, K.; Ryoo, R.; Ko, S. H.; Choi, H.-S. Facile Synthesis of Carbon Dot-Au Nanoraspberries and their Application as High-Performance Counter Electrodes in Quantum Dot-Sensitized Solar Cells. *Carbon* **2016**, *96*, 139-144.

90. Briscoe, J.; Marinovic, A.; Sevilla, M.; Dunn, S.; Titirici, M. Biomass-Derived Carbon Quantum Dot Sensitizers for Solid-State Nanostructured Solar Cells. *Angew. Chem. Int. Ed.* **2015**, *54*, 4463-4468.

91. Wang, Y.; Yan, L.; Ji, G.; Wang, C.; Gu, H.; Luo, Q.; Chen, Q.; Chen, L.; Yang, Y.; Ma, C. Q.; Liu, X. Synthesis of N,S-Doped Carbon Quantum Dots for Use in Organic Solar Cells as the ZnO Modifier To Eliminate the Light-Soaking Effect. *ACS Appl. Mater. Interfaces* **2019**, *11*, 2243-2253.

92. Zhang, R.; Zhao, M.; Wang, Z.; Wang, Z.; Zhao, B.; Miao, Y.; Zhou, Y.; Wang, H.; Hao, Y.; Chen, G.; Zhu, F. Solution-Processable ZnO/Carbon Quantum Dots Electron Extraction Layer for Highly Efficient Polymer Solar Cells. *ACS Appl. Mater. Interfaces* **2018**, *10*, 4895-4903.

Chapter 2

Boron Doped Carbon Dots with Unusually High Photoluminescence Quantum Yield for Ratiometric Intracellular pH Sensing

Herein we report that boron doping in carbon dots results in increased photoluminescence (PL) quantum yield, which could be used for ratiometric intracellular pH sensing in cancer cell lines. Using a mixture of citric acid monohydrate, thiourea, and boric acid, microwave-assisted synthesis of boron doped blue emitting carbon dots (B-Cdots) with an average size of 3.5 ± 1.0 nm was achieved. For B-Cdots, the maximum quantum yield (QY) was observed to be 25.8% (11.1% (w/w) H_3BO_3 input concentration), whereas, the same was calculated to be 16.9% and 11.4% for Cdots (synthesized from citric acid monohydrate and thiourea only) and P-Cdots (phosphorus doped carbon dots; synthesized using citric acid monohydrate, thiourea and phosphoric acid) (11.1% (w/w) H_3PO_4 input concentration), respectively. The observed luminescence efficiencies as obtained from steady state and time-resolved photoluminescence measurements suggest an alternative emission mechanism due to boron/phosphorus doping in carbon dots. We furthermore demonstrated facile composite formation using B-Cdots and another carbon dots with orange emission in presence of polyvinyl alcohol (PVA), resulting in white light emission (0.31, 0.32; λ_{ex} 380 nm). B-Cdots were preferred for composite preparation due to their measured high QY and maximum photo stability as compared to other two Cdot systems. The white light emitting composite enabled ratiometric pH sensing in the aqueous medium and showed favorable uptake properties by cancerous cells for intracellular pH sensing as well.

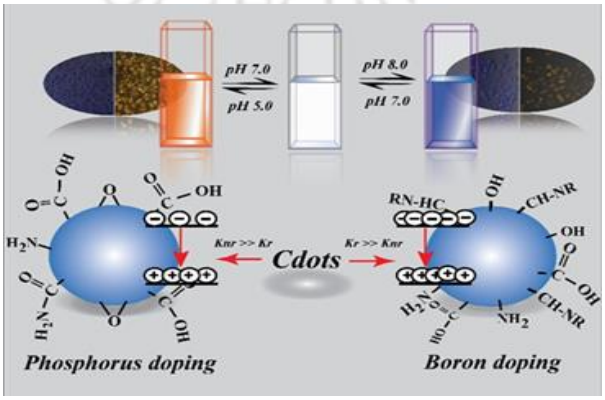

**[ChemPhysChem 2019, 20, 1018–1027] - Reproduced by permission from John Wiley and Sons.*

2.1 Experimental Section

2.1.1 Materials. Citric acid monohydrate (99 %, 210.14 g mol^{-1}), boric acid (61.83 g mol^{-1}), and ortho phosphoric acid (88 %, 98 g mol^{-1}) were purchased from Merck, India. Thiourea (99 %, 76.12 g mol^{-1}) was procured from Sigma-Aldrich. Also, poly vinyl alcohol (PVA), 1, 4-benzoquinone (98 %, 108.09 g mol^{-1}), ortho phenylenediamine (98 %, 108.14 g mol^{-1}) and dialysis membrane (benzoylated) were purchased from Sigma-Aldrich. All materials were used as procured without any further purification. Elix grade water from a MilliQ purification system was used for the experiments.

2.1.2 Synthesis of Carbon dots. Boron doped carbon dots i.e., B-Cdots were synthesized from citric acid monohydrate and thiourea in presence of boric acid. Typically, 210 mg (1 millimole) of citric acid monohydrate and 210 mg (2.76 millimole) of thiourea were dissolved first in 10 mL of water in a glass beaker. After that, the required amount of boric acid (such as 15.0 mg, 30.0 mg, 52.5 mg, 157.0 mg, 210.0 mg or 262.0 mg corresponding to 3.4%, 6.6%, 11.1 %, 27.2 %, 33.3% or 38.4% w/w respectively) was added to the reaction mixture followed by ultra-sonication up to 5 min. The resultant reaction mixture was then allowed for microwave treatment (600 W, make: Samsung; model: MC28H5023AK) for 5 min. After microwave treatment, the as-obtained product was cooled to room temperature and then was dissolved in 10 mL of water. Next, the dark brown solution was centrifuged at 15,000 rpm for 25 min (refrigerated centrifuge, SIGMA 3-30K). The collected supernatant part was then dialyzed (1 kDa dialysis membrane) for up to 12 h for further purification. Also, the powder of as-synthesized B-Cdots was collected after drying the purified dispersion at 60 ^{o}C for up to 48 h.

Similarly, to synthesize Cdots (without boron/phosphorus doping) only citric acid monohydrate (210 mg, 1 millimole) and thiourea (210 mg, 2.76 millimole) were used as the starting materials. After the completion of reaction, the obtained product was dissolved in 10 mL water followed by centrifugation at 15,000 rpm for 25 min. Finally, the collected supernatant was dialyzed for 12 h for further purification. The as-synthesized Cdots were dried at 60 ^{o}C for 48 h to get their powdered form.

Also, to synthesize phosphorus doped carbon dots i.e., P-Cdots, the required amount of phosphoric acid with successively ascending input concentrations (such as 30 µL, 90 µL, 120 µL or 150 µL corresponding to 11.1 %, 27.2%, 33.3% or 38.4% w/w respectively) was reacted with citric acid monohydrate (210 mg, 1 millimole) and thiourea (210 mg, 2.76 millimole) under microwave (600 W) irradiation for 5 min. After treatment, the obtained product was dissolved in 10 mL water followed by centrifugation at 15,000 rpm for 25 min. Finally, the collected supernatant was dialyzed for 12 h for purification. The as-synthesized P-Cdots were dried at 60 ^{o}C for 48 h to get the powdered sample.

2.1.3 Synthesis of Orange Luminescent Carbon dots (Cdots$_{orange}$). For the synthesis of Cdots$_{orange}$, 27 mg of (0.25 millimole) 1, 4-benzoquinone and 27 mg (0.25 millimole) of *ortho* phenylenediamine were dispersed well in 20 mL water through sonication up to 30 min. After that, 5 mL of *ortho* phosphoric acid was added dropwise to reaction mixture. The resultant reaction mixture was then allowed to stir under reflux condition for up to 8 h.

2.1.4 Preparation of Nanocomposite. For the synthesis of nanocomposite (Cdot/PVA), the as-obtained Cdots$_{orange}$ solution was diluted 10 times to its original concentration. Subsequently, 50 µL of the diluted Cdots$_{orange}$ solution was added to 2 mL of 20 mg/mL PVA solution and stirred well for 15 min. After that, 6 µL of B-Cdots (synthesized from 11.1 % w/w H_3BO_3 input concentration, QY 25.8%) solution with 40 times dilution was added to the final mixture and stirred for another 30 min so that carbon dots were encapsulated well inside the polymeric matrix.

2.1.5 Instruments. After synthesis, carbon dots and the composite material were characterized using field emission transmission electron microscopy (JEOL JEM-2100F FETEM) running at an accelerating voltage of 200 kV, X-ray photoelectron spectroscopy (XPS) (PHI 5000 Versa Probe II; FEI Inc.) and Fourier-transform infrared spectroscopy (Perkin Elmer spectrometer). UV-vis spectroscopy analyses were performed using Hitachi U-2900 spectrophotometer. Fluorescence spectroscopy was studied on Horiba Fluoromax-4 spectrofluorometer. Also, time resolved photo-luminescence study (TRPL) was done on Edinburgh Life-Spec-II spectrofluorometer along with 375 nm pulsed diode laser source (PDL). Corresponding analyses were

performed in FAST software. Energy dispersive X-ray (EDX) analyses were carried out in a Carl Zeiss, Sigma instrument. Zeiss LSM 880 microscope with 405 nm laser excitation source was used for confocal imaging. CIE coordinates along with CRI and CCT were calculated using the OSRAM color calculator (CIE-1931 color space).

2.1.6 Quantum Yield Calculation. Quantum yield (QY) values of carbon dots were calculated with respect to quinine sulfate in 0.1M H_2SO_4 as the standard using the following equation.

$$Q_S = Q_R \times \frac{I_S}{I_R} \times \frac{A_R}{A_S} \times \frac{\eta_S^2}{\eta_R^2} \qquad \text{equation 1.1}$$

Here, Q_S= quantum yield of the sample; Q_R = quantum yield of the reference; I_S = area under the PL curve of the sample; I_R = area under the PL curve of reference; A_R = absorbance of the reference; A_S = absorbance of the sample; η_S = refractive index of the sample solution; η_R = refractive index of reference.

QY of quinine sulphate = 0.54. Refractive index of water = 1.33.

Concentrations of the sample and the reference quinine sulphate were adjusted so that the optical densities of all the samples were 0.1±0.01 at the excitation wavelength of 360 nm.

Absorbance of quinine sulphate (A_R) = 0.098. Area under the PL curve (I_R) = 1.66×10^8 (a.u.).

Table 2.1. Quantum Yield Calculations.

Sample	Area under the PL curve (I_s) at 360 nm excitation (a.u.)	Absorbance at 360 nm (A_s)	Quantum yield (%) (Q_s)
B-Cdots	7.84×10^7	0.097	25.8
P-Cdots	3.6×10^7	0.1	11.4
Cdots	5.4×10^7	0.102	16.9

$Q_{B\text{-}Cdots}$ = [0.54 × (7.84×10^7 / 1.66×10^8) × (0.098 / 0.097) × (1.332 / 1.332)] × 100 % = 25.8 %.

$Q_{P\text{-}Cdots}$ = [0.54 × (3.6 × 10^7 / 1.66 × 10^8) × (0.098 / 0.1) × (1.332 / 1.332)] × 100 % = 11.4 %.

Q_{Cdots}= [0.54 × (5.4 × 10^7 / 1.66 × 10^8) × (0.098 / 0.102) × (1.332 / 1.332)] × 100 % = 16.9 %.

2.1.7 Cell Culture Studies. The in vitro cellular studies were carried out with HEK 293T human embryonic kidney cell lines and HeLa cervical cancer cell lines as procured from National Centre for Cell Sciences, Pune, India. The cell culture was pursued in Dulbecco's modified Eagle's medium supplemented with penicillin (50 units mL^{-1}), L-glutamine (4 mM), streptomycin (50 mg mL^{-1}) from Sigma Aldrich and fetal bovine serum (10% v/v, PAA Laboratories, Austria) in a 5% CO_2 humidified incubator at 37 °C for 24 h.

2.1.8 Cellular Uptake Studies. The cellular localization of nanocomposite was assessed using confocal microscopy in HEK 293T human embryonic kidney cell lines and HeLa cervical cancer cell lines. For confocal microscopy experiments, 1 × 10^5 HEK 293T and HeLa cells were seeded on coverslips in 35 mm culture dishes and were grown in a 5% CO_2 humidified incubator for 24 h at 37 °C. Subsequently, the cells were incubated with nanocomposite (20%, v/v) for 4 h. After washing the coverslips with phosphate buffered saline, the cell lines were fixed with 0.1% formaldehyde and 70% chilled ethanol. Next, the coverslips were mounted on glass slides with the ends sealed. Finally, the cover slips were observed under a confocal microscope at an excitation of 405 nm. HEK 293T and HeLa cells without any treatment with PFBT-BM NPs were kept as the control.

2.1.9 MTT Assay. The cell viability of HEK 293T and HeLa cells was determined through MTT [3-(4, 5-dimethylthiazol-2-yl)-2, 5-diphenyltetrazolium bromide] assay. For this, 1 × 10^5 cells/well of HEK 293T and HeLa cells were seeded in a 96-well plate and were cultured overnight at 37 °C in a 5% CO_2 humidified incubator. Subsequently, the cell lines were treated with varying concentrations of nanocomposite (such as 5 %, 15 % or 20 % (v/v), respectively) and the varying concentration of carbon dots (0 mg mL^{-1} (no carbon dots added), 0.05 mg mL^{-1}, 0.125 mg mL^{-1} or 0.15 mg mL^{-1}) for 24 h,

followed by the addition of MTT solution, which in turn was reduced to colored formazan crystals by the mitochondria of the viable cells. Finally, the absorbance of the formazan dye was measured at 570 nm, which directly relates to the number of viable cells. The percentage of cell viability was calculated using equation 2, where absorbance at 690 nm (due to the background interference) was subtracted. [1]

$$\text{Cell viability (\%)} = \frac{(\text{Abs}_{570} - \text{Abs}_{690})\ \text{of treated cells}}{(\text{Abs}_{570} - \text{Abs}_{690})\ \text{of control cells}} \times 100 \qquad \text{equation 1.2}$$

2.1.10 Intracellular pH Sensing Experiment. For intracellular pH sensing experiments, 1×10^5 HeLa cells were seeded on wells of a 96 well plate and grown in a 5% CO_2 humidified incubator for 24 h at 37 °C. Subsequently, the cells were incubated with nanocomposite 20% (v/v) for 4 h. The cells were then washed with phosphate buffered saline and were subjected to treatment with intracellular pH calibration buffer of various pH such as 4.5, 5.5, 6.5 or 7.5 for 10 min using Thermo Fisher intracellular pH calibration buffer kit. Thereafter, the cells were taken to observe under the confocal microscope at an excitation of 405 nm. Additionally, a separate set of experiments was performed where the HeLa and HEK cells were treated with the composite in culture media with pH adjusted to approximately 4.0 and 7.0. Next, the treated cells were fixed in 0.1% formaldehyde and 70% chilled ethanol. The cover slips were mounted onto glass slides and sealed. The samples were then observed using confocal microscopy.

2.2 Results and Discussion

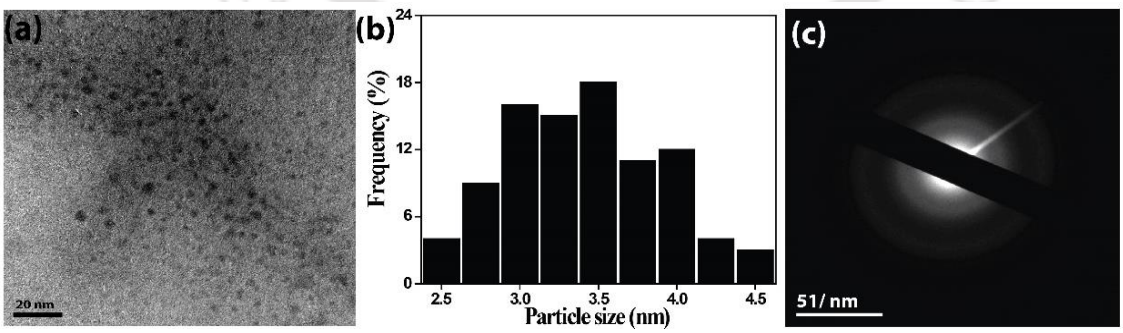

Figure 2.1. (a) TEM image of B-Cdots. (b) Particle size distribution of B-Cdots. Average calculated size was 3.5±1.0 nm. The distribution was calculated using several TEM images (with 100 particles). (c) Result corresponding to SAED study revealing amorphous nature of the as-synthesized B-Cdots.

Field emission transmission electron microscopy (FETEM) measurements (Figure 2.1.a) of B-Cdots revealed formation of well separated spherical particles with average size of 3.5±1.0 nm (Figure 2.1.b). Further, the selected area electron diffraction (SAED) study confirmed amorphous nature of the as-synthesized B-Cdots (Figure 2.1.c).

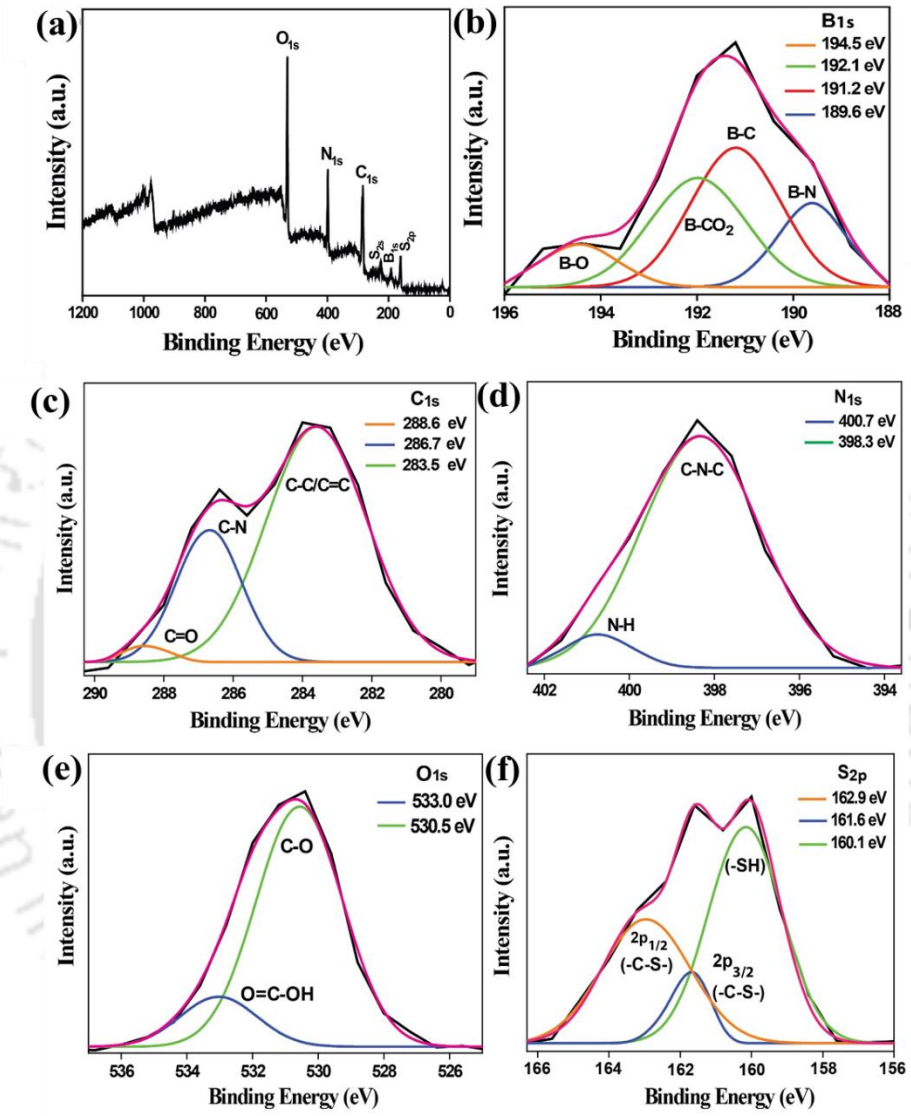

Figure 2.2. (a) XPS results for B-Cdots (H_3BO_3, 11.1 % (w/w)) (full range) showing the presence of C, N, O, S and B. (b) Deconvoluted XPS peaks at 194.5 eV, 192.1 eV, 191.2 eV and 189.6 eV for B_{1s} in B-Cdots, which correspond to B-O, B-CO_2, B-C and B-N bonds, respectively. (c-f) Deconvoluted peaks for C_{1s}, N_{1s}, O_{1s} and S_{2p} signals.

X-ray photoelectron spectroscopy (XPS) measurements revealed that B-Cdots consisted of a sharp peak for B_{1s} signal along with C_{1s}, N_{1s}, O_{1s} and S_{2p} peaks (Figure 2.2.a). High resolution B_{1s} signal could be deconvoluted into four components owing to B-O (194.5 eV), B-CO_2 (192.1 eV), B-C (191.2 eV) and B-N (189.6 eV) bonds present

in B-Cdots (Figure 2.2.b).[2] Other signals corresponding to C_{1s}, N_{1s}, O_{1s} and S_{2p}, observed for B-Cdots, were deconvoluted and are presented with details analysis result in the Figure 2.2.c-f.

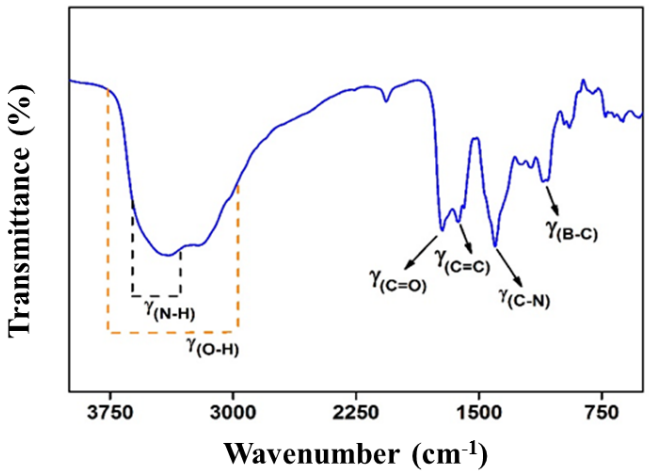

Figure 2.3. Fourier transform infrared (FTIR) spectrum of B-Cdots.

Fourier transform infrared (FTIR) spectroscopy analysis revealed the presence of broad peaks due to O-H and N-H groups (Figure 2.3). Additionally, sharp peaks, appearing at 1726 cm^{-1} and 1616 cm^{-1} owing to C=O and C=C bond stretching, respectively.[3] Strong signals were observed at 1400 cm^{-1} and 1110 cm^{-1} as well, corresponding to C-N and B-C stretching vibrations respectively, in the as-synthesized carbon nanostructure. Also, relatively weaker peaks appearing from 950 to 730 cm^{-1} could be due to symmetric stretching vibration of B-O bond in BO_3 and/or BO_4 units, being present in B-Cdots.[4]

Following this, we studied the optical properties of the B-Cdots in aqueous medium. UV-vis spectrum of B-Cdots (Figure 2.4.a) consisted of a broad absorption band at ~ 340 nm, which is related to n-π* transitions in the carbon nanostructure. Further, the absorption band appearing ~ 276 nm is assigned to π -π* transition.[5] Photoluminescence (PL) spectra unveiled excitation dependent tunability in the B-Cdot emission (Figure 2.4.b). Calculated fluorescence quantum yield (QY) was found to be 25.8 % at the excitation wavelength of 360 nm and emission wavelength of 450 nm.

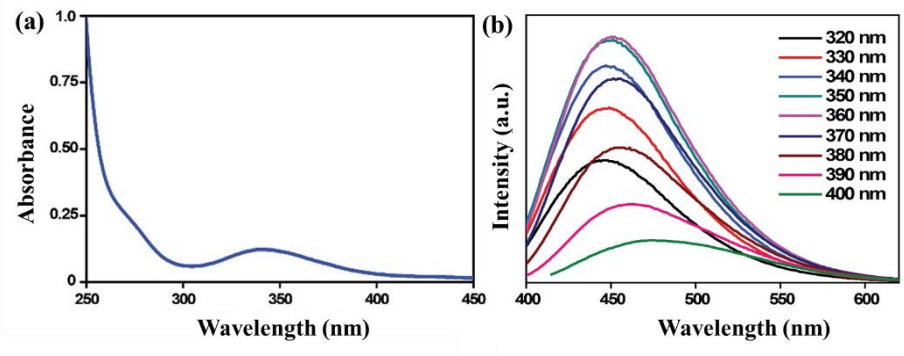

Figure 2.4. (a) UV-vis absorption spectra of B-Cdots. (b) Emission spectra of B-Cdots.

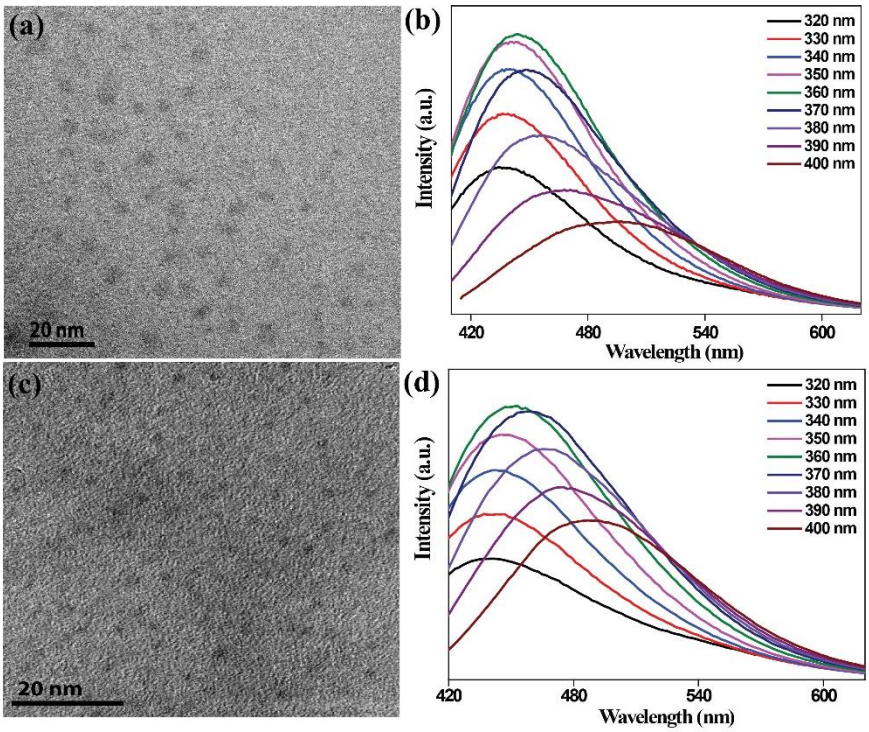

Figure 2.5. (a) FETEM image and (b) excitation dependent tunable emission spectra of Cdots. (c) FETEM image and (d) emission spectra of the P-Cdots with excitation dependent tenability.

In order to have detailed insight on the effect of introducing boron into the carbon nano structure and corresponding photo physical properties, we further synthesized carbon dots using only citric acid monohydrate and thiourea (termed as Cdots here) by following the same method. After synthesis, Cdots were characterized using FETEM analysis and photoluminescence studies (Figure 2.5.a, b). Figure 2.5.b demonstrates excitation dependent emission of Cdots. The calculated luminescence QY for the same was found to be 16.9% at 360 nm excitation wavelength, which was

considerably less as compared to boron doped carbon dots (B-Cdots). Notably, when we further doped phosphorus (instead of boron) into the same carbon dot system by adding phosphoric acid (11.1 % H_3PO_4 (w/w)) as the phosphorus source during reaction between citric acid monohydrate and thiourea, under similar reaction conditions, we observed considerable loss in the luminescence QY in the resultant carbon dot system (P-Cdots). The calculated photoluminescence QY for P-Cdots was found to be 11.4% at 360 nm excitation wavelength. FETEM image and fluorescence spectra of P-Cdots are represented in Figure 2.5.c and d as well.

Literature reports suggest that introduction hetero atom like phosphorus in carbon based nanostructure assists in improving luminescence efficiency.[6] However, during present study an opposite trend in photoluminescence property was observed for carbon dot system. Interestingly, after introduction of boron into the Cdots, a significant increase in the luminescence quantum yield was observed, whereas continuous decrease was monitored for the same in case of phosphorus doping.

Next, we performed time resolved photoluminescence study (TRPL) in order to understand the effect of introduction of boron/phosphorus on the photophysical properties of the as- synthesized carbon dot systems (Figure 2.6.b).

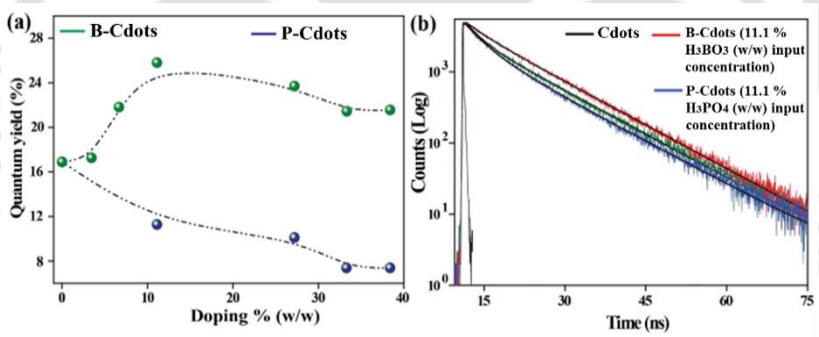

Figure 2.6. (a) Quantum yield study of B-Cdots synthesized from increasing H_3BO_3 input concentrations (such as 3.4%, 6.6%, 11.1 %, 27.2%, 33.3% or 38.4% w/w, respectively) and also of P-Cdots in presence of varying H_3PO_4 input concentrations (such as 11.1 %, 27.2%, 33.3% or 38.4% w/w, respectively). (b) Time resolved photoluminescence spectra of Cdots, B-Cdots (11.1 % H_3BO_3 input concentration) and P-Cdots (11.1 % H_3PO_4 input concentration), recorded at 375 nm excitation and 450 nm emission wavelengths.

Analyses were done using a 375 nm pulsed diode laser source at the emission wavelength of 450 nm. For all the three as-synthesized carbon dots such as Cdots (QY 16.9%), B-Cdots (with QY of 25.8% at 11.1 % (w/w) H_3BO_3 input concentration), and P-Cdots (11.1 % (w/w) H_3PO_4 with QY 11.4%) the plots followed bi-exponential decay

patterns (Table 2.2). As mentioned in Table 2.3, average luminescence lifetime τ_{av} for Cdots was found to be 10.2 ns. However, after doping boron into carbon nanostructure (i.e., in case of B-Cdots) the calculated average lifetime was found to be 10.52 ns and that for phosphorus doped carbon dots (P-Cdots) was found to be 9.5 ns. Also, corresponding radiative and non-radiative recombination rates were calculated taking all the luminescence data into consideration.

In case of Cdots, radiative decay rate constant (K_r) was found to be 1.6×10^7 sec^{-1} and that for non-radiative decay (K_{nr}) was measured to be 8.1×10^7 sec^{-1} (Table 2.3). However, after doping boron in carbon nanostructure, rate of radiative decay rate constant increased to 2.4×10^7 sec^{-1}. Also, calculated non-radiative decay rate constant (K_{nr}) for the same was found to be 7.0×10^7 sec^{-1} (Table 2.3). For P-Cdots, on the other hand, radiative decay rate constant (K_r) was calculated to be least as compared to that of B-Cdots and Cdots, which was 1.1×10^7 sec^{-1}. Besides, the non-radiative decay rate constant (K_{nr}) for P-Cdots was found to be 9.3×10^7 sec^{-1}.

Thus, aforementioned results indicated that boron doping in the carbon nanostructure not only assisted in improving the luminescence efficiency but also increased the radiative recombination rate in carbon dots. On the other hand, doping with phosphorus reduced the quantum efficiency of the carbon dots along with a considerable decrease in the radiative recombination rate of excitons.

Table 2.2. Calculated parameters, as-obtained from time resolved photoluminescence study of the three carbon dots i.e., Cdots, B-Cdots and P-Cdots.

Carbon dot Samples	λ^2	First component (α_1) (%)	First component lifetime (τ_1) (ns)	Second component (α_2) (%)	Second component lifetime (τ_2) (ns)
Cdots	1.07	13.8	2.4	86.2	10.52
B-Cdots (11.1% H_3BO_3, w/w)	1.01	6.0	2.9	94.0	10.66
P-Cdots (11.1% H_3PO_4, w/w)	1.09	18.2	2.4	81.8	9.94

Table 2.3. Measured quantum yield, average lifetime and corresponding radiative, non-radiative decay rate constants of the three carbon dot systems.

Carbon dot Samples	Measured quantum yield ϕ_D (%)	Calculated average lifetime τ_{av} (ns)	Radiative decay rate constant K_r (sec^{-1})	Non-radiative decay rate constant K_{nr} (sec^{-1})
Cdots	16.9 [a]	10.2 [d]	1.6×10^7	8.1×10^7
B-Cdots (11.1% H_3BO_3, w/w)	25.8 [b]	10.52 [e]	2.4×10^7	7.0×10^7
P-Cdots (11.1% H_3PO_4, w/w)	11.4 [c]	9.5 [f]	1.1×10^7	9.3×10^7

[a] ± 2.7 %. [b] ±1.2 %. [c] ±1.3 %. [d] ± 0.2 ns. [e] ± 0.04 ns. [f] ± 0.2 ns

The photoluminescence characteristics of carbon nanomaterials are understood to have two origins: one is established on the basis of size of the particles and the other is correlated to the defect state emission.[7] Notably, the quantum size effect, which typically originates due to graphitized carbon core, is known to be responsible for intrinsic emission.[8] On the other hand, the defect state emission, also known as trap state emission, originates due to various surface functional groups attached to the carbon core.[9]

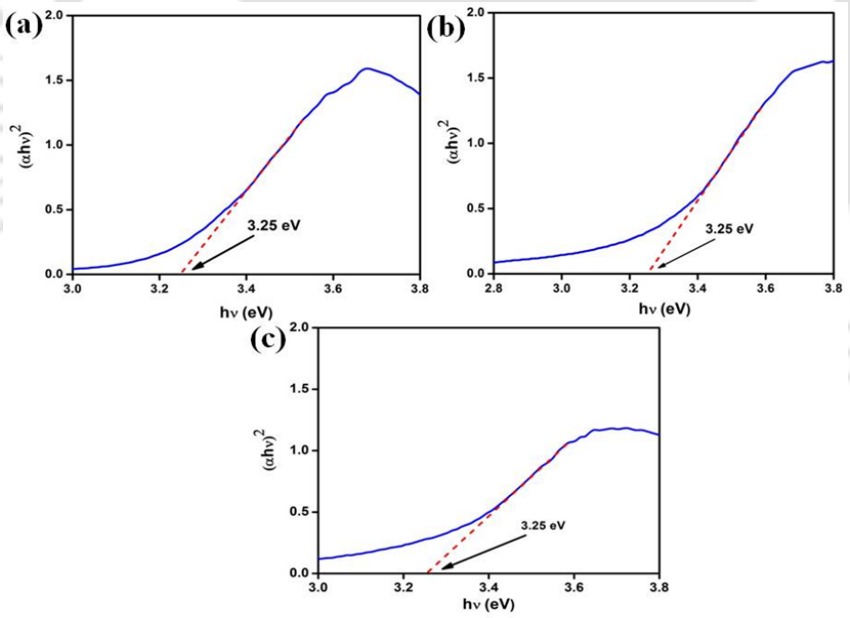

Figure 2.7. Tauc plot corresponding to optical band gap in B-Cdots (a), Cdots (b) and P-Cdots (c).

Figure 2.7.a, b and c represent Tauc plots of the three as-synthesized carbon dots suggesting identical band gap (3.25 eV) between the valence band and conduction band. Therefore, the emission mechanism based on quantum size effect can be discounted in all the three carbon dot systems. Besides, as can be found from emission

lifetime decay analyses, carbon dots exhibited bi-exponential decay pattern, resulting in two distinct lifetime components τ_1 and τ_2. The faster component τ_1 corresponds to the intrinsic emission, arising from core structure in carbon dots while the slower component τ_2 is assigned to the defect state emission.[10] As presented in Table 2.2, the fractional contribution corresponding to slower component i.e., α_2 (due to defect states) was found to be maximum in case of all the three carbon dots (i.e., B-Cdots (α_2 = 94 %); Cdots (α_2 = 86.2%); P-Cdots (α_2 = 81.8%)). The aforementioned results suggest that photoluminescence properties in all the three systems here were dominated by surface defect emissions. On the other hand, boron is a powerful reducing element.[11] Thus, doping with boron in presence of boric acid might have resulted in the reduction of the surface functional groups mostly to -CONHR, -CHNR which facilitates radiative recombination of excitons.[12] Microwave treatment in presence of phosphoric acid (resulting doping of phosphorus in carbon nano structure), on the other hand, assists in rapid high temperature carbonization along with oxidation to the surface functional groups (mostly in to carbonyl, epoxy, -COOH groups) which allows non-radiative recombination of the excitons in P-Cdot system. [12] Furthermore, energy dispersive X-ray (EDX) results indicated higher degree of surface passivation for samples doped with boron as nitrogen content considerably increased in case of B-Cdot system. As presented in Figure 2.8, B-Cdots consisted of 18.5 % nitrogen (N) while the same was found to be 13.2 % in case of P-Cdots (16.1 % in case of Cdots). Hence, it could be inferred that reduction of the surface functional groups along with higher degree of surface passivation resulted in increasing the PL efficiency of B-Cdots. In case of P-Cdots, on the contrary, surface oxidation along with lesser degree of surface passivation resulted in continuous decrease in the PL efficiency.[13] Also, it is noteworthy that presence of boric acid makes the reaction highly exothermic, which allows rapid high temperature carbonization of the starting materials. However, input concentration more than 11.1 % (w/w) resulted in incomplete carbonization of the starting materials. Therefore, under present reaction condition addition of excess boron in the reaction mixture led to further lowering in reaction efficiency along with the luminescence quantum yield of the as-obtained carbon dots.

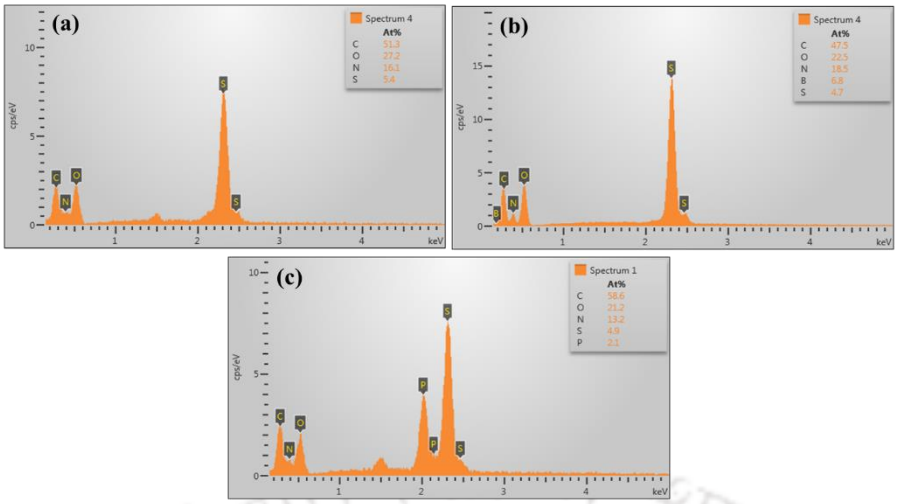

Figure 2.8. Energy dispersive X-ray (EDX) analysis results for (a) Cdots, (b) B-Cdots and (c) P-Cdots.

After that, we were interested in pursuing the development of a composite, based on carbon dots with two widely separated emission maxima. This was expected to provide pH sensitive emission changes of the component carbon dot peaks. Typically, the results would be a composite, and the emission of which would provide ratiometric pH sensing. This was achieved through incorporation of the as-synthesized blue emitting B-Cdots (with emission maximum at 450 nm) having highest luminescence quantum yield and another orange emitting carbon dots (with emission maximum at 570 nm, QY 4.4 %; Figure 2.9) in poly vinyl alcohol (PVA) matrix. The orange emitting carbon dots ($Cdots_{orange}$) were synthesized from 1, 4-benzoquinone and *ortho* phenylenediamine in presence of *ortho* phosphoric acid. The details of the synthesis procedure of the same are explained in the experimental section.

We preferred B-Cdots for this particular implementation over the other two carbon dots (i.e., Cdots and P-Cdots) due to several reasons. Firstly, B-Cdots showed maximum luminescence efficiency (H_3BO_3 input concentration 11.1 % (w/w), QY 25.8 %) as compared to Cdots (QY 16.9 %) and P-Cdots (H_3PO_4 input concentration 11.1 % (w/w), QY 11.4 %). Secondly, Figure 2.10, corresponding to the photo stability studies of all the three carbon dots (i.e., B-Cdots, Cdots and P-Cdots) for 1 h time period suggested that intensity decay of B-Cdots was considerably less in comparison with Cdots and P-Cdots under 360 nm excitation wavelength. Besides, PVA solution (20 mg/mL) was selected for the composite preparation as it helped embedding the component carbon dots homogeneously inside the polymeric matrix. This resulted in

uniform dispersion of components inside the matrix without changing their emission characteristics and also decreasing self-aggregation tendency of the particles due to coating of carbon dot surfaces with PVA. Also, PVA hydrogel is known to have good biocompatibility which could help carrying homogeneously embedded particles inside cells for biological applications as well.[14] The details of the composite (Cdot/PVA) synthesis are elaborated in the experimental section and the results of the same are included in Figure 2.11.

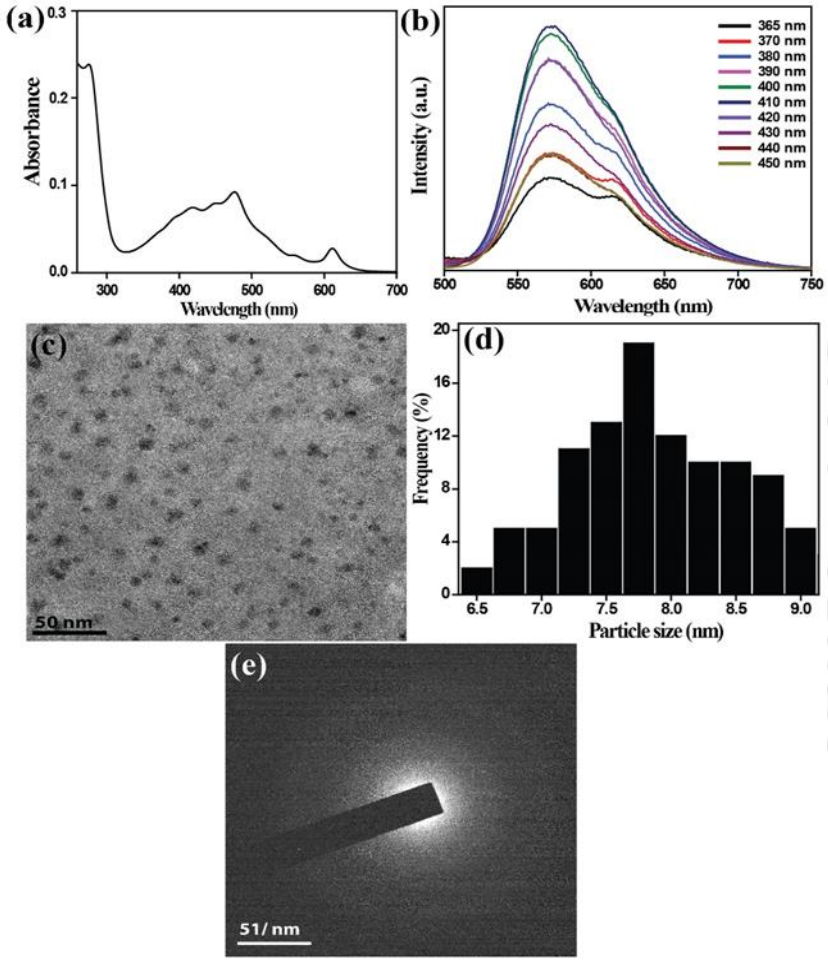

Figure 2.9. (a) UV-vis absorption spectrum of Cdots$_{orange}$. (b) Photoluminescence spectra of the as-synthesized Cdots$_{orange}$. Corresponding excitation wavelengths are mentioned in the legend. (c) FETEM image of Cdots$_{orange}$, confirming the formation of particles with average diameter of 7.75±1.25 nm (d). (e) SAED result corresponding to Cdots$_{orange}$, confirming their amorphous nature.

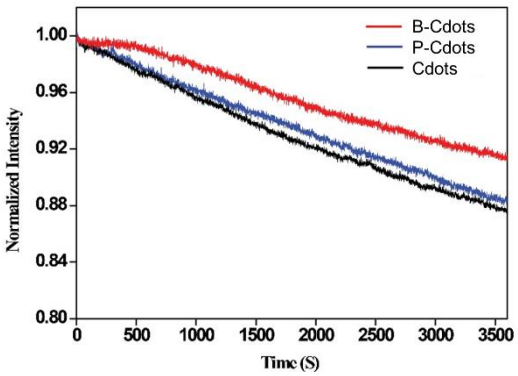

Figure 2.10. Time scan of luminescence intensity of the three as-synthesized carbon dots (i.e., B-Cdots, Cdots and P-Cdots). Observed photo degradation rate was minimum for B-Cdots compared to the other two carbon dots (i.e., Cdots and P-Cdots) over continuous irradiation with Xe lamp for 1 h time period.

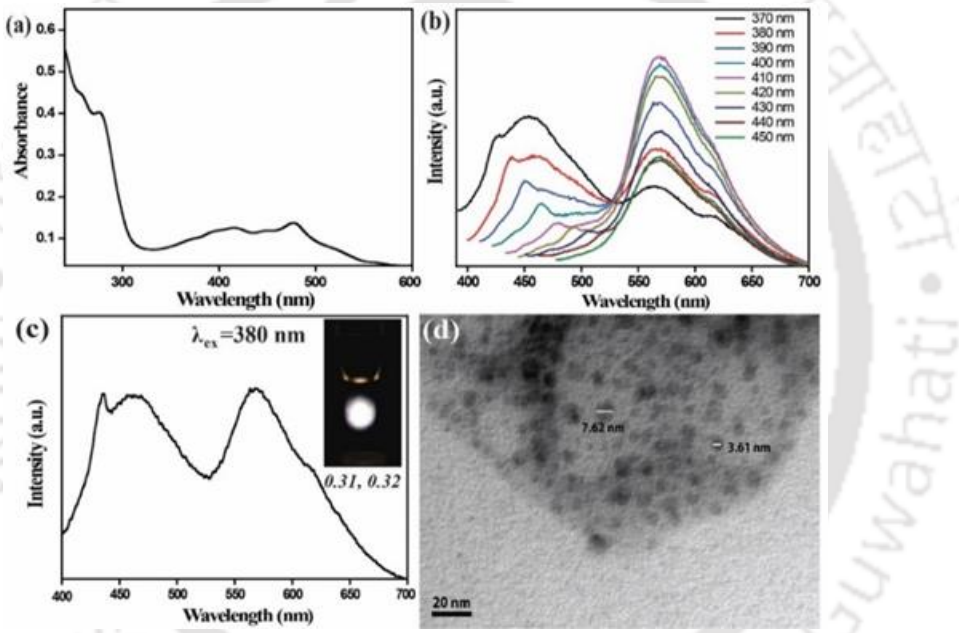

Figure 2.11. (a) UV-vis absorption spectrum of the Cdot/PVA composite. (b) Excitation dependent emission spectra of the as-synthesized composite. (c) Emission spectrum of the composite when excited with 380 nm excitation wavelength showing white light emission. Corresponding digital photograph of the composite dispersion is presented in the inset picture. (d) FETEM image of the composite nanomaterial, confirming the presence of both B-Cdots (diameter of 3.61 nm) and $Cdots_{orange}$ (diameter of 7.62 nm) inside the polymer layer.

Figure 2.11.a, b represent absorption and emission spectra of the as-synthesized nano composite (Cdot/PVA). The absorption spectrum of the composite material was found to be much similar to that of $Cdots_{orange}$ (Figure 2.9.a), due to higher loading concentration of the same as compared to B-Cdots. Strong absorption band appearing ~ 276 nm was due to π -π* transitions in the carbon dot system. Besides, the absorption

band, appearing at ~ 416 to 478 nm (due to $Cdots_{orange}$) was attributed to transitions from multiple surface groups leading to smaller electronic bandgaps in as-synthesized carbon dots (Figure 2.11.a).[15] On the other hand, the results in Figure 2.11.b indicated that emissions from two independent carbon dots could be discerned with widely separated peaks, even under same excitation. The change in intensity ratio of the peaks with the changing wavelength supported possible tuning of the emission characteristics as well. In addition, the results also showed (as is evident from Figure 2.11.c) that the intensity ratios of the contributing peaks (I_b/I_{or}, corresponding to the peaks at 450 nm and 570 nm) is nearly unity upon excitation at 380 nm wavelength. Significantly, the emission profile, shown by the Cdot/PVA nano composite was found to be very close to perfect and bright white light emission with chromaticity coordinate of 0.31, 0.32 (λ_{ex} = 380 nm); Figure 2.11.c. Figure 2.11.d corresponds to the FETEM image of the composite, confirming that both B-Cdots (3.61 nm, as assigned in Figure 2.11.d) and $Cdots_{orange}$ (diameter of 7.62 nm as measured) were embedded inside the polymer matrix after synthesis.

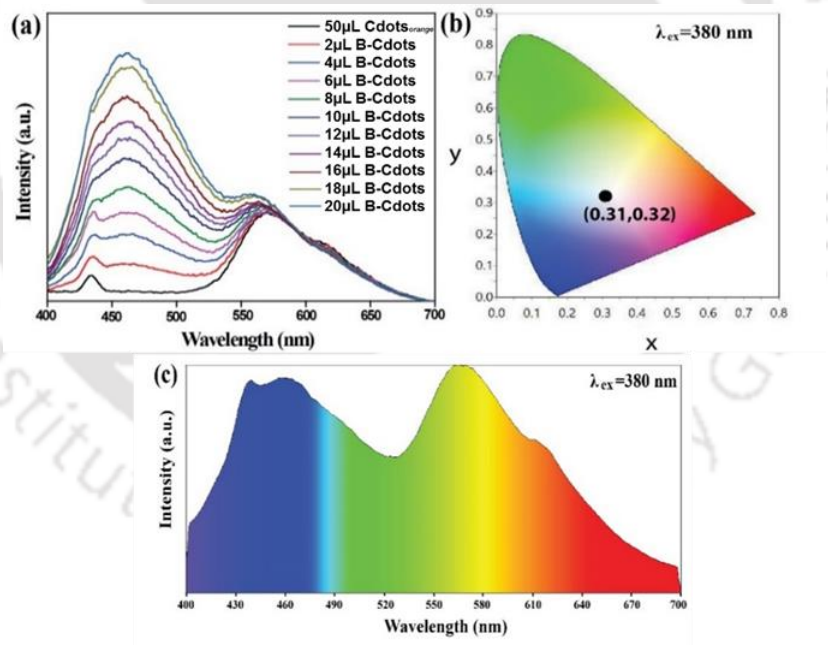

Figure 2.12. (a) Photoluminescence spectra of the Cdot/PVA nanocomposite synthesized with varying B-Cdot input concentrations. (b) CIE chromaticity diagram of the composite, synthesized from 6 µL B-Cdots and 50 µL of $Cdots_{orange}$, added to 2 mL of (20 mg/ mL) PVA solution. (c) Emission spectrum (λ_{ex} = 380 nm) corresponding to the chromaticity diagram in Figure S10b of the composite. Color rendering indices (CRI) and correlated color temperatures (CCT) were calculated to be 82 and 6300K, respectively.

The color rendering index (CRI) and correlated color temperature (CCT) of the same were calculated to be 82 and 6300K respectively (Figure 2.12.b, c). The emission characteristics of Cdot/PVA composite, synthesized with different B-Cdot loading concentrations were also studied and are represented in Figure 2.12.a.

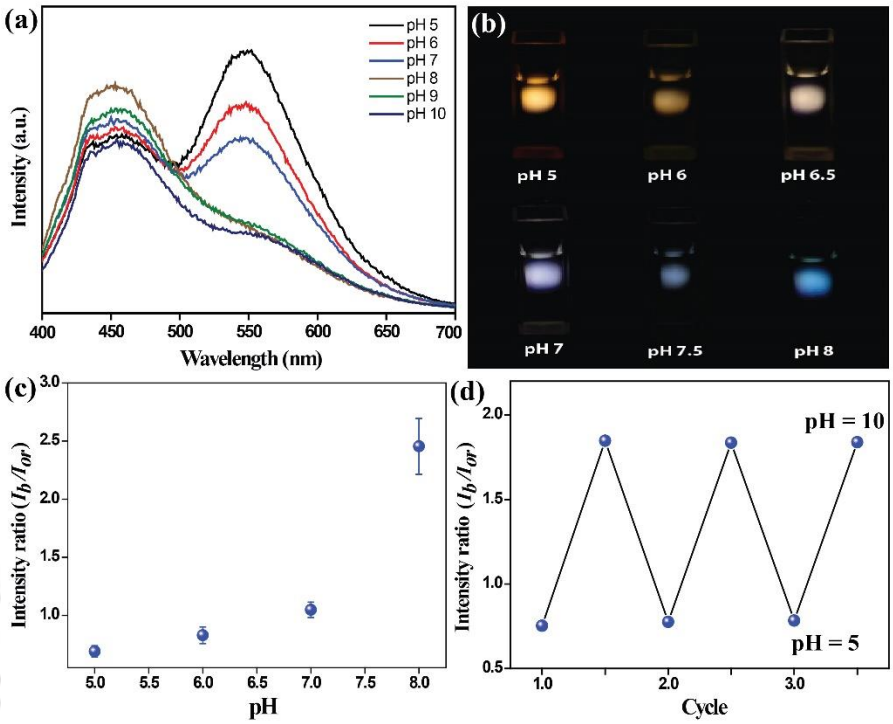

Figure 2.13. (a) pH response study of the as-synthesized Cdot/PVA composite. PL spectra of composite were recorded in 0.1 M PBS solution with varying pH conditions mentioned in the legend. (b) Digital photographs of the Cdot/PVA composite at 380 nm excitation wavelength. Distinct color change of the composite material could be monitored with changing pH (at λ_{ex} = 380 nm) of the medium. (c) Ratiometric changes in the fluorescence intensity duo of the composite (I_b/I_{or}) under varying pH conditions (λ_{ex} = 380 nm). (d) Fluorescence reversibility results of intensity ratios (I_b/I_{or}) of the composite between pH 5.0 and 10.0.

For ratiometric pH sensing study, as-synthesized Cdot/PVA composite was excited at 380 nm, where both the components in the composite exhibited similar emission intensity. Input concentration ratios of the carbon dots were same in the composite for which the spectra are reported in Figure 2.11. The pH sensing assay was carried out by monitoring the changes in intensity ratios between the two peaks (I_b/I_{or}). In this regard, pH dependent changes in emission spectra of the composite in separately prepared 0.1 M phosphate-buffered saline (PBS) of different pH is represented in Figure 2.13.a. As can be found in Figure 2.13.a, when the pH was lower, the intensity contribution from longer wavelength component was considerably high along with blue

shifting in the emission maximum (λ_{em} was shifted from 570 nm to 550 nm) and thus lowering the intensity ratio (I_b/I_{or}) value of the composite. However, with increasing pH, the intensity contribution from the blue component (I_b) was found to be predominant. Therefore, fluorescence intensity ratios i.e., I_b/I_{or} of the Cdot/PVA composite significantly increased with increasing pH between 5.0 to 10.0. Corresponding color changes of the composite nano material under 380 nm excitation source were recorded and are included in Figure 2.13.b. Intensity ratios of the composite were further calculated from pH dependent luminescence plots, which unveiled continuous increase in the intensity ratios (I_b/I_{or}) with increasing pH of the medium (Figure 2.13.c). Next, the luminescence intensity ratios of the composite were plotted for multiple cycles as well at optimum pH conditions (Figure 2.13.d), supporting reproducibility of the observed intensity ratio values of the composite over switching of the pH in the aqueous medium.

The pH dependent changes in emission characteristics of the nano composite, as presented in Figure 2.13.a, clearly substantiated that varying pH conditions can induce effective surface modification in terms of protonation-deprotonation equilibrium [16] of the surface functional groups present in carbon dot systems, and thus effecting significant change in the emission of the as-synthesized composite. It was observed that emission intensity of B-Cdots steadily increased with increasing basicity of the medium up to pH 8 followed by decrease of the same with further increase in the pH of the medium (Figure 2.13.a). $Cdots_{orange}$ on the other hand indicated the reverse trend, i.e., a continuous decrease in the luminescence intensity was observed with increasing medium pH (between pH 5 to 10). The pK_a values for B-Cdots and $Cdots_{orange}$ were calculated to be 7.3 (which corresponds to phenol ↔ phenolate equilibrium, with pK_a ranging typically between 8-10) and 6.2 (corresponding to carboxylic ↔ carboxylate equilibrium, with pK_a ranging typically between 4-5) respectively (Figure 2.14).

Further, in order to confirm interaction between B-Cdots and $Cdots_{orange}$, zeta potential (ζ) values of both the carbon dots were measured under varying pH conditions. Table 2.4 substantiates a systematic decrease in negative zeta potential values with decreasing pH of the medium for B-Cdots (ζ= -19.6 mV at pH 10; ζ = -3.4mV at pH 5). In case of $Cdots_{orange}$, on the other hand, the opposite trend was observed (i.e., ζ = 2.4 mV at pH 10; ζ = 19.1 mV at pH 5). Also, the absorption spectra

of the Cdot/PVA nano composite was recorded under varying pH conditions (Figure 2.15). Notably, the intense broad bands appearing at ~ 478 nm and ~ 448 nm (due to $Cdots_{orange}$) were significantly blue shifted at higher pH. Indeed, a single broad absorbance band was observed ~ 437 nm at pH 5, ~ 430 nm at pH 7 and ~ 421 nm at pH 10 for the nano composite material.

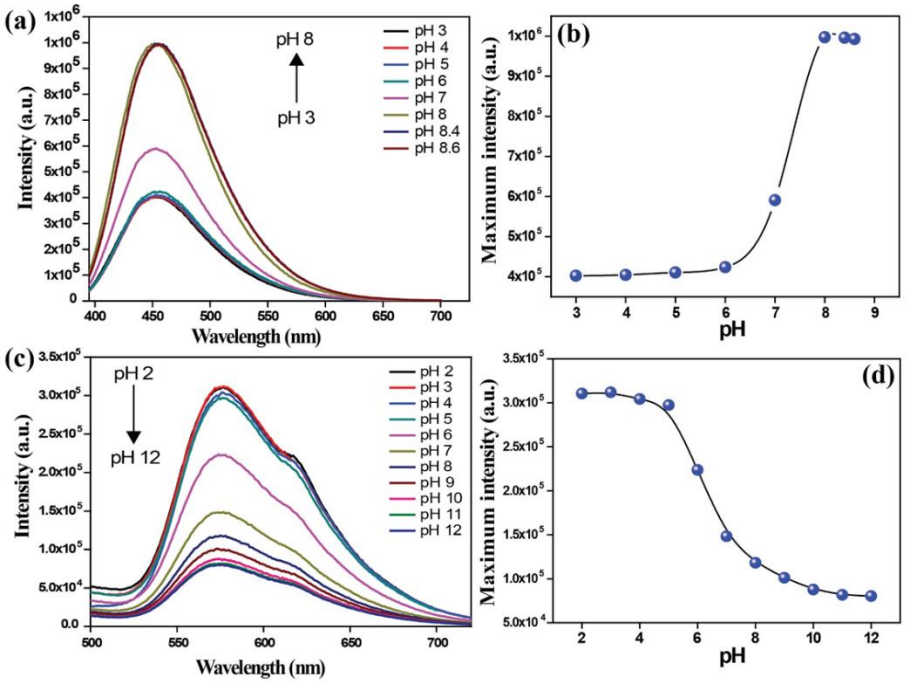

Figure 2.14. (a) Emission spectra of B-Cdots recorded at 380 nm excitation wavelength with different pH conditions such as 3.0, 4.0, 5.0, 6.0, 7.0, 8.0, 8.4 and 8.6. (b) Variation of intensity maximum with pH. For B-Cdots, the maximum intensity was observed at pH 8. From the point of inflection corresponding to the sigmoidal curve, the pK_a value for B-Cdots was measured to be 7.3. (c) Emission spectra of $Cdots_{orange}$ recorded at 380 nm excitation wavelength with different pH conditions such as 2.0, 3.0, 4.0, 5.0, 6.0, 7.0, 8.0, 9.0, 10.0, 11.0 and 12.0. The maximum emission intensity was recorded at pH 3 followed by continuous decrease in the same with change in the pH. (d) Observed sigmoidal pattern of emission intensity variation with pH. pK_a value from the curve was calculated to be 6.2.

Table 2.4. Measured zeta potential (ζ)values of B-Cdots and $Cdots_{orange}$ under the varying pH conditions.

pH of the carbon dots medium	Zeta potential (ζ) (B-Cdot solution) (mV)	Zeta potential (ζ) ($Cdots_{orange}$ solution) (mV)
pH 10	-19.6	2.4
pH 7	-11.1	12.5
pH 5	-3.4	19.1

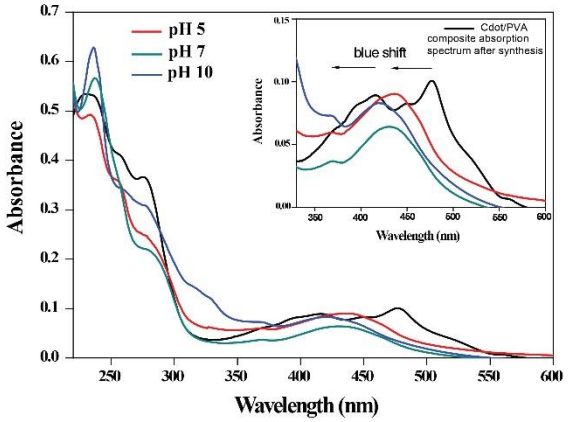

Figure 2.15. Absorption spectra of the Cdot/PVA composite under varying pH conditions such as pH 5, pH 7 and pH 10. The inset Figure consists of enlarged view of the same between 330-600 nm wavelength.

Hence, based on the experimental evidences, we conclude that the extent of variation in emission intensities of the two carbon dots differs due to different pK_a values (affecting the protonation-deprotonation equilibrium in surface functional groups with changing pH of the medium). In case of B-Cdots under acidic condition, surface functional groups get protonated and thereby the emissive sites become inactive, which leads to quenching of luminescence intensity. [17] On the other hand, under acidic condition higher degree of protonation in $Cdots_{orange}$ results in higher net surface charge, which induces strong hydrophilic properties and stability in water, effecting intense photoluminescence. [18] Besides, under varying pH conditions, strong electrostatic interaction between $Cdots_{orange}$ and B-Cdots through surface functional groups (as evident from zeta potential results and pH dependent observed blue shift in $Cdots_{orange}$ absorbance spectrum) effect new surface states (termed as E_2 here) with enhanced energy gap near the inherent E_1 energy level, which is responsible for blue shift in the emission maxima (λ_{max}) of $Cdots_{orange}$ (Scheme 2.1). Possible energy transfer between B-Cdots and $Cdots_{orange}$ (apparent from calculated Förster distance (R_0) value; R_0 = 21.78 Å and overlap integral (J_λ) = 2.02×10^{13} M^{-1} cm^{-1} nm^4, Figure 2.16) also assists in enhancing the λ_{max} intensity of $Cdots_{orange}$ (Figure 2.12.a) along with preferential radiative recombination from newly generated surface states (due to interaction with B-Cdots) in $Cdots_{orange}$. Such energy transfer is maximum under strong acidic condition because of high positive surface charge density over $Cdots_{orange}$. This might have led to enhanced energy transfer at lower pH, which resulted increased PL intensity of $Cdots_{orange}$.

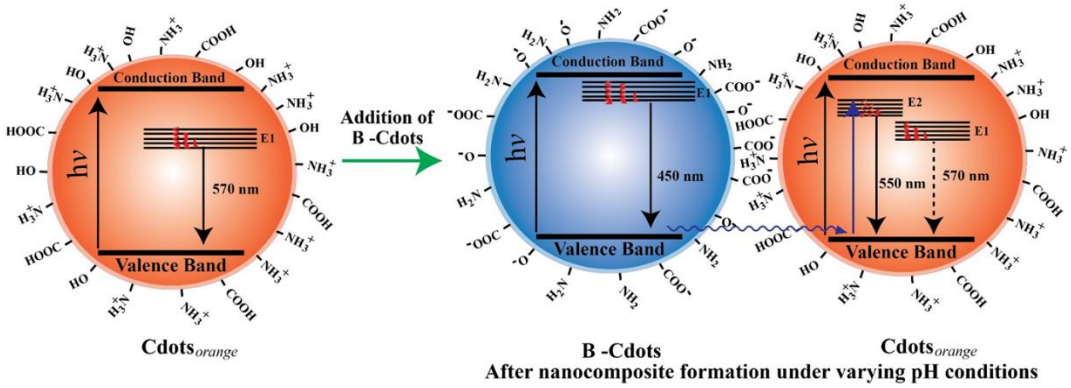

Scheme 2.1. Proposed schematic representation corresponding to the emission mechanism of $Cdots_{orange}$, followed by B-Cdots induced changes in the emission mechanism of the same after composite formation (depicting blue-shift in $Cdots_{orange}$ λ_{max}).

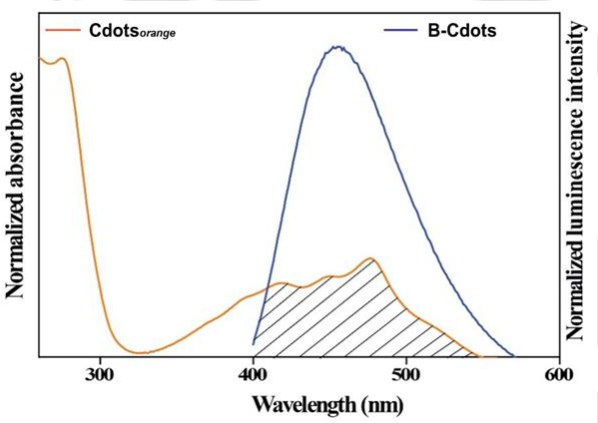

Figure 2.16. Spectral overlap between normalized B-Cdots emission spectrum and $Cdots_{orange}$ absorption spectrum (normalized). The overlap integral value (J_λ) was calculated to be 2.02×10^{13} M^{-1} cm^{-1} nm^4. The Förster distance (R_0) corresponding to interactions between the two components ($Cdots_{orange}$ and B-Cdots) was measured to be 21.78 Å, which is well in the range of 10–100 Å for Förster resonance energy transfer (FRET) to occur.

Next, we attempted to apply the newly designed optically stable Cdot/PVA nanocomposite as the nano probe for ratiometric intracellular pH sensing in cancerous cells further. First, in order to check the biocompatibility of Cdot/PVA nanocomposite, MTT [3-(4,5-dimethylthiazol-2-yl)-2,5-diphenyltetrazolium bromide] based analyses were carried out by incubating nanocomposite with human embryonic kidney (HEK 293T) cell lines and HeLa cervical cancer cell lines for up to 24 h. As represented in Figure 2.17, for concentration up to 20% (v/v) of the composite material added to the cell culture medium, 77% and 81% of the HEK 293T cells (Figure 2.17.a) and HeLa cells (Figure 2.17.b) were viable, respectively. Thus, the composite nanomaterial was found to be less toxic to the cells, and could be used further for bioimaging.

Additionally, the cell viability assay results corresponding to Cdot samples are included in Figure 2.18. Subsequently, the uptake analyses of nanocomposite were investigated in both the HeLa cell lines and HEK 293T cell lines. Interestingly, confocal laser scanning microscopy (CLSM) images, shown in Figure 2.19.a, b and c revealed efficient uptake of the Cdot/PVA composite by cancerous (HeLa) cell line only. On the other hand, no significant uptake of the same was found in HEK 293T cell lines, as represented in Figure 2.19.d, e and f. Such selectivity was possibly due to higher metabolic/growth rate of the cancer cells compared to normal cells leading to increased uptake of the Cdot/PVA composite in HeLa cells. [19] The results supported the potential of the duel emitting Cdot/PVA nano composite material for use in imaging cancer cell lines (HeLa cells in present study).

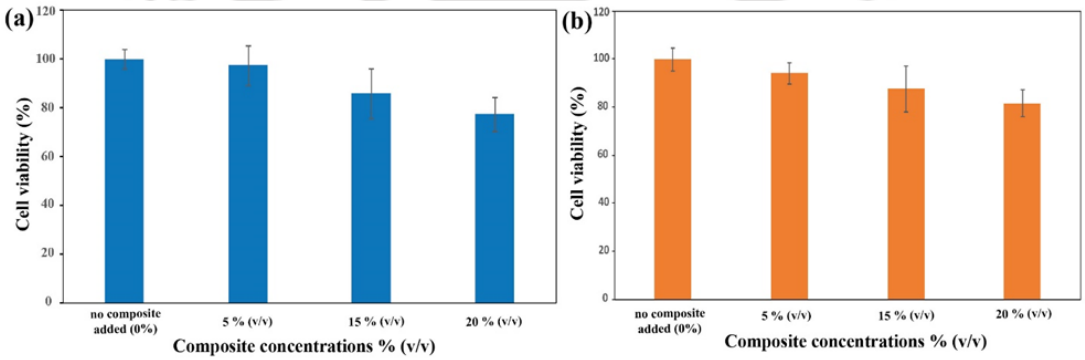

Figure 2.17. (a) MTT [3-(4,5-dimethylthiazol-2-yl)-2,5-diphenyltetrazolium bromide] based cell viability assay result of HEK 293T cells and (b) HeLa cells after 24 h treatment with varying concentrations of Cdot/PVA composite.

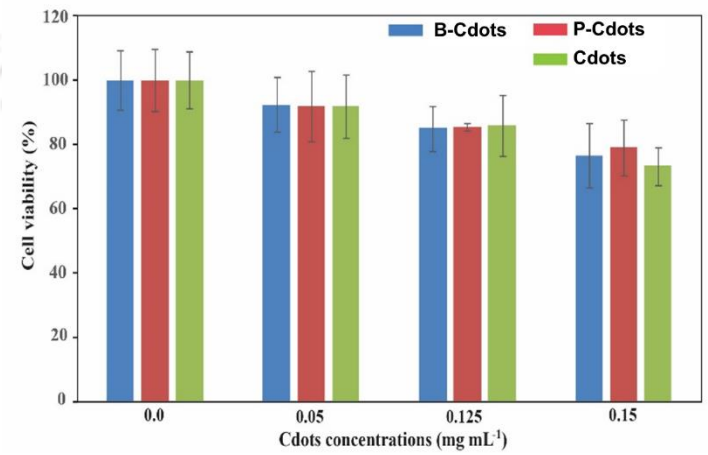

Figure 2.18. MTT based cell viability study of HEK 293T cells after 24 h treatment with varying concentrations of B-Cdots, P-Cdots and Cdots.

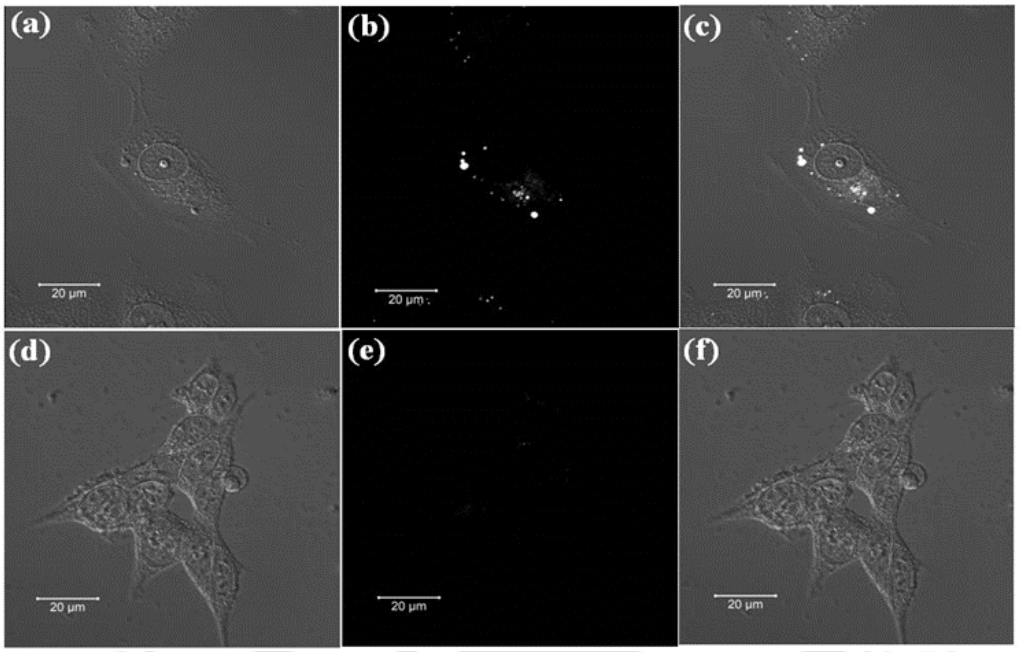

Figure 2.19. Confocal laser scanning microscopy (CLSM) images recorded for cellular uptake study of the Cdot/PVA composite. (a) Bright field image, (b) composite fluorescence image and (c) merged fluorescence image of HeLa cells, observed after the treatment with composite up to 4 h. Dual emission (white color) from inside cells come due to efficient up take of the composite material by treated HeLa cells (d) Bright field image of the HEK 293T cells following treatment with composite up to 4 h. (e) Fluorescence image and (f) merged fluorescence image of the same. No discernible emission was observed from the treated HEK 293T cells (confirming poor uptake of the composite material).

For the intracellular pH sensing assay, HeLa cells were incubated first with Cdot/PVA composite for 4 h at 37 ^{o}C in cell culture medium. After that, the medium was removed and cells were washed well with PBS buffer solution followed by further treatment with pH calibration buffer solution (Thermo Fisher) of different pH such as pH 4.5, 5.5, 6.5 and 7.5 for 10 min (as per manufacturer's protocol). Details are mentioned in the experimental section. Figure 2.20.a demonstrates the CLSM images of Cdot/PVA treated HeLa cells using a 405 nm laser excitation source under varying intracellular pH conditions. As can be seen in Figure 2.20.a, with increasing intracellular pH between 4.5 to 7.5, the fluorescence intensity ratios of composite between the two channels (channel 2; blue component 420-500 nm and channel 3; orange component 540-700 nm) continuously increased (as the intensity contribution from channel 3 significantly reduced along with slight change of the same in channel 2). Next, the average fluorescence intensities in channel 2 and channel 3 were quantified using ImageJ software, and the results for the same are presented in Figure

2.20.b. As can be found in Figure 2.20.b, with increasing the intracellular pH between 4.5 to 7.5 the peak intensity ratios i.e. I_b/I_{or} of the composite material increased continuously, which was also similar to the observed trend in aqueous medium, as mentioned earlier (Figure 2.13.c). Therefore, the as-synthesized Cdot/PVA nanocomposite demonstrated crucial changes in the emission intensity ratios (Figure 2.20.a, b) of its component peaks in the pH level between 4.5 to 7.5 in treated HeLa cells and acting as nanoprobe for the determination of intra cellular pH changes in cancerous cell. Also, the results for control experiment in case of cells without treatment are included in Figure 2.21.

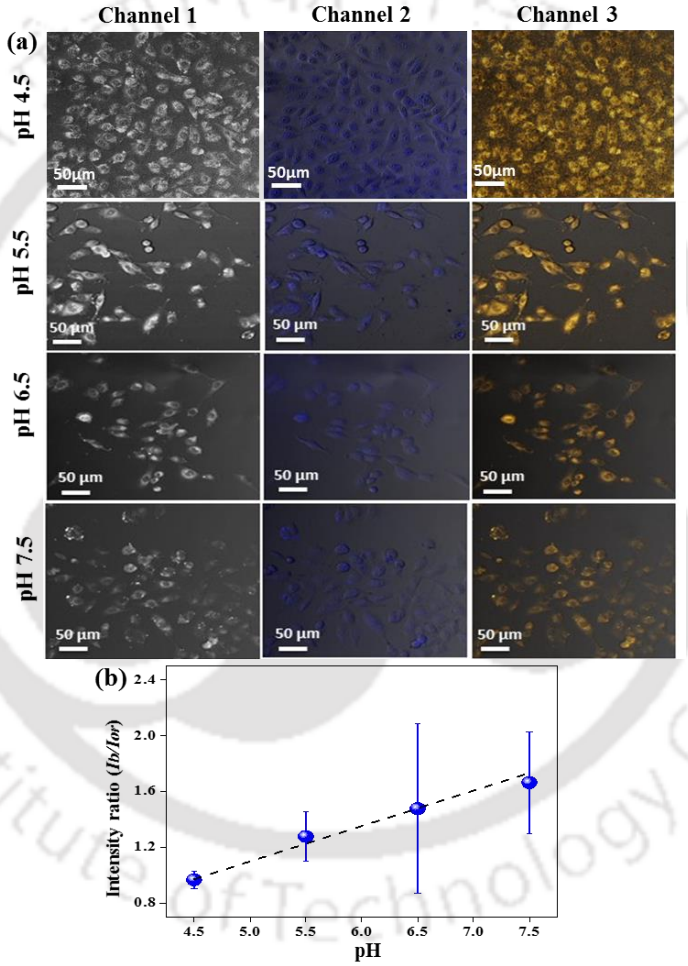

Figure 2.20. (a) Confocal microscopy images of HeLa cells labeled with Cdot/PVA composite under varying pH conditions. Cells were incubated with composite material (150 µL) first, followed by treatment with pH calibration buffer solution. During imaging, the emission wavelength in channel 1 was set between 420-700 nm at λ_{ex} = 405 nm. Also, the measuring wavelengths in channel 2 and channel 3 were set between 420-500 nm and 540-700 nm respectively. (b) Plot of intensity ratio versus varying pH for intracellular pH sensing in treated HeLa cells using Cdot/PVA nano composite.

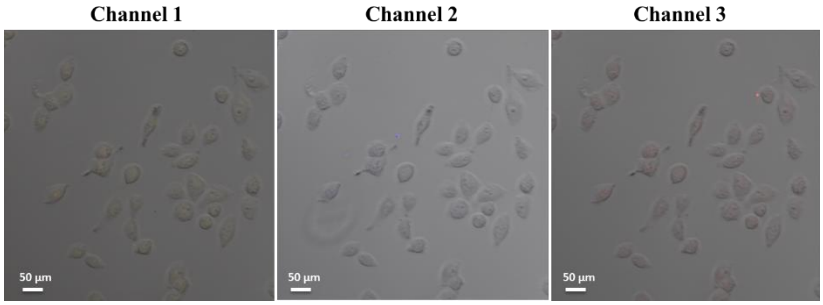

Figure 2.21. Confocal images of the control HeLa cells (in absence of composite) under 405 nm laser excitation source. Emission region of Channel 1 was set between 420-700 nm. Also, the wavelengths of emission for Channel 2 and Channel 3 were set between 420-500 nm and 540-700 nm, respectively.

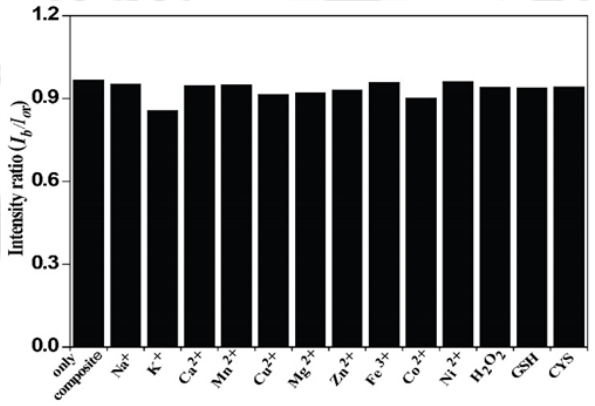

Figure 2.22. Observed fluorescence intensity ratios (I_b/I_{or}) of the Cdot/PVA composite in presence of interfering essential metal ions (1M, 5µL), ROS (5µL) species and biothiols (1M, 5µL) under the 380 nm excitation wavelength. No significant change in the intensity ratio of the composite was observed in presence of aforementioned interfering species.

Besides, for intracellular pH sensing, interference from various metal ions, that remains present in the biological system, should be avoided. Earlier reports suggest that the emission of carbon dots are typically sensitive to trace amount of metal ions (like Fe^{3+}, Cu^{2+}), [20] bio thiols (such as cysteine (Cys), [21] glutathione (GSH) [22] and reactive oxygen species (ROS), [23] which could limit their potential application in bioimaging and bio sensing. Therefore, the emission characteristics of the Cdot/PVA composite were further investigated in presence of several essential metal ions such as Na^+, K^+, Ca^{2+}, Mn^{2+}, Cu^{2+}, Mg^{2+}, Zn^{2+}, Fe^{3+}, Co^{2+}, Ni^{2+} (5 µL of 1 M solution added). Also, emission intensity ratios of the composite material were monitored in presence of biothiols (such as GSH and Cys; 5 µL of 1 M solution) and ROS species (36 % H_2O_2; 5 µL). As presented in Figure 2.22, no significant change in the intensity ratios between

two contributing peaks i.e. I_b/I_{or} was monitored during sensing assay using the as-synthesized Cdot/PVA composite and thus selectively acting as a pH sensing probe.

2.3 Conclusion. In conclusion, we demonstrate that, by introducing boron and phosphorus in carbon dots, the photoluminescence quantum yields/quantum efficiency could be increased and decreased (respectively) as opposed to established literature. In effect, detailed spectroscopic analyses such as steady state and time resolved photoluminescence measurements indicated that doping with boron helped enhancing the radiative decay rate hence increased quantum yield (maximum QY 25.8% at 11.1% (w/w) H_3BO_3 input concentration) in present carbon dot system. Whereas doping with phosphorus showed the opposite trend in optical property of the same system (11.4% QY at 11.1% (w/w) H_3PO_4 input concentration). Taking advantage of higher quantum efficiency and improved optical stability of as-synthesized boron doped carbon dots (i.e., B-Cdots), a carbon nano material based white light emitting ratiometric pH sensor was fabricated. The Cdot/PVA nano composite showed considerable change in its emission intensity ratios under varying pH conditions and thus acting as sensor for the same. Finally, pH dependent emission of the composite was successfully implemented for monitoring intracellular pH of the cancerous cells (HeLa cell). Compared to previously reported pH sensitive nano composite materials, the ease of our as-synthesized nano probe includes strong emissive nature, photo stability, low cytotoxicity and rapid cellular uptake. We believe that our as-fabricated white light emission based composite nanoprobe can be applied as a promising material for intra cellular pH sensing in cancer cell lines.

References

1. Sahoo, A. K.; Sailapu, S. K.; Dutta, D.; Banerjee, S.; Ghosh, S. S.; Chattopadhyay, A. DNA-Templated Single Thermal Cycle Based Synthesis of Highly Luminescent Au Nanoclusters for Probing Gene Expression. *ACS Sustainable Chem. Eng.* **2018**, *6*, 2142-2151.

2. Sadhanala, H. K.; Nanda, K. K. Boron and Nitrogen Co-doped Carbon Nanoparticles as Photoluminescent Probes for Selective and Sensitive Detection of Picric Acid. *J. Phys. Chem. C* **2015**, *119*, 13138-13143.

3. Nie, H.; Li, M.; Li, Q.; Liang, S.; Tan, Y.; Sheng, L.; Shi, W.; Zhang, S. X. A. Carbon Dots with Continuously Tunable Full-Color Emission and Their Application in Ratiometric pH Sensing. *Chem. Mater.* **2014**, *26*, 3104-3112.

4. Wei, Q.; Zhang, Y.; Song, Y.;Yang, G.; Zou, X. A Series of Inorganic–organic Hybrid Cadmium Borates with Novel Cd-centred $[Cd@B_{14}O_{20}(OH)_6]^{2-}$ clusters. *Dalton Trans.* **2016**, *45*, 13937- 13943.

5. Yang, Z.; Xu, M.; Liu, Y.;He, F.; Gao, F.; Su, Y.; Wei, H. ; Zhang, Y. Nitrogen-doped, Carbon-rich, Highly Photoluminescent Carbon Dots from Ammonium Citrate. *Nanoscale* **2014**, *6*, 1890-1895.

6. Ananthanarayanan, A.; Wang, Y.; Routh, P.; Sk, M. A.; Than, A.; Lin, M.; Zhang, J.; Chen, J.; Sun, H.; Chen, P. Nitrogen and Phosphorus Co-doped Graphene Quantum Dots: Synthesis from Adenosine Triphosphate, Optical Properties, and Cellular Imaging. *Nanoscale* **2015**, *7*, 8159-8165.

7. Li, H.; He, X.; Kang, Z.; Huang, H.; Liu, Y.; Liu, J.; Lian, S.; Tsang, C. A.; Yang, X.; Lee, S. Water-Soluble Fluorescent Carbon Quantum Dots and Photocatalyst Design. *Angew. Chem. Int. Ed.* **2010**, *49*, 4430-4434.

8. Kwon, W.; Do, S.; Kim, J.; Jeong, M.; Rhee, S. Control of Photoluminescence of Carbon Nanodots via Surface Functionalization using Para Substituted Anilines. *Sci. Rep.* **2015**, *5*, 12604.

9. Mei, Q.; Zhang, K.; Guan, G.; Liu, B.; Wang, S.; Zhang, Z. Highly Efficient Photoluminescent Graphene Oxide with Tunable Surface Properties. *Chem. Commun.* **2010**, *46*, 7319-7321.

10. Kiermasch, D.; Rieder, P.; Tvingstedt, K.; Baumann, A.; Dyakonov, V. Improved Charge Carrier Lifetime in Planar Perovskite Solar Cells by Bromine Doping. *Sci. Rep.* **2016**, *6*, 39333; doi: 10.1038/srep39333.

11. Bissinger, P.; Braunschweig, H.; Damme, A.; Hçrl, C.; Krummenacher, I.; Kupfer, T. Boron as a Powerful Reductant: Synthesis of a Stable Boron-Centered Radical-Anion Radical-Cation Pair. *Angew. Chem. Int. Ed.* **2015**, *54*, 359 -362.

12. Zhu, S.; Zhang, J.; Tang, S.; Qiao, C.; Wang, L.; Wang, H.; Liu, X.; Li, B.; Li, Y.; Yu, W.; Wang, X.; Sun, H.;Yang, B. Surface Chemistry Routes to Modulate the Photoluminescence of Graphene Quantum Dots: From Fluorescence Mechanism to Up-Conversion Bioimaging Applications. *Adv. Funct. Mater.* **2012**, *22*, 4732-4740.

13. Meiling, T.; Schürmann, R.; Vogel, S.; Ebel, K.; Nicolas, C.; Milosavljevic, A.; Bald, I. Photophysics and Chemistry of Nitrogen-Doped Carbon Nanodots with High Photoluminescence Quantum Yield. *J. Phys. Chem. C* **2018**, *122*, 10217-10230.

14. Canfarotta, F.; Piletsky, S. A. Engineered Magnetic Nanoparticles for Biomedical Applications. *Adv. Healthcare Mater.* **2014**, *3*, 160-175.

15. Schneider, J.; Reckmeier, C. J.; Xiong, Y.; Seckendorff, M.; Susha, A.; Kasák, P.; Rogach, A. Molecular Fluorescence in Citric Acid-Based Carbon Dots. *J. Phys. Chem. C* **2017**, *121*, 2014-2022.

16. Song, Y.; Zhu, S.; Xiang, S.; Zhao, X.; Zhang, J.; Zhang, H.; Fu, Y.; Yang, B. Investigation into the Fluorescence Quenching Behaviors and Applications of Carbon dots. *Nanoscale* **2014**, *6*, 4676-4682.

17. Li, L.; Wu, G.; Yang, G.; Peng, J.; Zhao, J.; Zhu, J. Focusing on Luminescent Graphene Quantum dots: Current Status and Future Perspectives. *Nanoscale* **2013**, *5*, 4015-4039.

18. Liu, Y.; Liu, Y.; Park, S.; Zhang, Y.; Kim, T.; Chae, S.; Park, M.; Kim, H. One-step Synthesis of Robust Nitrogen-doped Carbon dots: Acid-evoked Fluorescence Enhancement and their Application in Fe^{3+} Detection. *J. Mater. Chem. A* **2015**, *3*, 17747-17754.

19. Romero-Garcia, S.; Lopez-Gonzalez, J. S.; Báez-Viveros, J. L.; Aguilar-Cazares, D.; Prado-Garcia, H. Tumor cell metabolism. *Cancer Biol. Ther.* **2011**,*12*, 939-948.

20. Yang, Q.; Wei, L.; Zheng, X.; Xiao, L. Single Particle Dynamic Imaging and Fe^{3+} Sensing with Bright Carbon Dots Derived from Bovine Serum Albumin Proteins. *Sci. Rep.* **2015**, *5*, 1-12.

21. Zong, J.; Yang, X.; Trinchi, A.; Hardin, S.; Cole, I.; Zhu, Y.; Li, C.; Muster, T.; Wei, G. Carbon Dots as Fluorescent Probes for "Off-On" Detection of Cu^{2+} and L-Cysteine in Aqueous Solution. *Biosens. Bioelectron.* **2014**, *51*, 330-335.

22. Wang, Y.; Jiang, K.; Zhu, J.; Zhang, L.; Lin, H. A FRET-based Carbon Dot–MnO_2 Nanosheet Architecture for Glutathione Sensing in Human Whole Blood Samples. *Chem. Commun.* **2015**, *51*, 12748-12751.

23. Gong, Y.; Yu, B.; Yang, W.; Zhang, X. Phosphorus, and Nitrogen Co-doped Carbon Dots as a Fluorescent Probe for Real-Time Measurement of Reactive Oxygen and Nitrogen Species Inside Macrophages. *Biosens. Bioelectron.* **2016**, *79*, 822-828.

Chapter 3

Conducting Carbon Dot-Polypyrrole Nanocomposite for Sensitive Detection of Picric acid

The conducting nature of carbon dots (Cdots), synthesized from citric acid monohydrate and ethylene diamine has been reported here. After that, a conducting nanocomposite material has been prepared using the as-synthesized Cdots and polypyrrole (PPy), which showed higher electrical conductivity in comparison to the components i.e., Cdots or PPy. It is important mentioning here that, PPy is a biofriendly conducting polymer that can easily be synthesized from commercially available precursors and is also amenable to functionalization. On the other hand, the demonstrated ease of pursuing chemistry of Cdots under typically "green" reaction conditions, makes them appropriate for composite based organic polymer devices. The conductive nature of both Cdots and the Cdot-PPy nano composite film was studied based on *I-V* characteristics. It was found that introduction of conducting Cdots in to PPy helped improving the electrical conductivity of the as-synthesized nanocomposite material. The maximum conductivity of composite film was measured to be 2.60 mS m^{-1} and that for PPy film was found to be 0.23 mS m^{-1}. Finally, Cdots embedded nanocomposite film was successfully utilized for highly sensitive and selective detection of picric acid, both in water as well as in soil, based on the changes in *I-V* characteristics. Measured limit of detection for picric acid was found to be 1.40×10^{-7} M (32 ppb) in aqueous phase and 5.7 ng mg^{-1} of the soil. The technique described here is highly selective and the device can potentially be made flexible and portable for field applications.

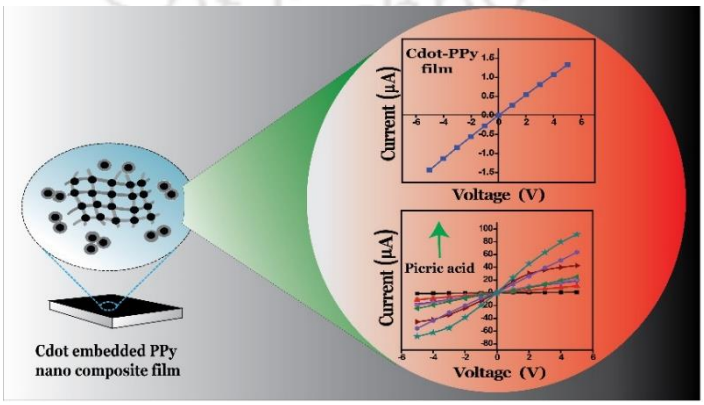

**[ACS Appl. Mater. Interfaces 2016, 8(9), 5758–5762] - Reproduced with permission from the American Chemical Society.*

3.1 Experimental Section

3.1.1 Materials. Citric acid monohydrate, ethylene diamine and H_2O_2 (50% as purchased; 29% as estimated) were purchased from Merck, India. Also, dialysis membrane (dialysis tubing, benzoylated) was procured from Sigma-Aldrich. Pyrrole (synthesis grade) was purchased from Spectrochem private limited, India. All the materials were used without further purification. Conducting silver paste was purchased from Alfa-Aesar. Elix grade water from a MilliQ purification system was used during the experiment. All chemicals were used without further purification.

3.1.2 Synthesis of Cdot-polypyrrole (Cdot-PPy) Nanocomposite. First, Cdots were prepared from a mixture of citric acid monohydrate and ethylene diamine by using induction coil heating method as reported earlier.[1] This was followed by dialysis of the final product using 1KDa dialysis membrane for 24 h. Acidic solution of pyrrole (Py) was prepared by stirring 268 µL of Py added to 4.0 mL of 1N HCl at room temperature for 30 min. The Cdot-PPy composite was synthesized by addition of acidic solution of Py to the freshly prepared aqueous solution of 4.0 mL Cdots (7.3 mg/mL) following which 200 µL H_2O_2 (29 %) was added. The solution was constantly stirred. The color of the reaction mixture gradually changed from brownish to black as polymerization of pyrrole started to occur in the presence of Cdots. The reaction was allowed to continue for 12 h for complete polymerization. In order to get the black powder of the composite, it was filtered first, followed by washing with water and methanol for several times. Finally, the filtrate was collected and dried at 50 ^oC for 12 h.

3.1.3 Synthesis of Polypyrrole (PPy) in HCl Medium. 268 µL of Py was dissolved first in 4.0 mL of 1N HCl by stirring at room temperature for 30 min. 200 µL of H_2O_2 (29 %) was added to the HCl solution of Py subsequently and the mixture was stirred under room temperature for 12 h. After complete polymerization, the dark colored precipitate of PPy was collected by decantation, washed well with water and methanol for several times and then dried at 50 ^oC for 12 h before further characterization.

3.1.4 Characterization Methods. Cdot-PPy composite was characterized using UV-vis absorption spectroscopy (Perkin Elmer Lambda 750 spectrophotometer), photoluminescence spectroscopy (Horiba Fluoromax-4 spectrofluorometer), Fourier transform infrared spectroscopy (Perkin Elmer spectrometer) and transmission electron microscopy (JEOL 2100UHR-TEM operating at an accelerating voltage 200 KV). Raman spectroscopy was done in Horiba LabRAM HR800 and powder X-ray diffraction analysis was carried out using Rigaku TTRAX III diffractometer, operating with Cu Kα source (λ=1.54Å). Thermogravimetric analysis (TGA) was performed with SDT Q600 in the temperature range of 70-700 ^{o}C under nitrogen atmosphere at a heating rate of 10 ^{o}C/min. Surface morphologies of the PPy and the composite films were studied using field-emission scanning electron microscope (Carl Zeiss, Sigma VP). Elemental analysis was performed using EuroEA Elemental Analyser.

3.1.5 Quantum Yield Calculation. Quantum yield (QY) of Cdot-PPy composite was calculated with respect to quinine sulphate in 0.1M H_2SO_4 as the standard and at an excitation wavelength of 365 nm, using the following equation.[2,3]

$$Q_S = Q_R \times \frac{I_S}{I_R} \times \frac{A_R}{A_S} \times \frac{\eta_S^2}{\eta_R^2} \qquad \text{equation 3.1}$$

Here, Q_S = quantum yield of the sample (Cdot-PPy composite); Q_R = quantum yield of the reference; I_S = area under the PL curve of the sample; I_R = area under the PL curve of reference; A_R = absorbance of the reference (quinine sulphate); A_S = absorbance of the sample (here Cdot-PPy composite); η_R = refractive index of quinine sulphate dissolved in 0.1M H_2SO_4; η_S = refractive index of sample. QY of quinine sulphate = 0.54. Refractive index of water = 1.33.

The concentrations of the sample and the reference quinine sulphate were adjusted so that the optical densities of all the samples were 0.1 ± 0.01 at the excitation wavelength of 365 nm.

3.1.6 Preparation of Cdot-PPy Film for *I-V* Characteristic Study. Conductive Cdot-PPy nanocomposite film was prepared over glass surface by using drop casting method. Before coating, glass slides were first washed well with aqua-regia, water and then acetone. The slides were finally dried for 1 h in oven. In a typical procedure, 100 μL (40 mg/mL) of sample was drop-cast over (0.9 x 0.9) cm^2 glass slide and was then kept at 50 ^oC for up to 2 h until the film was dried completely. After that, two contact points were made with conducting silver paste to connect the copper electrodes with dimension of (4.5 x 0.7) cm^2 to the composite film and the current (*I*) changes were measured applying different voltages (*V*) by using Keithley 2400 source meter.

3.1.7 Preparation of Cdot Film. After the synthesis and purification, 100 μL (7.3 mg/mL) of pure Cdot dispersion was drop-cast over (0.9 x 0.9) cm^2 glass slide and was kept at 80 ^oC for 2 days until the film dried completely. Two contact points were then made with conducting silver paste over the film as mentioned earlier and the current (*I*) changes were measured applying different voltages (*V*) by using source meter.

3.1.8 Detection of Picric Acid. The change in *I-V* characteristic of the composite film after addition of 2.0 μL of water was measured first as the reference. Next to that, 2.0 μL aqueous solution of picric acid was added over the composite film and changes in current, after applying different voltages were measured. In this regard, *I-V* characteristics for a range of concentrations from 1.0 μM to 1.0 mM solution of picric acid were recorded. *I-V* characteristics were also measured for other analytes by similar procedure.

3.1.9 Soil Test. During the experiment, 60 mg of soil was weighed first, followed by addition of 15 μL of picric acid and the mixture was allowed to dry for a week. Before recording the *I-V* characteristics, 15 μL of water was added to the soil sample and which was then spread uniformly over the composite film. During conductivity measurement soil sample containing picric acid was transferred over the film in such a way that it did not come into the contact with the two electrodes directly. As the concentration of picric acid was increased from 0.08 mM to 0.5 mM (as in the parent solution) in the soil, the corresponding *I-V* characteristics showed distinct increase in

current in the composite film. Finally, 15 µL of water was mixed to the soil sample to check the corresponding *I-V* characteristic plot also as the reference.

3.2 Results and Discussion

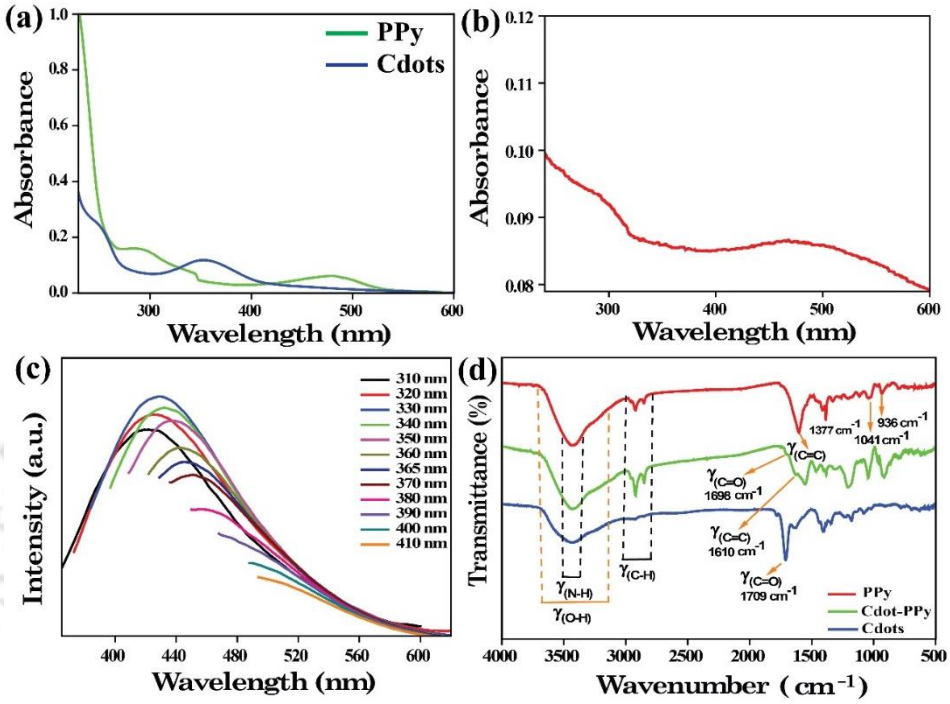

Figure 3.1. UV−vis absorption spectra of (a) Cdots and PPy and (b) the composite in water. (c) Emission spectra of Cdot-PPy composite. The excitation wavelengths are indicated in the legends. (d) FTIR spectra of PPy, Cdot-PPy composite and Cdots.

Figure 3.1. a and b correspond to absorption study of the as-synthesized materials. UV-vis spectrum of the aqueous dispersion of the composite consisted of broad absorption bands at ~290 nm and ~468 nm (Figure 3.1.b). The characteristic absorption peak at ~290 nm is assigned to π-π* transition, which became broad and redshifted compared to that from PPy, appearing at ~280 nm (Figure 3.1.a). Interestingly, the sharp bipolaron transition of PPy [4] at 475 nm appeared as broad absorption band from 350 to 600 nm in the composite, which might be due to interaction (overlap) between bipolaron transition band in PPy and the n-π* transition band, centered at 360 nm in the Cdot absorption spectrum (Figure 3.1).

Photoluminescence (PL) spectra (Figure 3.1.c) revealed retention of wavelength tunable emission due to the Cdots in the composite; however, the intensity was significantly reduced as compared to Cdots. The fluorescence quantum yield (QY) of Cdot-PPy composite was found to be 0.04% at the excitation wavelength of 365 nm.

The details of the QY calculations are mentioned in the experimental section. It is worth mentioning here that electron transfer through non-radiative pathway between Cdots and PPy could have resulted in the lowering of luminescence quantum yield in the emission spectrum.[5] However, contribution of PPy to the overall absorbance in the composite might also have led to the lowering of the measured QY as well.

Fourier transform infrared (FTIR) spectroscopic measurement of the composite material revealed the presence of characteristic peak at 1610 cm^{-1} due to typical C=C stretching vibration of the PPy ring (Figure 3.1.d).[6] The C=O stretching vibration in Cdot-PPy composite was shifted to 1698 cm^{-1} (from 1709 cm^{-1}) due to hydrogen bonding interaction between C=O group present on the surface of Cdots and the N–H of Py rings in polymer as well as π–π interaction between aromatic Py rings and C=O in Cdots. Weak absorption for C=O stretching of Cdots may be due to its low concentration in the composite. Additional peaks at 1377, 1041 and 936 cm^{-1}, in the fingerprint region of PPy FTIR spectrum, correspond to the bipolaron bands originating from the doped state of PPy. The bands are consistent with the literature reports.[6,7]

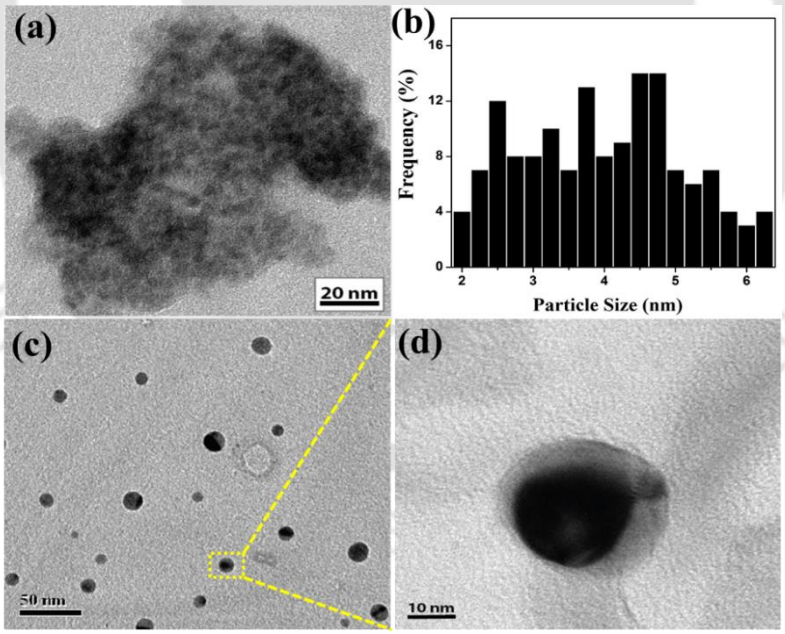

Figure 3.2. (a)TEM image of Cdots inside the polymer matrix. (b) Particle size distribution of Cdots present in the polymer matrix. The distribution was calculated using several TEM images (with more than 100 particles). (c) TEM image of PPy coated Cdots observed outside the larger polymer matrix. Scale bar is 50 nm. (b) Enlarged view of the same in 10 nm scale bar.

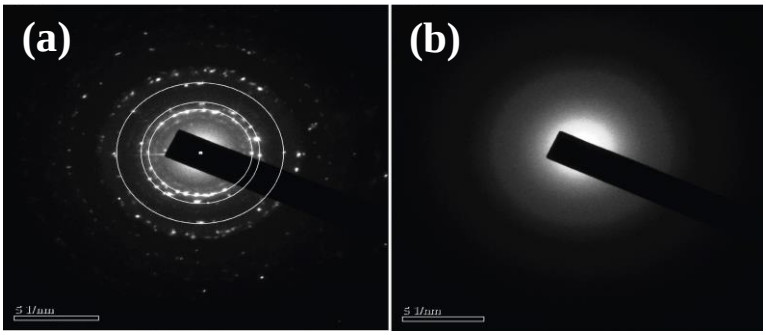

Figure 3.3. Selected area electron diffraction (SAED) pattern of the Cdot-PPy composite material revealing (a) clear patterns at 0.35, 0.28 and 0.20 nm due to the crystalline part present in the composite; (b) no such pattern was observed in the amorphous content of the composite.

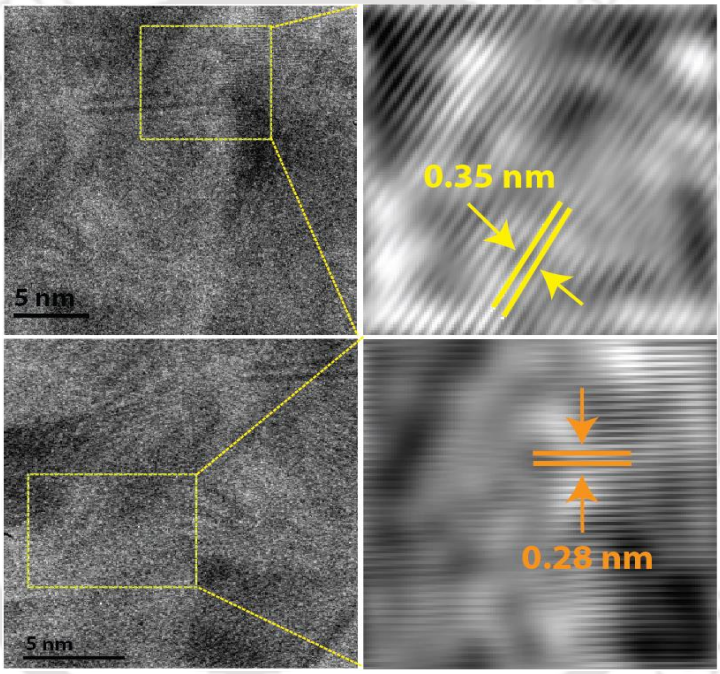

Figure 3.4. HRTEM and corresponding inverse fast Fourier transform (IFFT) images of the composite material with corresponding d spacing of 0.35 and 0.28 nm.

Next, the formation of nanocomposite was confirmed by the transmission electron microscopy (TEM) study, which revealed that smaller Cdots with average size of 4.5 ± 2 nm were embedded in the polymer matrix (Figure 3.2.a, b), along with the presence of individual PPy-coated Cdots (Figure 3.2.c, d). Further, Cdot-PPy composite material was observed to have been semi-crystalline in nature (Figure 3.3.a, b). Crystalline nature of the material was established by selected area electron diffraction (SAED) measurement (Figure 3.3.a). High-resolution TEM (HRTEM) images showed the presence of fringes with lattice spacing of 0.35 and 0.28 nm (Figure 3.4), which

correspond to the inter planar distance between aromatic pyrrole to pyrrole rings and face-to-face stacking, respectively.[8, 9]

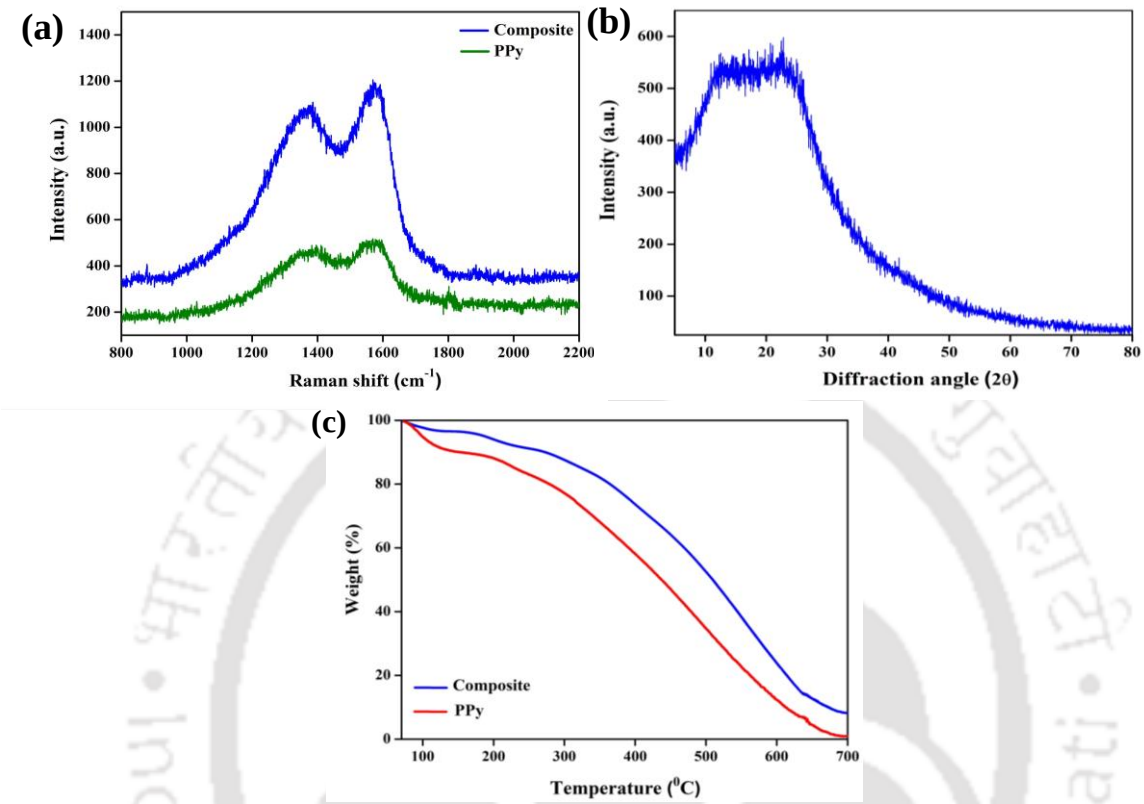

Figure 3.5. (a) Raman spectra of PPy and Cdot-PPy composite. (b) Powder X-ray diffraction pattern of Cdot-PPy composite. (c) Thermogravimetric analysis corresponding to PPy and Cdot-PPy composite.

The Raman spectra of PPy and the composite material were recorded with laser wavelength set at 488 nm (Figure 3.5.a). Two typical bands appeared for PPy at 1383 and 1574 cm^{-1} due to the ring stretching mode and the C=C backbone stretching of PPy.[10] Importantly, when Cdots were introduced into the polymer, both the bands were observed at 1369 and 1567 cm^{-1}, respectively.

The X-ray diffraction (XRD) study (Figure 3.5.b) showed two broad peaks at 15° and 25°. However, due to the broad diffractions from the amorphous component, it might have been difficult to observe the sharper diffractions from the crystalline component of the composite in the XRD pattern.

Additionally, thermal stability studies of PPy and Cdot-PPy composite were carried out in nitrogen atmosphere at a heating rate of 10 °C/min. As shown in Figure 3.5.c, the initial weight loss for both the materials in temperature range of 70 to 130 °C was due to evaporation of residual water. Subsequent weight loss in the range of 220 to 700 °C was due to the continuous degradation of the polymer. Importantly, the thermogravimetric study revealed that the rate of weight loss for the composite was less as compared to that of PPy, suggesting higher thermal stability of the Cdot-PPy composite than PPy.

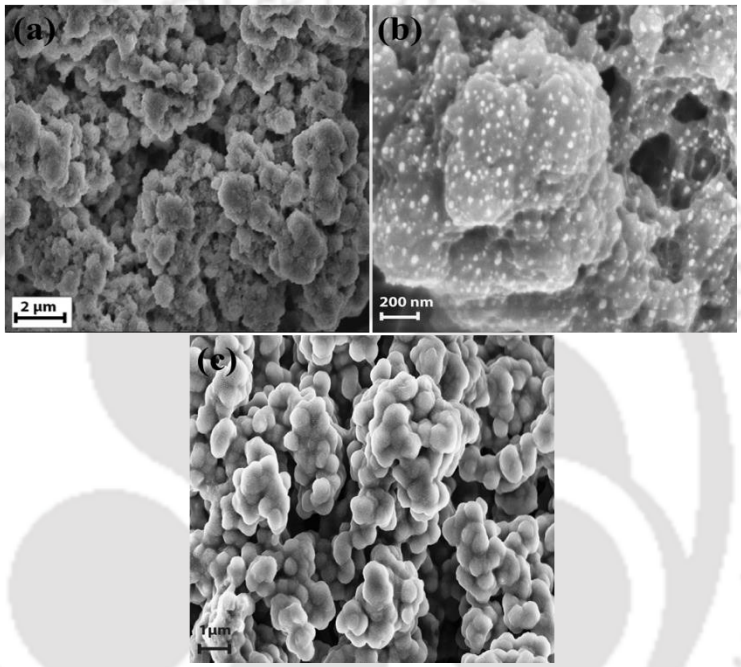

Figure 3.6. (a) FESEM image of Cdot-PPy composite film. (b) Enlarged view for the same in 200 nm scale bar revealing that nanoscale particulate forms were present over the polymer. (c) FESEM image of the PPy film. Scale bar is 1 µm.

The field-emission scanning electron microscopy (FESEM) images (Figure 3.6.a) of the composite thin film demonstrated the presence of uneven surface of the polymeric layer, with possible incorporation of Cdots and PPy coated Cdots as represented by the presence of nanoscale particles (Figure 3.6.b). Elemental analysis confirmed that the composite film contained 55.74% C, 5.05% H, 15.33% N, and 23.88% O (as calculated).

A plausible mechanism for the formation of the composite could be proposed to be based on the interaction between Cdots and Py moiety, occurring through hydrogen bonding and π-π interactions between sp^2 bonded carbon atoms of both the materials,

leading to the proximity of the components.[11] Subsequently, reaction with H_2O_2 led to the formation of polymeric layer over Cdot-surface during chemical oxidation polymerization of Py.

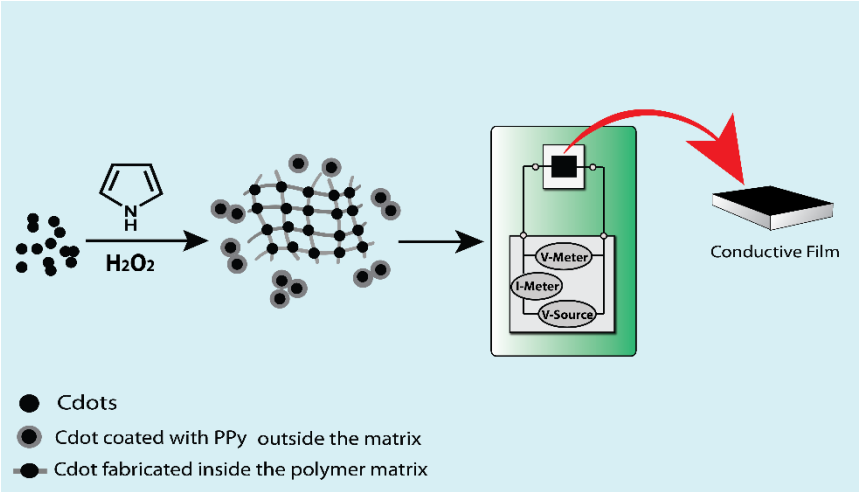

Scheme 3.1. Schematic Representation of the synthesis of Cdot-PPy composite and corresponding experimental set-up for *I-V* characteristic study of the composite Film.

The current vs voltage (*I-V*) characteristic plot for Cdot film was recorded, revealing the electrically conducting nature of the as-synthesized Cdots (Figure 3.7.a). Linear *I-V* characteristic plot demonstrated the metallic behavior of the film. The conductivity of Cdot film could be attributed to the presence of sp^2 C-C bonds, which allow conjugation of the adjacent π-bonds to form the π- and π*-bands.[12] Further introductions of Cdots into the polymeric matrix of PPy revealed the higher conductivity of the composite nanomaterial as compared to PPy. The *I-V* characteristic plots presented in Figure 3.7.b clearly indicated improved electrical conductivity of Cdot-PPy film in comparison to PPy film. The maximum conductivity for composite film was measured to be 2.60 mS m^{-1} and that for PPy film was 0.23 mS m^{-1}. A digital photograph of the composite film is presented in Figure 3.7.b (inset) and the circuit configuration for the study of *I-V* characteristics is included in Figures 3.7.c. Also, the details of the measurement procedures are mentioned in the experimental section.

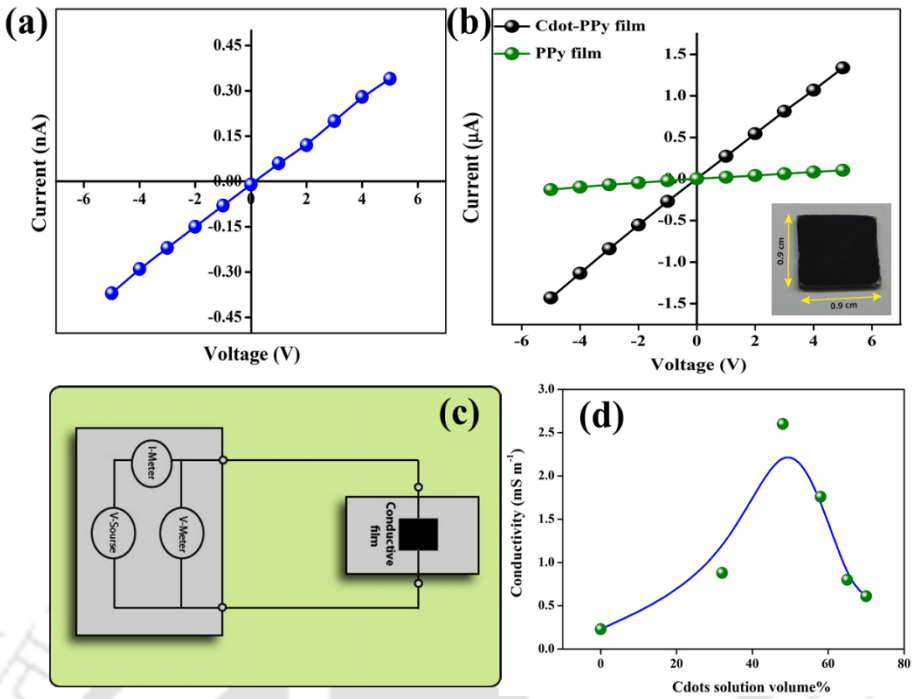

Figure 3.7. Plots of *I-V* characteristics of (a) Cdot film and (b) Cdot-PPy and PPy films. Digital photograph (inset) of a Cdot-PPy nanocomposite film. (c) Circuit diagram for *I-V* characteristic measurement system for Cdot-PPy composite film. (d) Conductivity change due to the variation of Cdot content in composite film. Plot of conductivity of the composite film in terms of initial concentration of Cdot in the reaction mixture (which is expressed in terms of volume percentage).

PPy, being a p-type of semiconductor, mainly conducts through holes.[13] Therefore, the conductivity of the composite is expected to be higher, as positive charge density increases in the polymer backbone. The charge carrier density in the composite might have been enhanced in the presence of Cdots, which are excellent electron acceptors.[14] This resulted in the higher conductivity of the composite as compared to PPy. Concentration dependent change in conductivity was also studied by varying the Cdot concentration in the composite material. As shown in Figure 3.7.d, conductivity of the composite was observed to increase initially with the increase in Cdot content; however, at higher concentrations of Cdot the conductivity decreased. The maximum conductivity of the film was obtained when it was prepared from a reaction mixture containing 4.0 mL of 7.3 mg/ mL Cdot dispersion and 268 μL of Py added to 4.0 mL of 1N HCl medium.

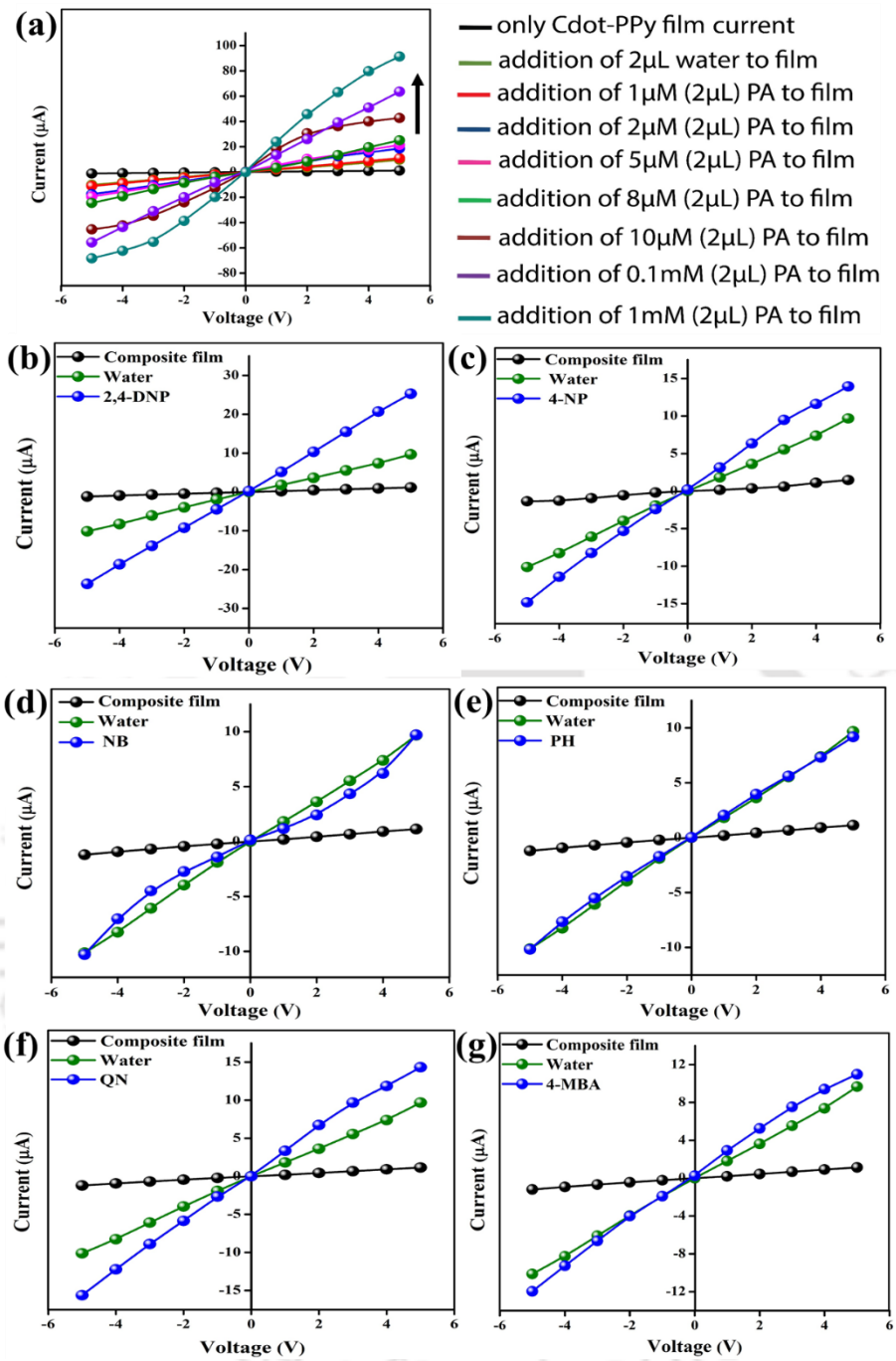

Figure 3.8. (a) *I-V* characteristics of the composite film in presence of different concentrations of picric acid (PA) solutions. Changes in *I-V* characteristics of composite film due to addition of 2.0 μL of 1.0 mM (b) 2,4-dinitrophenol (2, 4-DNP) or (c) 4-nitrophenol (4-NP). Also, changes in *I-V* characteristic plot of the composite film due to addition of 2.0 μL of 1.0 mM (d) nitrobenzene (NB) and (e) phenol (PH) have been represented. Change in *I-V* characteristic plot of the composite film due to addition of 2.0 μL of 1.0 mM (f) 1,4-benzoquinone (QN) and (g) 4-methoxybenzoic acid (4-MBA).

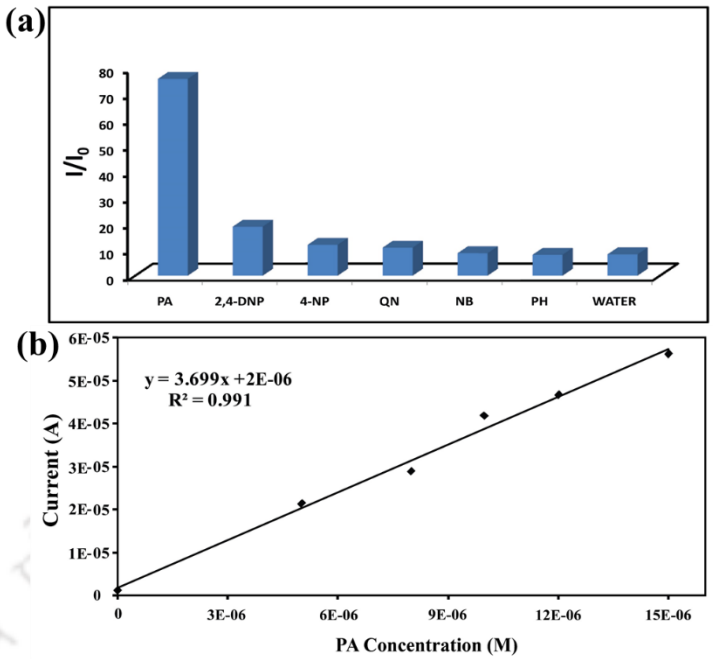

Figure 3.9. (a) The ratios of current flowing through the composite film after adding 2.0 μL 1.0 mM aqueous solution of different analytes to the film only. In the figure PA = picric acid, 2,4-DNP = 2,4-dinitrophenol, 4-NP = 4-nitrophenol, NB = nitrobenzene, PH = phenol, QN = 1,4- benzoquinone, 4-MBA= 4- methoxybenzoic acid. The measurements were made at +5 V. (b) Sensor response curve of the Cdot-PPy composite film in presence of different concentrations of picric acid.

Finally, Cdot-PPy composite film was used for the detection of picric acid, based on the changes in *I-V* characteristics. Interestingly, we found significant increase in current due to the addition of aqueous solutions of picric acid with increasing concentrations on the composite film. Concentration dependent distinct changes in the *I-V* characteristics of the composite film in the presence of picric acid (Figure 3.8.a) indicated higher degree of protonation to aromatic ring in the PPy backbone, thus allowing higher charge carrier density. As is illustrated in Figure 3.8.a-g and Figure 3.9.a, the response of the composite film was much higher toward picric acid in comparison to other nitro phenol derivatives such as 2,4-dinitrophenol (2,4-DNP), 4-nitrophenol (4-NP) and phenol (PH), thus indicating selectivity for the preferential detection of picric acid. Additional experiment, corresponding to the *I-V* characteristic study of the composite film with electron acceptor molecule, 1,4- benzoquinone (QN) and electron donor molecule like 4-methoxy benzoic acid (MBA) were performed, for which the sensitivities were found to be low (Figure 3.8. f, g). It is worth mentioning here that the limit of detection of picric acid was found to be 1.40×10^{-7} M (32 ppb),

revealing higher sensitivity of the composite film, as compared to earlier reported results (Figure 3.9. b).[15-17]

Determination of Limit of Detection (LOD)

Limit of Detection (LOD) for PA was calculated according to the following formula. [18, 19]

$$LOD = \frac{3\sigma}{K} \qquad \text{equation 3.2}$$

Here, σ corresponds to standard deviation of measured current for the blank composite film and *K* denotes the gradient of current vs. concentration plot.

As calculated, σ for the blank composite film was found to be 1.72 X 10^{-7} A. Gradient of current vs. PA concentration plot (*K*) was found to be 3.699 (A/M). Introducing the obtained values in the above equation, the calculated value of LOD was found to be 1.40 X 10^{-7} M (32 ppb).

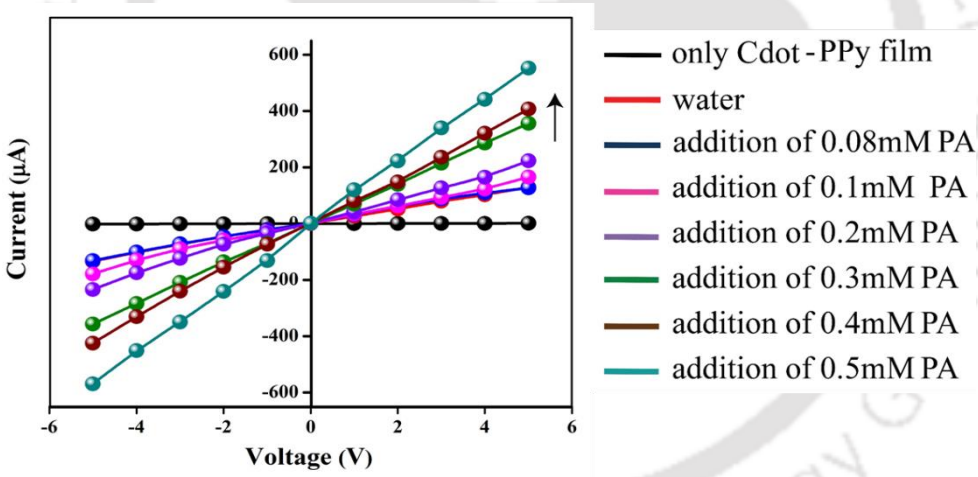

Figure 3.10. *I-V* characteristics of the composite film in presence of different concentrations of PA mixed in soil.

It was observed that the Cdot-PPy composite film was also able to detect trace amount of picric acid present in soil sample (Figure 3.10) with appreciable changes in *I-V* characteristics at low concentrations of the acid. The minimum concentration of picric acid detected by the film was 5.7 ng per mg of the soil.

3.3 Conclusion. In conclusion, in this chapter we have reported the electrical conducting property of Cdots and also developed a facile method of synthesis of conducting Cdot-PPy nanocomposite, which showed enhanced electrical conductivity compared to both Cdot and PPy films. The maximum conductivity for composite film was measured to be 2.60 mS m^{-1} and that for PPy film was 0.23 mS m^{-1}. Further, the as-synthesized composite film exhibited higher selectivity and sensitivity toward detection of trace amount of picric acid present in aqueous phase as well as in the soil. Notably, the limit of detection of picric acid was found to be 1.40×10^{-7} M (32 ppb) in aqueous phase and 5.7 ng mg^{-1} of the soil respectively. The above results indicated the potential of Cdot, being present in a composite polymer film, for versatile sensing applications especially in flexible nano electronics.

References

1. Sk, M. P.; Chattopadhyay, A. Induction Coil Heater Prepared Highly Fluorescent Carbon Dots as Invisible Ink and Explosive Sensor. *RSC Adv*. **2014**, *4*, 31994-31999.
2. Hu, S.; Niu, K.; Sun, J.; Yang, J.; Zhao, N.; Du, X. One-Step Synthesis of Fluorescent Carbon Nanoparticles by Laser Irradiation. *J. Mater. Chem*. **2009**, *19*, 484-488.
3. Murphy, J. E.; Beard, M. C.; Norman, A. G.; Ahrenkiel, S. P.; Johnson, J. C.; Yu, P.; Micic, O. I.; Ellingson, R. J.; Nozik, A. J. PbTe Colloidal Nanocrystals: Synthesis, Characterization, and Multiple Exciton Generation. *J. Am. Chem. Soc*. **2006**, *128*, 3241-3247.
4. Choudhary, M.; Islam, R.; Witcomb, M. J.; Mallick, K. In Situ Generation of a High-Performance Pd-Polypyrrole Composite with Multi-Functional Catalytic Properties. Dalton Trans. 2014, 43, 6396-6405.
5. Barman, M.; Jana, B.; Bhattacharyya, S.; Patra, A. Photophysical Properties of Doped Carbon Dots (N, P, and B) and Their Influence on Electron/Hole Transfer in Carbon Dots−Nickel (II) Phthalocyanine Conjugates. *J. Phys. Chem. C* **2014**, *118*, 20034-20041.
6. Chen, A.; Wang, H.; Li, X. One-Step Process to Fabricate Ag–Polypyrrole Coaxial Nanocables. *Chem. Commun*. **2005**, 1863-1864.
7. Tian, B.; Zerbi, G. Lattice Dynamics and Vibrational Spectra of Pristine and Doped Polypyrrole: Effective Conjugation Coordinate. *J.Chem. Phys*. **1990**, *92*, 3892–3898.
8. Carrasco, P.; Grande, H.; Cortazar, M.; Alberdi, J.; Areizaga, J.; Pomposo, J. Structure-Conductivity Relationships in Chemical Polypyrroles of Low, Medium and High conductivity. *Synth. Met.* **2006**, *156*, 420-425.
9. Jeeju, P.; Varma, S.; Xavier, P. A.; Sajimol, A. M.; Jayalekshmi, S. Novel Polypyrrole Films with Excellent Crystallinity and Good Thermal Stability. *Mater. Chem. Phys.* **2012**, *134*, 803-808.
10. Lim, S.; Pandikumar, A.; Lim, Y.; Huang, N.; Lim, H. In-situ Electrochemically Deposited Polypyrrole Nanoparticles Incorporated Reduced Graphene Oxide as an Efficient Counter Electrode for Platinum-free Dye-sensitized Solar Cells. *Sci. Rep.***2014**, *4*, 5305.

11. Xu, C.; Sun, J.; Gao, L. Synthesis of Novel Hierarchical Graphene/Polypyrrole Nanosheet Composites and Their Superior Electrochemical Performance. *J. Mater. Chem.* **2011**, *21*, 11253-11258.

12. Eda, G.; Lin, Y.; Mattevi, C.; Yamaguchi, H.; Chen, H.; Chen, I.; Chen, C.; Chhowalla, M. Blue Photoluminescence from Chemically Derived Graphene Oxide. *Adv. Mater*. **2010**, *22*, 505-509.

13. Chen, X.; Jenekhe, S. Bipolar Conducting Polymers: Blends of p-Type Polypyrrole and an n-Type Ladder Polymer. *Macromolecules* **1997**, *30*, 1728-1733.

14. Wang, X.; Cao, L.; Lu, F.; Meziani, M.; Li, H.; Qi, G.; Zhou, B.; Harruff, B.; Kermarrec, F.; Sun, Y. Photoinduced Electron Transfers with Carbon Dots. *Chem. Commun*. **2009**, 3774-3776.

15. Huang, J.; Wang, L.; Shi, C.; Dai, Y.; Gu, C.; Liu, J. Selective Detection of Picric Acid Using Functionalized Reduced Graphene Oxide Sensor Device. *Sens. Actuators B* **2014**, *196*, 567-573.

16. Ma, J.; Lin, T.; Pan, X.; Wang, W. Graphene-Like Molecules Based on Tetraphenylethene Oligomers: Synthesis, Characterization, and Applications. *Chem. Mater.* **2014**, *26*, 4221-4229.

17. Dinda, D.; Gupta, A.; Shaw, B.; Sadhu, S.; Saha, S. Highly Selective Detection of Trinitrophenol by Luminescent Functionalized Reduced Graphene Oxide through FRET Mechanism. *ACS Appl. Mater. Interfaces* **2014**, *6*, 10722-10728.

18. Huang, J.; Wang, L.; Shi, C.; Dai, Y.; Gua, C.; Liu, J. Selective Detection of Picric Acid Using Functionalized Reduced Graphene Oxide Sensor Device. *Sens. Actuators, B* **2014**, *196*, 567-573.

19. Ang, C.; Tan, S.; Wu, S.; Qu, Q.; Wong, M.; Luo, Z.; Li, P.; Selvan, S.; Zhao, Y. A Dual Responsive "Turn-On" Fluorophore for Orthogonal Selective Sensing of Biological Thiols and Hydrogen Peroxide. *J. Mater. Chem. C* **2015**, DOI: 10.1039/c5tc01465d.

Chapter 4

Phosphorus Induced Crystallinity in Carbon dots for Solar Light Assisted Seawater Desalination

A highly ordered crystalline structure in carbon dots can substantially enhance the gamut of their applications in conversion, transfer and transport of energy; however, achievement of such crystallinity in a controlled manner has been elusive. Herein, we report a facile method for the synthesis of highly crystalline doped carbon dots with an average diameter of 2.8 ± 0.8 nm. The extent of crystallinity was dependent on the phosphorus content in the doped carbon dots. We attempt to understand the nature of phosphorus doping into as-synthesized carbon nanostructures (P-Cdots) via spectroscopic and microscopic techniques. Based on computational refinement of the powder X-ray diffraction pattern via the LeBail method we propose an orthorhombic crystal structure for P-Cdots. Importantly, the crystallinity in P-Cdots significantly enhanced the bulk solar photothermal evaporation efficiency to 83.6%. This phenomenon was further implemented towards successful and efficient solar light-based seawater desalination. Recent studies reveal that Cdot based nanocomposite materials such as iron oxide-Cdot nanoparticles or Cdot functionalized gold nanorods can be efficiently used for laser assisted photothermal therapy to kill cancer cells. However, the use of Cdots in solar thermal conversion or seawater desalination has not yet been reported. This could have its origin in the lack of long-range order in the Cdot structure, unlike in other carbon allotropes such as graphene, carbon nanotubes or diamond.

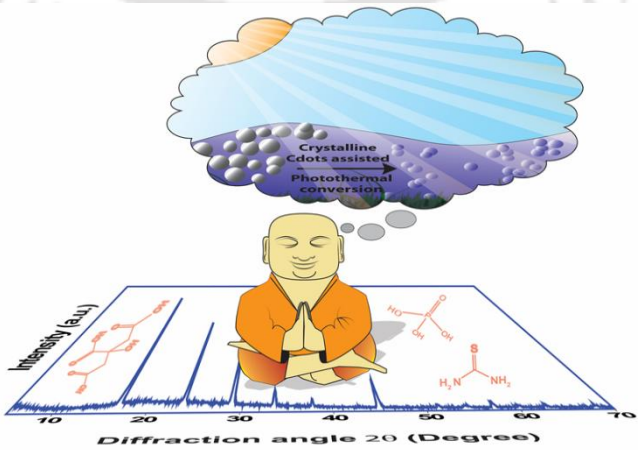

**[J. Mater. Chem. A 2018, 6, 4111-4118] - Reproduced with permission from the Royal Society of Chemistry.*

4.1 Experimental Section

4.1.1 Materials. Citric acid monohydrate (99%), *ortho* phosphoric acid (88%) and urea (99.5%) were purchased from Merck, India. Also, thiourea (99%) and the dialysis membrane (dialysis tubing, benzoylated) were purchased from Sigma-Aldrich. All materials were used without further purification. Elix grade water from a MilliQ purification system was used during the experiments.

4.1.2 Synthesis of Carbon dots. First, 210 mg (1 millimole) of citric acid monohydrate and 210 mg (2.76 millimole) of thiourea were dissolved in 10 mL water in a glass beaker. Subsequently, the required amount of phosphoric acid (such as 10 μL, 15 μL, 30 μL and 45 μL corresponding to 4.0%, 5.9%, 11.1% and 16.0% w/w respectively) was added dropwise to the mixture of starting materials under stirring. The reaction mixture was then treated under microwave radiation (600 W, make: Samsung; model: MC28H5023AK) for 5 min. After the completion of the reaction, the final product was cooled to room temperature and dissolved in 10 mL of water. The as-obtained dark brown solution was then centrifuged (15 000 rpm, 25 min, refrigerated centrifuge, SIGMA 3-30K) followed by dialysis (1 kDa dialysis membrane) of the collected supernatant part up to 12 h for further purification. In order to get dark brown powder of phosphorus doped Cdots (P-Cdots), the solution, after purification, was dried at 60 ^{o}C for 48 h.

For the synthesis of carbon dots, without phosphorus doping (Cdots), 210 mg of citric acid monohydrate and 210 mg of thiourea were dissolved in 10 mL water in a glass beaker and subsequently the reaction mixture was treated under microwave radiation (600 W) for 5 min. After synthesis, the final product was centrifuged (15 000 rpm, 25 min) followed by dialysis of the supernatant (1 kDa dialysis membrane, up to 12 h) for further purification as well.

For P-Cdots, the calculated weight percentage of the yield was ca. 62% with respect to citric acid, used as the carbon source before purification. After purification, the calculated yield of the material was ca. 17%. On the other hand, for un-doped carbon dots (termed as Cdots), the calculated yields were found to be ca. 59% and ca. 20% before and after purification, respectively, with respect to citric acid.

4.1.3 Characterization Methods. Cdots and P-Cdots were characterized using UV-vis spectroscopy (Hitachi U-2900 spectrophotometer), photoluminescence spectroscopy (Horiba Fluoromax-4 spectrofluorometer), X-ray photoelectron spectroscopy (XPS) (PHI 5000 Versa Probe II; FEI Inc.) and Fourier-transform infrared spectroscopy (Perkin Elmer spectrometer). Field emission transmission electron microscopy was done using a JEOL JEM-2100F FETEM operating at an accelerating voltage of 200 kV. Powder X-ray diffraction analysis was performed using a Rigaku TTRAX III diffractometer, operating with a Cu K_α source (λ = 1.54 Å). Matrix-assisted laser desorption/ionization time-of-flight mass spectrometry (MALDI-TOF MS) was performed on a Bruker Autoflex Speed MALDI-TOF system using 355 nm nitrogen laser pulse. Thermogravimetric analysis was done using a Netzsch STA 449F3 thermal analyzer system. Also, a Perkin Elmer Lambda 750 spectrophotometer was used to record NIR absorption spectra.

4.1.4 Quantum Yield Calculation. Quantum yields (QY) of P-Cdots as well as Cdots were calculated with respect to quinine sulphate in 0.1M H_2SO_4 as the standard using the following equation.

$$Q_S = Q_R \times \frac{I_S}{I_R} \times \frac{A_R}{A_S} \times \frac{\eta_S^2}{\eta_R^2} \qquad \text{equation 4.1}$$

Here, Q_S= quantum yield of the sample; Q_R = quantum yield of the reference; I_S = area under the PL curve of the sample; I_R = area under the PL curve of reference; A_R = absorbance of the reference; A_S = absorbance of the sample; η_S = refractive index of the sample solution; η_R = refractive index of reference.

QY of quinine sulphate = 0.54. Refractive index of water = 1.33.

Absorbance of quinine sulphate (A_R) = 0.098. Area under the PL curve (I_R) = 1.66 × 10^8.

Table 4.1.

Sample	Area under the PL curve (I_s) at 360 nm excitation (a.u.)	Absorbance at 360 nm (A_s)	Quantum yield (%) (Q_s)
P-Cdots	3.50×10^7	0.099	11.27
Cdots	4.32×10^7	0.097	14.20

$Q_{P\text{-}Cdot} = [0.54 \times (3.50 \times 10^7 / 1.66 \times 10^8) \times (0.098 / 0.099) \times (1.33^2/1.33^2)] \times 100\ \%$

$= 11.27\ \%$

$Q_{Cdot} = [0.54 \times (4.32 \times 10^7 / 1.66 \times 10^8) \times (0.098 / 0.097) \times (1.33^2/1.33^2)] \times 100\ \%$

$= 14.2\ \%$

4.1.5 Sample Preparation for MALDI-TOF MS. Saturated matrix solution of 2, 5-dihydroxybenzoic acid (DHB) (50 mg/ mL) was prepared in acetonitrile /water containing 0.1% trifluoroacetic acid (TFA) (3:2, v/v). To prepare sample-matrix solution, 2 µL of 1 mg/ mL P-Cdot dispersion was added to 2 µL of DHB solution and mixed well. Finally, 2 µL from the resulting mixture was spotted over MALDI target plate and air-dried before sample analysis.

4.1.6 Laser Assisted Photothermal Heating Experiment. To study photothermal performance by P-Cdots and Cdots, aqueous dispersions with ascending concentrations (5 mg/mL, 25 mg/mL, 50 mg/mL, 100 mg/mL, 175 mg/mL, 250 mg/mL) were taken in a 45 mm × 12.5 mm × 12.5 mm quartz cuvette. The sample cuvette was then irradiated with a laser source (high power focusable 2W 808 nm IR laser; MOD808-2W, Laser type: diode) for 8 min with stirring, for homogenous heat distribution through the aqueous dispersions. Corresponding temperature increase in different time intervals were carefully measured using a K-type digital thermometer (Model: Generiac K-type). During irradiation, path length between source and the sample cuvette was maintained at 250 mm. For control experiment, only water (without any Cdots) was irradiated with the laser source as well, maintaining all the aforementioned experimental conditions.

4.1.7 Evaporation Experiment. P-Cdot and Cdot assisted efficient water evaporation experiment was carried out by using rotary evaporator assisted vertical condensation technique (Buchi rotavapor, model: R-100). At first, during the process

temperature of vertically aligned condenser was made stable to 10 ^{o}C by circulating ice water for 15 min. After the stabilization of condenser temperature, different concentrations (4.5 mg/mL, 10 mg/mL, 20 mg/mL, 30 mg/mL, 40 mg/mL, 80 mg/mL) of homogeneously dispersed P-Cdot and Cdot solutions were taken in 1liter evaporation flask and were irradiated with simulated solar illumination (1 W/ cm^2) for 15 min. We found that the presence of both P-Cdots and Cdots in water could significantly increase water evaporation rate because of their extensive photothermal heat generation efficiency as compared to the normal water evaporation. P-Cdot was found to be even more efficient than Cdot. After completion of each experiment, the amount of excess water evaporation, assisted by carbon nano material was measured and corresponding evaporation efficiency was calculated. During all the measurements, typical pressure inside the evaporation flask was maintained at 35 mbar.

4.1.8 Calculation of Evaporation Efficiency. For calculation of evaporation efficiency η, we carried out separate sets of experiments where the pressure inside the evaporation flask was the standard atmospheric pressure of 1.01 bar. The water-evaporation efficiency under the experimental setup was calculated by the formula:

$$\eta = \frac{h_e \times m}{E} \qquad \text{equation 4.2}$$

Here h_e is the specific enthalpy of water vapor, m is the mass of evaporated water per unit time, and E is total energy input per unit time.

We use standard value of 2260 J/g for h_e as heat of evaporation of water at the pressure of 1.01 bar.[1] The energy input E for the experimental setup is the incident simulated solar energy of 5 J/s and m corresponds to the mass of water evaporated in 15 min, i.e. 900 seconds.

4.1.9 Sea Water Desalination Technique. For P-Cdot and Cdot assisted (concentration - 80 mg/mL) photothermal sea water evaporation, the aforementioned experimental procedure was followed in presence of simulated solar radiation (1 W/ cm^2). Salinity and pH of the water samples were carefully measured using a salinity measurement probe (model: HI98194).

4.2 Results and Discussion

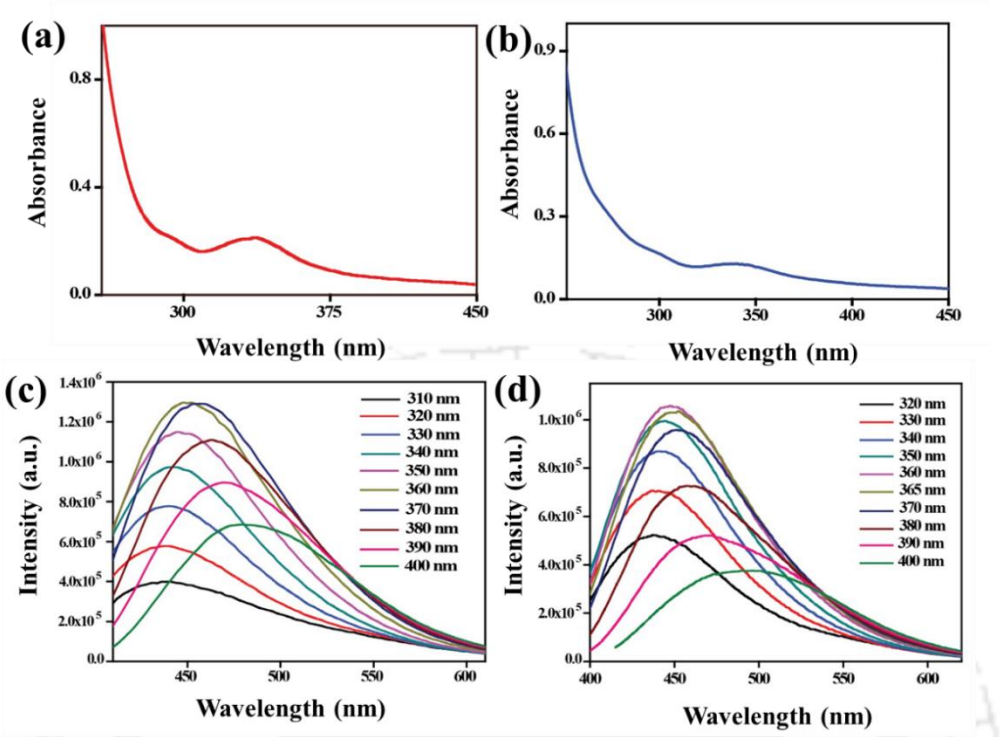

Figure 4.1. UV-vis absorption spectra of (a) Cdots (without phosphorus doping), (b) P-Cdots. Excitation dependent emission spectra of (c) P-Cdots and (d) Cdots. Corresponding excitation wavelengths are mentioned in the legends.

UV-vis spectrum of Cdots (Figure 4.1.a) consisted of two absorption bands at ~ 293 nm and ~ 340 nm, due to π -π* transitions and n-π* transitions, respectively. After doping phosphorus into the carbon nanostructure (i.e., P-Cdots), the π -π* transition band was blue shifted to 271 nm and a new absorption band appeared at 304 nm, indicating presence of additional surface states (Figure 4.1.b).[2]

Photoluminescence (PL) studies revealed wavelength tunable emission of both the P-Cdots and Cdots (Figure 4.1.c and d). Excitation-dependent tunability of carbon nano dots originated due to surface defects, capturing excitons, caused by heteroatoms and thus tuning the trap state emission.[3] The luminescence quantum yield (QY) of P -Cdots and Cdots were measured to be 11.27 % and 14.2 % respectively, at the excitation wavelength of 360 nm and emission wavelengths of 450 nm and 447 nm, respectively.

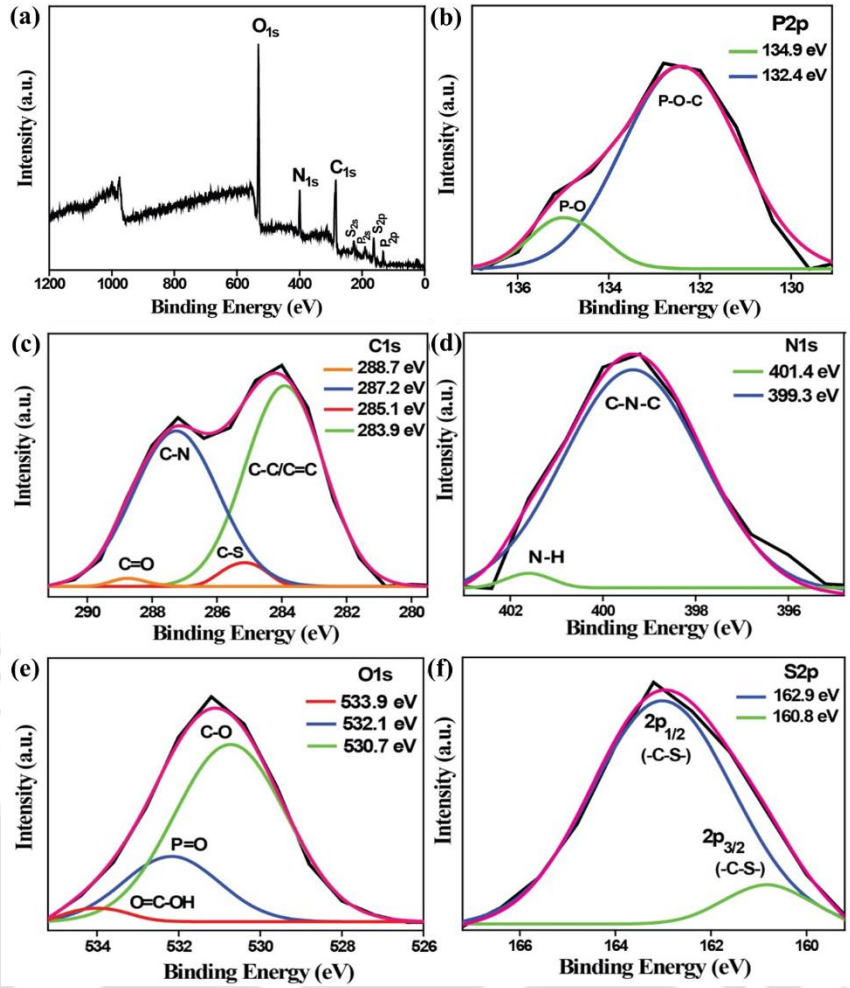

Figure 4.2. (a) X-ray photoelectron spectroscopy (XPS) results for P-Cdots (phosphoric acid, 11.1 % (w/w)) (full range) showing the presence of C, N, O, S and P and (b) deconvoluted XPS peaks at 134.9 eV and 132.4 eV for P_{2p} in P-Cdots, which correspond to P-O and P-O-C bonds respectively. [4,5] Deconvoluted XPS results for (c) C_{1s}, (d) N_{1s}, (e) O_{1s} and (f) S_{2p} peaks in P-Cdots.[6-9] Minor intensity deconvoluted peaks for O=C-OH and C=O groups were observed due to dangling groups present on the surface of crystalline P-Cdots.

We used X-ray photoelectron spectroscopy (XPS) analysis in order to understand the chemical bonding and surface groups present in both types of Cdots. As illustrated in Figure 4.2.a, the XPS spectrum of P-Cdots demonstrated sharp peaks due to P_{2s} and P_{2p}, confirming the successful doping of phosphorus into the Cdot nanostructure. The high resolution P_{2p} spectrum (Figure 4.2.b) could be deconvoluted into two signals at 134.9 eV and 132.4 eV, corresponding to P-O and P-O-C bonds, respectively.[4,5] Other signals appearing for both P-Cdots and Cdots were deconvoluted as well and are included in Figure 4.2.c-f and Figure 4.3.a-e respectively. Subsequently, atomic percentages in both Cdots were also calculated and are mentioned in Table 4.2.

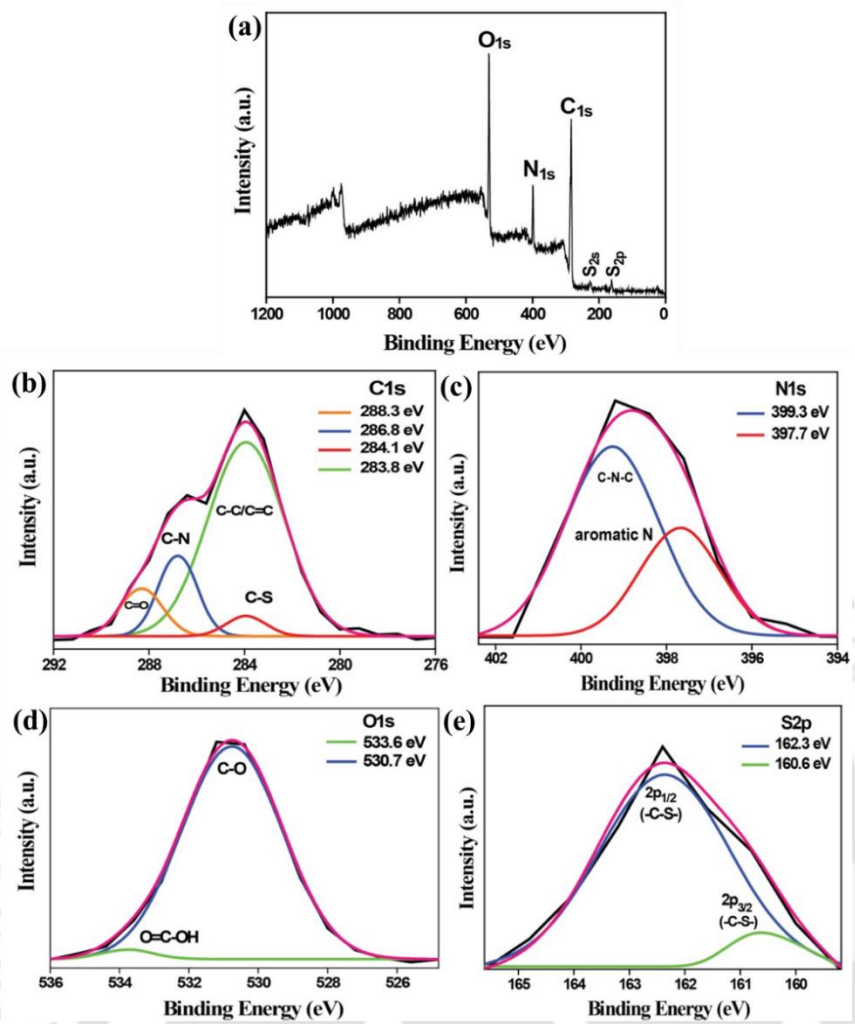

Figure 4.3. (a) XPS analysis plot for Cdots, showing the presence of C, N, O and S. Deconvoluted XPS results for (b) C_{1s}, (c) N_{1s}, (d) O_{1s} and (e) S_{2p} peaks in Cdots.

Table 4.2. Atomic concentration table of the as-synthesized carbon dots calculated based on XPS data.

P-Cdots (atomic %)		Cdots (without phosphorus-doped) (atomic %)	
C	47.44	C	63.53
N	13.57	N	13.49
O	32.23	O	21.44
S	4.08	S	1.54
P	2.68	-	-

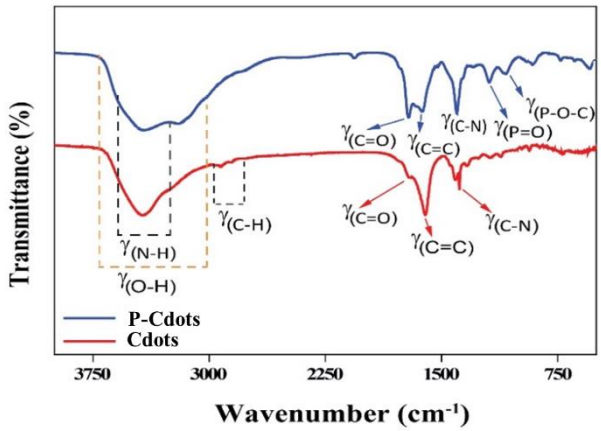

Figure 4.4. FTIR spectra of P-Cdots and Cdots.

XPS data were further corroborated by Fourier-transform infrared (FTIR) spectroscopy (Figure 4.4). In P-Cdots, peaks emerged at 1712 cm^{-1} and 1626 cm^{-1} due to C=O and C=C stretching vibrations, respectively, were similar to those in Cdots as well.[10] Besides, a strong signal was found at 1404 cm^{-1} due to C-N stretching, which was also present in Cdots, but with comparatively less intensity at 1385 cm^{-1}. Furthermore, peaks appearing at 1194 cm^{-1} and 1083 cm^{-1} can be attributed to P=O and P-O-C stretching vibrations in P-Cdots and these intense peaks were particularly absent in Cdots. [11] The results further confirmed the presence of phosphorus in the as-synthesized P-Cdots.

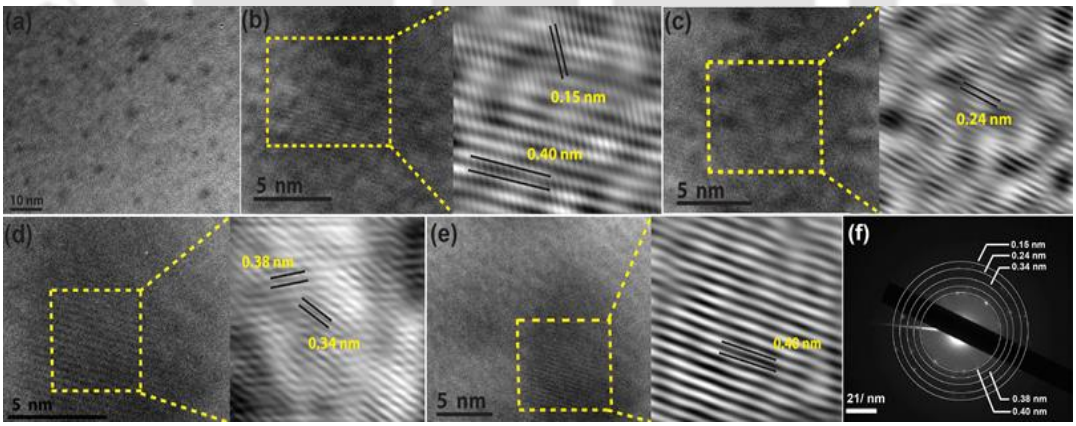

Figure 4.5. (a) TEM image of P -Cdots. High-resolution TEM (HRTEM) and corresponding inverse fast Fourier transform (IFFT) images, recorded for P-Cdots with corresponding d-spacing of (b) 0.15 nm, 0.40 nm, (c) 0.24 nm, (d) 0.34 nm, 0.38 nm and (e) 0.40 nm. (f) Corresponding selected area electron diffraction (SAED) patterns.

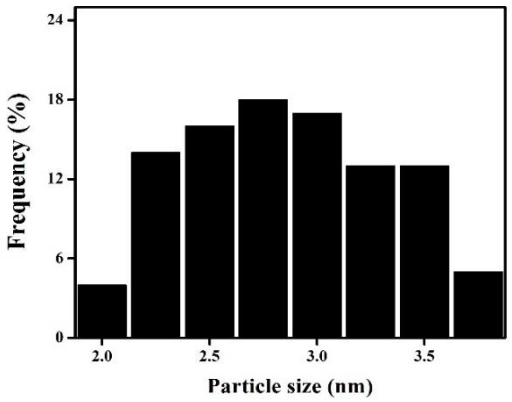

Figure 4.6. Particle size distribution of P-Cdots. The distribution was calculated using several TEM images (with 100 particles).

Next, we performed transmission electron microscopy (TEM) to explore the structure and morphologies of the two types of carbon nano dot systems. Figure 4.5.a, corresponding to the TEM image of P-Cdots, suggests the formation of uniform spherical particles with an average size of 2.8 ± 0.8 nm (Figure 4.6). Significantly, we discovered that the as-synthesized P-Cdots were exceptionally crystalline in nature, as is evident from the high-resolution TEM (HRTEM) measurements (Figure 4.5.b-e) and sharp patterns in the selected area electron diffraction (SAED) study (Figure 4.5.f). Typical HRTEM images and corresponding IFFT patterns in Figure 4.5.b-e confirmed the presence of several distinct fringes in P-Cdots with lattice spacings of 0.15 nm, 0.24 nm, 0.34 nm, 0.38 nm, and 0.40 nm.

On the other hand, TEM analysis of the Cdots (with a relatively larger size of 6.5 ± 1.5 nm, Figure 4.7.a and b) revealed their predominantly amorphous, quasi-graphitic nature. The HRTEM results in Figure 4.7c and d confirmed a single lattice spacing of 0.28 nm corresponding to the (020) diffraction plane (Figure 4.7.e) of graphite carbon, agreed well with earlier reports.[12] However, no additional planes were found in the SAED pattern of Cdots. Therefore, from the results of TEM analysis we presumed that doping of phosphorus could help induce a highly crystalline order in the structure.

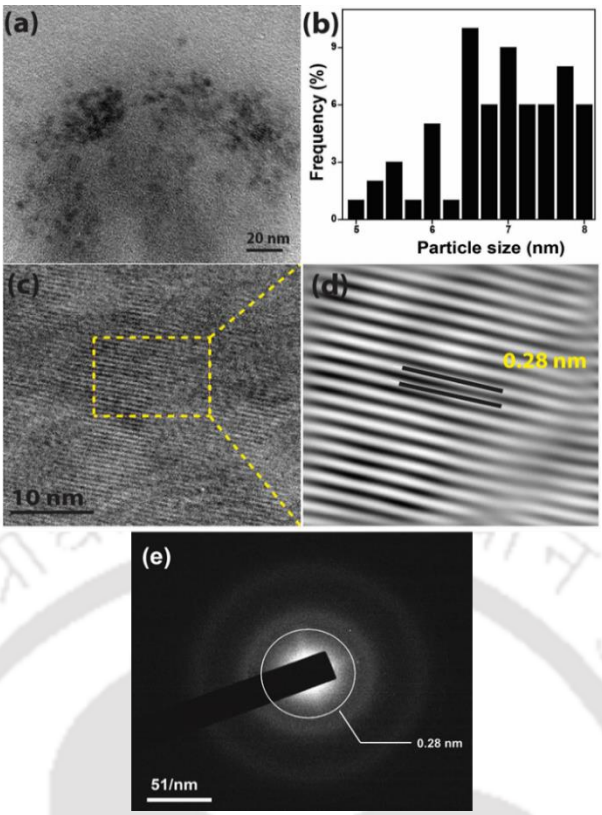

Figure 4.7. (a) TEM image of Cdots. (b) Particle size distribution of Cdots. Average calculated size was 6.5±1.5 nm. The distribution was calculated using several TEM images (with 100 particles). (c) HRTEM and (d) IFFT images corresponding to the d-spacing of 0.28 nm. (e) SAED pattern of Cdots.

After observing the exceptional polycrystalline nature of P-Cdots in TEM, we further investigated those by powder X-ray diffraction (powder XRD) analysis to confirm crystal quality and its origination.

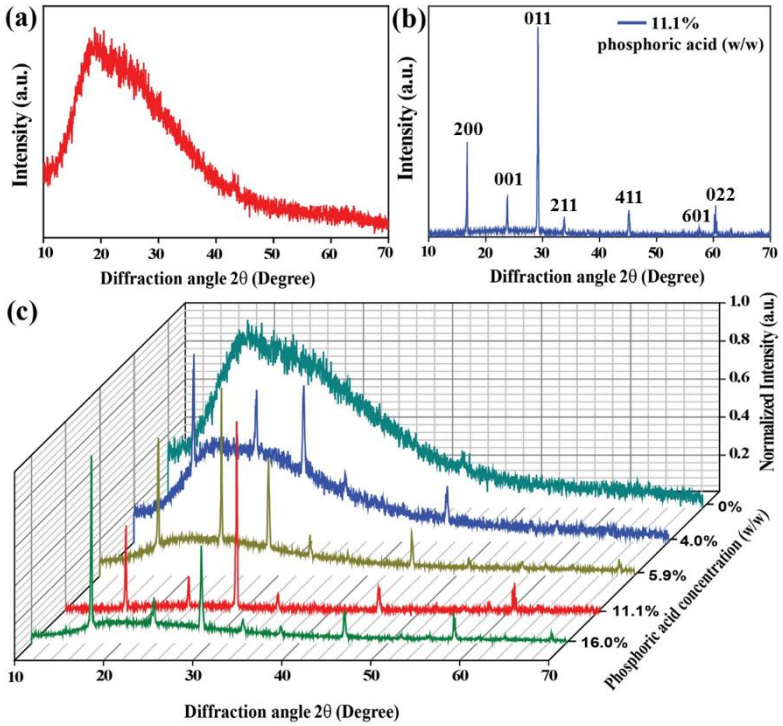

Figure 4.8. Powder X-ray diffraction patterns (powder XRD) of (a) amorphous Cdots (without phosphorus doping) and (b) crystalline P-Cdots. (c) Powder XRD patterns of P-Cdots with different phosphoric acid concentrations, added to the reaction mixture such as 0% (no phosphorus doping), 4.0%, 5.9%, 11.1% and 16.0%. The maximum crystalline nature was achieved at an optimum phosphoric acid input concentration of 11.1% (w/w).

The powder XRD patterns of both Cdots and P-Cdots are presented in Figure 4.8.a and b. In the case of the Cdots, we found a low intensity broad diffraction peak, asymmetrically centered at a 2θ value of 20^{o} (Figure 4.8.a). This is indicative of an amorphous disordered structure in Cdots, consistent with the earlier reports.[13, 14] However, the diffraction pattern of P-Cdots (with H_3PO_4:11.1% (w/w)) consisting of sharp peaks was remarkable. The results revealed the formation of a well-ordered highly crystalline structure (Figure 4.8.b) in the P-Cdots, supporting the aforementioned TEM results. As represented in Figure 4.8.b, the XRD pattern of P-Cdots included sharp peaks at 2θ = 16.7 ^{o}, 23.7 ^{o}, 29.0 ^{o}, 33.6 ^{o}, 45.05 ^{o} and 60.26 ^{o}. Besides, some additional peaks at higher angles were also observed, though with less intensity, demonstrating the highly ordered structure in P-Cdots. Subsequently, we found a gradual change in the degree of crystallinity during X-ray diffraction analysis of P-Cdots with varying phosphorus doping percentages (Figure 4.8.c). Figure 4.8.c and Figure 4.9 clearly substantiate that increasing the phosphorus content up to a certain value in P-Cdots increased the crystalline nature. The finest diffraction pattern with the

lowest amorphous background and maximum number of crystalline peaks was observed for the sample prepared with a phosphoric acid concentration of 11.1% (w/w).

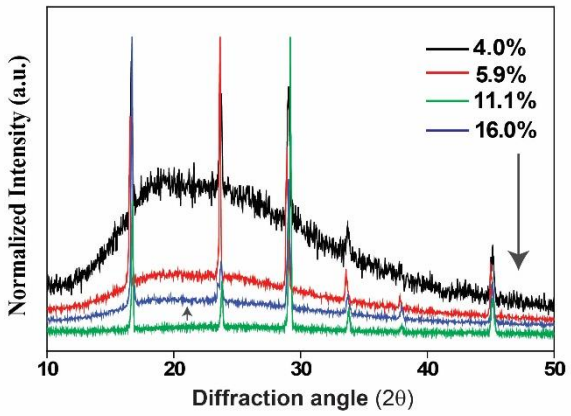

Figure 4.9. Enlarged image of the amorphous part of P-Cdot X-ray diffraction patterns with different phosphoric acid input ratios, showing continuous decrease in the intensity for amorphous region (I^{am}) with increasing phosphorus percentage. After 11.1 % (w/w), further increase in the amorphous content in P-Cdot system was observed. Calculated intensity ratio was found to be $I_{4.0}^{am} : I_{5.9}^{am} : I_{11.1}^{am} : I_{16.0}^{am}$ = 1: 0.4: 0.05: 0.23.

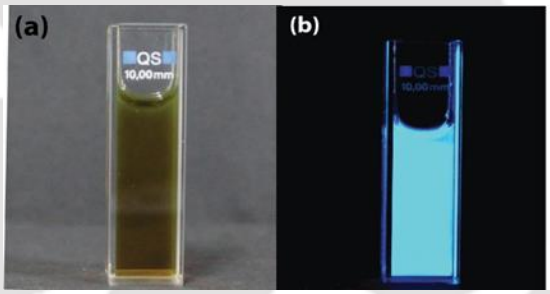

Figure 4.10. (a) Dark brown dispersion obtained, after dilution following synthesis of P-Cdots under visible light. (b) P-Cdot dispersion under UV light (365 nm).

In order to confirm the exceptional crystalline nature in P-Cdots, caused by phosphorus doping, additional control experiments under the same reaction conditions were carried out. Interestingly, microwave treatment of the starting materials with different possible combinations such as only thiourea in the presence of phosphoric acid or only citric acid monohydrate in the presence of phosphoric acid did not result in any carbon dots formation under similar experimental conditions (Figure 4.11.a and b; 4.11.c and d). Previous studies reported formation of amorphous carbon dots from only citric acid using high temperature pyrolysis for longer duration.[15] In our case, treatment of only citric acid monohydrate with microwave resulted in unsuccessful carbon dot

formation under the applied reaction conditions (Figure 4.11. e and f). An additional experiment, such as the reaction between citric acid monohydrate and urea (instead of thiourea) in the presence of phosphoric acid, was also performed to ascertain the role of phosphorus in achieving crystalline carbon dots. First, carbon dot formation was confirmed by PL measurements (Figure 4.12. a and b), which unveiled wavelength tunable emission properties in both the systems. Interestingly, in this carbon dot system (having no S), we observed phosphorus induced crystallinity as well, along with identical XRD pattern and similar peak positions (Figure 4.12. c and d).

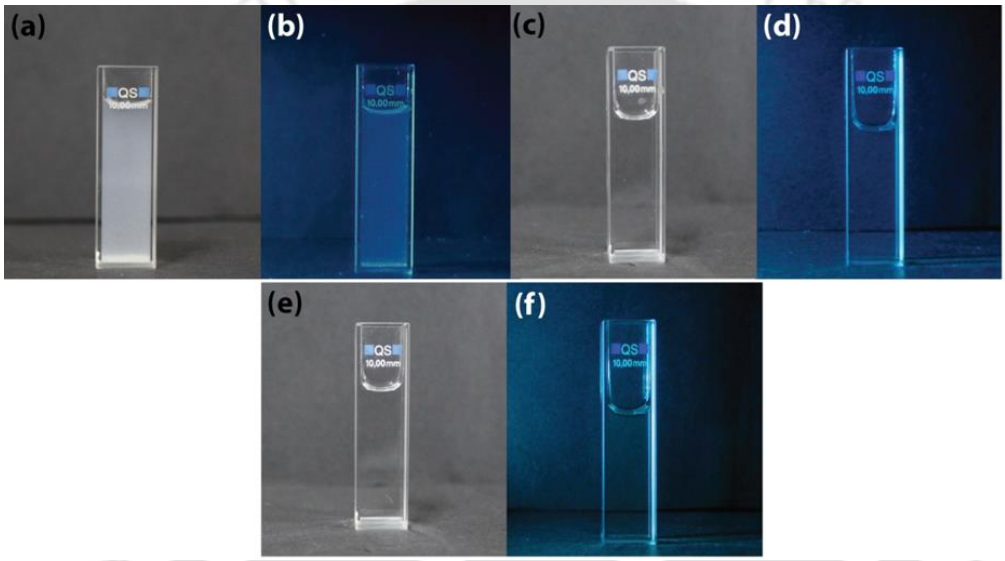

Figure 4.11. Control experiments. (a) Dispersion of the unreacted material obtained after microwave treatment of thiourea and phosphoric acid followed by dilution. (b) Dispersion under UV light (365 nm). No emission was observed, confirming unsuccessful synthesis of Cdots. (c) Dispersion of the material obtained after microwave treatment of citric acid monohydrate and phosphoric acid followed by dilution. (d) Dispersion under UV light (365 nm). In this case no emission was found due to no carbon dot formation. (e) Aqueous dispersion of the material obtained after microwave treatment of only citric acid monohydrate followed by dilution. (f) Solution under UV light (365 nm) having no photoluminescence.

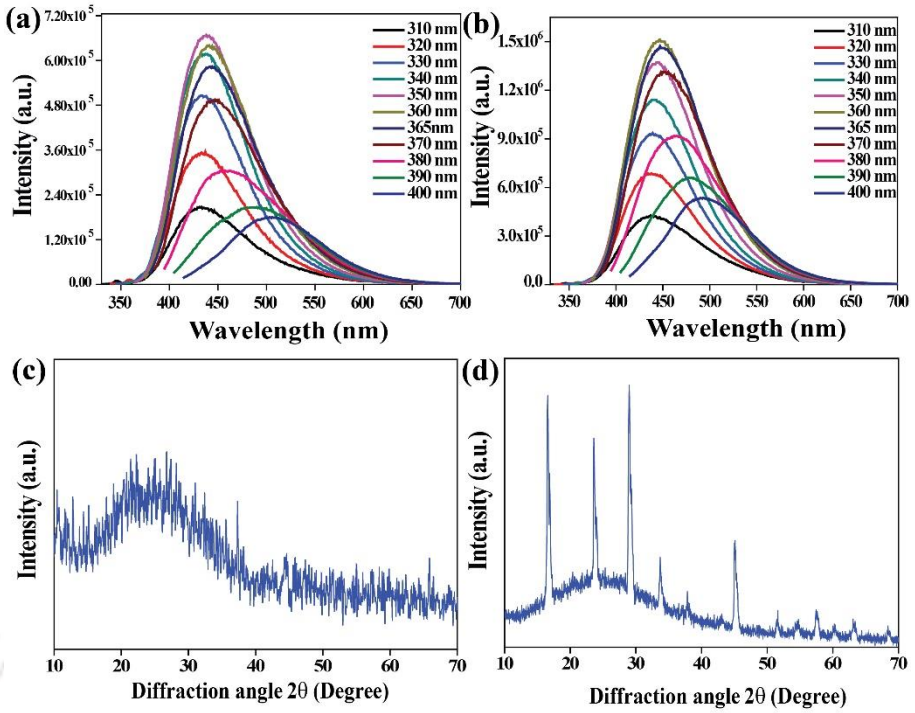

Figure 4.12. Wavelength tunable emission spectra of resultant materials, synthesized from (a) citric acid monohydrate and urea, (b) citric acid monohydrate and urea in presence of phosphoric acid (11.1 %, w/w as the phosphorus source) confirming the formation of carbon dots during microwave treatment of aforementioned starting materials. Powder XRD pattern of the carbon dots without phosphorus inside the structure (c) and with phosphorus, doped inside the structure (d). All reaction parameters such as microwave power, starting materials' amount (210 mg) were similar as mentioned in the experimental section.

The results presented above suggested that doping of phosphorus not only induced very high macro-crystallinity in P-Cdots but also helped in improving the structural order within the carbon nanostructure. On the other hand, the presence of nitrogen facilitates the formation of polycyclic fragments in the carbon nano structures under applied reaction conditions.

Furthermore, we performed structural analyses *via* the LeBail method using the Fullprof suite of utilities (Figure 4.13.a) to solve the powder XRD pattern of P-Cdots, which was obtained with a Rigaku TTRAX-III instrument. The instrumental parameters (such as the illuminated area outside the sample) were carefully recorded and were utilized during pattern refinement.

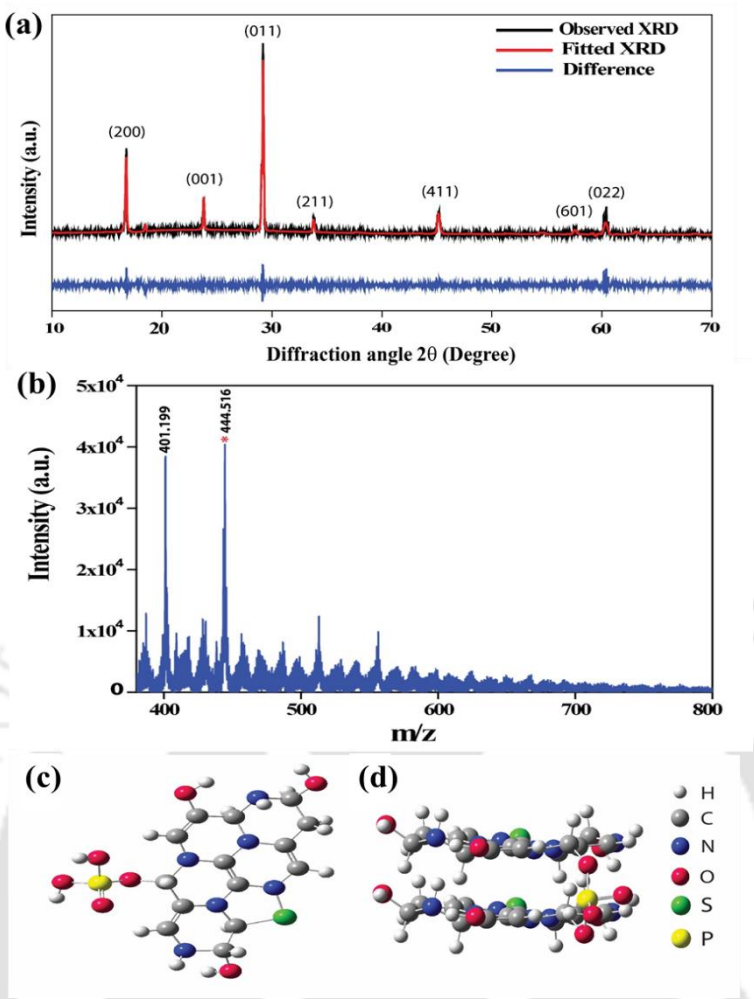

Figure 4.13. (a) Computational refinement of the powder XRD pattern of P-Cdots (11.1% (w/w)). The black line corresponds to the observed pattern and red line is for the calculated LeBail fit. Blue line shows difference between observed and fitted plots in the crystal structure. (b) MALDI-TOF mass spectrum of P-Cdots. Major sharp peak (m/z 444.516) corresponding to molecular formula of $C_{14}H_{17}N_6O_7PS$ in P-Cdot structure is identified. Another intense peak (m/z 401.19) is due to the product following loss of -CH (OH) NH- fragment and subsequently termination of two hydrogen atoms (M_w = 2.02) into the primary building unit. (c) Representative schematic of the proposed smallest repeating unit in crystalline P-Cdot structure (top view) (molecular formula $C_{14}H_{17}N_6O_7PS$) (d) Horizontal view of the phosphate ligated bilayer structure.

The crystal structure that matched well with the best fitted value had an orthorhombic unit cell with space group P_{mmm} and unit cell parameters of a = 10.6211 Å, b = 5.3899 Å, c = 3.7471 Å and $\alpha=\beta=\gamma=90^o$. We found that the calculated d-spacing values of 0.15 nm, 0.24 nm, 0.35 nm and 0.37 nm with orthorhombic crystal structure, obtained via computational refinement, matched well with the values obtained from the SAED pattern and HRTEM analysis for P-Cdots. Besides, we could also assign indices

to the higher-angle peaks in the powder XRD results via corresponding computational refinement, which are included in Table 4.3 along with the assigned *hkl* values.

Table 4.3. Calculated *hkl* plains and corresponding d-spacing values of the diffraction plains obtained after computational refinement of the P-Cdot XRD pattern.

Diffraction angle (2θ) (degree)	*hkl*	d-spacing (Å)
16.681	200	5.31053
23.726	001	3.74714
25.182	101	3.53367
28.998	011	3.07668
33.723	211	2.66217
37.833	410	2.38192
45.064	411	2.01017
57.536	601	1.60057
60.260	022	1.53834

Next, in order to find the mass of the plausible structural units of P-Cdots, we performed matrix-assisted laser desorption/ionization time-of-fight mass spectrometry (MALDI-TOF MS) in 2, 5-dihydroxybenzoic acid (DHB) matrix. The spectrum reproducibly exhibited intense sharp peak at m/z 444.516 (Figure 4.13.b). Taking note of the fact that the starting reagents comprised of thiourea and citric acid monohydrate in ~ 3:1 molar ratio, the carbonization that took place under the reaction conditions was likely to lead to fused polycyclic rings that contain fragments resembling citrazinic acid. Multiple layers of such fragments could then be connected via phosphate groups to bring a crystalline order to carbon dots and their aggregates. Based upon the entire structural and compositional information obtained from the analyses as indicated above, a representative phosphate ligated fragment with nominal molecular formula of $C_{14}H_{17}N_6O_7PS$ (formula weight 444.36 g/ mol) is schematized as the smallest repeating unit in the P-Cdot structure. Corresponding structural formula unit is represented as a ball-and-stick model in Figure 4.13. c and d.

It is noteworthy that carbon dots are formed through two successive steps: polymerization followed by carbonization. During the synthesis of P-Cdots, presence of

phosphoric acid made the reaction highly exothermic. This would allow rapid condensation polymerization of starting materials along with generation of excess heat. We surmise that in consequent steps, the excess heat was utilized for high temperature carbonization, which led to the growth of highly ordered structure inside carbon core. Besides, we observed considerable decrease in the particle size in P-Cdots in comparison with Cdots. We assume that, introduction of phosphorus into carbon nanostructure restricted the catenation property of carbon, thus inhibiting continuous uncontrolled growth of carbogenic fragments during the polymerization followed by high temperature carbonization.

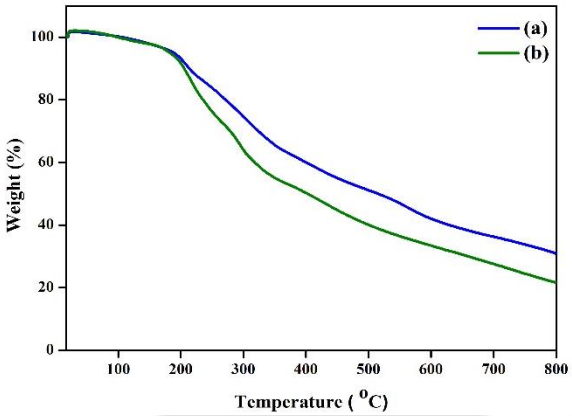

Figure 4.14. Thermogravimetric study corresponding to (a) P-Cdots and (b) Cdots. The analyses were carried out in argon atmosphere at a heating rate of 10 °C/ min.

Thermal stability studies of the two carbon dots were carried out under argon atmosphere. As represented in Figure 4.14, the rate of weight loss for P-Cdots was less as compared to that of Cdots, suggesting higher thermal stability of the P-Cdots than Cdots. Initial minor weight loss for both the materials up to 200 °C was due to elimination of water. After that, subsequent weight loss up to 800 °C was due to continuous degradation of carbogenic framework.

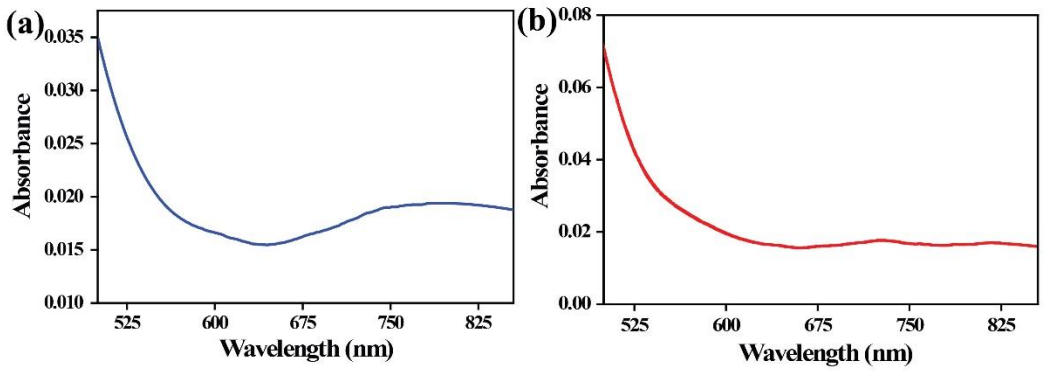

Figure 4.15. NIR absorption spectra of (a) P-Cdot and (b) Cdot. In P-Cdot spectrum, broad absorption band was observed in the range of 700-850 nm. For Cdots broad absorption was observed as well, with two minor intensity absorption peaks around 730 nm and 820 nm.

Finally, we accomplished a comparative study on the photothermal activity of the two carbon dots. We chose this particular implementation due to several reasons. First, the synthesized carbon dots, absorb well in near-infrared (NIR) region (Figure 4.15) and significantly, 52% of total solar energy come from NIR radiation. [16] Second, carbon dots can be synthesized by processes that are more economical and scalable as compared to other materials which researchers have earlier used for this purpose. To confirm the photothermal activity of P-Cdots and Cdots in water, we first studied the rise in temperature of the dispersions due to NIR-laser irradiation (2W, 808 nm IR laser). Details are mentioned in experimental section. Upon irradiation with the laser source, though we found both the carbon dots caused a rise in the temperature of the dispersion, P-Cdots were found to be more efficient than Cdots. Figure 4.16. a and b represent concentration dependent heating of the aqueous medium in presence of P-Cdots and Cdots. Notably, we found that in presence of P-Cdots (with concentration up to 250 mg/mL) the maximum average temperature reached to 89.5 ^{o}C from room temperature (25.1 ^{o}C) in 8 min (Figure 4.16.a), and, on the other hand, for Cdots (250 mg/mL), though less, maximum average temperature reached up to 67.7 ^{o}C (Figure 4.16.b) under identical experimental conditions.

In order to probe further the enhanced photothermal performance due to phosphorus doping, similar experiments were performed with P-Cdots, synthesized from different phosphoric acid input concentrations (i.e., 0 % (no phosphorus doping), 4.0 %, 5.9 %, 11.1 % and 16.0 %). Figure 4.17 clearly demonstrates that increasing phosphorus input amount in carbon dots during synthesis caused a steady rise in the temperature of their corresponding aqueous dispersions, irradiated with 808 nm laser up

to an optimum concentration of 11.1% (w/w). The temperature of carbon dot dispersion decreased under same experimental conditions when phosphoric acid input concentration was increased further (i.e. in case of 16%). This trend strongly correlates with the trend in crystallinity of the phosphorus doped carbon dots. Thus, it is the crystallinity, and not the mere amount of phosphorus present in carbon nanostructure that helps achieving the enhanced photothermal conversion.

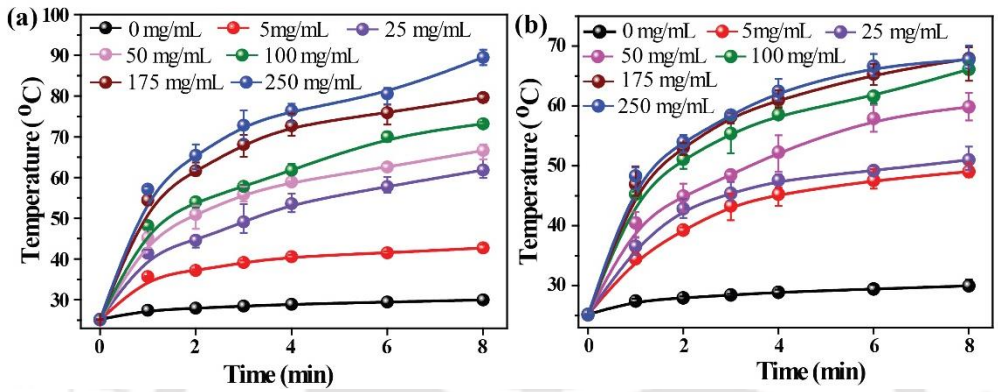

Figure 4.16. Concentration dependent temperature increase of (a) P-Cdot - water dispersion and (b) Cdot - water dispersion in the presence of 808 nm laser irradiation at various time intervals.

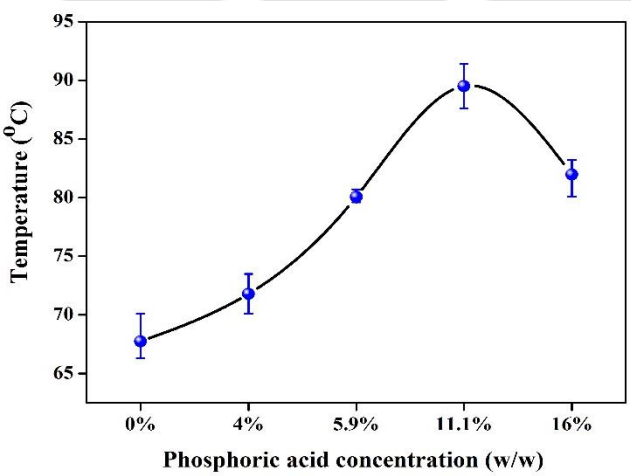

Figure 4.17. Photothermal study of P-Cdot - water dispersion (250 mg/mL) under 808 nm laser irradiation (for 8 min). Different concentrations of phosphoric acid were added prior to microwave treatment such as 0 % (no phosphorus doping), 4.0 %, 5.9 %, 11.1 % and 16.0 %. The temperature in the y-axis refers to the dispersion temperature. The maximum temperature was achieved at an optimum phosphoric acid input concentration of 11.1% (w/w).

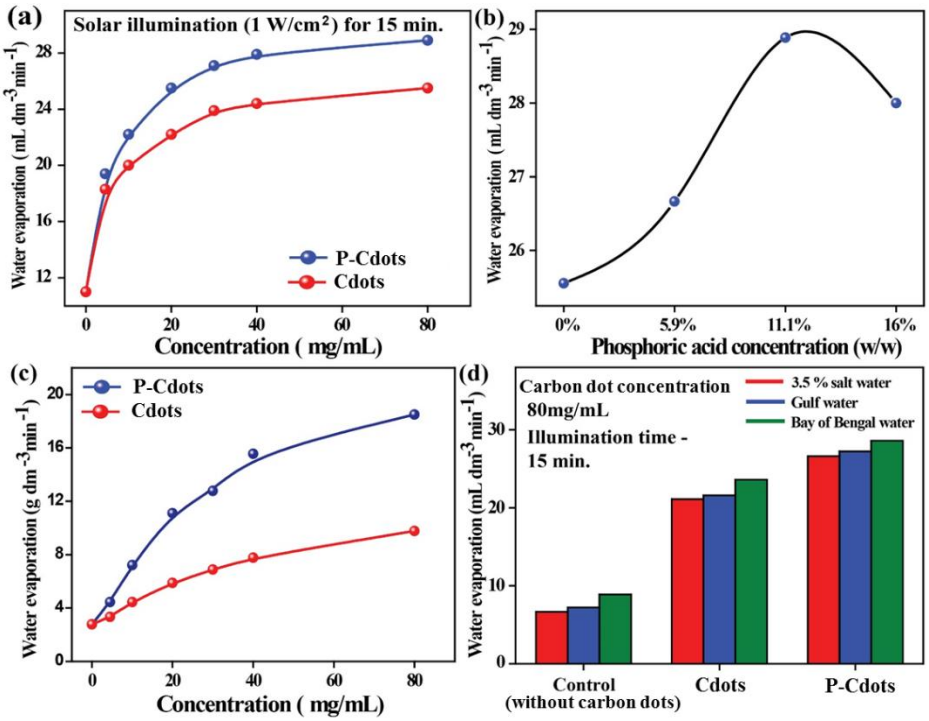

Figure 4.18. (a) Plot showing carbon dot concentration dependent water evaporation under solar illumination at 35 mbar. (b) Solar light assisted water evaporation in presence of P-Cdots (80 mg/mL), synthesized with different phosphoric acid concentrations (0%, 5.9%, 11.1%, 16%) as added to the reaction mixture. Evaporation was maximum with P-Cdots synthesized from 11.1 % (w/w) phosphoric acid. (c) Water evaporation in presence of different P-Cdot and Cdot concentrations under standard atmospheric pressure and simulated solar illumination (1W/ cm^2, 15 min illumination time). (d) Extent of sea water desalinated using as-synthesized carbon dots (80 mg/ mL) under solar illumination at 35 mbar.

Further, in order to substantiate efficient light-to-heat conversion by the carbon dots, water evaporation experiments with different carbon dot concentrations were carried out under simulated concentrated solar illumination (1 W/cm^2) using rotary evaporator assisted vertical condensation technique. Figure 4.18.a substantiates that, addition of carbon dots helped in achieving faster and efficient water evaporation under simulated solar illumination and 35 mbar pressure, as compared to the control sample of water, without any carbon dots. Interestingly, as shown in Figure 4.18.a, adding up to 80 mg/mL of P-Cdots in water could result in 43.5% evaporation of the initial volume within 15 min, with the evaporation rate of 28.9 mL dm^{-3} min^{-1}. Cdots, on the other hand, could evaporate 38.3 % of the initial volume in the same time interval with 25.5 mL dm^{-3} min^{-1} evaporation rate. Also, as demonstrated in Figure 4.18.b, water evaporation efficiency was maximum for 11.1 % (w/w) phosphoric acid, added during

carbon dot synthesis. This result further confirmed the effect of higher crystallinity in achieving higher photothermal effect as well as efficient solar thermal evaporation using as-synthesized carbon nanomaterial. Evaporation efficiencies of both the carbon dots were calculated taking different concentrations of carbon dots, dispersed in aqueous medium under standard atmospheric pressure (Figure 4.18.c). Calculated solar thermal evaporation efficiencies for P-Cdots and Cdots were found to be 83.6 % and 44.2 %, respectively, under standard atmospheric pressure (Table 4.4). It is essential to note that typically, when photon absorption material is dispersed in the bulk of the liquid to be evaporated, the energy conversion efficiency remains low due to heat dissipation in the entire liquid volume. [17] This trend is followed by the Cdots. However, despite bulk-liquid dispersion, the P-Cdots are able to yield an evaporation efficiency that is higher than the efficiencies previously reported for bulk-heated systems [18] and even surface-heated systems[19] under similar solar illumination intensity. The above result substantiates P-Cdot as a significantly higher efficient material for solar assisted light-to-heat conversion and water evaporation.

Table 4.4. Calculated efficiencies for evaporation by P-Cdots and Cdots under simulated concentrated solar illumination (1W/cm^2). Milli-Q^{TM} water of resistivity 18 MΩ.cm without any additive was used as the control sample.

Sl. No.	Name of the Sample	η (%)
1.	Dispersion of 80 mg/mL P-Cdots in Milli-Q water	83.6
2.	Dispersion of 80 mg/mL Cdots in Milli-Q water	44.2
3.	Mili-Q water without any additive (control)	12.6

Finally, carbon dot assisted solar desalination was carried out taking three water samples with different salinities. Initially measured salinity and pH of the water samples (collected from the Bay of Bengal, Persian Gulf water, and the sample with average sea water salinity) are mentioned in Table 4.5. As shown in Figure 4.18.d, presence of carbon dots significantly improved sea-water evaporation rate compared to control experiment, performed without Cdots. Importantly, P-Cdots were found to be more efficient than Cdots. Maximum desalination rate was achieved with P-Cdots in the Bay of Bengal water sample (28.6 mL dm^{-3} min^{-1}; 43.0 % evaporation of the initial volume taken, in 15 min), which was higher than that in presence of Cdots (23.6 mL

dm^{-3} min^{-1}; 35.5 % evaporation in 15 min) and the control experiment (without any Cdots, 8.8 mL dm^{-3} min^{-1}; 13.3 % evaporation of the initial volume for the Bay of Bengal water sample). After the desalination process salinity of collected water samples were further measured and are included in Table 4.6 as well. Average dissolved salt concentrations after P-Cdot and Cdot assisted purifications were measured to be 0.02 psu and 0.016 psu respectively, which are well within the limits of the permissible level in safe drinking water (0.2 psu).[20] After conducting the solar-based seawater desalination experiment, the carbon dots were left in the reaction vessel along with residual seawater, forming a brown slurry. In the subsequent cycle, desalination experiment was conducted after adding more seawater (equal in volume to the evaporated seawater) to the remaining slurry. This process was repeated for multiple cycles, in order to check the effect of excess salt concentration on carbon dot evaporation performance. Figure 4.19 clearly shows that P-Cdots can retain up to 78% (water evaporation rate: 27 mL dm^{-3} min^{-1} after first cycle; 21.1 mL dm^{-3} min^{-1} after the completion of ninth cycle) of their original desalination rate even after ninth cycle of usage, without any backflush with freshwater in between. Additionally, in order to remove excess marine salts from carbon dots after desalination, dialysis was pursued for both the carbon dots. After 24 h of purification, the average salt concentrations were measured to be 0.11 psu for P-Cdots dispersion and 0.16 psu for Cdots dispersion.

Table 4.5. Measured salinity with corresponding pH values of the collected water samples before purification.

Sample	Salinity (psu)	pH
Persian Gulf water	39.51	7.59
3.5 % dissolved salt water	33.52	6.91
Water sample collected from the Bay of Bengal	21.07	7.67

Table 4.6. Salinity with corresponding pH values of the collected water samples measured after carbon dot assisted purification through evaporation.

Sample	**Gulf water**		**Sample with average sea water salinity (3.5 %)**		**Bay of Bengal water**	
Analyte concentration- 80 mg/ mL	Salinity	pH	Salinity	pH	Salinity	pH
P-Cdots	0.01	6.38	0	5.98	0.05	6.81
Cdots	0.02	6.32	0.02	5.50	0.01	6.22

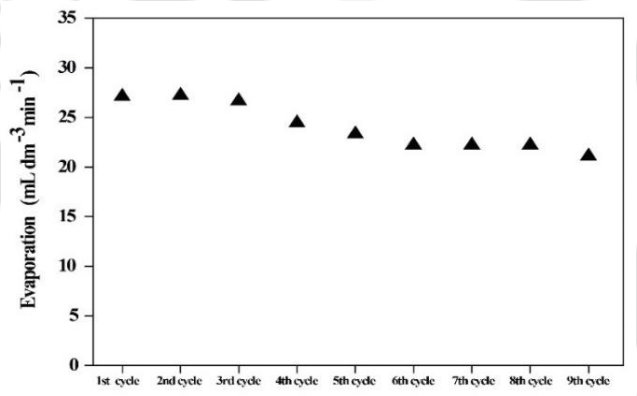

Figure 4.19. Solar light assisted desalination performance by P-Cdots during several cycles. In each cycle 80 mg/mL Cdot dispersion was illuminated under 1 W/cm^2 simulated concentrated solar light. After ninth cycle, P-Cdots retained up to 78% of the original desalination rate in first cycle (water evaporation rate: 27 mL dm^{-3} min^{-1} after first cycle; 21.1 mL dm^{-3} min^{-1} after the completion of ninth cycle).

The photothermal conversion efficiency of nanomaterial dispersion is directly proportional to the photon absorption cross section and thermal conductivity of the material.[21] Cdots and P-Cdots exhibit similar UV-vis and NIR absorption trends. Further, calculated mass extinction coefficient (ε) for Cdot was 0.98 × 10^3 mL g^{-1} cm^{-1} and that for P-Cdot was 0.93× 10^3 mL g^{-1} cm^{-1} at 808 nm wavelength (Figure 4.20). This indicates that increased photon absorption cross section is not the significant factor for enhancement of photothermal performance by P-Cdots in present study. However, as indicated by the low luminescence quantum yield values, a large portion of the absorbed radiation might have been converted into phononic rather than photonic energy. Further, comprehensive experimental evidences, as discussed in preceding

sections, revealed that the photothermal conversion ability of the P-Cdot was correlated to the extent of crystallinity rather than to the dopant content. It is likely that the heat transport within the bulk of the P-Cdots was enhanced on account of their high crystallinity, which is expected to reduce phonon scattering losses.[22] The distance between the fused polycyclic layers in P-Cdots (0.374 nm) is higher than the interlayer spacing of 0.28 nm between the quasi-graphitic layers in Cdots. This 'opening up' of the layer structure on account of intercalated phosphates is likely to assist with enhanced heat transfer from the P-Cdot to the solvent. Thus, we propose that the enhancement in phonon transport and transfer due to crystallinity in structure resulted in the improved photothermal performance of the P-Cdot in overall study.

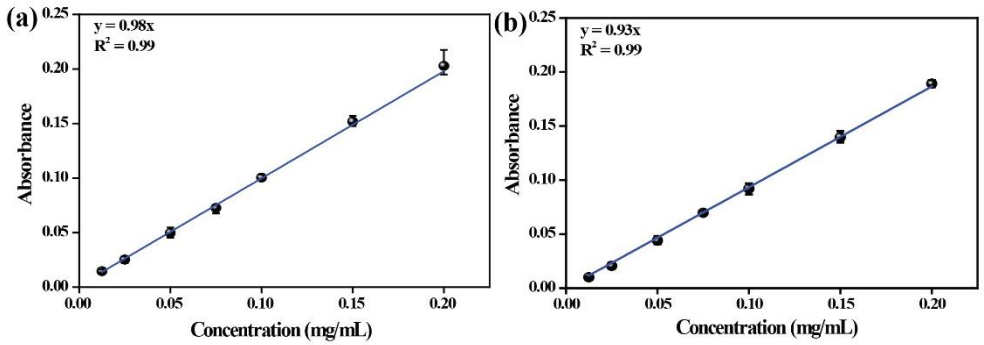

Figure 4.20. Concentration dependent absorbance measurement for (a) Cdots and (b) P-Cdots. Experiments were carried out by taking 0.2 mg/mL, 0.15 mg/mL, 0.1 mg/mL, 0.075 mg/mL, 0.05 mg/mL, 0.025 mg/mL and 0.0125 mg/mL of both the samples in cuvettes with path length (l) of 1 cm.

During experiments path length (l) was 1 cm (10 mm).

For Cdots, $\frac{A}{c}$ = 0.98 $(mg/mL)^{-1}$ (obtained from the slope of Figure 4.20.a)

Hence, $\varepsilon = 0.98/1$ $(mg/mL)^{-1}$ cm^{-1}

= 0.98 mL mg^{-1} cm^{-1}

= 0.98 × 10^3 mL g^{-1} cm^{-1}

Similarly, in case of P-Cdots, $\frac{A}{c}$ = 0.93 $(mg/mL)^{-1}$ and calculated mass extinction coefficient (ε) = 0.93 × 10^3 mL g^{-1} cm^{-1} (Figure 4.20.b).

4.3 Conclusion. In conclusion, we have designed an advanced synthetic technique for generating crystallinity in carbon dots by doping phosphorus (P-Cdots) into a carbon nanostructure. Based on detailed experimental analyses followed by computational refinement, we propose formation of the orthorhombic crystalline pattern of the unit cell in the carbon dot structure. This excellent crystallinity made P-Cdots conducive to efficient light-to-heat conversion and solar light assisted sea water desalination. We observed that, in the presence of P-Cdots and Cdots, the temperature of aqueous medium could rise up to 89.5 ^{o}C and 67.7 ^{o}C, respectively, within 8 min under NIR-laser irradiation. Besides, bulk solar photothermal evaporation efficiency was measured to be to 83.6% for the as-prepared crystalline P-Cdots, which was much higher than that of the Cdots (having limited graphitic crystallinity; η = 44.2 %). To the best of our knowledge, achieving a highly ordered crystalline structure in carbon dots is exceptional, and may prove crucial in the near future for their far-reaching applications in metal-free photothermal conversion, organic photovoltaics and organic electronics research.

References:

1. Zhang, L.; Tang, B.; Wu, J.; Li, R.; Wang, P. Hydrophobic Light-to-Heat Conversion Membranes with Self-Healing Ability for Interfacial Solar Heating. *Adv. Mater.* **2015**, *27*, 4889-4894.

2. Ding, H.; Yu, S. B.; Wei, J. S.; Xiong, H. M. Full-Color Light-Emitting Carbon Dots with a Surface-State-Controlled Luminescence Mechanism. *ACS Nano* **2016**, *10*, 484-491.

3. Roy, P.; Chen, P. C.; Periasamy, A. P.; Chen, Y. N.; Chang, H. T. Photoluminescent Carbon Nanodots: Synthesis, Physicochemical Properties and Analytical Applications. *Mater. Today* **2015**, *18*, 447-458.

4. Kim, S.-O.; Manthiram, A. The Facile Synthesis and Enhanced Sodium-storage Performance of a Chemically Bonded CuP_2/C Hybrid Anode. *Chem. Commun.* **2016**, *52*, 4337-4340.

5. Qi, W.; Zhao, H., Wu, Y.; Zeng, H., Tao, T.; Chen, C.; Kuang, C.; Zhou, S.; Huang, Y. Facile Synthesis of Layer Structured GeP_3/C with Stable Chemical Bonding for Enhanced Lithium-Ion Storage. *Sci. Rep.* **2017**, *7*, 43582.

6. Liu, S.; Tian, J.; Wang, L.; Zhang, Y.; Qin, X.; Luo, Y.; Asiri, A. M.; Al-Youbi, A. O.; Sun, X. Hydrothermal Treatment of Grass: A Low-Cost, Green Route to Nitrogen-Doped, Carbon-Rich, Photoluminescent Polymer Nanodots as an Effective Fluorescent Sensing Platform for Label-Free Detection of Cu(II) Ions. *Adv. Mater.* **2012**, *24*, 2037-2041.

7. Liu, J.; Lu, S.; Tang, Q.; Zhang, K.; Yu, W.; Sun, H.; Yang, B. One-step Hydrothermal Synthesis of Photoluminescent Carbon Nanodots with Selective Antibacterial Activity Against Porphyromonas Gingivalis. *Nanoscale* **2017**, *9*, 7135-7142.

8. Xu, Q.; Liu, Y.; Gao, C.; Wei, J.; Zhou, H.; Chen, Y.; Dong, C.; Sreeprasad, T. S.; Li, N.; Xia, Z. Synthesis, Mechanistic Investigation, and Application of Photoluminescent Sulfur and Nitrogen Co-doped Carbon Dots. *J. Mater. Chem. C* **2015**, *3*, 9885-9893.

9. Wang, C.; Sun, D.; Zhuo, K.; Zhang, H.; Wang, J. Simple and Green Synthesis of Nitrogen-, Sulfur and Phosphorus-co-doped Carbon Dots with Tunable Luminescence Properties and Sensing Application. *RSC Adv.* **2014**, *4*, 54060-54065.

10. Liu, Y.; Xiao, N.; Gong, N.; Wang, H.; Shi, X.; Gu, W.; Ye, L. One-step Microwave-assisted Polyol Synthesis of Green Luminescent Carbon Dots as Optical Nano probes. *Carbon N. Y.* **2014**, *68*, 258-264.

11. Wang, C.; Sun, D.; Zhuo, K.; Zhang, H.; Wang, J. Simple and Green Synthesis of Nitrogen-, Sulfur-, and Phosphorus-co-doped Carbon Dots with Tunable Luminescence Properties and Sensing Application. *RSC Adv.* **2014**, *4*, 54060-54065.

12. Zheng, M.; Liu, S.; Li, J.; Qu, D.; Zhao, H.; Guan, X.; Hu, X.; Xie, Z.; Jing, X.; Sun, Z. Integrating Oxaliplatin with Highly Luminescent Carbon Dots: An Unprecedented Theranostic Agent for Personalized Medicine. *Adv. Mater.* **2014**, *26*, 3554-3560.

13. Yang, Y.; Ji, X.; Jing, M.; Hou, H.; Zhu, Y.; Fang, L.; Yang, Chen, X. Q.; Banks, C. E. Carbon Dots Supported Upon N-doped TiO_2 Nano Rods Applied into Sodium and Lithium Ion Batteries. *J. Mater. Chem. A* **2015**, *3*, 5648-5655.

14. Liu, Y.; Zhou, L.; Li, Y.; Deng, R.; Zhang, H. Highly Fluorescent Nitrogen-doped Carbon Dots with Excellent Thermal and Photo Stability Applied as Invisible Ink for Loading Important Information and Anti-counterfeiting. *Nanoscale* **2017**, *9*, 491-496.

15. Bagheri, Z.; Ehtesabi, H.; Rahmandoust, M.; Ahadian, M.; Hallaji, Z.; Eskandari, F.; Jokar, E. New Insight into the Concept of Carbonization Degree in Synthesis of Carbon Dots to Achieve Facile Smartphone Based Sensing Platform. *Sci. Rep.***2017**, *7*, 11013.

16. Levinson, R.; Berdahl, P.; Akbari, H. Solar Spectral Optical Properties of Pigments-Part I: Model for Deriving Scattering and Absorption Coefficients from Transmittance and Reflectance Measurements. *Sol. Energy Mater. Sol. Cells* **2005**, *89*, 319-349.

17. Liu, Z.; Song, H.; Ji, D.; Li, C.; Cheney, A.; Liu, Y.; Zhang, N.; Zeng, X.; Chen, B.; Gao, J.; Li, Y.; Liu, X.; Aga, D.; Jiang, S.; Yu, Z.; Gan, Q. Extremely Cost-Effective and Efficient Solar Vapor Generation under Nonconcentrated Illumination Using Thermally Isolated Black Paper. *Glob. Challenges* **2017**, *1*, 1600003.

18. Durkaieswaran, P.; Murugavel, K. K. Various Special Designs of Single Basin Passive Solar Still - A Review. *Renew. Sustain. Energy Rev.* **2015**, *49*, 1048-1060.

19. Bae, K.; Kang, G.; Cho, S. K.; Park, W.; Kim, K.; Padilla, W. J. Flexible Thin-film Black Gold Membranes with Ultra Broad Band Plasmonic Nano Focusing for Efficient Solar Vapour Generation. *Nat. Commun.* **2015**, *6*, 10103.

20. Li, X.; Xu, W.; Tang, M.; Zhou, L.; Zhu, B.; Zhu, S.; Zhu, J. Graphene Oxide-based Efficient and Scalable Solar Desalination Under One Sun with a Confined 2D Water Path. *Proc. Natl. Acad. Sci.* **2016**, *113*, 13953-13958.

21. Neumann, O.; Urban, A. S.; Day, J.; Lal, S.; Nordlander, P.; Halas, N. J. Solar Vapor Generation Enabled by Nanoparticles. *ACS Nano* **2013**, *7*, 42-49.

22. Klett, J. W.; Mcmillan, A. D.; Gallego, N. C.; Walls, C. A. The Role of Structure on the Thermal Properties of Graphitic Foams. *J. Mater. Sci.* **2004**, *39*, 3659-3676.

Chapter 5

Zinc Ion Induced Assembly of Crystalline Carbon Dots with Excellent Supercapacitor Performance

Crystalline carbon dots with size of 3.2±1.0 nm have been assembled into 3D crystalline structures via complexation between Cdot surface functional groups (especially phosphate) and zinc ions (Zn^{2+}). The unprecedented crystalline nature in the Cdot assembly was investigated using spectroscopic and microscopic techniques. Experimental evidences suggest that addition of Zn^{2+} to crystalline Cdot dispersion resulted in a template free controlled growth of orthorhombic hopeite structures over the surface, which further assisted in initiating assembled crystalline Cdot system. Importantly, crystallinity in Cdot assembly helped in improving the electrochemical performance and charge storage ability of electrodes significantly. Finally, the so generated crystalline assembly was successfully applied towards fabrication of Cdot based supercapacitor electrodes with excellent specific capacitance (743.2 F/g) and high energy density (20 Wh kg^{-1} at 110 W kg^{-1}). Although, report on the graphitic Cdot-supported supramolecular assembly suggests its superior use for white light generation, the hierarchical assembly of non-graphitic Cdots into a crystalline structure is yet to be reported. Further, to the best of our knowledge, this is the first report on usage of crystalline carbon dots towards boosting charge storage ability.

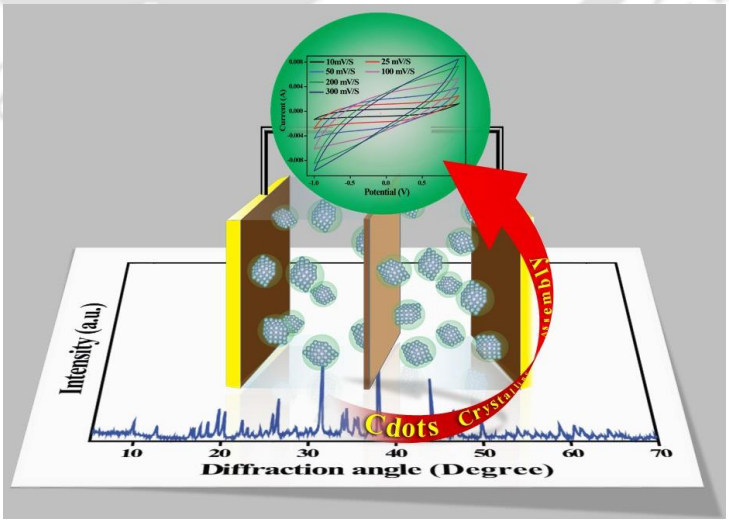

** [J. Phys. Chem. C 2019, 123, 19421−19428]- Reproduced with permission from the American Chemical Society.*

5.1 Experimental Section

5.1.1 Materials. Citric acid monohydrate (99 %, 210.14 g mol^{-1}), *ortho* phosphoric acid (88 %, 98 g mol^{-1}) and zinc acetate dihydrate (219.49 g mol^{-1}) were purchased from Merck, India. Thiourea (99 %, 76.12 g mol^{-1}) and dialysis membrane (benzoylated) were procured from Sigma-Aldrich. All materials were used as purchased without any further purification. Elix grade water from a MilliQ purification system was used for the experiments.

5.1.2 Synthesis of Carbon dots (Cdots). In order to prepare phosphorus doped Cdots (termed as P-Cdots), citric acid monohydrate (210 mg, 1 millimole) and thiourea (210 mg, 2.76 millimole) were dissolved in 10 mL of water, which was followed by addition of 30 µL (11.1% w/w) of *ortho* phosphoric acid to the reaction mixture. The resultant mixture was then subjected to microwave treatment (600W; model: MC28H5023AK, Samsung; 100% power) for 5 min. The final product as-obtained was dissolved in 10 mL of water and then was centrifuged at 15 000 rpm for 25 min (refrigerated centrifuge, SIGMA 3-30K). After that, the collected supernatant part was dialyzed for 12 h (using 1 kDa dialysis membrane) for purification of the product and finally dried at 60 ^{o}C for 48 h in order to obtain powdered sample.[1]

In order to make surface complexation mediated P-Cdot crystalline assembly (termed as Zn, P-Cdots), a stock solution of 2 mg/mL P-Cdot was first prepared. After that, 1 mL of zinc acetate dihydrate aqueous solution (80 mg/mL) was added dropwise to 1 mL of the Cdot dispersion, which led to the appearance of white color precipitation. The solution was then allowed to settle for 15 min followed by centrifugation of the same at 15 000 rpm for 25 min (refrigerated centrifuge, SIGMA 3-30K). Next, the resulting pellet as-obtained after centrifugation was washed repeatedly with ethanol (for five times) followed by water (for five times as well) to remove excess salts. After washing, the final white color pallet was collected carefully and was dried at 50 ^{o}C overnight before further characterizations.

5.1.3 Characterization Methods. Field emission transmission electron microscopy analyses were performed using a JEOL JEM-2100F FETEM instrument (acceleration voltage of 200 kV). Rigaku TTRAX III diffractometer, running with a Cu Kα source (λ = 1.54 Å), was used to analyze powder X-ray diffraction pattern of the

samples. A PHI 5000 Versa Probe II; FEI Inc. instrument was used for X-ray photoelectron spectroscopy (XPS) analyses. Perkin Elmer spectrometer was used to record Fourier-transform infrared spectroscopy data. Also, after the synthesis, P-Cdots and Zn, P-Cdots were characterized using UV-vis spectroscopy (Hitachi U2900 spectrophotometer), fluorescence spectroscopy (Horiba Fluoromax-4 spectrofluorometer) and time resolved photoluminescence spectroscopy (Edinburgh Life-Spec-II spectrofluorometer). Thermogravimetric analysis was done using a Netzsch STA 449F3 thermal analyzer system. Field emission scanning electron microscopy (FESEM) was done using a Zeiss, Sigma 300 instrument. Also, N_2 adsorption-desorption isotherm analyses were performed using a Quantachrome Autosorb-IQ MP gas sorption analyzer.

5.1.4 Quantum Yield Calculation. Quantum yield (QY) was calculated with respect to quinine sulfate in 0.1M H_2SO_4 as the reference using the following equation

$$Q_S = Q_R \times \frac{I_S}{I_R} \times \frac{A_R}{A_S} \times \frac{\eta_S^2}{\eta_R^2} \qquad \text{equation 5.1}$$

Here, Q_S= quantum yield of the sample; Q_R = quantum yield of the reference; I_S = area under the PL curve of the sample; I_R = area under the PL curve of reference; A_R = absorbance of the reference; A_S = absorbance of the sample; η_S = refractive index of the sample solution; η_R = refractive index of reference.

QY of quinine sulphate = 0.54. Refractive index of water = 1.33.

Absorbance of quinine sulphate (A_R) = 0.098. Area under the emission curve (I_R) = 1.66×10^8 (a.u.).

Table 5.1.

Sample	Area under the PL curve (I_s) at 360 nm excitation (a.u.)	Absorbance at 360 nm (A_s)	Quantum yield (%) (Qs)
P-Cdots	3.7×10^7	0.098	12.0
Zn, P-Cdots	7.6×10^6	0.099	2.4

$Q_{P\text{-}Cdots} = [0.54\times(3.7 \times 10^7/1.66 \times 10^8)\times(0.098 / 0.098)\times(1.33/1.33)]\times 100\ \% = 12\ \%.$

$Q_{Zn,P\text{-}Cdots} = [0.54\times(7.6 \times 10^6/1.66 \times 10^8)\times(0.098 / 0.099)\times(1.33/1.33)]\times 100\ \% = 2.4\ \%.$

5.1.5 Preparation of Active Material and Electrode Fabrication. In order to study the electrochemical property, 20 mg of Zn, P-Cdot assembled system (powdered) was first added to 60 mg of activated carbon powder (1:3 ratio) followed by dropwise addition of 200 µL of water-methanol (1:1) to the same. After that, 30 µL of polytetrafluoroethylene (PTFE, 60 wt %; Sigma-Aldrich) was added to the dispersion and mixed well in an ultrasonic bath for up to 20 min.

EDL capacitor electrodes were fabricated over nickel (Ni) substrates. Before device fabrication, Ni-plates of (1.5 × 1.0) cm^2 dimensions were rubbed with sand paper in order to get rough plate surface. After that, Ni-plates were washed well with water through sonication for up to 1 h and then acetone. Finally, after washing, plates were dried at 50 ^oC for 30 min. In a typical procedure, 10 µL of resultant slurry was drop-cast over Ni-plates followed by doctor-blade coating of the same in order to get thin film. The as-obtained films were dried at 50 ^oC for 6 h. After drying, the coated Ni-substrates were pressed (in a hydraulic pellet press) at 50 kg/cm^2 for preferable binding of the active material with substrate. During measurements typical dimension of the films were maintained at (0.8 × 0.6) cm^2.

Next, two electrodes were placed in parallel with one over the other such that the active material film in each electrode faced each other. During experiment, cellulose filter paper (Whatman grade 1; thickness 180 µm) soaked with 0.2 M KOH solution was used as the separator between two electrodes. A Gamry reference 600+ instrument was used for performing all the electrochemical measurements.

Similarly, in order to build AC/P-Cdot supercapacitor, 20 mg of P-Cdot powder was added to 60 mg of activated carbon maintaining 1:3 ratio, followed by dropwise addition of 200 µL of water-methanol (1:1) and 30 µL of PTFE to the same. The resultant mixture was continuously stirred in an ultrasonic bath for up to 20 min to get resultant slurry of the electrode material. Similar procedure, as mentioned in the preceding section was followed for super capacitor electrode (SCE) fabrication and measurements.

Also, to fabricate activated carbon based super capacitor electrodes (SCEs), 60 mg of activated carbon powder was mixed well with 30 µL of PTFE in presence of 200 µL of water-methanol (1:1), followed by vigorous mixing in an ultrasonic bath for 20 min. The resultant slurry was then coated over Ni-substrate by following the aforementioned procedure to prepare electrodes.

5.1.6 Calculation of Specific Capacitance. The specific capacitance values of the as-prepared single electrodes under the experimental setup were calculated from the discharge curves by the formula: [2]

$$\text{Specific capacitance} = \frac{2 \times I_s \times \Delta t}{\Delta V} \qquad \text{equation 5.2}$$

Here, I_s corresponds to discharge current density (i.e., I/m), Δt is the total discharge time and ΔV refers to voltage range. The multiplier of 2 adjusts cell capacitance to the capacitance of single electrode.

5.1.7 Calculation of Energy Density and Power Density. The energy density (E) and power density values (P) were calculated according to following equations. [2]

$$E = \frac{C_{sp} \times \Delta v^2}{2 \times 3.6} \qquad \text{equation 5.3}$$

$$\boldsymbol{P = \frac{E}{\Delta t} \times 3600} \qquad \text{equation 5.4}$$

Here E is the energy density (Wh kg^{-1}), C_{sp} is the specific capacitance (F/g) and Δv is the voltage difference (Volt). P corresponds to power density (W kg^{-1}) and Δt is the discharge time.

Scheme 5.1. Schematic representation for the synthesis of 3D- Cdot assembly and fabrication of corresponding electrical double layer (EDL) capacitor. Also, a pictorial representation for the enhanced supercapacitor performance has been depicted.

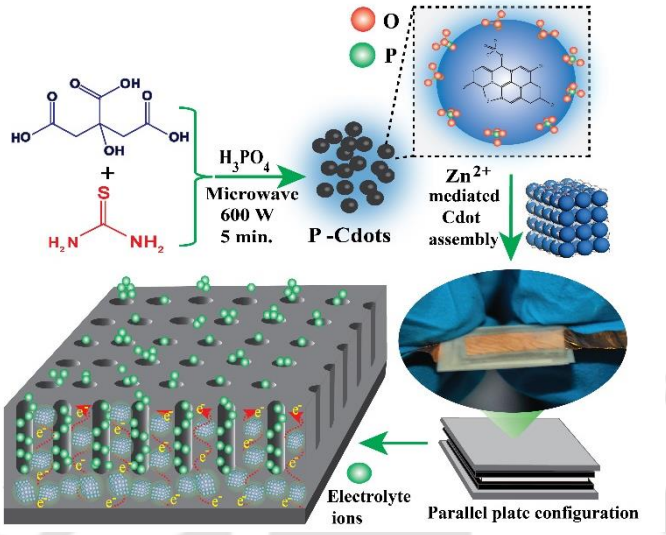

5.2 Results and Discussion

Crystalline P-Cdots were synthesized using citric acid monohydrate, thiourea and *ortho* phosphoric acid in the presence of microwave radiation, based on a reported protocol. [1] Addition of zinc acetate dihydrate to the as-synthesized Cdots led to the formation of white color precipitate, which was separated by centrifugation and then collected for further analyses and use. The details of the synthesis procedure are included in the experimental section.

Transmission electron microscopy (TEM) image (Figure 5.1.a) of Zn, P-Cdots indicated the formation of assembly of particles of diameter 3.2±1.0 nm (Figure 5.1.b). Importantly, these constituent particles of the assembly had diameters almost similar to those of the precursor P-Cdots (3.0±1.0 nm, Figure 5.1.c, d)). A careful investigation of the TEM images for Zn, P-Cdots revealed the presence of distinct polycrystalline domains in the assembled nanostructure. Selected area electron diffraction (SAED) study (Figure 5.2) of the assembled system discerned their polycrystalline nature. HRTEM results and corresponding inverse fast Fourier transform (IFFT) images of Zn, P-Cdots revealed lattice spacing of 0.15, 0.20, 0.26, 0.29, 0.33, 0.45 and 0.91 nm (Figure 5.3.a-e). These calculated d-spacing values matched well with the SAED pattern of the same (Figure 5.2). Additional lattice spacing values corresponding to crystalline plains in Zn, P-Cdots are also presented in Figure 5.4. Phosphorus doping in

carbon nanostructure helps inducing non-graphitic crystallinity, and indeed the lattice distances of 0.15 nm, 0.20 nm and 0.27 nm in the present study correspond to crystallinity in the carbon nanostructure itself. [1] However, the additional lattice fringes and corresponding d-spacing coexisting with P-Cdot crystal planes are presumed to have originated from the zinc ion mediated crystalline assembly of Cdots. Also, high-resolution TEM images corresponding to Zn P-Cdots were recorded from different spots showing that Cdot crystal planes were present together with newly generated lattice planes due to Zn^{2+} inclusion (Figure 5.5).

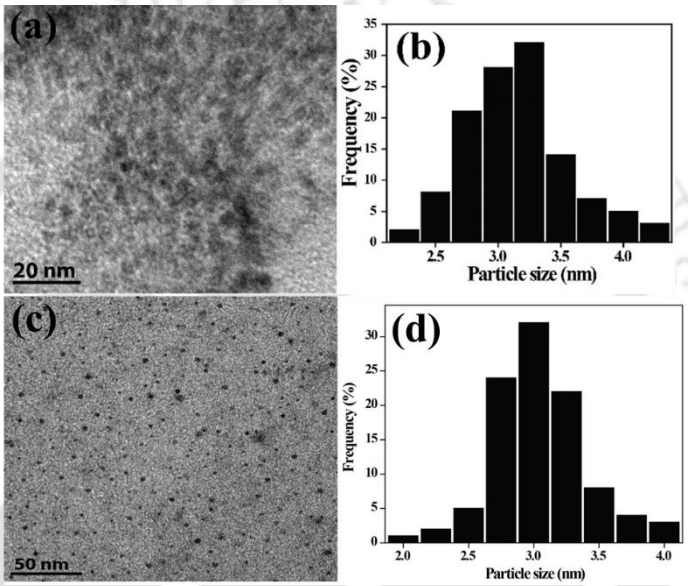

Figure 5.1. (a) TEM image of Zn, P-Cdot assembly. (b) Average size distribution plot of the assembled particles in Zn, P-Cdots. Several TEM images were used to calculate the distribution (with 100 particles). (c) TEM image of P-Cdots. (d) Particle size distribution plot of P-Cdots calculated form several TEM images (more than 100 particles). Average diameter of the same was calculated to be 3.0±1 nm.

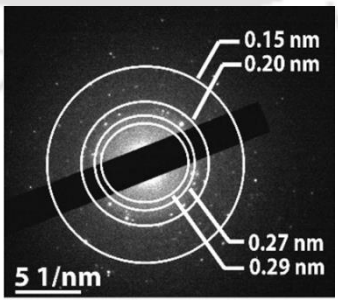

Figure 5.2. Selected area electron diffraction (SAED) patterns of the assembled nanostructures.

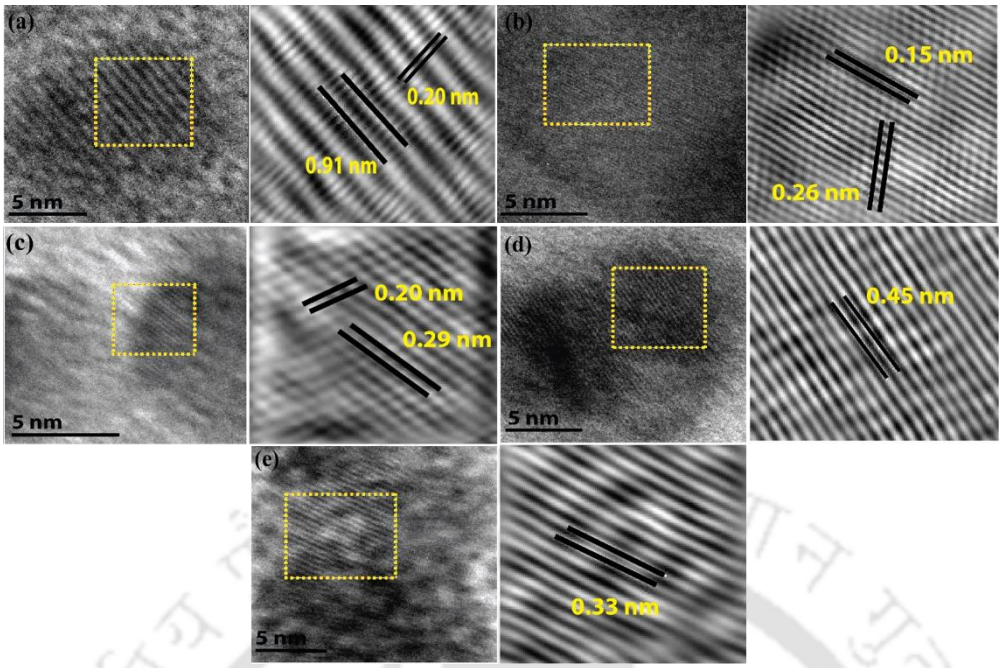

Figure 5.3. High-resolution TEM (HRTEM) images and Inverse fast Fourier transform (IFFT) patterns observed for Zn, P-Cdots corresponding to lattice spacing of (a) 0.20 nm, 0.91 nm, (b) 0.15 nm, 0.26 nm, (c) 0.20 nm, 0.29 nm, (d) 0.45 nm, and (e) 0.33 nm respectively.

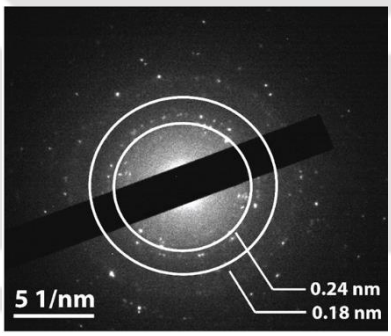

Figure 5.4. Additional SAED patterns corresponding to d-spacing values of 0.18 nm and 0.24 nm, observed in Zn, P-Cdot assembly. Sharp peaks due to aforementioned d-spacing values were also identified in the powder XRD pattern of the same at 49.9^{o} and 37.0^{o}, respectively.

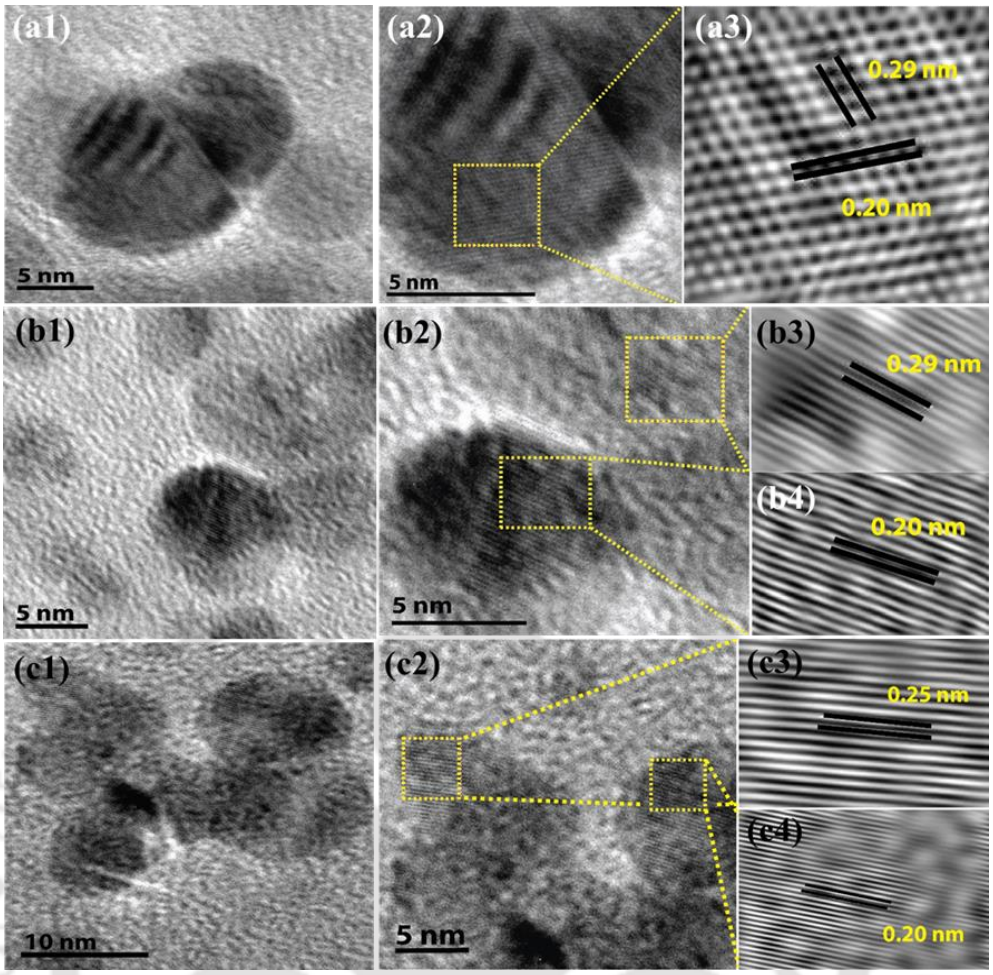

Figure 5.5. Additional TEM and high-resolution TEM images corresponding to Zn, P-Cdots assembly were recorded from different spots confirming coexistence of lattice plains observed due to both P-Cdots and Zn^{2+} induced newly generated crystallinity (lattice spacing of 0.20 nm assigned to P-Cdots; 0.25 and 0.29 nm lattice spacing assigned to additional crystal planes generated following Zn^{2+} addition).

Literature reports suggest usual amorphous nature of Cdots. [3] However, as we have reported earlier, [1] microwave treatment of the precursors in the presence of phosphoric acid results in the formation of crystalline Cdots (P-Cdots) with characteristic X-ray diffraction (XRD) patterns (Figure 5.6.a, b). The diffraction pattern of Zn, P-Cdots, comprising of multiple sharp peaks, was remarkable (Figure 5.6.c), revealing formation of well-ordered nanostructure in the as-synthesized residuals with exceptional crystallinity. As represented in Figure 5.6.c, the diffraction pattern of Cdot assembly consisted of intense characteristic peaks at 2θ values of 9.64, 16.7, 17.4, 18.2, 19.38, 20.1, 22.2, 22.9, 23.58, 24.4, 25.7, 26.28, 27.6, 28.7, 29.6, 30.16 and 31.3° along with other peaks between 33.72° to 60.6°, substantiating high degree of crystallinity. Interestingly, apart from the assigned peak positions due to P-Cdot crystalline domains

(23.58, 28.7, 33.7, 45.2, 57.7 and 60.6°), the observed XRD pattern consisted of several other peaks corresponding to characteristic diffraction pattern of orthorhombic hopeite structure ($Zn_3(PO_4)_2$, $4H_2O$) (JCPDS file no. 33-1474).[4] Also, it is important to mention here that the observed d-spacing values of 0.26 nm, 0.29 nm, 0.33 nm, 0.45 nm and 0.91 in HRTEM analyses (Figure 5.3.a-e) and 0.18 nm and 0.24 nm (Figure 5.4) were found to be substantially similar to the d-spacing values of orthorhombic hopeite structure. The observed peak positions as well as assigned peak details are included in Table 5.2 in this regard.

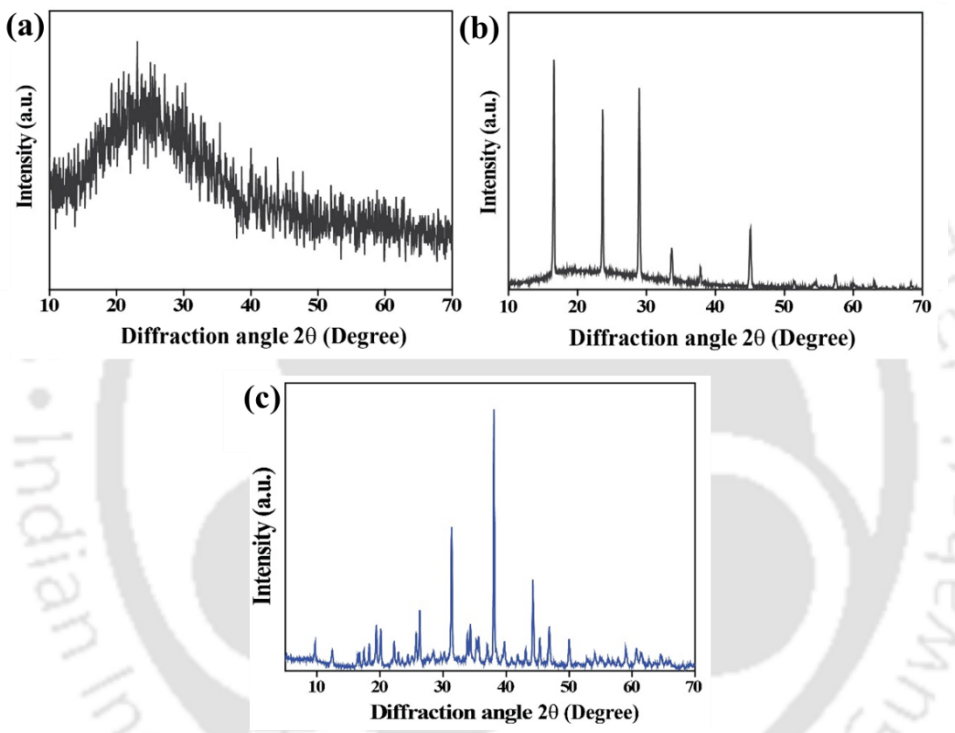

Figure 5.6. Powder XRD pattern of (a) the Cdots without phosphorus in the structure showing amorphous nature of the same and (b) P-Cdots synthesized from citric acid monohydrate (210 mg), thiourea (210 mg) and phosphoric acid (11.1 % w/w, input concentration) (c) Powder X-ray diffraction pattern of the Zn, P-Cdot crystalline assembly.

Table 5.2. Detailed observed peak positions in the Zn, P-Cdots XRD pattern along with assigned *hkl* planes and corresponding d-spacing values. Here the peaks identified due to P-Cdots and zinc phosphate crystallinity (due to orthorhombic hopeite arrangement) on Cdot surface are assigned as CDs and ZnP, respectively.

Diffraction angle (2θ)	Peak assignments	Assigned *hkl*	Corresponding d-spacing (Å)	Diffraction angle (2θ)	Peak assignments	Assigned *hkl*	Corresponding d-spacing (Å)
9.64	ZnP	020	9.16	33.72	CDs	211	2.66
16.7	ZnP	200	5.31	34.30	ZnP	331	2.6
17.4	ZnP	210	5.09	35.34	ZnP	161	2.53
18.2	ZnP	011	4.85	35.66	ZnP	002	2.51
19.38	ZnP	040	4.57	37.02	ZnP	112/022	2.4
20.1	ZnP	111	4.41	38.04	ZnP	261	2.34
22.2	ZnP	230	4.0	39.74	ZnP	171	2.26
22.90	ZnP	031	3.88	40.88	ZnP	222/042	2.20
23.58	CDs	001	3.74	41.82	ZnP	142	2.15
24.4	ZnP	131/201	3.64	43.04	ZnP	280/361	2.1
25.7	ZnP	240	3.46	45.24	CDs	411	2.01
26.28	ZnP	221	3.3	49.96	ZnP	402	1.82
27.6	ZnP	141	3.22	54.06	ZnP	442	1.82
28.7	CDs	011	3.07	54.88	ZnP	182	1.67
29.6	ZnP	250	3.01	57.7	CDs	601	1.6
30.16	ZnP	051	2.9	60.6	CDs	022	1.5
31.3	ZnP	241	2.85				

Thus, based on aforementioned experimental evidences we surmise that addition of zinc acetate dihydrate into P-Cdots led to the growth of orthorhombic hopeite structure over Cdot surface, which further resulted in the formation of surface complexation mediated crystalline self-assembled Cdots (evident from synchronized lattice planes during TEM analysis). An orthorhombic zinc phosphate tetrahydrate crystal structure with a = 10.61Å, b = 18.31Å, c = 5.03Å and α=β=γ=90^{o} is illustrated in Figure 5.7.a. Also, possible arrangement of Zn^{2+} ions and PO_4^{3-} groups over Cdot surface during complexation along with a 3D structure corresponding to the assembled system is represented in Figure 5.7.b and c respectively. Further, simulated XRD pattern (obtained using VESTA 3.4.5 analyzer) corresponding to orthorhombic hopeite structure has been represented in Figure 5.7.d substantiating identical peak positions observed in case of Zn, P-Cdot XRD pattern.

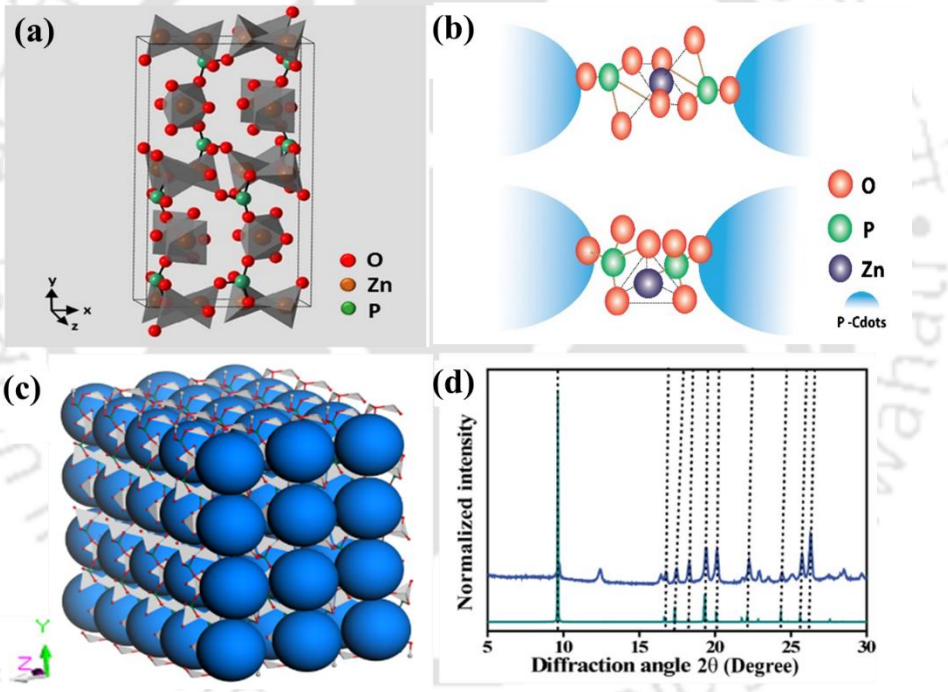

Figure 5.7. (a) Orthorhombic zinc phosphate tetrahydrate structure. (b) Schematic representation for Zn-octahedral and Zn-tetrahedral arrangement in the occurrence of Cdot assembly. (c) 3D visual corresponding to zinc ion mediated Cdot assembly. (d) Simulated powder XRD pattern corresponding to orthorhombic arrangement in zinc phosphate tetrahydrate crystal structure, as represented in Figure 5.7.a. The figure shows similarities in the peak positions between the simulated pattern and the observed Zn, P-Cdot assembly powder XRD pattern. This supports formation of orthorhombic zinc phosphate tetrahydrate crystal structure over Cdot surface during the formation of Cdot assembly as well.

It is important mentioning here that, the role of *ortho* phosphoric acid during the synthesis of P-Cdots is crucial as it allows exothermic, rapid polymerization of the starting materials followed by high temperature carbonization in the successive steps. This results in the generation of highly ordered structure inside the carbon core. [1] Also, the as-synthesized Cdots consist of excess PO_4^{3-} groups over the surface. Addition of zinc acetate dihydrate in the Cdot medium effects selective binding of the free PO_4^{3-} groups with added Zn^{2+} ions in an octahedral/tetrahedral fashion resulting in the zinc phosphate crystallization decorated over the surface of P-Cdots.

X-ray photoelectron spectroscopy (XPS) analyses (Figure 5.8 and 5.9) exhibited that the spectrum of Zn, P-Cdots (Figure 5.8.a) consisted of major sharp peaks at 1043.7 eV and 1020.8 eV, identified as Zn $2p_{1/2}$ and Zn $2p_{3/2}$ peaks, respectively. [5] Besides, other major peaks observed due to Cdots in both the Zn, P-Cdot system and P-Cdots, corresponding to those of C, N, O, S and P are presented in Figure 5.8, 5.9 following deconvolution. The results indicated successful incorporation of zinc in the crystalline assembled system. Fourier-transform infrared (FTIR) spectrum (Figure 5.10 and Table 5.3) showed peaks appearing at 1710 cm^{-1} and 1628 cm^{-1} in P-Cdots, due to stretching vibrations from C=O and C=C bonds, respectively. [6] Zn, P-Cdots, on the other hand, revealed a sharp peak at 1608 cm^{-1}, which was identified as that of C=C stretching mode. Additional peaks appearing at 1189 cm^{-1} and 1100 cm^{-1} in P-Cdots were assigned as P=O and P-O stretching vibrations, respectively.[6] The said peaks appeared at lower wavenumber region for Zn, P-Cdots i.e., at 1112 cm^{-1} and 1068 cm^{-1} as well, possibly due to interaction with zinc. Furthermore, the peaks at 1025 cm^{-1}, 947 cm^{-1} and 632 cm^{-1} were assigned as Zn-OH stretching and Zn-O translational mode [7] and these vibrational modes were particularly absent in P-Cdots.

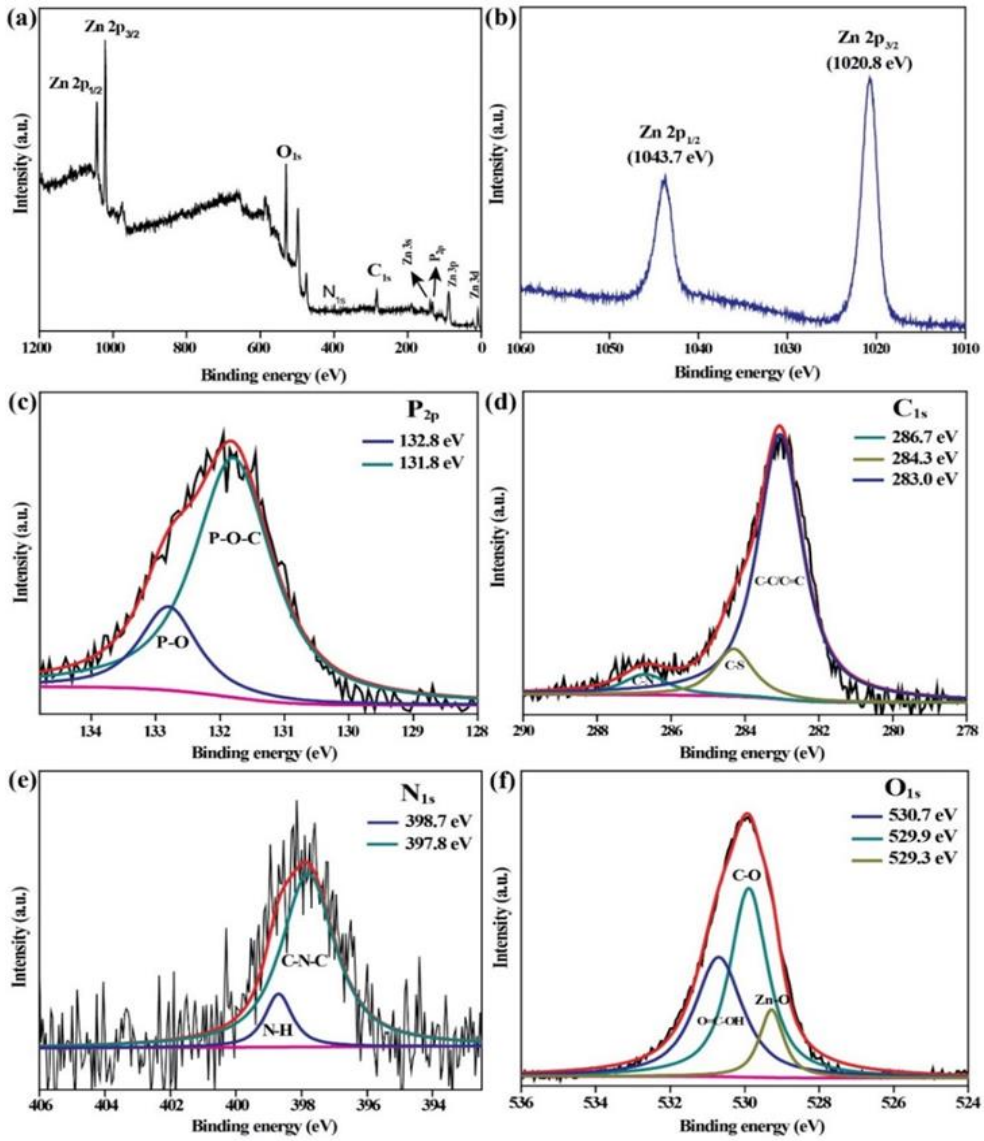

Figure 5.8. (a) XPS analysis plot (full range) for Cdot assembly consisting of peaks due to zinc. (b) Enlarged plots for Zn $2p_{1/2}$ and Zn $2p_{3/2}$ peaks, observed at 1043.7 eV and 1020.8 eV respectively, confirming the presence of zinc along with Cdots in the assembled nano structure. Deconvoluted XPS plots for (c) $P_{2p,}$ (d) $C_{1s,}$ (e) N_{1s} and (f) O_{1s} signals, present in the Zn, P-Cdots (or the Cdot assembly here) XPS plot. The peak appearing at 529.3 eV is due to Zn-O bond in Zn, P-Cdot assembly structure.[8-10]

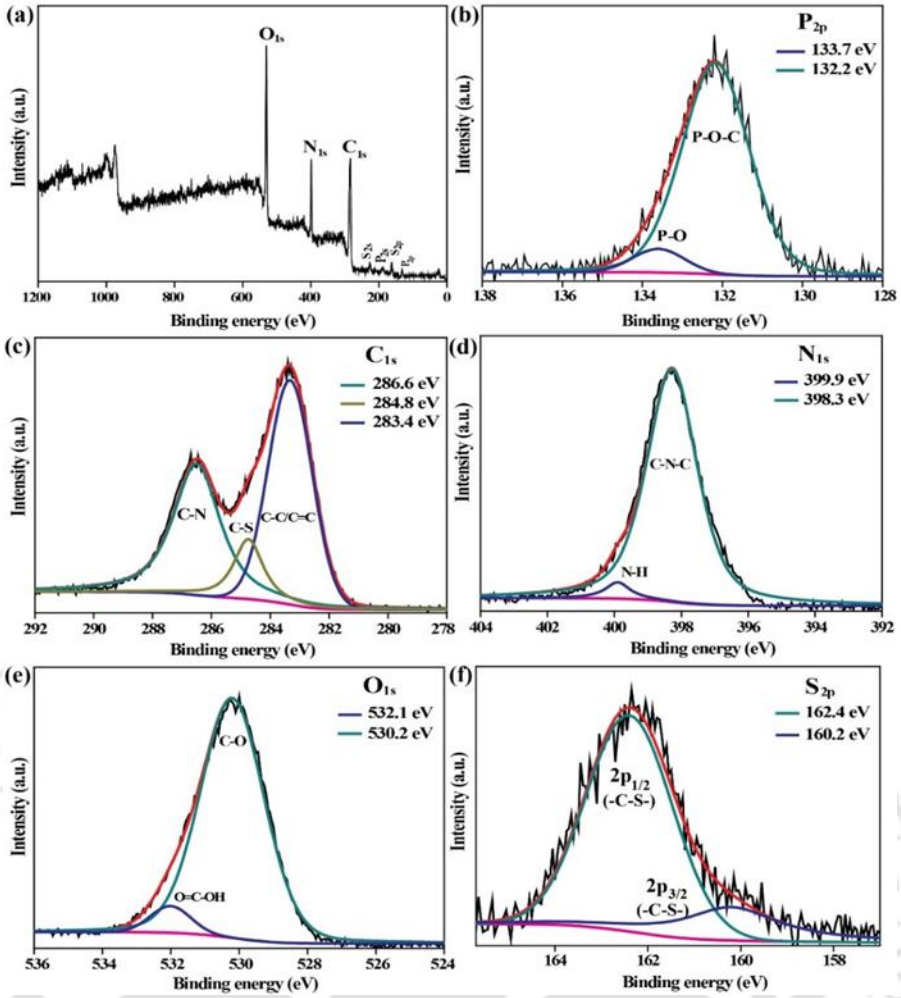

Figure 5.9. (a) XPS results (full range) for P-Cdots confirming presence of phosphorus along with C, N, O and S in the structure. Also, the deconvoluted XPS results for (b) P_{2P}, (c) C_{1S}, (d) N_{1S}, (e) O_{1S} and (f) S_{2P} are represented.

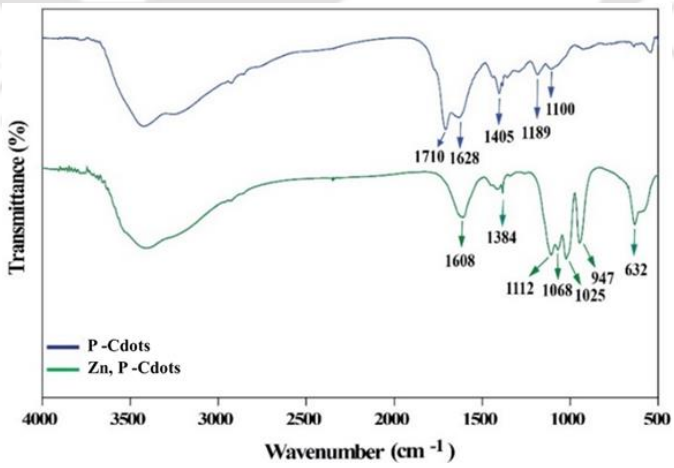

Figure 5.10. FTIR spectra of P-Cdots and Zn, P-Cdots.

Table 5.3. Tabulated vibrational frequencies and corresponding band assignments recorded for P-Cdots and Zn, P-Cdots.

P-Cdots		Zn, P-Cdots	
Vibrational frequency (cm^{-1})	**Bonds present**	**Vibrational frequency (cm^{-1})**	**Bonds present**
1710	C=O stretching	1608	C=C stretching
1628	C=C stretching	1384	C-N stretching
1405	C-N stretching	1112	P=O
1189	P=O	1068	P-O
1100	P-O	1025, 947	Zn-OH
--	--	632	Zn-O translational mode

UV-vis spectrum of P-Cdots showed absorption bands at ~274 nm and ~338 nm, which correspond to π–π* transitions and n–π* transitions, respectively (Figure 5.11.a). [11] Dispersion of the as-obtained white precipitate of Zn, P-Cdots also exhibited absorbance at ~278 nm and ~342 nm thus indicating the integration of Cdots inside the structure (Figure 5.11.b). Photoluminescence studies of P-Cdots confirmed excitation wavelength dependent tunable emission, with excitation maximum at 360 nm (corresponding λ_{em} = 450 nm, Figure 5.11.c). Such excitation-dependent tunable emissive nature in Cdots has its origin in the surface defects caused due to heteroatom doping. [12] Zn, P-Cdots showed excitation dependent tunability due to Cdots as well, along with shifting of the excitation maximum to 370 nm (corresponding λ_{em} was found to be at 460 nm, Figure 5.11.d). The result also supported that the white residual, obtained after zinc addition followed by purification retained Cdots inside the structure. Besides, red shifting in the emission characteristics indicated interaction between Cdots remaining inside the structure and the Zn^{2+} ions added to the system. Excitation spectra of both the P-Cdots and Zn, P-Cdots were also recorded, corresponding to λ_{em} of 450 nm and 460 nm wavelengths, respectively and are presented in Figure 5.11.e, f. The photoluminescence quantum yield (QY) of P-Cdots and Zn, P-Cdots were found to be 12 % and 2.4 % at 360 nm excitation wavelength and 450 nm, 460 nm emission wavelength, respectively. Details of the calculations are mentioned in the experimental section. Considerable loss in the luminescence QY (80 % loss in QY) was due to attainment of additional crystallinity suggesting interactions amongst the Cdots and with Zn^{2+} ions further.

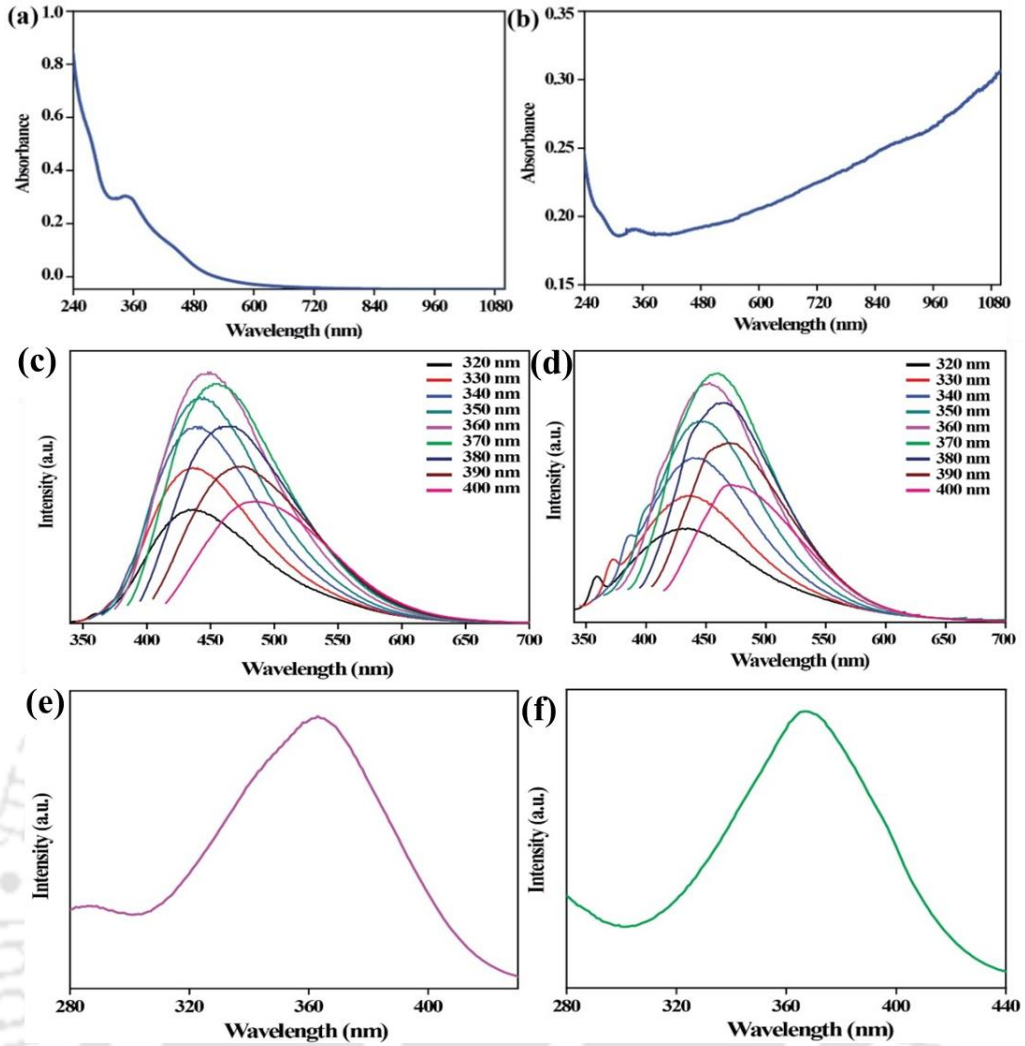

Figure 5.11. Absorption spectra of (a) P-Cdots and (b) Zn, P-Cdots. Emission spectra of (c) P-Cdots and (d) Zn, P-Cdots, confirming excitation dependent tunable nature of emission. Corresponding excitation wavelengths are mentioned in the legends. Excitation spectra of (e) P-Cdots and (f) Zn, P-Cdots. The emission maxima were set at 450 nm and 460 nm wavelengths for P-Cdots and Zn, P-Cdots, respectively.

Time resolved photoluminescence (TRPL) studies, using a 375 nm pulsed diode laser source, indicated shortening of lifetime following the formation of Zn, P-Cdots. (Figure 5.12). As mentioned in Table 5.4 and 5.5, the average photoluminescence lifetime for P-Cdots was calculated to be 9.2 ns and that for Zn, P-Cdots was 8.2 ns. Corresponding radiative (K_r) and non-radiative (K_{nr}) decay rate constants are presented in Table 5.4. Interestingly, for Zn, P-Cdots, K_{nr} was found to be 1.1×10^8 s^{-1}, which was found to be much higher than that of P-Cdots ($K_{nr} = 9.5 \times 10^7$ s^{-1}), indicating considerable loss of the absorbed energy into non-radiative pathways for the former.

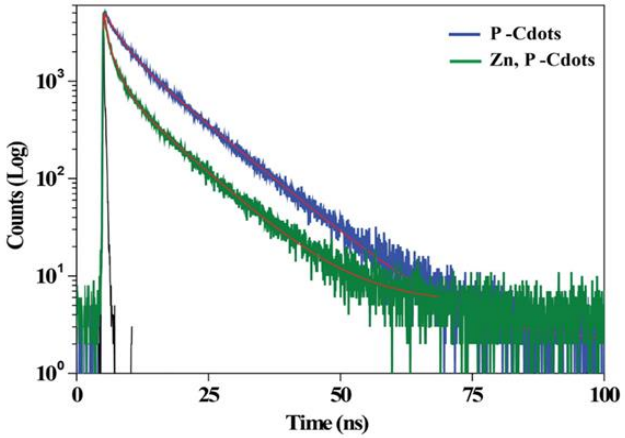

Figure 5.12. Time resolved photoluminescence (TRPL) spectra of P-Cdots and Zn, P-Cdots (assembly) recorded using a 375 nm pulsed diode laser (PDL) source.

Table 5.4. Measured quantum yield values (refer to Table 5.1), average lifetime and corresponding radiative and non-radiative decay rate constants of the as-synthesized P-Cdots and Zn, P-Cdots.

Samples	Quantum yield (φ_D) (%)	Average lifetime (τ_{av}) (ns)	Radiative decay rate constant (K_r) (s^{-1})	Non radiative decay rate constant (K_{nr}) (s^{-1})
P-Cdots	12.0	9.2	1.3×10^7	9.5×10^7
Zn, P-Cdots	2.4	8.2	2.9×10^6	1.1×10^8

Table 5.5. Calculated parameters, as-obtained during time resolved photoluminescence study, of P-Cdots and Zn, P-Cdots.

Sample	λ^2	α_1 (%)	Lifetime (τ_1) (ns)	α_2 (%)	Lifetime (τ_2) (ns)	α_3 (%)	Lifetime (τ_3) (ns)
P-Cdots	1.2	21.1	2.9	78.9	9.7	-	-
Zn, P-Cdots	1.1	10.8	0.3	29.4	1.9	59.8	8.9

Thermogravimetric analysis (TGA) under argon atmosphere (Figure 5.13) showed discernible weight loss for Zn, P-Cdots up to 200 °C (~14 % degradation) as compared to P-Cdots. However, beyond that temperate the rate of thermal degradation was found to be much higher for P-Cdots, whereas the Zn, P-Cdots were considerably stable till 800 °C.

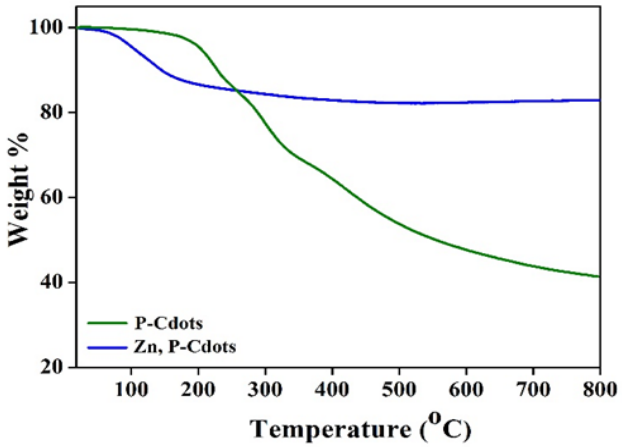

Figure 5.13. Thermogravimetric analysis (TGA) plot corresponding to P-Cdots and Zn, P-Cdot assembly under argon atmosphere (10 °C/ min).

Field emission scanning electron microscopy (FESEM) and N_2 adsorption-desorption isotherm analyses have been performed in order to understand surface morphologies and porosity of Zn, P-Cdot and P-Cdot adsorbed in activated carbon (AC). Large specific surface area along with appropriate structural porosity are conducive towards facile electrolyte diffusion as well as ion transportations, discussed in the subsequent sections. Figure 5.14. (a-f) represents the FESEM images of AC/Zn, P-Cdot, AC/P-Cdot and activated carbon films, respectively. The images clearly illustrate porous morphology of all the three as-prepared films. Also, result corresponding to N_2 adsorption-desorption analysis is represented in Figure 5.15. (a-c). Measured surface area along with total pore volumes are included in Table 5.6. The surface area and total pore volume for activated carbon were found to 756.4 m^2/g and 0.50 cc/g, respectively. However, after addition of Zn, P-Cdots and P-Cdots separately to activated carbon both the surface area and total pore volume were found to have been decreased. For AC/P-Cdots, surface area and total pore volume were measured to be 673.4 m^2/g and 0.46 cc/g; whereas the same for AC/Zn, P-Cdot film were found to be 630.8 m^2/g and 0.44 cc/g, respectively.

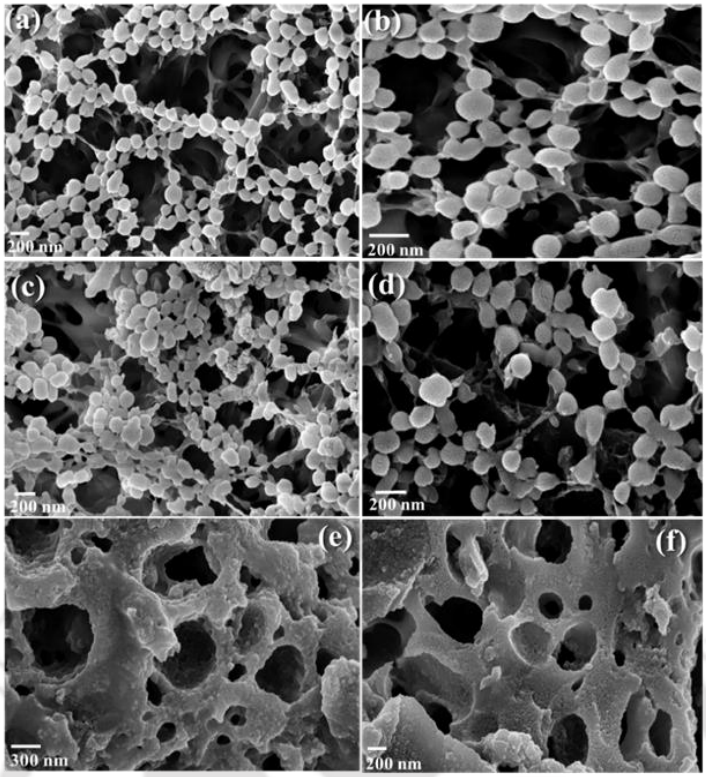

Figure 5.14. FESEM images (a, b) of AC/Zn, P-Cdot film. Also, (c, d) and (e, f) correspond to morphologies of AC/ P-Cdot and only activated carbon films, respectively. Highly porous morphologies have been identified for all the three systems, which were deemed suitable for facile electron / ion transportation.

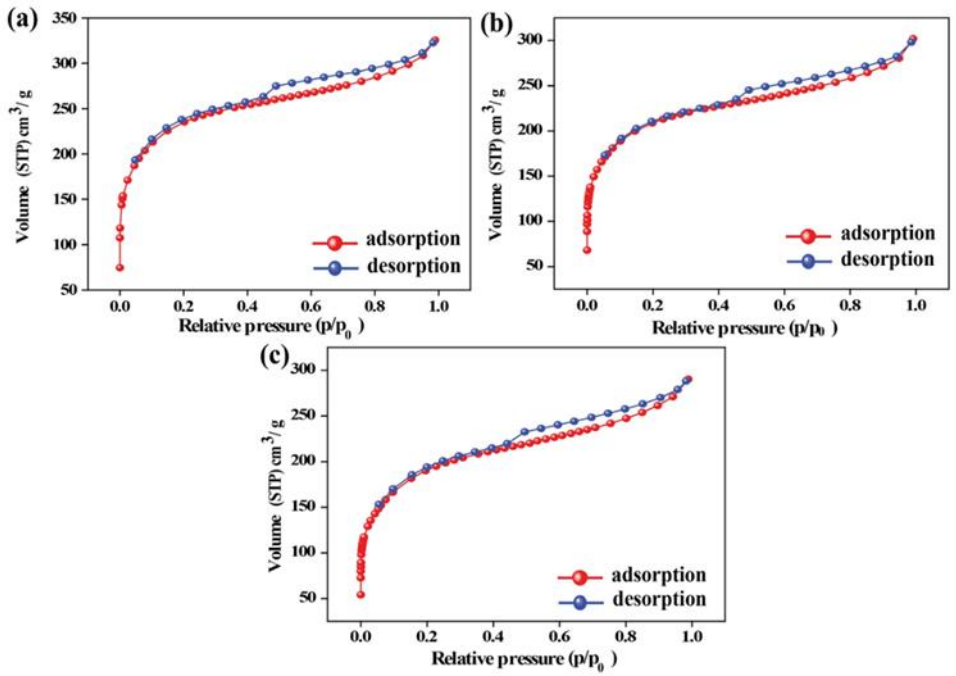

Figure 5.15. N_2 adsorption-desorption isotherms for (a) activated carbon, (b) AC/P-Cdots and (b) AC/Zn, P-Cdots.

Table 5.6. Measured surface area and total pore volume from N_2 adsorption-desorption isotherm for activated carbon, AC/P-Cdot and AC/Zn, P-Cdot active materials used for supercapacitor electrode fabrication.

Sample	Surface area (m^2/g)	Total pore volume (cc/g)
Activated carbon	756.4	0.50
AC/P-Cdot	673.4	0.46
AC/Zn, P-Cdot	630.8	0.44

Finally, the exceptional crystallinity in P-Cdot assembly was tested for electrochemical properties and charge storage ability in an electric double layer (EDL) capacitor. For this, P-Cdots and the crystalline assembled system of the same (Zn, P-Cdots) were first adsorbed separately inside activated carbon material followed by deposition over nickel (Ni) substrate in order to device EDL capacitor electrodes. The details of the device fabrication techniques have been mentioned in the experimental section. We chose our materials for this implementation because of their exceptional crystallinity, which would create additional ion channel through the crystalline networks for conducting electrolytes to pass. On the other hand, activated carbon (AC) has been chosen due to low cost, good electrochemical stability and high surface area.

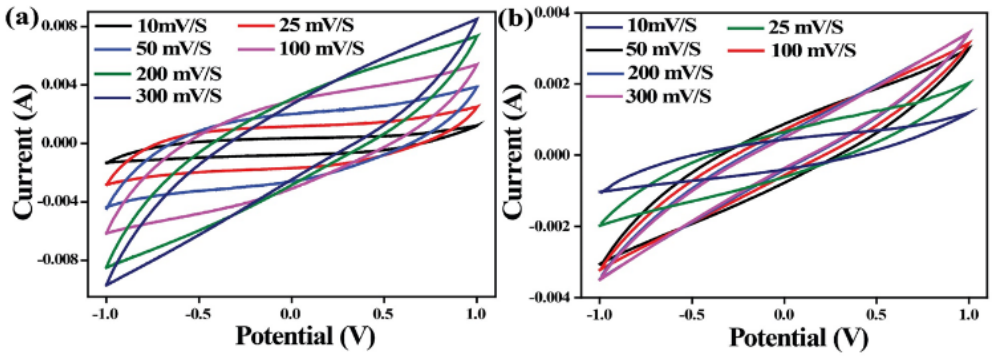

Figure 5.16. CV plots corresponding to (a) AC/Zn, P-Cdot and (b) AC/P-Cdot electrodes under varying scan rates (10, 25, 50, 100, 200 and 300 mV/S).

The electrochemical properties of as-prepared AC/Zn, P-Cdot and AC/ P-Cdot electrodes were first investigated using cyclic voltammetry (CV). Figure 5.16 represents the cyclic voltammograms of two different types of electrodes under varying scan rates. The symmetrical CV curves in Figure 5.16.a suggest a nearly ideal EDL capacitive (EDLC) behavior (or the electrochemical performance) of AC/Zn, P-Cdot electrode. In comparison, the CV curves for AC/P-Cdot and only activated carbon were recorded under identical conditions as the control, indicating lower integrated areas under the voltammogram plots and hence lower capacitive behavior of the same (Figure 5.16.b and 5.17.a). A schematic illustration of parallel plate supercapacitor construction is represented in Figure 5.17.b. Figure 5.18.a and b represent galvanostatic charge-discharge curves (CDC) of AC/Zn, P-Cdot and AC/P-Cdot electrodes, respectively, under different current densities. Most importantly, less voltage drop with time and triangular symmetry in CDCs corresponding to AC/Zn, P-Cdot electrode signify outstanding EDLC behavior of the same as compared to AC/P-Cdot or activated carbon electrodes (Figure 5.18.a, b and c). The calculated maximum specific capacitances (based on equation 5.2) were found to be 743.2, 263.6 and 144.3 F/g for AC/Zn, P-Cdot, AC/P-Cdot and activated carbon electrodes, respectively, at 0.25 A/g current density. Also, changes in specific capacitance values under different current densities for all the three electrodes have been shown in Figure 5.19 and Table 5.7.

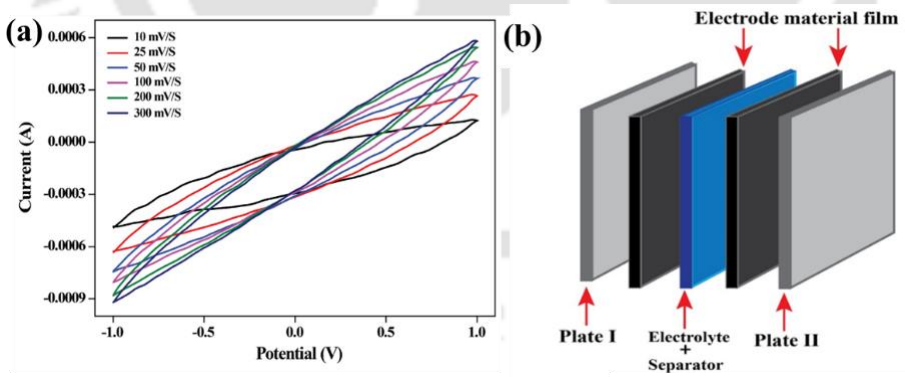

Figure 5.17. (a) CV plots corresponding to activated carbon electrode based supercapacitor under varying scan rates (10, 25, 50, 100, 200 and 300 mV/S). (b) Schematic representation for parallel plate arrangement.

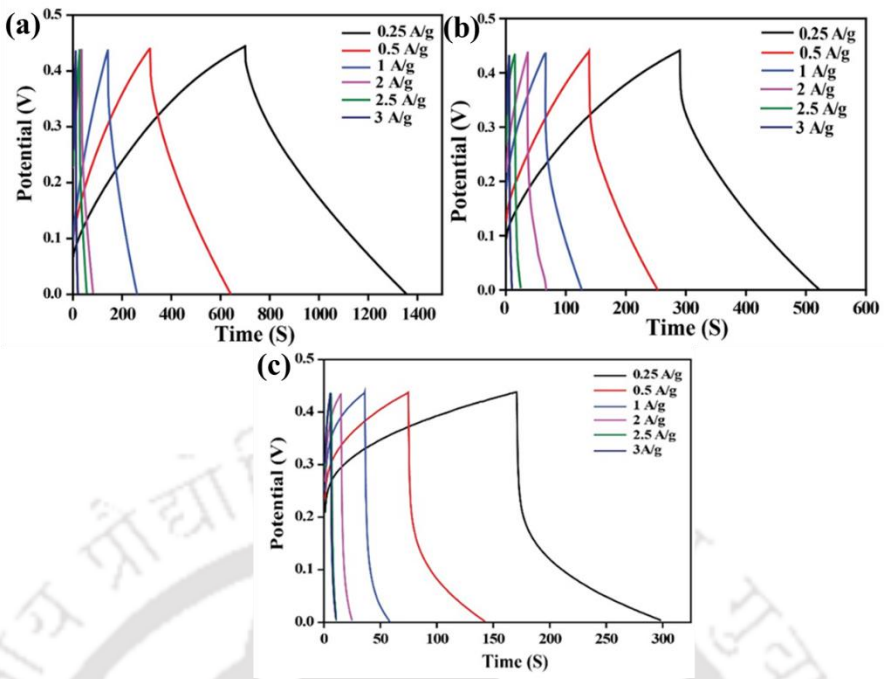

Figure 5.18. Galvanostatic charge-discharge curves (CDC) corresponding to (a) AC/Zn, P-Cdot (b) AC/P-Cdot and (c) activated carbon based supercapacitor electrodes under varying current densities.

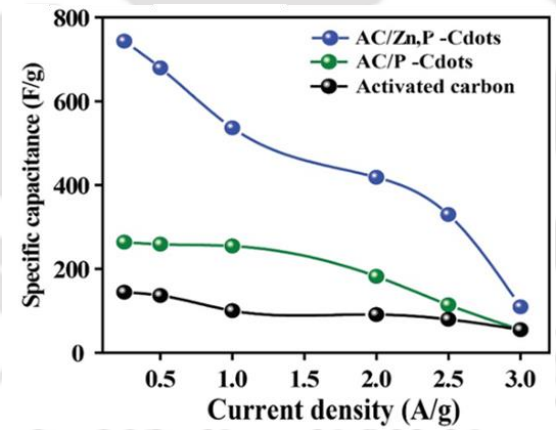

Figure 5.19. Comparison of the rate performance of the as-prepared supercapacitor electrodes (SCEs).

Table 5.7. Calculated specific capacitance values corresponding to different supercapacitors under varying current densities.

Sample SCs	Calculated specific capacitance (F/g)					
	0.25 A/g	0.5 A/g	1 A/g	2 A/g	2.5 A/g	3 A/g
AC/Zn, P-Cdot	743.2	679.5	536.4	418.2	329.5	109
AC/P-Cdot	263.6	259.0	254.5	181.8	114.0	54.5
Activated carbon	144.3	136.4	100.0	90.9	79.5	54.5

Electrochemical impedance spectroscopy (EIS) measurements were further performed in order to study electrochemical performance of the electrodes. Principally, at lower frequency region, the Nyquist plot of an ideal EDL capacitor is a straight line. In other words, the more perpendicular the line, the more intently the supercapacitor acts like an ideal capacitor. Figure 5.20.a corresponds to EIS measurement plots of AC/Zn, P-Cdot and AC/P-Cdot systems. The Nyquist plot for AC/Zn, P-Cdot electrode consisted of smaller semicircle part at the higher frequency region along with a straight line, which is closely parallel to imaginary axis at lower frequency region as compared with AC/P-Cdot electrode. Also, the obtained Nyquist plot for as-prepared activated carbon based supercapacitor electrode (SCE) has been represented in Figure 5.20.b, showing relatively larger semicircle at high frequency and the straight line more inclined towards Z' at lower frequency region. Further studies corresponding to increasing Zn, P-Cdot input ratios (0 i.e. no Zn, P-Cdot added to activated carbon, 1:10, 1:6, 1:3) confirmed improved electrochemical performance and charge storage behavior of the electrodes (Figure 5.21.a, b and 5.22.a, b; Table 5.8).

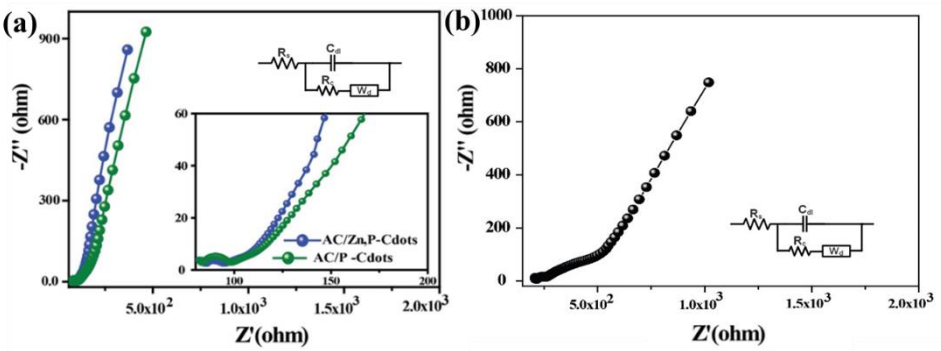

Figure 5.20. (a) Electrochemical impedance spectroscopy (EIS) plots for AC/Zn, P-Cdot and AC/P-Cdot. Enlarged view at higher frequency. (b) EIS plot for activated carbon supercapacitor electrode. Corresponding equivalent circuit diagram has been represented in the inset.

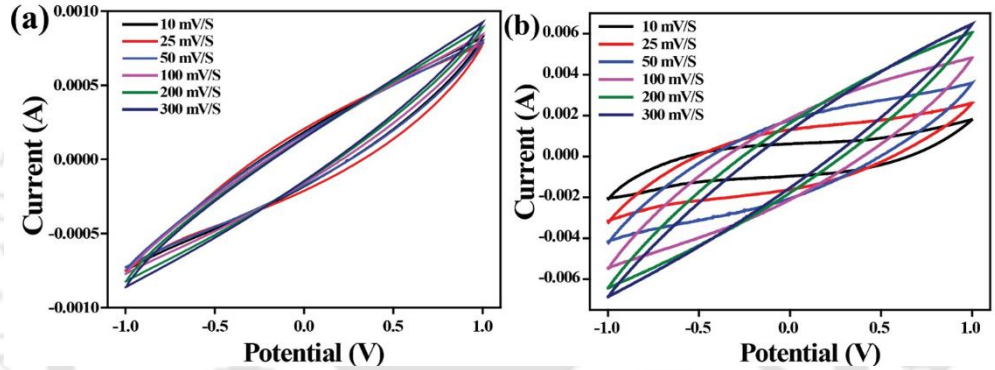

Figure 5.21. Electrochemical performance of the electrodes prepared with varying concentrations of Zn, P-Cdots added to activated carbon. CV curves for AC/Zn, P-Cdots under different scan rates for (a) 1:10 ratio and (b) 1:6 ratios.

Table 5.8. Calculated specific capacitance values corresponding to EDL capacitors prepared with varying Zn, P-Cdots concentrations.

Zn, P-Cdot: AC concentration ratio	Measured specific capacitance (F/g)
0 (i.e., no Zn, P-Cdot added to activated carbon)	144.3
1:10	256.8
1:6	454.5
1:3	743.2

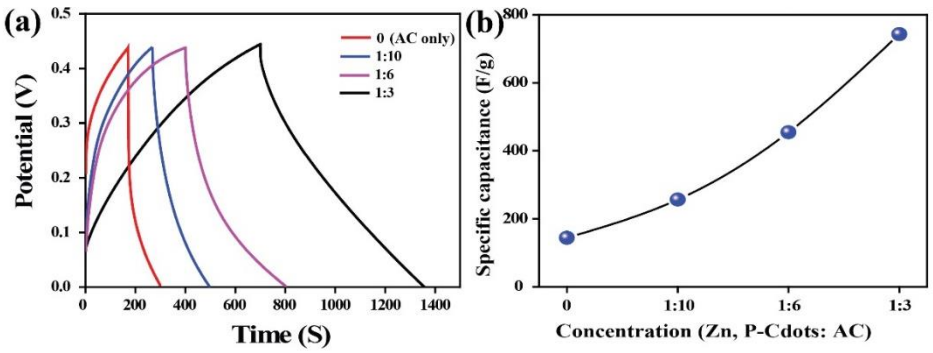

Figure 5.22. (a) Galvanostatic charge-discharge curves for varying Zn, P-Cdot concentrations such as 0 (i.e., no Zn, P-Cdot added to activated carbon), 1:10, 1:6, 1:3 ratios (Zn, P-Cdot: AC) at 0.25 A/g. (b) Measured specific capacitances for the electrodes.

It is important mentioning here that despite of having high surface area and porosity for activated carbon, the CV analyses, galvanostatic charge-discharge and EIS results indicate AC/Zn, P-Cdot (with having the lowest surface area and total pore volume; Table 5.6) as the finest electrode material for supercapacitors. We surmise that highly crystalline Zn, P-Cdots generated overall conductive channels in the composite structure with activated carbon, which was effective in improving the electron and/or ion transportations through the micro pores of activated carbon and thus enhancing the capacitive behavior (as is evident from Figure (5.16-5.22)). Additionally, Figure 5.23 represents energy density (*E*) vs. power density (*P*) plots for the as-prepared devices, indicating the highest performance of the AC/Zn, P-Cdot supercapacitor devices (20 Wh kg^{-1} at 110 W kg^{-1} and 2.9 Wh kg^{-1} at 1320 W kg^{-1}) as compared to AC/P-Cdot or activated carbon based supercapacitor devices. Moreover, AC/Zn, P-Cdot SCE demonstrated remarkable cyclic stability. After 4000 cycles, the discharge capacity was measured to be 95.45 F/g at 3A/g with only 12.5% loss (Figure 5.24). The above results indicated a potentially new and important material in the form of crystalline assembled P-Cdots, wherein specific capacitance values of SCEs along with energy densities were found to be much higher as compared to literature reports.[13-20] The details are summarized in Table 5.9.

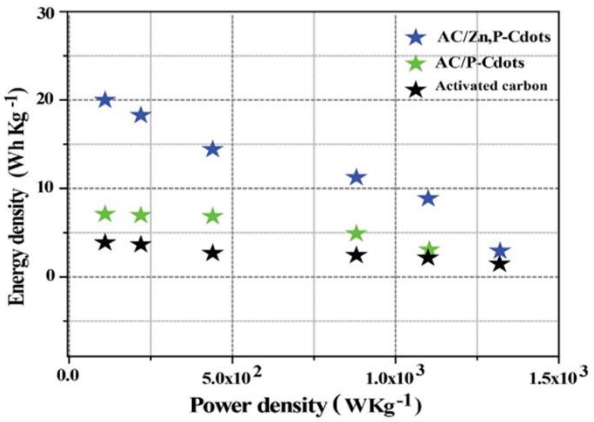

Figure 5.23. Ragone plot related to the energy and power densities.

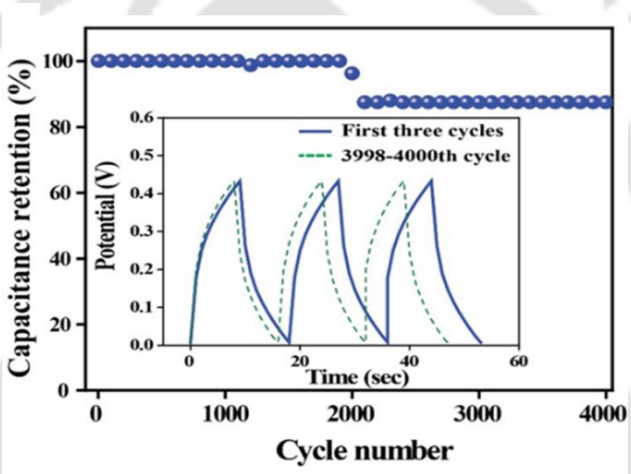

Figure 5.24. Cycling performance of AC/Zn, P-Cdot capacitor electrode at 3 A/g. Inset picture showing charge-discharge curves corresponding to first three cycles and the same for 3998-4000 cycles.

Table 5.9. Tabulated form of the comparison of different porous carbon based active materials for supercapacitors in two electrode system.

Ref. No.	Journals	Materials	Surface area (m^2/g)	Electrolyte	Current density /Scan rate	Specific capacitance (F/g)	Energy density ($Wh\ kg^{-1}$)
This work	*Present work*	*Crystalline Cdot assembly embedded activated carbon*	*630.8*	*0.2 M KOH (aqueous)*	*0.25 A/g*	*743.2*	*20*
13	*Nano Energy* **2018**, *47*, 547-555.	O-N-S co-doped three-dimensional hierarchical porous carbons	2650	6 M KOH *aqueous*	0.1 A/g	352	12
14	*Adv. Mater.* **2017**, *29*, 1604569.	Porous 3D Graphene-like Carbon	1545	6 mol L^{-1} KOH *aqueous*	1 A/g	231	4.2
15	*J. Mater. Chem. A* **2013**,*1*, 6462-6470.	Porous graphene-like nano sheets (PGNSs)	1874	6 M KOH *aqueous*	1 A/g	69	9.58
16	*Adv. Funct. Mater.* **2018**, *28*, 1805898.	Ultra-microporous carbons puzzled by GQDs	1730	6 M KOH *aqueous*	0.5 A/g	240	9.38
17	*Adv. Energy Mater.* **2015**, *5*, 1401761.	Porous carbon nanosheets	2770	6 M KOH *aqueous*	1 A/g	228	6.6
18	*small* **2016**, *12, No. 23, 3134-3142*	Hollow microporous carbon Spheres	816	6 M KOH *aqueous*	2 mV/ s	240	5.4
19	*Nanoscale* **2018**, *10*, 22871-22883.	N-doped graphene quantum dots/ porous carbon	704.1	1 M H_2SO_4 *aqueous*	0.5 A/g	294.1	10.2
20	*J. Phys. Chem. C* **2016**, *120*, 13406-13413.	Cdots (PEG-400) modified activated carbon	723	6 M KOH *aqueous*	1 A/g	134	-

5.3 Conclusion. In summary, we have demonstrated that crystalline assembly of carbon dots provides a new platform for improving the electrochemical performance of supercapacitor electrodes. Assisted by multiple spectroscopic (photoluminescence, X-ray photoelectron, and infrared) and microscopic (high resolution transmission electron microscopy, and selected area electron diffraction) characterizations, we propose that Zn^{2+} ions ligated in alternative octahedral/tetrahedral fashion with free phosphate groups over Cdot surface were likely present in the assembled system. Also, a representative three-dimensional structure of the same has been proposed. Generation of excellent crystallinity made P-Cdots conducive towards favorable electron and/or ion transportations, which was finally implemented for boosting the electrochemical performance of activated carbon. Conductive networks, induced by crystalline Cdot assembly maximized ion transportation, charge storage ability (743.2 F/g) and provided highest energy density (20 Wh kg^{-1} at 110 W kg^{-1}). Arranging Cdots into well-defined structure is remarkable and such programmed assembly of crystalline Cdots can be considered to provide a bio-friendly alternative in the fields of organic electronics, organic photovoltaics and energy storage devices in the near future.

References:

1. Pal, A.; Natu, G.; Ahmad, K.; Chattopadhyay, A. Phosphorus Induced Crystallinity in Carbon Dots for Solar Light Assisted Seawater Desalination. *J. Mater. Chem. A* **2018**, *6*, 4111-4118.

2. Li, Z.; Bu, F.; Wei, J.; Yao, W.; Wang, L.; Chen, Z.; Pan, D.; Wu, M. Boosting the Energy Storage Densities of Supercapacitors by Incorporating N-doped Graphene Quantum Dots into Cubic Porous Carbon. *Nanoscale* **2018**, *10*, 22871-22883.

3. Georgakilas, V.; Perman, J. A.; Tucek, J.; Zboril, R. Broad Family of Carbon Nanoallotropes: Classification, Chemistry, and Applications of Fullerenes, Carbon Dots, Nanotubes, Graphene, Nanodiamonds, and Combined Superstructures. *Chem. Rev.* **2015**, *115*, 4744-4822.

4. Zhou, X.; Bai, H.; Ma, H.; Li, H.; Yuan, W.; Du, H.; Zhang, P.; Xin, H. Synthesis of Zinc Phosphate and Zinc Ammonium Phosphate Nanostructures with Different Morphologies through pH Control. *Mater. Charact.* **2015,** *108*, 22-28.

5. Zhang, Z.; Shao, C.; Li, X.; Wang, C.; Zhang, M.; Liu, Y. Electrospun Nanofibers of p-Type NiO/n-Type ZnO Heterojunctions with Enhanced Photocatalytic Activity. *ACS Appl. Mater. Interfaces* **2010**, *2*, 2915-2923.

6. Wang, C.; Sun, D.; Zhuo, K.; Zhang, H.; Wang, J. Simple and Green Synthesis of Nitrogen-, Sulfur-, and Phosphorus-co-doped Carbon dots with Tunable Luminescence Properties and Sensing Application. *RSC Adv.* **2014**, *4*, 54060-54065.

7. Qin, N.; Xiang, Q.; Zhao, H.; Zhang, J.; Xu, J. Evolution of ZnO Microstructures from Hexagonal Disk to Prismoid, Prism and Pyramid and their Crystal Facet-dependent Gas Sensing Properties. *CrystEngComm* **2014,** *16*,7062-7073.

8. Zhang, Z.; Shao, C.; Li, X.; Wang, C.; Zhang, M.; Liu, Y. Electrospun Nanofibers of p-Type NiO/n-Type ZnO Heterojunctions with Enhanced Photocatalytic Activity. *ACS Appl. Mater. Interfaces* **2010**, *2(10)*, 2915-2923.

9. Qi, W.; Zhao, H.; Wu, Y.; Zeng, H.; Tao, T.; Chen, C.; Kuang, C.; Zhou, S.; Huang, Y. Facile Synthesis of Layer Structured GeP_3/C with Stable Chemical Bonding for Enhanced Lithium-Ion Storage. *Sci. Rep.* **2017**, *7*, 43582.

10. Xu, Q.; Liu, Y.; Gao, C.; Wei, J.; Zhou, H.; Chen, Y.; Dong, C.; Sreeprasad, T. S.; Li, N.; Xia, Z. Synthesis, Mechanistic Investigation, and Application of

Photoluminescent Sulfur and Nitrogen Co-Doped Carbon Dots. *J. Mater. Chem. C* **2015**, *3*, 9885-9893.

11. Chen, Y.; Lian, H.; Wei, Y.; He, X.; Chen, Y.; Wang, B.; Zeng, Q.; Lin, J. Concentration-induced Multi-colored Emissions in Carbon Dots: Origination from Triple Fluorescent Centers. *Nanoscale* **2018**, *10*, 6734-6743.

12. van Dam, B.; Nie, H.; Ju, B.; Marino, E.; Paulusse, J. M. J.; Schall, P.; Li, M.; Dohnalova, K. Excitation-Dependent Photoluminescence from Single-Carbon Dots. *Small* **2017,** *13*,1702098.

13. Zhao, G.; Chen, C.; Yu, D.; Sun, L.; Yang, C.; Zhang, H.; Sun, Y.; Besenbacher, F.; Yu, M. One-Step Production of O-N-S Co-Doped Three-Dimensional Hierarchical Porous Carbons for High-Performance Supercapacitors. *Nano Energy* **2018**,*47*, 547-555.

14. Zhao, J.; Jiang, Y.; Fan, H.; Liu, M.; Zhuo, O.; Wang, X.; Wu, Q.; Yang, L.; Ma, Y.; Hu, Z. Porous 3D Few-Layer Graphene-like Carbon for Ultrahigh-Power Supercapacitors with Well-Defined Structure-Performance Relationship. *Adv. Mater.* **2017**, *29*,1604569.

15. Sun, L.; Tian, C.; Li, M.; Meng, X.; Wang, L.; Wang, R.; Yin, J.; Fu, H. From coconut shell to porous graphene-like nanosheets for high-power supercapacitors. *J. Mater. Chem. A* **2013**, *1*,6462-6470.

16. Zhang, S.; Zhu, J.; Qing, Y.; Wang, L.; Zhao, J.; Li, J.; Tian, W.; Jia, D.; Fan, Z. Ultramicroporous Carbons Puzzled by Graphene Quantum Dots: Integrated High Gravimetric, Volumetric, and Areal Capacitances for Supercapacitors. *Adv. Funct. Mater.***2018**, *28*,1805898.

17. Fan, X.; Yu, C.; Yang, J.; Ling, Z.; Hu, C.; Zhang, M.; Qiu, J. A Layered-Nanospace-Confinement Strategy for the Synthesis of Two-Dimensional Porous Carbon Nanosheets for High-Rate Performance Supercapacitors. *Adv. Energy Mater.* **2015**, *5*, 1401761.

18. Wang, K.; Huang, L.; Razzaque, S.; Jin, S.; Tan, B. Fabrication of Hollow Microporous Carbon Spheres from Hyper-Crosslinked Microporous Polymers. *Small* **2016**, *12*, 3134-3142.

19. Li, Z.; Bu, F.; Wei, J.; Yao, W.; Wang, L.; Chen, Z.; Pan, D.; Wu, M. Boosting the energy storage densities of supercapacitors by incorporating N-doped graphene quantum dots into cubic porous carbon. *Nanoscale* **2018**, *10*, 22871-22883.

20. Kumar, V. B.; Borenstein, A.; Markovsky, B.; Aurbach, D.; Gedanken, A.; Talianker, M.; Porat, Z. Activated Carbon Modified with Carbon Nanodots as Novel Electrode Material for Supercapacitors. *J. Phys. Chem. C* **2016**, *120*, 13406-13413.

Chapter 6

Summary and Future Prospects

6.1 Summary

In summary, throughout the present thesis facile synthetic strategies have been reported in order to generate noble characteristics in carbon dot (Cdot) systems, which are as follows.

(i) Microwave assisted synthesis of hetero atom doped Cdots for improved photophysical properties is reported. During studies it has been observed that due to the introduction of boron and phosphorus in Cdots, the photoluminescence quantum yields/quantum efficiency could be increased and decreased (respectively) as opposed to established literature.

(ii) Conducting nature in Cdots has been demonstrated based on the *I-V* characteristic studies. Linear *I-V* characteristic plot confirmed the metallic behavior of the as-prepared film. In this work, the conductivity of Cdot film was attributed to the presence of sp^2 C–C bonds, which allowed conjugation of the adjacent π-bonds to form the π- and π*-bands.

(iii) Microwave assisted facile synthetic technique for generating dopant induced crystalline nature in Cdots has been reported. Based on detailed experimental analyses followed by computational refinement, formation of the orthorhombic crystalline pattern of the unit cells in the Cdot structure has been proposed.

(iv) Extent of crystallinity in Cdot structure was further improved by using zinc ion induced crystalline assembly. The so generated crystallinity in Cdot-assembly was found to improve electrochemical performance and charge storage ability of electrodes significantly.

Most importantly, based on the observed fundamental properties in carbon nano structures versatile applications of Cdots in different areas of nano science and nano technology have been demonstrated such as fluorescence based intracellular pH sensing, conductometric detection of nitro explosive compounds, solar light assisted sea water desalination and energy storage application. To conclude, the present thesis not

only showcases Cdots as good optical nano material, but also portrays their excellent crystalline nature and recommend them as future energy material.

6.2 Future Prospects

Discovery of non-graphitic crystallinity in Cdots is exceptional, as so far only amorphous or limited graphitic crystallinity in carbon nano structures are known. Besides, insufficient knowledge regarding their structures further put limitations on understanding their fundamental properties. Present thesis is believed to add a new dimension towards making arranged structural units in Cdot systems inducing crystalline property with improved qualities. Furthermore, it is believed that Cdots could be utilized as efficient energy material and using their crystalline nature miniaturized, low-cost, environment friendly devices, free from heavy metals can be fabricated for photocatalysis, photovoltaics, energy storage and energy conversion.

List of Publications

1. **Pal, A.**; Sk, M. P.; Chattopadhyay, A. Conducting Carbon dot-Polypyrrole Nanocomposite for Sensitive Detection of Picric acid. *ACS Appl. Mater. Interfaces* **2016**, *8(9)*, 5758-5762.

2. **Pal, A.**; Natu, G.; Ahmad, K.; Chattopadhyay, A. Phosphorous Induced Crystallinity in Carbon Dots for Solar Light Assisted Seawater Desalination. *J. Mater. Chem. A* **2018**, *6*, 4111-4118.

3. Ahmad, K.; **Pal, A.**; Pan, U.N.; Chattopadhyay, A.; Paul, A. Synthesis of Single-particle Level White-light-emitting Carbon dots via a One-step Microwave Method. *J. Mater. Chem. C* **2018**, *6*, 6691-6697.

4. **Pal, A.**; Ahmad, K.; Dutta, D.; Chattopadhyay, A. Boron Doped Carbon Dots with Unusually High Photoluminescence Quantum Yield for Ratiometric Intracellular pH Sensing. *ChemPhysChem* **2019**, *20*, 1018-1027.

5. **Pal, A.**; Bhakat, A.; Chattopadhyay, A. Zinc Ion-Induced Assembly of Crystalline Carbon Dots with Excellent Supercapacitor Performance. *J. Phys. Chem. C* **2019**, *123*, 19421-19428.

Conferences Attended

1. New Advances and Horizons in Nanoscience and Nanotechnology (NanoSci-2014) held at IASST, Guwahati, India. (National conference)
2. MEMS/NEMS and Theranostic Devices (NWNTD 2015) held at IIT Guwahati, India.
3. DAE-BRNS 6th Interdisciplinary Symposium on Materials Chemistry (ISMC-2016) held at BARC, Mumbai, India.
4. 5th International Conference on Advanced Nanomaterials and Nanotechnology (ICANN-2017) held at IIT Guwahati, India.
5. Frontiers in Chemical Sciences (FICS-2018) held at IIT Guwahati, India.
6. International Conference on Nano Science and Technology (ICONSAT-2018) held at IISc, Bengaluru, India

Permissions

Title: Graphitic Nitrogen Triggers Red Fluorescence in Carbon Dots

Author: Kateřina Holá, Mária Sudolská, Sergii Kalytchuk, et al

Publication: ACS Nano

Publisher: American Chemical Society

Date: Dec 1, 2017

PERMISSION/LICENSE IS GRANTED FOR YOUR ORDER AT NO CHARGE

This type of permission/license, instead of the standard Terms & Conditions, is sent to you because no fee is being charged for your order. Please note the following:

- Permission is granted for your request in both print and electronic formats, and translations.
- If figures and/or tables were requested, they may be adapted or used in part.
- Please print this page for your records and send a copy of it to your publisher/graduate school.
- Appropriate credit for the requested material should be given as follows: "Reprinted (adapted) with permission from (COMPLETE REFERENCE CITATION). Copyright (YEAR) American Chemical Society." Insert appropriate information in place of the capitalized words.
- One-time permission is granted only for the use specified in your request. No additional uses are granted (such as derivative works or other editions). For any other uses, please submit a new request.

If credit is given to another source for the material you requested, permission must be obtained from that source.

TH-2131_146122026

Title:	Full-Color Light-Emitting Carbon Dots with a Surface-State-Controlled Luminescence Mechanism
Author:	Hui Ding, Shang-Bo Yu, Ji-Shi Wei, et al
Publication:	ACS Nano
Publisher:	American Chemical Society
Date:	Jan 1, 2016

PERMISSION/LICENSE IS GRANTED FOR YOUR ORDER AT NO CHARGE

This type of permission/license, instead of the standard Terms & Conditions, is sent to you because no fee is being charged for your order. Please note the following:

- Permission is granted for your request in both print and electronic formats, and translations.
- If figures and/or tables were requested, they may be adapted or used in part.
- Please print this page for your records and send a copy of it to your publisher/graduate school.
- Appropriate credit for the requested material should be given as follows: "Reprinted (adapted) with permission from (COMPLETE REFERENCE CITATION). Copyright (YEAR) American Chemical Society." Insert appropriate information in place of the capitalized words.
- One-time permission is granted only for the use specified in your request. No additional uses are granted (such as derivative works or other editions). For any other uses, please submit a new request.

If credit is given to another source for the material you requested, permission must be obtained from that source.

BACK | CLOSE WINDOW

TH-2131_146122026

Royal Society of Chemistry LICENSE TERMS AND CONDITIONS

Jul 09, 2019

This is a License Agreement between AYAN PAL ("You") and Royal Society of Chemistry ("Royal Society of Chemistry") provided by Copyright Clearance Center ("CCC"). The license consists of your order details, the terms and conditions provided by Royal Society of Chemistry, and the payment terms and conditions.

All payments must be made in full to CCC. For payment instructions, please see information listed at the bottom of this form.

License Number	4624711091320
License date	Jul 09, 2019
Licensed content publisher	Royal Society of Chemistry
Licensed content title	Chemical communications
Licensed content date	Jan 1, 1996
Type of Use	Thesis/Dissertation
Requestor type	Academic institution
Format	Print, Electronic
Portion	image/photo
Number of images/photos requested	1
The requesting person/organization is:	Ayan Pal, IIT Guwahati
Title or numeric reference of the portion(s)	Chapter 1 (Introduction), Figure 1.3 (in thesis); Fig. 5 (in the original article).
Title of the article or chapter the portion is from	Classical oxidant induced chemiluminescence of fluorescent carbon dots.
Editor of portion(s)	N/A
Author of portion(s)	N/A
Volume of serial or monograph.	N/A
Page range of the portion	1051–1053
Publication date of portion	August 2019
Rights for	Main product
Duration of use	Life of current edition
Creation of copies for the disabled	no
With minor editing privileges	yes
For distribution to	Worldwide
In the following language(s)	Original language of publication
With incidental promotional use	no
The requested content will be used in number of	Up to 499

new product

Title	Towards Crystalline Carbon dots for Improved Application Potential
Institution name	IIT Guwahati, India
Expected presentation date	Aug 2019
Total (may include CCC user fee)	0.00 USD

Terms and Conditions

TERMS AND CONDITIONS
The following terms are individual to this publisher:

None

Other Terms and Conditions:
STANDARD TERMS AND CONDITIONS

1. Description of Service; Defined Terms. This Republication License enables the User to obtain licenses for republication of one or more copyrighted works as described in detail on the relevant Order Confirmation (the "Work(s)"). Copyright Clearance Center, Inc. ("CCC") grants licenses through the Service on behalf of the rightsholder identified on the Order Confirmation (the "Rightsholder"). "Republication", as used herein, generally means the inclusion of a Work, in whole or in part, in a new work or works, also as described on the Order Confirmation. "User", as used herein, means the person or entity making such republication.
2. The terms set forth in the relevant Order Confirmation, and any terms set by the Rightsholder with respect to a particular Work, govern the terms of use of Works in connection with the Service. By using the Service, the person transacting for a republication license on behalf of the User represents and warrants that he/she/it (a) has been duly authorized by the User to accept, and hereby does accept, all such terms and conditions on behalf of User, and (b) shall inform User of all such terms and conditions. In the event such person is a "freelancer" or other third party independent of User and CCC, such party shall be deemed jointly a "User" for purposes of these terms and conditions. In any event, User shall be deemed to have accepted and agreed to all such terms and conditions if User republishes the Work in any fashion.
3. Scope of License; Limitations and Obligations.
3.1 All Works and all rights therein, including copyright rights, remain the sole and exclusive property of the Rightsholder. The license created by the exchange of an Order Confirmation (and/or any invoice) and payment by User of the full amount set forth on that document includes only those rights expressly set forth in the Order Confirmation and in these terms and conditions, and conveys no other rights in the Work(s) to User. All rights not expressly granted are hereby reserved.
3.2 General Payment Terms: You may pay by credit card or through an account with us payable at the end of the month. If you and we agree that you may establish a standing account with CCC, then the following terms apply: Remit Payment to: Copyright Clearance Center, 29118 Network Place, Chicago, IL 60673-1291. Payments Due: Invoices are payable upon their delivery to you (or upon our notice to you that they are available to you for downloading). After 30 days, outstanding amounts will be subject to a service charge of 1-1/2% per month or, if less, the maximum rate allowed by applicable law. Unless otherwise specifically set forth in the Order Confirmation or in a separate written agreement signed by CCC, invoices are due and payable on "net 30" terms. While User may exercise the rights licensed immediately upon issuance of the Order Confirmation, the license is automatically revoked and is null and void, as if it had never been issued, if complete payment for the license is not received on a timely basis either from User directly or through a payment agent, such as a credit card company.
3.3 Unless otherwise provided in the Order Confirmation, any grant of rights to User (i) is one-time (including the editions and product family specified in the license), (ii) is non-

exclusive and non-transferable and (iii) is subject to any and all limitations and restrictions (such as, but not limited to, limitations on duration of use or circulation) included in the Order Confirmation or invoice and/or in these terms and conditions. Upon completion of the licensed use, User shall either secure a new permission for further use of the Work(s) or immediately cease any new use of the Work(s) and shall render inaccessible (such as by deleting or by removing or severing links or other locators) any further copies of the Work (except for copies printed on paper in accordance with this license and still in User's stock at the end of such period).

3.4 In the event that the material for which a republication license is sought includes third party materials (such as photographs, illustrations, graphs, inserts and similar materials) which are identified in such material as having been used by permission, User is responsible for identifying, and seeking separate licenses (under this Service or otherwise) for, any of such third party materials; without a separate license, such third party materials may not be used.

3.5 Use of proper copyright notice for a Work is required as a condition of any license granted under the Service. Unless otherwise provided in the Order Confirmation, a proper copyright notice will read substantially as follows: “Republished with permission of [Rightsholder’s name], from [Work's title, author, volume, edition number and year of copyright]; permission conveyed through Copyright Clearance Center, Inc. ” Such notice must be provided in a reasonably legible font size and must be placed either immediately adjacent to the Work as used (for example, as part of a by-line or footnote but not as a separate electronic link) or in the place where substantially all other credits or notices for the new work containing the republished Work are located. Failure to include the required notice results in loss to the Rightsholder and CCC, and the User shall be liable to pay liquidated damages for each such failure equal to twice the use fee specified in the Order Confirmation, in addition to the use fee itself and any other fees and charges specified.

3.6 User may only make alterations to the Work if and as expressly set forth in the Order Confirmation. No Work may be used in any way that is defamatory, violates the rights of third parties (including such third parties' rights of copyright, privacy, publicity, or other tangible or intangible property), or is otherwise illegal, sexually explicit or obscene. In addition, User may not conjoin a Work with any other material that may result in damage to the reputation of the Rightsholder. User agrees to inform CCC if it becomes aware of any infringement of any rights in a Work and to cooperate with any reasonable request of CCC or the Rightsholder in connection therewith.

4. Indemnity. User hereby indemnifies and agrees to defend the Rightsholder and CCC, and their respective employees and directors, against all claims, liability, damages, costs and expenses, including legal fees and expenses, arising out of any use of a Work beyond the scope of the rights granted herein, or any use of a Work which has been altered in any unauthorized way by User, including claims of defamation or infringement of rights of copyright, publicity, privacy or other tangible or intangible property.

5. Limitation of Liability. UNDER NO CIRCUMSTANCES WILL CCC OR THE RIGHTSHOLDER BE LIABLE FOR ANY DIRECT, INDIRECT, CONSEQUENTIAL OR INCIDENTAL DAMAGES (INCLUDING WITHOUT LIMITATION DAMAGES FOR LOSS OF BUSINESS PROFITS OR INFORMATION, OR FOR BUSINESS INTERRUPTION) ARISING OUT OF THE USE OR INABILITY TO USE A WORK, EVEN IF ONE OF THEM HAS BEEN ADVISED OF THE POSSIBILITY OF SUCH DAMAGES. In any event, the total liability of the Rightsholder and CCC (including their respective employees and directors) shall not exceed the total amount actually paid by User for this license. User assumes full liability for the actions and omissions of its principals, employees, agents, affiliates, successors and assigns.

6. Limited Warranties. THE WORK(S) AND RIGHT(S) ARE PROVIDED “AS IS”. CCC HAS THE RIGHT TO GRANT TO USER THE RIGHTS GRANTED IN THE ORDER CONFIRMATION DOCUMENT. CCC AND THE RIGHTSHOLDER DISCLAIM ALL OTHER WARRANTIES RELATING TO THE WORK(S) AND RIGHT(S), EITHER

EXPRESS OR IMPLIED, INCLUDING WITHOUT LIMITATION IMPLIED WARRANTIES OF MERCHANTABILITY OR FITNESS FOR A PARTICULAR PURPOSE. ADDITIONAL RIGHTS MAY BE REQUIRED TO USE ILLUSTRATIONS, GRAPHS, PHOTOGRAPHS, ABSTRACTS, INSERTS OR OTHER PORTIONS OF THE WORK (AS OPPOSED TO THE ENTIRE WORK) IN A MANNER CONTEMPLATED BY USER; USER UNDERSTANDS AND AGREES THAT NEITHER CCC NOR THE RIGHTSHOLDER MAY HAVE SUCH ADDITIONAL RIGHTS TO GRANT.

7. Effect of Breach. Any failure by User to pay any amount when due, or any use by User of a Work beyond the scope of the license set forth in the Order Confirmation and/or these terms and conditions, shall be a material breach of the license created by the Order Confirmation and these terms and conditions. Any breach not cured within 30 days of written notice thereof shall result in immediate termination of such license without further notice. Any unauthorized (but licensable) use of a Work that is terminated immediately upon notice thereof may be liquidated by payment of the Rightsholder's ordinary license price therefor; any unauthorized (and unlicensable) use that is not terminated immediately for any reason (including, for example, because materials containing the Work cannot reasonably be recalled) will be subject to all remedies available at law or in equity, but in no event to a payment of less than three times the Rightsholder's ordinary license price for the most closely analogous licensable use plus Rightsholder's and/or CCC's costs and expenses incurred in collecting such payment.

8. **Miscellaneous.**

8.1 User acknowledges that CCC may, from time to time, make changes or additions to the Service or to these terms and conditions, and CCC reserves the right to send notice to the User by electronic mail or otherwise for the purposes of notifying User of such changes or additions; provided that any such changes or additions shall not apply to permissions already secured and paid for.

8.2 Use of User-related information collected through the Service is governed by CCC's privacy policy, available online here:
http://www.copyright.com/content/cc3/en/tools/footer/privacypolicy.html.

8.3 The licensing transaction described in the Order Confirmation is personal to User. Therefore, User may not assign or transfer to any other person (whether a natural person or an organization of any kind) the license created by the Order Confirmation and these terms and conditions or any rights granted hereunder; provided, however, that User may assign such license in its entirety on written notice to CCC in the event of a transfer of all or substantially all of User's rights in the new material which includes the Work(s) licensed under this Service.

8.4 No amendment or waiver of any terms is binding unless set forth in writing and signed by the parties. The Rightsholder and CCC hereby object to any terms contained in any writing prepared by the User or its principals, employees, agents or affiliates and purporting to govern or otherwise relate to the licensing transaction described in the Order Confirmation, which terms are in any way inconsistent with any terms set forth in the Order Confirmation and/or in these terms and conditions or CCC's standard operating procedures, whether such writing is prepared prior to, simultaneously with or subsequent to the Order Confirmation, and whether such writing appears on a copy of the Order Confirmation or in a separate instrument.

8.5 The licensing transaction described in the Order Confirmation document shall be governed by and construed under the law of the State of New York, USA, without regard to the principles thereof of conflicts of law. Any case, controversy, suit, action, or proceeding arising out of, in connection with, or related to such licensing transaction shall be brought, at CCC's sole discretion, in any federal or state court located in the County of New York, State of New York, USA, or in any federal or state court whose geographical jurisdiction covers the location of the Rightsholder set forth in the Order Confirmation. The parties expressly submit to the personal jurisdiction and venue of each such federal or state court.If you have

TH-2131_146122026

any comments or questions about the Service or Copyright Clearance Center, please contact us at 978-750-8400 or send an e-mail to info@copyright.com.
v 1.1

Questions? customercare@copyright.com or +1-855-239-3415 (toll free in the US) or +1-978-646-2777.

TH-2131_146122026

JOHN WILEY AND SONS LICENSE TERMS AND CONDITIONS

Jul 08, 2019

This Agreement between AYAN PAL ("You") and John Wiley and Sons ("John Wiley and Sons") consists of your license details and the terms and conditions provided by John Wiley and Sons and Copyright Clearance Center.

License Number	4624130387370
License date	Jul 08, 2019
Licensed Content Publisher	John Wiley and Sons
Licensed Content Publication	Advanced Materials
Licensed Content Title	Bright Multicolor Bandgap Fluorescent Carbon Quantum Dots for Electroluminescent Light-Emitting Diodes
Licensed Content Author	Fanglong Yuan, Zhibin Wang, Xiaohong Li, et al
Licensed Content Date	Nov 23, 2016
Licensed Content Volume	29
Licensed Content Issue	3
Licensed Content Pages	6
Type of use	Dissertation/Thesis
Requestor type	University/Academic
Format	Print and electronic
Portion	Figure/table
Number of figures/tables	3
Original Wiley figure/table number(s)	Figure 1b, Figure 2b, Figure 3a
Will you be translating?	No
Title of your thesis / dissertation	Towards Crystalline Carbon dots for Improved Application Potential
Expected completion date	Aug 2019
Expected size (number of pages)	150
Requestor Location	AYAN PAL IIT GUWAHATI, ASSAM, INDIA IIT GUWAHATI, ASSAM, INDIA GUWAHATI, ASSAM 781039 India Attn: AYAN PAL
Publisher Tax ID	EU826007151
Total	0.00 USD
Terms and Conditions	

TERMS AND CONDITIONS

This copyrighted material is owned by or exclusively licensed to John Wiley & Sons, Inc. or one of its group companies (each a"Wiley Company") or handled on behalf of a society with

YH-2131_4461220260

which a Wiley Company has exclusive publishing rights in relation to a particular work (collectively "WILEY"). By clicking "accept" in connection with completing this licensing transaction, you agree that the following terms and conditions apply to this transaction (along with the billing and payment terms and conditions established by the Copyright Clearance Center Inc., ("CCC's Billing and Payment terms and conditions"), at the time that you opened your RightsLink account (these are available at any time at http://myaccount.copyright.com).

Terms and Conditions

- The materials you have requested permission to reproduce or reuse (the "Wiley Materials") are protected by copyright.

- You are hereby granted a personal, non-exclusive, non-sub licensable (on a stand-alone basis), non-transferable, worldwide, limited license to reproduce the Wiley Materials for the purpose specified in the licensing process. This license, **and any CONTENT (PDF or image file) purchased as part of your order,** is for a one-time use only and limited to any maximum distribution number specified in the license. The first instance of republication or reuse granted by this license must be completed within two years of the date of the grant of this license (although copies prepared before the end date may be distributed thereafter). The Wiley Materials shall not be used in any other manner or for any other purpose, beyond what is granted in the license. Permission is granted subject to an appropriate acknowledgement given to the author, title of the material/book/journal and the publisher. You shall also duplicate the copyright notice that appears in the Wiley publication in your use of the Wiley Material. Permission is also granted on the understanding that nowhere in the text is a previously published source acknowledged for all or part of this Wiley Material. Any third party content is expressly excluded from this permission.

- With respect to the Wiley Materials, all rights are reserved. Except as expressly granted by the terms of the license, no part of the Wiley Materials may be copied, modified, adapted (except for minor reformatting required by the new Publication), translated, reproduced, transferred or distributed, in any form or by any means, and no derivative works may be made based on the Wiley Materials without the prior permission of the respective copyright owner.**For STM Signatory Publishers clearing permission under the terms of the STM Permissions Guidelines only, the terms of the license are extended to include subsequent editions and for editions in other languages, provided such editions are for the work as a whole in situ and does not involve the separate exploitation of the permitted figures or extracts,** You may not alter, remove or suppress in any manner any copyright, trademark or other notices displayed by the Wiley Materials. You may not license, rent, sell, loan, lease, pledge, offer as security, transfer or assign the Wiley Materials on a stand-alone basis, or any of the rights granted to you hereunder to any other person.

- The Wiley Materials and all of the intellectual property rights therein shall at all times remain the exclusive property of John Wiley & Sons Inc, the Wiley Companies, or their respective licensors, and your interest therein is only that of having possession of and the right to reproduce the Wiley Materials pursuant to Section 2 herein during the continuance of this Agreement. You agree that you own no right, title or interest in or to the Wiley Materials or any of the intellectual property rights therein. You shall have no rights hereunder other than the license as provided for above in Section 2. No right, license or interest to any trademark, trade name, service mark or other branding ("Marks") of WILEY or its licensors is granted hereunder, and you agree that you

TH-2131_146122026

shall not assert any such right, license or interest with respect thereto

- NEITHER WILEY NOR ITS LICENSORS MAKES ANY WARRANTY OR REPRESENTATION OF ANY KIND TO YOU OR ANY THIRD PARTY, EXPRESS, IMPLIED OR STATUTORY, WITH RESPECT TO THE MATERIALS OR THE ACCURACY OF ANY INFORMATION CONTAINED IN THE MATERIALS, INCLUDING, WITHOUT LIMITATION, ANY IMPLIED WARRANTY OF MERCHANTABILITY, ACCURACY, SATISFACTORY QUALITY, FITNESS FOR A PARTICULAR PURPOSE, USABILITY, INTEGRATION OR NON-INFRINGEMENT AND ALL SUCH WARRANTIES ARE HEREBY EXCLUDED BY WILEY AND ITS LICENSORS AND WAIVED BY YOU.

- WILEY shall have the right to terminate this Agreement immediately upon breach of this Agreement by you.

- You shall indemnify, defend and hold harmless WILEY, its Licensors and their respective directors, officers, agents and employees, from and against any actual or threatened claims, demands, causes of action or proceedings arising from any breach of this Agreement by you.

- IN NO EVENT SHALL WILEY OR ITS LICENSORS BE LIABLE TO YOU OR ANY OTHER PARTY OR ANY OTHER PERSON OR ENTITY FOR ANY SPECIAL, CONSEQUENTIAL, INCIDENTAL, INDIRECT, EXEMPLARY OR PUNITIVE DAMAGES, HOWEVER CAUSED, ARISING OUT OF OR IN CONNECTION WITH THE DOWNLOADING, PROVISIONING, VIEWING OR USE OF THE MATERIALS REGARDLESS OF THE FORM OF ACTION, WHETHER FOR BREACH OF CONTRACT, BREACH OF WARRANTY, TORT, NEGLIGENCE, INFRINGEMENT OR OTHERWISE (INCLUDING, WITHOUT LIMITATION, DAMAGES BASED ON LOSS OF PROFITS, DATA, FILES, USE, BUSINESS OPPORTUNITY OR CLAIMS OF THIRD PARTIES), AND WHETHER OR NOT THE PARTY HAS BEEN ADVISED OF THE POSSIBILITY OF SUCH DAMAGES. THIS LIMITATION SHALL APPLY NOTWITHSTANDING ANY FAILURE OF ESSENTIAL PURPOSE OF ANY LIMITED REMEDY PROVIDED HEREIN.

- Should any provision of this Agreement be held by a court of competent jurisdiction to be illegal, invalid, or unenforceable, that provision shall be deemed amended to achieve as nearly as possible the same economic effect as the original provision, and the legality, validity and enforceability of the remaining provisions of this Agreement shall not be affected or impaired thereby.

- The failure of either party to enforce any term or condition of this Agreement shall not constitute a waiver of either party's right to enforce each and every term and condition of this Agreement. No breach under this agreement shall be deemed waived or excused by either party unless such waiver or consent is in writing signed by the party granting such waiver or consent. The waiver by or consent of a party to a breach of any provision of this Agreement shall not operate or be construed as a waiver of or consent to any other or subsequent breach by such other party.

- This Agreement may not be assigned (including by operation of law or otherwise) by you without WILEY's prior written consent.

TH-2131_146122026

- Any fee required for this permission shall be non-refundable after thirty (30) days from receipt by the CCC.

- These terms and conditions together with CCC's Billing and Payment terms and conditions (which are incorporated herein) form the entire agreement between you and WILEY concerning this licensing transaction and (in the absence of fraud) supersedes all prior agreements and representations of the parties, oral or written. This Agreement may not be amended except in writing signed by both parties. This Agreement shall be binding upon and inure to the benefit of the parties' successors, legal representatives, and authorized assigns.

- In the event of any conflict between your obligations established by these terms and conditions and those established by CCC's Billing and Payment terms and conditions, these terms and conditions shall prevail.

- WILEY expressly reserves all rights not specifically granted in the combination of (i) the license details provided by you and accepted in the course of this licensing transaction, (ii) these terms and conditions and (iii) CCC's Billing and Payment terms and conditions.

- This Agreement will be void if the Type of Use, Format, Circulation, or Requestor Type was misrepresented during the licensing process.

- This Agreement shall be governed by and construed in accordance with the laws of the State of New York, USA, without regards to such state's conflict of law rules. Any legal action, suit or proceeding arising out of or relating to these Terms and Conditions or the breach thereof shall be instituted in a court of competent jurisdiction in New York County in the State of New York in the United States of America and each party hereby consents and submits to the personal jurisdiction of such court, waives any objection to venue in such court and consents to service of process by registered or certified mail, return receipt requested, at the last known address of such party.

WILEY OPEN ACCESS TERMS AND CONDITIONS

Wiley Publishes Open Access Articles in fully Open Access Journals and in Subscription journals offering Online Open. Although most of the fully Open Access journals publish open access articles under the terms of the Creative Commons Attribution (CC BY) License only, the subscription journals and a few of the Open Access Journals offer a choice of Creative Commons Licenses. The license type is clearly identified on the article.

The Creative Commons Attribution License

The Creative Commons Attribution License (CC-BY) allows users to copy, distribute and transmit an article, adapt the article and make commercial use of the article. The CC-BY license permits commercial and non-

Creative Commons Attribution Non-Commercial License

The Creative Commons Attribution Non-Commercial (CC-BY-NC)License permits use, distribution and reproduction in any medium, provided the original work is properly cited and is not used for commercial purposes.(see below)

Creative Commons Attribution-Non-Commercial-NoDerivs License

The Creative Commons Attribution Non-Commercial-NoDerivs License (CC-BY-NC-ND) permits use, distribution and reproduction in any medium, provided the original work is properly cited, is not used for commercial purposes and no modifications or adaptations are made. (see below)

Use by commercial "for-profit" organizations

Use of Wiley Open Access articles for commercial, promotional, or marketing purposes requires further explicit permission from Wiley and will be subject to a fee.
Further details can be found on Wiley Online Library
http://olabout.wiley.com/WileyCDA/Section/id-410895.html

Other Terms and Conditions:

v1.10 Last updated September 2015

Questions? customercare@copyright.com or +1-855-239-3415 (toll free in the US) or +1-978-646-2777.

TH-2131_146122026

Royal Society of Chemistry LICENSE TERMS AND CONDITIONS

Jul 09, 2019

This is a License Agreement between AYAN PAL ("You") and Royal Society of Chemistry ("Royal Society of Chemistry") provided by Copyright Clearance Center ("CCC"). The license consists of your order details, the terms and conditions provided by Royal Society of Chemistry, and the payment terms and conditions.

All payments must be made in full to CCC. For payment instructions, please see information listed at the bottom of this form.

License Number	4624710664828
License date	Jul 09, 2019
Licensed content publisher	Royal Society of Chemistry
Licensed content title	Chemical communications
Licensed content date	Jan 1, 1996
Type of Use	Thesis/Dissertation
Requestor type	Academic institution
Format	Print, Electronic
Portion	image/photo
Number of images/photos requested	2
The requesting person/organization is:	Ayan Pal, IIT Guwahati
Title or numeric reference of the portion(s)	Chapter 1(Introduction), Figure 1.5 (in thesis); Scheme 1 and TOC in the original article
Title of the article or chapter the portion is from	A gold–carbon nanoparticle composite as an efficient catalyst for homocoupling reaction
Editor of portion(s)	N/A
Author of portion(s)	N/A
Volume of serial or monograph.	N/A
Page range of the portion	8235-8237
Publication date of portion	August 2019
Rights for	Main product
Duration of use	Life of current edition
Creation of copies for the disabled	no
With minor editing privileges	yes
For distribution to	Worldwide
In the following language(s)	Original language of publication
With incidental promotional use	no
The requested content will be used in my thesis	Up to 499

new product

Title	Towards Crystalline Carbon dots for Improved Application Potential
Institution name	IIT Guwahati, India
Expected presentation date	Aug 2019
Total (may include CCC user fee)	0.00 USD

Terms and Conditions

TERMS AND CONDITIONS
The following terms are individual to this publisher:

None

Other Terms and Conditions:
STANDARD TERMS AND CONDITIONS

1. Description of Service; Defined Terms. This Republication License enables the User to obtain licenses for republication of one or more copyrighted works as described in detail on the relevant Order Confirmation (the "Work(s)"). Copyright Clearance Center, Inc. ("CCC") grants licenses through the Service on behalf of the rightsholder identified on the Order Confirmation (the "Rightsholder"). "Republication", as used herein, generally means the inclusion of a Work, in whole or in part, in a new work or works, also as described on the Order Confirmation. "User", as used herein, means the person or entity making such republication.
2. The terms set forth in the relevant Order Confirmation, and any terms set by the Rightsholder with respect to a particular Work, govern the terms of use of Works in connection with the Service. By using the Service, the person transacting for a republication license on behalf of the User represents and warrants that he/she/it (a) has been duly authorized by the User to accept, and hereby does accept, all such terms and conditions on behalf of User, and (b) shall inform User of all such terms and conditions. In the event such person is a "freelancer" or other third party independent of User and CCC, such party shall be deemed jointly a "User" for purposes of these terms and conditions. In any event, User shall be deemed to have accepted and agreed to all such terms and conditions if User republishes the Work in any fashion.
3. Scope of License; Limitations and Obligations.
3.1 All Works and all rights therein, including copyright rights, remain the sole and exclusive property of the Rightsholder. The license created by the exchange of an Order Confirmation (and/or any invoice) and payment by User of the full amount set forth on that document includes only those rights expressly set forth in the Order Confirmation and in these terms and conditions, and conveys no other rights in the Work(s) to User. All rights not expressly granted are hereby reserved.
3.2 General Payment Terms: You may pay by credit card or through an account with us payable at the end of the month. If you and we agree that you may establish a standing account with CCC, then the following terms apply: Remit Payment to: Copyright Clearance Center, 29118 Network Place, Chicago, IL 60673-1291. Payments Due: Invoices are payable upon their delivery to you (or upon our notice to you that they are available to you for downloading). After 30 days, outstanding amounts will be subject to a service charge of 1-1/2% per month or, if less, the maximum rate allowed by applicable law. Unless otherwise specifically set forth in the Order Confirmation or in a separate written agreement signed by CCC, invoices are due and payable on "net 30" terms. While User may exercise the rights licensed immediately upon issuance of the Order Confirmation, the license is automatically revoked and is null and void, as if it had never been issued, if complete payment for the license is not received on a timely basis either from User directly or through a payment agent, such as a credit card company.
3.3 Unless otherwise provided in the Order Confirmation, any grant of rights to User (i) is one-time (including the editions and product family specified in the license), (ii) is non-

exclusive and non-transferable and (iii) is subject to any and all limitations and restrictions (such as, but not limited to, limitations on duration of use or circulation) included in the Order Confirmation or invoice and/or in these terms and conditions. Upon completion of the licensed use, User shall either secure a new permission for further use of the Work(s) or immediately cease any new use of the Work(s) and shall render inaccessible (such as by deleting or by removing or severing links or other locators) any further copies of the Work (except for copies printed on paper in accordance with this license and still in User's stock at the end of such period).

3.4 In the event that the material for which a republication license is sought includes third party materials (such as photographs, illustrations, graphs, inserts and similar materials) which are identified in such material as having been used by permission, User is responsible for identifying, and seeking separate licenses (under this Service or otherwise) for, any of such third party materials; without a separate license, such third party materials may not be used.

3.5 Use of proper copyright notice for a Work is required as a condition of any license granted under the Service. Unless otherwise provided in the Order Confirmation, a proper copyright notice will read substantially as follows: “Republished with permission of [Rightsholder’s name], from [Work's title, author, volume, edition number and year of copyright]; permission conveyed through Copyright Clearance Center, Inc. ” Such notice must be provided in a reasonably legible font size and must be placed either immediately adjacent to the Work as used (for example, as part of a by-line or footnote but not as a separate electronic link) or in the place where substantially all other credits or notices for the new work containing the republished Work are located. Failure to include the required notice results in loss to the Rightsholder and CCC, and the User shall be liable to pay liquidated damages for each such failure equal to twice the use fee specified in the Order Confirmation, in addition to the use fee itself and any other fees and charges specified.

3.6 User may only make alterations to the Work if and as expressly set forth in the Order Confirmation. No Work may be used in any way that is defamatory, violates the rights of third parties (including such third parties' rights of copyright, privacy, publicity, or other tangible or intangible property), or is otherwise illegal, sexually explicit or obscene. In addition, User may not conjoin a Work with any other material that may result in damage to the reputation of the Rightsholder. User agrees to inform CCC if it becomes aware of any infringement of any rights in a Work and to cooperate with any reasonable request of CCC or the Rightsholder in connection therewith.

4. Indemnity. User hereby indemnifies and agrees to defend the Rightsholder and CCC, and their respective employees and directors, against all claims, liability, damages, costs and expenses, including legal fees and expenses, arising out of any use of a Work beyond the scope of the rights granted herein, or any use of a Work which has been altered in any unauthorized way by User, including claims of defamation or infringement of rights of copyright, publicity, privacy or other tangible or intangible property.

5. Limitation of Liability. UNDER NO CIRCUMSTANCES WILL CCC OR THE RIGHTSHOLDER BE LIABLE FOR ANY DIRECT, INDIRECT, CONSEQUENTIAL OR INCIDENTAL DAMAGES (INCLUDING WITHOUT LIMITATION DAMAGES FOR LOSS OF BUSINESS PROFITS OR INFORMATION, OR FOR BUSINESS INTERRUPTION) ARISING OUT OF THE USE OR INABILITY TO USE A WORK, EVEN IF ONE OF THEM HAS BEEN ADVISED OF THE POSSIBILITY OF SUCH DAMAGES. In any event, the total liability of the Rightsholder and CCC (including their respective employees and directors) shall not exceed the total amount actually paid by User for this license. User assumes full liability for the actions and omissions of its principals, employees, agents, affiliates, successors and assigns.

6. Limited Warranties. THE WORK(S) AND RIGHT(S) ARE PROVIDED “AS IS”. CCC HAS THE RIGHT TO GRANT TO USER THE RIGHTS GRANTED IN THE ORDER CONFIRMATION DOCUMENT. CCC AND THE RIGHTSHOLDER DISCLAIM ALL OTHER WARRANTIES RELATING TO THE WORK(S) AND RIGHT(S), EITHER

EXPRESS OR IMPLIED, INCLUDING WITHOUT LIMITATION IMPLIED WARRANTIES OF MERCHANTABILITY OR FITNESS FOR A PARTICULAR PURPOSE. ADDITIONAL RIGHTS MAY BE REQUIRED TO USE ILLUSTRATIONS, GRAPHS, PHOTOGRAPHS, ABSTRACTS, INSERTS OR OTHER PORTIONS OF THE WORK (AS OPPOSED TO THE ENTIRE WORK) IN A MANNER CONTEMPLATED BY USER; USER UNDERSTANDS AND AGREES THAT NEITHER CCC NOR THE RIGHTSHOLDER MAY HAVE SUCH ADDITIONAL RIGHTS TO GRANT.

7. Effect of Breach. Any failure by User to pay any amount when due, or any use by User of a Work beyond the scope of the license set forth in the Order Confirmation and/or these terms and conditions, shall be a material breach of the license created by the Order Confirmation and these terms and conditions. Any breach not cured within 30 days of written notice thereof shall result in immediate termination of such license without further notice. Any unauthorized (but licensable) use of a Work that is terminated immediately upon notice thereof may be liquidated by payment of the Rightsholder's ordinary license price therefor; any unauthorized (and unlicensable) use that is not terminated immediately for any reason (including, for example, because materials containing the Work cannot reasonably be recalled) will be subject to all remedies available at law or in equity, but in no event to a payment of less than three times the Rightsholder's ordinary license price for the most closely analogous licensable use plus Rightsholder's and/or CCC's costs and expenses incurred in collecting such payment.

8. **Miscellaneous.**

8.1 User acknowledges that CCC may, from time to time, make changes or additions to the Service or to these terms and conditions, and CCC reserves the right to send notice to the User by electronic mail or otherwise for the purposes of notifying User of such changes or additions; provided that any such changes or additions shall not apply to permissions already secured and paid for.

8.2 Use of User-related information collected through the Service is governed by CCC's privacy policy, available online here:
http://www.copyright.com/content/cc3/en/tools/footer/privacypolicy.html.

8.3 The licensing transaction described in the Order Confirmation is personal to User. Therefore, User may not assign or transfer to any other person (whether a natural person or an organization of any kind) the license created by the Order Confirmation and these terms and conditions or any rights granted hereunder; provided, however, that User may assign such license in its entirety on written notice to CCC in the event of a transfer of all or substantially all of User's rights in the new material which includes the Work(s) licensed under this Service.

8.4 No amendment or waiver of any terms is binding unless set forth in writing and signed by the parties. The Rightsholder and CCC hereby object to any terms contained in any writing prepared by the User or its principals, employees, agents or affiliates and purporting to govern or otherwise relate to the licensing transaction described in the Order Confirmation, which terms are in any way inconsistent with any terms set forth in the Order Confirmation and/or in these terms and conditions or CCC's standard operating procedures, whether such writing is prepared prior to, simultaneously with or subsequent to the Order Confirmation, and whether such writing appears on a copy of the Order Confirmation or in a separate instrument.

8.5 The licensing transaction described in the Order Confirmation document shall be governed by and construed under the law of the State of New York, USA, without regard to the principles thereof of conflicts of law. Any case, controversy, suit, action, or proceeding arising out of, in connection with, or related to such licensing transaction shall be brought, at CCC's sole discretion, in any federal or state court located in the County of New York, State of New York, USA, or in any federal or state court whose geographical jurisdiction covers the location of the Rightsholder set forth in the Order Confirmation. The parties expressly submit to the personal jurisdiction and venue of each such federal or state court.If you have

TH-2131_146122026

any comments or questions about the Service or Copyright Clearance Center, please contact us at 978-750-8400 or send an e-mail to info@copyright.com.
v 1.1

Questions? customercare@copyright.com or +1-855-239-3415 (toll free in the US) or +1-978-646-2777.

TH-2131_146122026

Title: Synthesis of N,S-Doped Carbon Quantum Dots for Use in Organic Solar Cells as the ZnO Modifier To Eliminate the Light-Soaking Effect

Author: Yaling Wang, Lingpeng Yan, Guoqi Ji, et al

Publication: Applied Materials

Publisher: American Chemical Society

Date: Jan 1, 2019

PERMISSION/LICENSE IS GRANTED FOR YOUR ORDER AT NO CHARGE

This type of permission/license, instead of the standard Terms & Conditions, is sent to you because no fee is being charged for your order. Please note the following:

- Permission is granted for your request in both print and electronic formats, and translations.
- If figures and/or tables were requested, they may be adapted or used in part.
- Please print this page for your records and send a copy of it to your publisher/graduate school.
- Appropriate credit for the requested material should be given as follows: "Reprinted (adapted) with permission from (COMPLETE REFERENCE CITATION). Copyright (YEAR) American Chemical Society." Insert appropriate information in place of the capitalized words.
- One-time permission is granted only for the use specified in your request. No additional uses are granted (such as derivative works or other editions). For any other uses, please submit a new request.

If credit is given to another source for the material you requested, permission must be obtained from that source.

TH-2131_146122026

JOHN WILEY AND SONS LICENSE TERMS AND CONDITIONS

Jul 08, 2019

This Agreement between AYAN PAL ("You") and John Wiley and Sons ("John Wiley and Sons") consists of your license details and the terms and conditions provided by John Wiley and Sons and Copyright Clearance Center.

License Number	4624150049150
License date	Jul 08, 2019
Licensed Content Publisher	John Wiley and Sons
Licensed Content Publication	ChemPhysChem
Licensed Content Title	Boron Doped Carbon Dots with Unusually High Photoluminescence Quantum Yield for Ratiometric Intracellular pH Sensing
Licensed Content Author	Ayan Pal, Kafeel Ahmad, Deepanjalee Dutta, et al
Licensed Content Date	Apr 8, 2019
Licensed Content Volume	20
Licensed Content Issue	8
Licensed Content Pages	10
Type of use	Dissertation/Thesis
Requestor type	Author of this Wiley article
Format	Print and electronic
Portion	Full article
Will you be translating?	No
Title of your thesis / dissertation	Towards Crystalline Carbon dots for Improved Application Potential
Expected completion date	Aug 2019
Expected size (number of pages)	150
Requestor Location	AYAN PAL IIT GUWAHATI, ASSAM, INDIA IIT GUWAHATI, ASSAM, INDIA GUWAHATI, ASSAM 781039 India Attn: AYAN PAL
Publisher Tax ID	EU826007151
Total	0.00 USD
Terms and Conditions	

TERMS AND CONDITIONS

This copyrighted material is owned by or exclusively licensed to John Wiley & Sons, Inc. or one of its group companies (each a"Wiley Company") or handled on behalf of a society with which a Wiley Company has exclusive publishing rights in relation to a particular work (collectively "WILEY"). By clicking "accept" in connection with completing this licensing transaction, you agree that the following terms and conditions apply to this transaction (along with the billing and payment terms and conditions established by the Copyright

Clearance Center Inc., ("CCC's Billing and Payment terms and conditions"), at the time that you opened your RightsLink account (these are available at any time at http://myaccount.copyright.com).

Terms and Conditions

- The materials you have requested permission to reproduce or reuse (the "Wiley Materials") are protected by copyright.

- You are hereby granted a personal, non-exclusive, non-sub licensable (on a stand-alone basis), non-transferable, worldwide, limited license to reproduce the Wiley Materials for the purpose specified in the licensing process. This license, **and any CONTENT (PDF or image file) purchased as part of your order,** is for a one-time use only and limited to any maximum distribution number specified in the license. The first instance of republication or reuse granted by this license must be completed within two years of the date of the grant of this license (although copies prepared before the end date may be distributed thereafter). The Wiley Materials shall not be used in any other manner or for any other purpose, beyond what is granted in the license. Permission is granted subject to an appropriate acknowledgement given to the author, title of the material/book/journal and the publisher. You shall also duplicate the copyright notice that appears in the Wiley publication in your use of the Wiley Material. Permission is also granted on the understanding that nowhere in the text is a previously published source acknowledged for all or part of this Wiley Material. Any third party content is expressly excluded from this permission.

- With respect to the Wiley Materials, all rights are reserved. Except as expressly granted by the terms of the license, no part of the Wiley Materials may be copied, modified, adapted (except for minor reformatting required by the new Publication), translated, reproduced, transferred or distributed, in any form or by any means, and no derivative works may be made based on the Wiley Materials without the prior permission of the respective copyright owner.**For STM Signatory Publishers clearing permission under the terms of the STM Permissions Guidelines only, the terms of the license are extended to include subsequent editions and for editions in other languages, provided such editions are for the work as a whole in situ and does not involve the separate exploitation of the permitted figures or extracts,** You may not alter, remove or suppress in any manner any copyright, trademark or other notices displayed by the Wiley Materials. You may not license, rent, sell, loan, lease, pledge, offer as security, transfer or assign the Wiley Materials on a stand-alone basis, or any of the rights granted to you hereunder to any other person.

- The Wiley Materials and all of the intellectual property rights therein shall at all times remain the exclusive property of John Wiley & Sons Inc, the Wiley Companies, or their respective licensors, and your interest therein is only that of having possession of and the right to reproduce the Wiley Materials pursuant to Section 2 herein during the continuance of this Agreement. You agree that you own no right, title or interest in or to the Wiley Materials or any of the intellectual property rights therein. You shall have no rights hereunder other than the license as provided for above in Section 2. No right, license or interest to any trademark, trade name, service mark or other branding ("Marks") of WILEY or its licensors is granted hereunder, and you agree that you shall not assert any such right, license or interest with respect thereto

- NEITHER WILEY NOR ITS LICENSORS MAKES ANY WARRANTY OR REPRESENTATION OF ANY KIND TO YOU OR ANY THIRD PARTY, EXPRESS, IMPLIED OR STATUTORY, WITH RESPECT TO THE MATERIALS

TH-21[illegible]2016

OR THE ACCURACY OF ANY INFORMATION CONTAINED IN THE MATERIALS, INCLUDING, WITHOUT LIMITATION, ANY IMPLIED WARRANTY OF MERCHANTABILITY, ACCURACY, SATISFACTORY QUALITY, FITNESS FOR A PARTICULAR PURPOSE, USABILITY, INTEGRATION OR NON-INFRINGEMENT AND ALL SUCH WARRANTIES ARE HEREBY EXCLUDED BY WILEY AND ITS LICENSORS AND WAIVED BY YOU.

- WILEY shall have the right to terminate this Agreement immediately upon breach of this Agreement by you.

- You shall indemnify, defend and hold harmless WILEY, its Licensors and their respective directors, officers, agents and employees, from and against any actual or threatened claims, demands, causes of action or proceedings arising from any breach of this Agreement by you.

- IN NO EVENT SHALL WILEY OR ITS LICENSORS BE LIABLE TO YOU OR ANY OTHER PARTY OR ANY OTHER PERSON OR ENTITY FOR ANY SPECIAL, CONSEQUENTIAL, INCIDENTAL, INDIRECT, EXEMPLARY OR PUNITIVE DAMAGES, HOWEVER CAUSED, ARISING OUT OF OR IN CONNECTION WITH THE DOWNLOADING, PROVISIONING, VIEWING OR USE OF THE MATERIALS REGARDLESS OF THE FORM OF ACTION, WHETHER FOR BREACH OF CONTRACT, BREACH OF WARRANTY, TORT, NEGLIGENCE, INFRINGEMENT OR OTHERWISE (INCLUDING, WITHOUT LIMITATION, DAMAGES BASED ON LOSS OF PROFITS, DATA, FILES, USE, BUSINESS OPPORTUNITY OR CLAIMS OF THIRD PARTIES), AND WHETHER OR NOT THE PARTY HAS BEEN ADVISED OF THE POSSIBILITY OF SUCH DAMAGES. THIS LIMITATION SHALL APPLY NOTWITHSTANDING ANY FAILURE OF ESSENTIAL PURPOSE OF ANY LIMITED REMEDY PROVIDED HEREIN.

- Should any provision of this Agreement be held by a court of competent jurisdiction to be illegal, invalid, or unenforceable, that provision shall be deemed amended to achieve as nearly as possible the same economic effect as the original provision, and the legality, validity and enforceability of the remaining provisions of this Agreement shall not be affected or impaired thereby.

- The failure of either party to enforce any term or condition of this Agreement shall not constitute a waiver of either party's right to enforce each and every term and condition of this Agreement. No breach under this agreement shall be deemed waived or excused by either party unless such waiver or consent is in writing signed by the party granting such waiver or consent. The waiver by or consent of a party to a breach of any provision of this Agreement shall not operate or be construed as a waiver of or consent to any other or subsequent breach by such other party.

- This Agreement may not be assigned (including by operation of law or otherwise) by you without WILEY's prior written consent.

- Any fee required for this permission shall be non-refundable after thirty (30) days from receipt by the CCC.

- These terms and conditions together with CCC's Billing and Payment terms and conditions (which are incorporated herein) form the entire agreement between you and WILEY concerning this licensing transaction and (in the absence of fraud) supersedes

all prior agreements and representations of the parties, oral or written. This Agreement may not be amended except in writing signed by both parties. This Agreement shall be binding upon and inure to the benefit of the parties' successors, legal representatives, and authorized assigns.

- In the event of any conflict between your obligations established by these terms and conditions and those established by CCC's Billing and Payment terms and conditions, these terms and conditions shall prevail.

- WILEY expressly reserves all rights not specifically granted in the combination of (i) the license details provided by you and accepted in the course of this licensing transaction, (ii) these terms and conditions and (iii) CCC's Billing and Payment terms and conditions.

- This Agreement will be void if the Type of Use, Format, Circulation, or Requestor Type was misrepresented during the licensing process.

- This Agreement shall be governed by and construed in accordance with the laws of the State of New York, USA, without regards to such state's conflict of law rules. Any legal action, suit or proceeding arising out of or relating to these Terms and Conditions or the breach thereof shall be instituted in a court of competent jurisdiction in New York County in the State of New York in the United States of America and each party hereby consents and submits to the personal jurisdiction of such court, waives any objection to venue in such court and consents to service of process by registered or certified mail, return receipt requested, at the last known address of such party.

WILEY OPEN ACCESS TERMS AND CONDITIONS

Wiley Publishes Open Access Articles in fully Open Access Journals and in Subscription journals offering Online Open. Although most of the fully Open Access journals publish open access articles under the terms of the Creative Commons Attribution (CC BY) License only, the subscription journals and a few of the Open Access Journals offer a choice of Creative Commons Licenses. The license type is clearly identified on the article.

The Creative Commons Attribution License

The Creative Commons Attribution License (CC-BY) allows users to copy, distribute and transmit an article, adapt the article and make commercial use of the article. The CC-BY license permits commercial and non-

Creative Commons Attribution Non-Commercial License

The Creative Commons Attribution Non-Commercial (CC-BY-NC)License permits use, distribution and reproduction in any medium, provided the original work is properly cited and is not used for commercial purposes.(see below)

Creative Commons Attribution-Non-Commercial-NoDerivs License

The Creative Commons Attribution Non-Commercial-NoDerivs License (CC-BY-NC-ND) permits use, distribution and reproduction in any medium, provided the original work is properly cited, is not used for commercial purposes and no modifications or adaptations are made. (see below)

Use by commercial "for-profit" organizations

Use of Wiley Open Access articles for commercial, promotional, or marketing purposes requires further explicit permission from Wiley and will be subject to a fee.

Further details can be found on Wiley Online Library
http://olabout.wiley.com/WileyCDA/Section/id-410895.html

TH-2131_146122026

Other Terms and Conditions:

v1.10 Last updated September 2015

Questions? customercare@copyright.com or +1-855-239-3415 (toll free in the US) or +1-978-646-2777.

TH-2131_146122026

Title: Conducting Carbon Dot–Polypyrrole Nanocomposite for Sensitive Detection of Picric acid

Author: Ayan Pal, Md Palashuddin Sk, Arun Chattopadhyay

Publication: Applied Materials

Publisher: American Chemical Society

Date: Mar 1, 2016

PERMISSION/LICENSE IS GRANTED FOR YOUR ORDER AT NO CHARGE

This type of permission/license, instead of the standard Terms & Conditions, is sent to you because no fee is being charged for your order. Please note the following:

- Permission is granted for your request in both print and electronic formats, and translations.
- If figures and/or tables were requested, they may be adapted or used in part.
- Please print this page for your records and send a copy of it to your publisher/graduate school.
- Appropriate credit for the requested material should be given as follows: "Reprinted (adapted) with permission from (COMPLETE REFERENCE CITATION). Copyright (YEAR) American Chemical Society." Insert appropriate information in place of the capitalized words.
- One-time permission is granted only for the use specified in your request. No additional uses are granted (such as derivative works or other editions). For any other uses, please submit a new request.

TH-2131_146122026

Royal Society of Chemistry LICENSE TERMS AND CONDITIONS

Jul 09, 2019

This is a License Agreement between AYAN PAL ("You") and Royal Society of Chemistry ("Royal Society of Chemistry") provided by Copyright Clearance Center ("CCC"). The license consists of your order details, the terms and conditions provided by Royal Society of Chemistry, and the payment terms and conditions.

All payments must be made in full to CCC. For payment instructions, please see information listed at the bottom of this form.

License Number	4624740365112
License date	Jul 09, 2019
Licensed content publisher	Royal Society of Chemistry
Licensed content title	Journal of materials chemistry. A, Materials for energy and sustainability
Licensed content date	Jan 1, 2013
Type of Use	Thesis/Dissertation
Requestor type	Academic institution
Format	Print, Electronic
Portion	chapter/article
The requesting person/organization is:	Ayan Pal, IIT Guwahati
Title or numeric reference of the portion(s)	Chapter 4; Phosphorus Induced Crystallinity in Carbon dots for Solar Light Assisted Seawater Desalination.
Title of the article or chapter the portion is from	Phosphorus Induced Crystallinity in Carbon dots for Solar Light Assisted Seawater Desalination.
Editor of portion(s)	N/A
Author of portion(s)	Ayan Pal
Volume of serial or monograph.	N/A
Issue, if republishing an article from a serial	4111-4118
Page range of the portion	
Publication date of portion	August 2019
Rights for	Main product
Duration of use	Life of current edition
Creation of copies for the disabled	no
With minor editing privileges	yes
For distribution to	Worldwide
In the following language(s)	Original language of publication
With incidental promotional use	no

TH-2131_146122026

The lifetime unit quantity of new product	Up to 499
Title	Towards Crystalline Carbon dots for Improved Application Potential
Institution name	IIT Guwahati, India
Expected presentation date	Aug 2019
Billing Type	Invoice
Billing Address	AYAN PAL IIT GUWAHATI, ASSAM, INDIA IIT GUWAHATI, ASSAM, INDIA GUWAHATI, India 781039 Attn: AYAN PAL
Total (may include CCC user fee)	0.00 USD
Terms and Conditions	

TERMS AND CONDITIONS

The following terms are individual to this publisher:

None

Other Terms and Conditions:

STANDARD TERMS AND CONDITIONS

1. Description of Service; Defined Terms. This Republication License enables the User to obtain licenses for republication of one or more copyrighted works as described in detail on the relevant Order Confirmation (the "Work(s)"). Copyright Clearance Center, Inc. ("CCC") grants licenses through the Service on behalf of the rightsholder identified on the Order Confirmation (the "Rightsholder"). "Republication", as used herein, generally means the inclusion of a Work, in whole or in part, in a new work or works, also as described on the Order Confirmation. "User", as used herein, means the person or entity making such republication.

2. The terms set forth in the relevant Order Confirmation, and any terms set by the Rightsholder with respect to a particular Work, govern the terms of use of Works in connection with the Service. By using the Service, the person transacting for a republication license on behalf of the User represents and warrants that he/she/it (a) has been duly authorized by the User to accept, and hereby does accept, all such terms and conditions on behalf of User, and (b) shall inform User of all such terms and conditions. In the event such person is a "freelancer" or other third party independent of User and CCC, such party shall be deemed jointly a "User" for purposes of these terms and conditions. In any event, User shall be deemed to have accepted and agreed to all such terms and conditions if User republishes the Work in any fashion.

3. Scope of License; Limitations and Obligations.

3.1 All Works and all rights therein, including copyright rights, remain the sole and exclusive property of the Rightsholder. The license created by the exchange of an Order Confirmation (and/or any invoice) and payment by User of the full amount set forth on that document includes only those rights expressly set forth in the Order Confirmation and in these terms and conditions, and conveys no other rights in the Work(s) to User. All rights not expressly granted are hereby reserved.

3.2 General Payment Terms: You may pay by credit card or through an account with us payable at the end of the month. If you and we agree that you may establish a standing account with CCC, then the following terms apply: Remit Payment to: Copyright Clearance Center, 29118 Network Place, Chicago, IL 60673-1291. Payments Due: Invoices are payable upon their delivery to you (or upon our notice to you that they are available to you for downloading). After 30 days, outstanding amounts will be subject to a service charge of 1-1/2% per month or, if less, the maximum rate allowed by applicable law. Unless otherwise

specifically set forth in the Order Confirmation or in a separate written agreement signed by CCC, invoices are due and payable on "net 30" terms. While User may exercise the rights licensed immediately upon issuance of the Order Confirmation, the license is automatically revoked and is null and void, as if it had never been issued, if complete payment for the license is not received on a timely basis either from User directly or through a payment agent, such as a credit card company.

3.3 Unless otherwise provided in the Order Confirmation, any grant of rights to User (i) is "one-time" (including the editions and product family specified in the license), (ii) is non-exclusive and non-transferable and (iii) is subject to any and all limitations and restrictions (such as, but not limited to, limitations on duration of use or circulation) included in the Order Confirmation or invoice and/or in these terms and conditions. Upon completion of the licensed use, User shall either secure a new permission for further use of the Work(s) or immediately cease any new use of the Work(s) and shall render inaccessible (such as by deleting or by removing or severing links or other locators) any further copies of the Work (except for copies printed on paper in accordance with this license and still in User's stock at the end of such period).

3.4 In the event that the material for which a republication license is sought includes third party materials (such as photographs, illustrations, graphs, inserts and similar materials) which are identified in such material as having been used by permission, User is responsible for identifying, and seeking separate licenses (under this Service or otherwise) for, any of such third party materials; without a separate license, such third party materials may not be used.

3.5 Use of proper copyright notice for a Work is required as a condition of any license granted under the Service. Unless otherwise provided in the Order Confirmation, a proper copyright notice will read substantially as follows: "Republished with permission of [Rightsholder's name], from [Work's title, author, volume, edition number and year of copyright]; permission conveyed through Copyright Clearance Center, Inc. " Such notice must be provided in a reasonably legible font size and must be placed either immediately adjacent to the Work as used (for example, as part of a by-line or footnote but not as a separate electronic link) or in the place where substantially all other credits or notices for the new work containing the republished Work are located. Failure to include the required notice results in loss to the Rightsholder and CCC, and the User shall be liable to pay liquidated damages for each such failure equal to twice the use fee specified in the Order Confirmation, in addition to the use fee itself and any other fees and charges specified.

3.6 User may only make alterations to the Work if and as expressly set forth in the Order Confirmation. No Work may be used in any way that is defamatory, violates the rights of third parties (including such third parties' rights of copyright, privacy, publicity, or other tangible or intangible property), or is otherwise illegal, sexually explicit or obscene. In addition, User may not conjoin a Work with any other material that may result in damage to the reputation of the Rightsholder. User agrees to inform CCC if it becomes aware of any infringement of any rights in a Work and to cooperate with any reasonable request of CCC or the Rightsholder in connection therewith.

4. Indemnity. User hereby indemnifies and agrees to defend the Rightsholder and CCC, and their respective employees and directors, against all claims, liability, damages, costs and expenses, including legal fees and expenses, arising out of any use of a Work beyond the scope of the rights granted herein, or any use of a Work which has been altered in any unauthorized way by User, including claims of defamation or infringement of rights of copyright, publicity, privacy or other tangible or intangible property.

5. Limitation of Liability. UNDER NO CIRCUMSTANCES WILL CCC OR THE RIGHTSHOLDER BE LIABLE FOR ANY DIRECT, INDIRECT, CONSEQUENTIAL OR INCIDENTAL DAMAGES (INCLUDING WITHOUT LIMITATION DAMAGES FOR LOSS OF BUSINESS PROFITS OR INFORMATION, OR FOR BUSINESS INTERRUPTION) ARISING OUT OF THE USE OR INABILITY TO USE A WORK, EVEN IF ONE OF THEM HAS BEEN ADVISED OF THE POSSIBILITY OF SUCH

DAMAGES. In any event, the total liability of the Rightsholder and CCC (including their respective employees and directors) shall not exceed the total amount actually paid by User for this license. User assumes full liability for the actions and omissions of its principals, employees, agents, affiliates, successors and assigns.

6. Limited Warranties. THE WORK(S) AND RIGHT(S) ARE PROVIDED "AS IS". CCC HAS THE RIGHT TO GRANT TO USER THE RIGHTS GRANTED IN THE ORDER CONFIRMATION DOCUMENT. CCC AND THE RIGHTSHOLDER DISCLAIM ALL OTHER WARRANTIES RELATING TO THE WORK(S) AND RIGHT(S), EITHER EXPRESS OR IMPLIED, INCLUDING WITHOUT LIMITATION IMPLIED WARRANTIES OF MERCHANTABILITY OR FITNESS FOR A PARTICULAR PURPOSE. ADDITIONAL RIGHTS MAY BE REQUIRED TO USE ILLUSTRATIONS, GRAPHS, PHOTOGRAPHS, ABSTRACTS, INSERTS OR OTHER PORTIONS OF THE WORK (AS OPPOSED TO THE ENTIRE WORK) IN A MANNER CONTEMPLATED BY USER; USER UNDERSTANDS AND AGREES THAT NEITHER CCC NOR THE RIGHTSHOLDER MAY HAVE SUCH ADDITIONAL RIGHTS TO GRANT.

7. Effect of Breach. Any failure by User to pay any amount when due, or any use by User of a Work beyond the scope of the license set forth in the Order Confirmation and/or these terms and conditions, shall be a material breach of the license created by the Order Confirmation and these terms and conditions. Any breach not cured within 30 days of written notice thereof shall result in immediate termination of such license without further notice. Any unauthorized (but licensable) use of a Work that is terminated immediately upon notice thereof may be liquidated by payment of the Rightsholder's ordinary license price therefor; any unauthorized (and unlicensable) use that is not terminated immediately for any reason (including, for example, because materials containing the Work cannot reasonably be recalled) will be subject to all remedies available at law or in equity, but in no event to a payment of less than three times the Rightsholder's ordinary license price for the most closely analogous licensable use plus Rightsholder's and/or CCC's costs and expenses incurred in collecting such payment.

8. **Miscellaneous.**

8.1 User acknowledges that CCC may, from time to time, make changes or additions to the Service or to these terms and conditions, and CCC reserves the right to send notice to the User by electronic mail or otherwise for the purposes of notifying User of such changes or additions; provided that any such changes or additions shall not apply to permissions already secured and paid for.

8.2 Use of User-related information collected through the Service is governed by CCC's privacy policy, available online here:
http://www.copyright.com/content/cc3/en/tools/footer/privacypolicy.html.

8.3 The licensing transaction described in the Order Confirmation is personal to User. Therefore, User may not assign or transfer to any other person (whether a natural person or an organization of any kind) the license created by the Order Confirmation and these terms and conditions or any rights granted hereunder; provided, however, that User may assign such license in its entirety on written notice to CCC in the event of a transfer of all or substantially all of User's rights in the new material which includes the Work(s) licensed under this Service.

8.4 No amendment or waiver of any terms is binding unless set forth in writing and signed by the parties. The Rightsholder and CCC hereby object to any terms contained in any writing prepared by the User or its principals, employees, agents or affiliates and purporting to govern or otherwise relate to the licensing transaction described in the Order Confirmation, which terms are in any way inconsistent with any terms set forth in the Order Confirmation and/or in these terms and conditions or CCC's standard operating procedures, whether such writing is prepared prior to, simultaneously with or subsequent to the Order Confirmation, and whether such writing appears on a copy of the Order Confirmation or in a separate instrument.

TH-2131_146122026

8.5 The licensing transaction described in the Order Confirmation document shall be governed by and construed under the law of the State of New York, USA, without regard to the principles thereof of conflicts of law. Any case, controversy, suit, action, or proceeding arising out of, in connection with, or related to such licensing transaction shall be brought, at CCC's sole discretion, in any federal or state court located in the County of New York, State of New York, USA, or in any federal or state court whose geographical jurisdiction covers the location of the Rightsholder set forth in the Order Confirmation. The parties expressly submit to the personal jurisdiction and venue of each such federal or state court.If you have any comments or questions about the Service or Copyright Clearance Center, please contact us at 978-750-8400 or send an e-mail to info@copyright.com.
v 1.1

Questions? customercare@copyright.com or +1-855-239-3415 (toll free in the US) or +1-978-646-2777.

TH-2131_146122026

Zinc Ion-Induced Assembly of Crystalline Carbon Dots with Excellent Supercapacitor Performance

Author: Ayan Pal, Arin Bhakat, Arun Chattopadhyay
Publication: The Journal of Physical Chemistry C
Publisher: American Chemical Society
Date: Aug 1, 2019

PERMISSION/LICENSE IS GRANTED FOR YOUR ORDER AT NO CHARGE

This type of permission/license, instead of the standard Terms & Conditions, is sent to you because no fee is being charged for your order. Please note the following:

- Permission is granted for your request in both print and electronic formats, and translations.
- If figures and/or tables were requested, they may be adapted or used in part.
- Please print this page for your records and send a copy of it to your publisher/graduate school.
- Appropriate credit for the requested material should be given as follows: "Reprinted (adapted) with permission from (COMPLETE REFERENCE CITATION). Copyright (YEAR) American Chemical Society." Insert appropriate information in place of the capitalized words.
- One-time permission is granted only for the use specified in your request. No additional uses are granted (such as derivative works or other editions). For any other uses, please submit a new request.

BACK CLOSE WINDOW